Universitat
de les Illes Balears

DOCTORAL THESIS
2022

METAGENOMIC CHARACTERIZATION OF HYPERSALINE ANAEROBIC SEDIMENTS OF S'AVALL SOLAR SALTERNS, AND EVALUATION OF SALINITY AS SELECTION FORCE IN THE TAXONOMIC STRUCTURE OF METHANOGENIC CONSORTIA

Francesca Font Verdera

Universitat de les Illes Balears

IMEDEA CSIC UIB

DOCTORAL THESIS
2022

Doctoral Programme in Environmental and Biomedical Microbiology

METAGENOMIC CHARACTERIZATION OF HYPERSALINE ANAEROBIC SEDIMENTS OF S'AVALL SOLAR SALTERNS, AND EVALUATION OF SALINITY AS SELECTION FORCE IN THE TAXONOMIC STRUCTURE OF METHANOGENIC CONSORTIA

Francesca Font Verdera

Thesis Supervisor: Dr. Ramon A. Rosselló Mora

Thesis Supervisor: Dr. Bartomeu A. Viver Pizà

Thesis Tutor: Dr. Elena I. García-Valdés Pukkits

Doctor by the Universitat de les Illes Balears

Ramon Antoni Rosselló Mora
Grupo de Microbiología Marina
Departamento de Biodiversidad
Animal y Microbiana
IMEDEA (UIB-CSIC)
Thesis Supervisor

Bartomeu Antoni Viver Pizà
Grupo de Microbiología Marina
Departamento de Biodiversidad
Animal y Microbiana
IMEDEA (UIB-CSIC)
Thesis Supervisor

Elena Isabel García-Valdés Pukkits
Grupo de Microbiología
Departamento de Biología
(UIB)
Thesis Tutor

Francesca Font Verdera

Universitat de les Illes Balears

Dr. Ramon A. Rosselló Mora, of Universitat de les Illes Balears

Dr. Bartomeu A. Viver Pizà, of Universitat de les Illes Balears

WE DECLARE:

That the thesis title *Metagenomic characterization of hypersaline anaerobic sediments of S'Avall solar salterns, and evaluation of salinity as selection force in the taxonomic structure of methanogenic consortia* presented by Francesca Font Verdera to obtain a doctoral degree, has been completed under our supervision and meets the requirements to opt for a Doctorate.

For all intents and purposes, we hereby sign this document

Ramon Antoni Rosselló Mora
Grupo de Microbiología Marina
Departamento de Biodiversidad
Animal y Microbiana
IMEDEA (UIB-CSIC)

Bartomeu Antoni Viver Pizà
Grupo de Microbiología Marina
Departamento de Biodiversidad
Animal y Microbiana
IMEDEA (UIB-CSIC)

Palma de Mallorca, January 31th 2022

Acknowledgments

I would thank the predoctoral fellowship from the Spanish Ministry of Science, Innovation and Universities (Nr. BES-2016-078138) supporting my own research activity and the projects also granted by the Spanish Ministry of Science, Innovation and Universities CLG2015_66686-C3-1-P (SALPLOMA) and PGC2018-096956-B-C41 (MICROMATES), which were both supported with European Regional Development Fund (FEDER) funds.

M'agradaria expressar la meva més sincera gratitud als meus directors de tesi, el Dr. Ramon Rosselló Móra i el Dr. Bartomeu Viver Pizà. Gràcies Ramon per obrir-me les portes al món de la microbiologia, per haver-me acceptat en el teu grup d'investigació ja per fer les pràctiques del màster, i sobretot per haver confiat amb mi de cara a fer el doctorat, encara que tingués un perfil acadèmic certament diferent al que s'adequa més amb la línia d'investigació del grup. Moltes gràcies pel teus consells, recolzament continu i tutela durant el doctorat.

I wish to show my appreciation to all the co-authors of the manuscript, for their comments, suggestions and contribution in the improvement of the published article. I wish to extend my special thanks to all those responsible of Salinas S'Avall (Colònia de Sant Jordi, Mallorca, Spain), for admittance to their installations and sampling permission.

No em puc creure que aquí es posi el punt i final, qui m'hauria dit a mi que hagués acabat realitzant una tesi doctoral i que, a més, fos en aquell edifici immens pel qual jo passava cada dia per davant. Perquè jo sabia que allà treballaven científics, però no en sabia més... i em preguntava... què investigaven exactament? Per a què servia allò? Com es podia entrar a treballar allà? Després de set anys formant part del IMEDEA, encara em queda molt per aprendre, però el que m'enduc a la motxilla és molt més valuós que el que duia quan vaig començar. Per uns pocs realitzar la tesi doctoral serà un treball que dura quatre anys, per altres un camí dur, ple d'entrebancs i contratemps que s'han d'anar esquivant, i per altres una experiència inoblidable (en el bon sentit de la paraula). Jo crec que la majoria de gent passa pels diferent estadis en menor o major mesura, però el realment important és ser conseqüent amb un mateix, no rendir-se i aguantar la pressió que a vegades ens vol ofegar en aquesta muntanya russa anomenada "tesi doctoral", i arribar a la meta, essent un poc més savi que al principi.

Estic profundament agraïda a tot el grup MMG, a tots els components que vaig conèixer quan vaig començar més o menys a finals de 2013, fins a l'actualitat. Dóna gust entrar a un lloc nou a treballar i que l'ambient sigui tan càlid i familiar, aquesta meravellosa sensació que sempre ha transmès el grup. M'he sentit com a casa (literal i figurativament). Moltes gràcies a tots els membres que han format o formen part del MMG: Aina, Albert, Anina, Arantxa, Esteban, Josep, Miquel, Sara *et al.* pel vostre recolzament i la vostra ajuda en cada una de les etapes de la investigació. Quiero agradecer especialmente a Raquel por su

inestimable contribución a la tesis. También hacer especial mención a dos personas que han significado mucho para mí durante mi estancia en IMEDEA, de los cuales he aprendido más de lo que puedo recordar: Merit y Raúl, un placer haber coincidido con vosotros en un tramo de este largo camino. Mercedes, gracias, gracias y gracias. Literalmente, no sé qué haríamos sin nuestra mamá particular, tanto dentro como fuera del laboratorio. I finalment, gràcies a en Tomeu (ara sí te toca), a en Joan i a na Carlota. Gràcies per tot, per ser com sou, per sempre estar allà, pels incontables moments de xerrades, de rialles, de festa... i d'amistat. Gràcies Tomeu pel teu ajut continu i per haver estat el millor codirector que podria desitjar. Gràcies Joan per ser el millor retallador... no, pel gran sentit de l'humor i companyerisme. Gràcies Carlota per ser el desastre més entranyable i millor amiga que m'he trobat durant el doctorat.

Vull estendre els meus agraïments a tots els "Imedeicos". Tanta gent i l'experiència tan enriquidora d'haver compartit aquest viatge amb vosaltres, ja sigui amb un cafè a l'àgora o donant-ho tot en una festa, però quin gust haver pogut ser part dels vostres èxits en algun moment. Tothom sap que l'IMEDEA és com una estació de metro, en la qual tot el temps n'hi ha que van i que vénen, però no puc deixar de ressaltar al Carlos, Pablo, Nayaret, Chiara, Mario, Guille i Flore. El meu sincer agraïment a l'Alex, Vero, Miguel, Tim, Albert, Ana, Paula, Marlene, Arancha, Núria, Julia, Melo, Almu, Laura, Pau, Inma, Emma, Dani, Àngels, Manu...segur que em deixo a moltíssima gent. Per tant, a tots els meus col·legues, amics i amigues que he conegut durant aquest trajecte, sabeu qui sou, i em tendreu pel que vulgueu i quan ho necessiteu. El final de l'etapa a IMEDEA no és la fi de la nostra amistat, i ja sabeu que tots teniu casa a Mallorca.

També vull agrair a les meves amigues de sempre, a les que m'han suportat en els meus dies millors i pitjors durant la tesi, a les que diuen que la seva amiga és "la científica", encara que jo cregui que aquest títol em ve un poc gran, però que m'enorgulleix que penseu això. Moltes gràcies Maria, Marga G., Xisca, Marina, Cris, Aina, Tita, Marga B. i Mary, per ser i estar sempre.

I no puc oblidar-me d'agrair a tota la meva família i als dos més importants, als que han respectat totes les decisions de la meva vida i m'han aplanat el camí per aconseguir tot el que m'he proposat. Agrair enormement als meus dos pilars, als meus pares, als que sempre han confiat en mi.

List of completed publications related to this Thesis:

Font-Verdera, F., Liébana, R., Aldeguer-Riquelme, B., Gangloff, V., Santos, F., Viver, T., and Rosselló-Móra, R. (2021) Inverted microbial community stratification and spatial–temporal stability in hypersaline anaerobic sediments from the S'Avall solar salterns. Syst Appl Microbiol 44: 126231.

Other publications produced during the Ph.D. period:

Mora-Ruiz, M. del R., Cifuentes, A., Font-Verdera, F., Pérez-Fernández, C., Farias, M.E., González, B., et al. (2018) Biogeographical patterns of bacterial and archaeal communities from distant hypersaline environments. Syst Appl Microbiol 41: 139–150.

TABLE OF CONTENTS

Abstract

The anaerobic hypersaline sediments of an ephemeral pond from the S'Avall solar salterns constituted an excellent study system because of their easy accessibility, as well as the analogy of their microbial assemblages with some known deep-sea hypersaline anaerobic brines. By means of shotgun metagenomics and 16S rRNA gene amplicon sequencing, the microbial composition of the sediment was shown to be stable in time and space. The communities were formed by prokaryote representatives with an inferred clear anaerobic metabolism, mainly related to the methane, sulfur and nitrate cycles. The most conspicuous finding was the inverted nature of the vertical stratification. Contrarily to what could be expected, a methanogenic archaeal metabolism was found to dominate in the upper layers, whereas Bacteria with fermentative and anaerobic respiration metabolisms increased with depth. We could demonstrate a putative methanogenic nature of the members of candidate lineages DHVE2 and MSBL1, which were present in high abundance in this system, and described, for the first time, viruses infecting these lineages. Members of the aerobic genera *Salinibacter* and *Halorubrum* putatively active were detected especially in the deepest layers for which we hypothesize that either oxygen could be sporadically available, or they could perform anaerobic metabolisms. We also report a novel repertoire of virus species thriving in these sediments, which had special relevance because of their lysogenic lifestyles.

Sediments underlying the solar salterns of S'Avall have been subjected to the evaluation of abiotic factors as salinity, substrate concentration (*Posidonia oceanica*) and antibiotic. The sediment composition was analysed by amplicon 16S rRNA gene sequencing. Salinity acted as the major selection force to structure microbial communities, influenced by ampicillin, that exerted a selective pressure, and the use of distinct concentrations of *P. oceanica*, which displayed a weaker effect. At high salinities, communities were dominated by extreme halophilic Archaea, whereas bacterial alpha diversity decreased with salinity, being highest at 5%. Besides, among the most competitive taxa and their metabolic role in the ecosystem, overall sulfate-reducers decreased with salinity and in turn methanogens increased as salt concentration did, especially at 25% were only methanogens dominated. Beta diversity between communities in microcosms with and without ampicillin displayed an increasing trend with dilution, although its real effect could be partially hidden by the salinity factor. However, no important effect was observed of carbon substrate concentration. Deterministic ecological factors did not affect microbial community assemblies, whereas stochastic processes predominantly prevailed on the microbial dynamics of the sediment as salinity increased. Dilution applied to the slurry (initial conditions), ranging from 30% to 5% of salinity (at which the highest compositional changes were detected) was the most relevant ecological factor.

Microbial communities from sediments of S'Avall demonstrated an understudied potential in methanogenesis, and halophilic methanogenic consortia from enriched microcosms were described in this study by means of metagenomics. With a broad range in cultivability requirements at eight different salinities, distinct substrate concentrations and ampicillin, the most efficient microcosms were selected in accordance to gas methane measurement through gas chromatography. These enrichments were subcultured and supplemented with organic compounds (acetate, formate and trimethylamine: ATF), which enhanced the methane production. The results showed the highest methane yield in microcosms at 5% of salinity with ampicillin and 10% w/w *P. oceanica*, and even more the supplemented with ATF, obtaining higher methane rates in comparison to reported until now. Among the prokaryotic diversity regarding the ATF supplement availability, *Methanosarcina* was more abundant in the no supplemented enrichment, whereas *Methanoculleus* with ATF. These genera within *Methanomicrobia* showed a taxonomic turnover in accordance to the supplement disposal. Besides, aceticlastic *Methanoculleus* genus exhibited high replication activity in comparison to the metabolically versatile *Methanosarcina*, which can produce methane using any of the methanogenesis pathways. Additionally, new members of *Bathyarchaeia* and *Lokiarchaeia* were also able to produce methane, specially *Bathyarchaeia* in the no-ATF supplemented enrichment and the putative hydrogenotrophic *Lokiarchaeia* class in the supplemented one. In fact, methanogenesis was performed mainly via aceticlastic route, with *Methanomicrobia* and *Bathyarchaeia* as the most representative, and the supplement based on the addition of acetate, trimethylamine and formate could be mainly metabolized by members affiliated with *Methanomicrobia* and *Lokiarchaeia*.

Resumen

Los sedimentos hipersalinos anaerobios de un estanque efímero de las salinas solares de S'Avall constituyeron un excelente sistema de estudio por su fácil accesibilidad, así como por la analogía de sus ensamblajes microbianos con algunos de salmueras anaerobias hipersalinas de aguas profundas conocidas (DHABS). Se demostró la estabilidad temporal y espacial de la composición microbiana del sedimento, mediante metagenómica y la secuenciación del amplicón del gen del ARNr 16S. Las comunidades estaban compuestas por representantes procariotas con un claro metabolismo anaerobio inferido, relacionado principalmente con los ciclos del metano, azufre y nitrato. El hallazgo más notorio fue la naturaleza invertida de la estratificación vertical. Contrariamente a lo que podría esperarse, se encontró que un metabolismo llevado a cabo por Archaea metanogénicas dominaba en las capas superiores, mientras que las bacterias con metabolismos respiratorios fermentativos y anaeróbicos aumentaron con la profundidad. Pudimos demostrar un comportamiento putativamente metanógeno para los miembros de los linajes candidatos DHVE2 y MSBL1, que eran muy abundantes en este sistema, y se describió, por primera vez, virus que infectan estos linajes. Se detectaron miembros de los géneros aerobios *Salinibacter* y *Halorubrum* supuestamente activos, especialmente en las capas más profundas, por lo que planteamos las hipótesis de que el oxígeno podría estar disponible esporádicamente o que estos microorganismos podrían realizar metabolismos anaerobios. Un repertorio novedoso de especies de virus que prosperan en estos sedimentos también fue encontrado, los cuales tuvieron especial relevancia debido a sus estilos de vida lisogénicos.

Los sedimentos subyacentes a las salinas solares de S'Avall se han sometido a la evaluación de factores abióticos como la salinidad, la concentración de sustrato (*Posidonia oceanica*) y antibiótico. La composición del sedimento se analizó mediante secuenciación del gen del ARNr 16S. La salinidad actuó como la fuerza principal de selección para estructurar las comunidades microbianas, influenciadas por la ampicilina, que ejerció una presión selectiva, y el uso de distintas concentraciones de *P. oceanica*, que mostraron un efecto más débil. En altas salinidades, las comunidades estuvieron dominadas por Archaea extremadamente halófilas, mientras que la diversidad alfa bacteriana disminuyó con la salinidad, siendo más alta al 5%. Además, entre los taxones más competitivos y su función metabólica en el ecosistema, en general los reductores de sulfato disminuyeron con la salinidad y, a su vez, los metanógenos aumentaron con la concentración de sal, especialmente al 25% dónde sólo dominaron los metanógenos. La beta-diversidad entre las comunidades de los microcosmos con y sin ampicilina mostró una tendencia creciente con la dilución, aunque su efecto real podría estar parcialmente oculto por el factor de salinidad. Sin embargo, no se observó ningún efecto importante proveniente de la concentración de sustrato de carbono. Los factores ecológicos deterministas no afectaron a los ensamblajes de comunidades microbianas, mientras que los procesos estocásticos prevalecieron

predominantemente sobre la dinámica microbiana del sedimento a medida que aumentaba la salinidad. La dilución aplicada al sedimento (en condiciones iniciales), la cual variaba del 30% al 5% de salinidad (en la que se detectaron los mayores cambios de composición) fue el factor ecológico más relevante.

Las comunidades microbianas de los sedimentos de S'Avall demostraron un potencial poco estudiado en la metanogénesis, y en este estudio se describieron consorcios metanogénicos halófilos a partir de microcosmos enriquecidos mediante metagenómica. Con una amplia gama de requisitos de cultivabilidad, a ocho salinidades diferentes, distintas concentraciones de sustrato y ampicilina, los microcosmos más eficientes fueron seleccionados de acuerdo a la medición de gas metano mediante cromatografía de gases. Estos enriquecimientos fueron subcultivados y suplementados con compuestos orgánicos (acetato, formiato y trimetilamina: ATF), que potenciaron la producción de metano. Los resultados mostraron el mayor rendimiento en metano en los microcosmos al 5% de salinidad con ampicilina y 10% de *P. oceanica*, y aún más en el suplementado con ATF, obteniendo tasas de metano más altas en comparación a lo descrito hasta el momento. Entre la diversidad procariota con respecto a la disponibilidad del suplemento ATF, *Methanosarcina* fue más abundante en el enriquecimiento no suplementado, mientras que *Methanoculleus* con ATF. Estos géneros pertenecientes a *Methanomicrobia* mostraron una clara evidencia de un recambio taxonómico entre ellos, de acuerdo con el suplemento disponible. Además, el género aceticlástico *Methanoculleus* exhibió una alta actividad de replicación en comparación con *Methanosarcina*, muy versátil metabólicamente por su capacidad de producir metano utilizando cualquiera de las vías de la metanogénesis. Además, los nuevos miembros de *Bathyarchaeia* y *Lokiarchaeia* también fueron capaces de generar gas metano, especialmente *Bathyarchaeia* en el enriquecimiento sin ATF y la clase hidrogenotrófica putativa *Lokiarchaeia* en el suplementado. De hecho, la metanogénesis se llevó a cabo principalmente por la vía aceticlástica, con *Methanomicrobia* y *Bathyarchaeia* como las comunidades microbianas más representativas, y el suplemento basado en la adición de acetato, trimetilamina y formiato pudo ser metabolizado principalmente por miembros afiliados a *Methanomicrobia* and *Lokiarchaeia*.

Resum

Els sediments hipersalins anaerobis d'un estany efímer de les salines de S'Avall van constituir un sistema d'estudi excel·lent per la seva fàcil accessibilitat, així com l'analogia dels seus acoblaments microbians amb els d'algunes salmorres anaeròbies hipersalines d'aigües profundes conegudes (DHABS). L'estabilitat temporal i espacial en la composició microbiana del sediment es va demostrar mitjançant metagenòmica i la seqüenciació del gen de l'ARNr 16S. Les comunitats estaven compostes per representants procariotes amb un clar metabolisme anaerobi inferit, relacionat principalment amb els cicles del metà, sofre i nitrat. La troballa més notòria va ser la naturalesa invertida de l'estratificació vertical. Contràriament al que es podria esperar, es va trobar que un metabolisme dut a terme per Archaea metanògenes dominava a les capes superiors, mentre que els bacteris amb metabolismes respiratoris fermentatius i anaeròbics van augmentar amb la profunditat. Vam poder demostrar un comportament putativament metanògen per als membres dels llinatges candidats DHVE2 i MSBL1, que eren molt abundants en aquest sistema, i es va descriure, per primera vegada, virus que infecten aquests llinatges. Es van detectar membres dels gèneres aerobis *Salinibacter* i *Halorubrum* suposadament actius, especialment a les capes més profundes, per la qual cosa plantegem les hipòtesis que l'oxigen podria estar disponible esporàdicament o que aquests microorganismes podrien realitzar metabolismes anaerobis. Un repertori innovador d'espècies víriques que prosperen en aquests sediments també va ser trobat, les quals van tenir especial rellevància a causa dels seus estils de vida lisogènics.

Els sediments subjacents a les salines solars de S'Avall han estat sotmesos a l'avaluació de factors abiòtics com la salinitat, la concentració de substrat (*Posidonia oceanica*) i antibiòtic. La composició del sediment es va analitzar mitjançant la seqüenciació del gen de l'ARNr de l'amplicó 16S. La salinitat va actuar com la força principal de selecció per a estructurar les comunitats microbianes, influenciades per l'ampicil·lina, que va exercir una pressió selectiva, i l'ús de diferents concentracions de *P. oceanica*, les quals van mostrar un efecte més feble. A elevades salinitats, les comunitats van estar dominades per Archaea extremadament halòfiles, mentre que la diversitat alfa bacteriana va disminuir amb la salinitat, essent més alta al 5%. A més, entre els tàxons més competitius i la seva funció metabòlica a l'ecosistema, en general els reductors de sulfat van disminuir amb la salinitat i, alhora, els metanògens van augmentar amb la concentració de sal, especialment al 25% on només van dominar els metanògens. La beta-diversitat entre les comunitats dels microcosmos amb ampicil·lina i sense va mostrar una tendència creixent amb la dilució, encara que el seu efecte real podria estar parcialment ocult pel factor de salinitat. No obstant això, no es va observar cap efecte important provinent de la concentració de substrat de carboni. Els factors ecològics deterministes no van afectar als assemblatges de les comunitats microbianes, mentre que els processos estocàstics van prevaldre predominantment sobre la dinàmica microbiana del sediment a mesura que augmentava la salinitat. La dilució aplicada al

sediment (en condicions inicials), la qual variava del 30% al 5% de salinitat (en què es van detectar els majors canvis de composició) va ser el factor ecològic més rellevant.

Les comunitats microbianes dels sediments de S'Avall van demostrar un potencial poc estudiat a la metanogènesi, i en aquest estudi es van descriure consorcis metanogènics halòfils a partir de microcosmos enriquits mitjançant metagenòmica. Amb una àmplia gamma de requisits de cultivabilitat, a vuit salinitats diferents, distintes concentracions de substrat i ampicil·lina, els microcosmos més eficients van ser seleccionats d'acord amb el mesurament de gas metà mitjançant cromatografia de gasos. Aquests enriquiments van ser subcultivats i suplementats amb compostos orgànics (acetat, formiat i trimetilamina: ATF), que van potenciar la producció de metà. Els resultats van mostrar el major rendiment en metà als microcosmos al 5% de salinitat amb ampicil·lina i 10% *P. oceanica*, i encara més al suplementat amb ATF, obtenint taxes de metà més altes en comparació al que s'ha descrit fins ara. Entre la diversitat procariota d'acord a la disponibilitat del suplement ATF, *Methanosarcina* va ser més abundant a l'enriquiment no suplementat, mentre que *Methanoculleus* amb ATF. Aquests gèneres pertanyents a *Methanomicrobia* van mostrar una evidència clara d'un recanvi taxonòmic entre ells, d'acord amb el suplement disponible. A més, el gènere aceticlàstic *Methanoculleus* va exhibir una alta activitat de replicació en comparació amb *Methanosarcina*, molt versàtil metabòlicament per la seva capacitat de produir metà utilitzant qualsevol de les vies de la metanogènesi. A més, els nous membres trobats de *Bathyarchaeia* i *Lokiarchaeia* també van ser capaços de generar gas metà, especialment *Bathyarchaeia* a l'enriquiment sense ATF i la classe hidrogenotròfica putativa *Lokiarchaeia* al suplementat. De fet, la metanogènesi es va dur a terme principalment per la via aceticlàstica, amb *Methanomicrobia* i *Bathyarchaeia* com les comunitats microbianes més representatives, i el suplement basat en l'adició d'acetat, trimetilamina i formiat va poder ser metabolitzat principalment per membres afiliats a *Methanomicrobia* i *Lokiarchaeia*.

I. INTRODUCTION

1. Hypersaline and anaerobic ecosystems

Hypersaline systems, defined as environments with saline concentrations above seawater (~35 g/L), characterized by the high concentration of salt, being this, the most important environmental factor conditioning the microbial communities living there (Ventosa and Arahal, 2009). Hypersaline environments are normally described as either thalassohaline (originated by seawater evaporation) or athalassohaline (ionic compostition different to seawater and depends of the origin of the substrate). In thalassohaline ecosystems, a high concentrations of the cations Na^+ (sodium), Mg^{2+} (magnesium), Ca^{2+} (calcium) and K^+ (potassium) and of anions Cl^- (chloride), SO_4^{2-} (sulfate) and CO_3^{2-}/HCO_3^- (carbonate and hydrogen-carbonate, although less common) have been reported, and the pH is near neutral to slightly alkaline (McGenity and Oren, 2012; López-López *et al.*, 2013; Gründger *et al.*, 2015).

The microbial diversity has been described in diverse hypersaline environments such as deep-sea basins (van der Wielen *et al.*, 2005; Yakimov *et al.*, 2015; Merlino *et al.*, 2018), solar salterns (López-López *et al.*, 2010, 2013; Viver *et al.*, 2019), dark buried evaporates (McGenity and Oren, 2012), biofilms and lakes (Jiang *et al.*, 2007; Swan *et al.*, 2010; Antunes *et al.*, 2011), hypersaline microbial mats (Fernandez *et al.*, 2016; McGenity and Sorokin, 2019) and even in plants (halophytes; Mora-Ruiz *et al.*, 2015, 2016); Figure I.1.

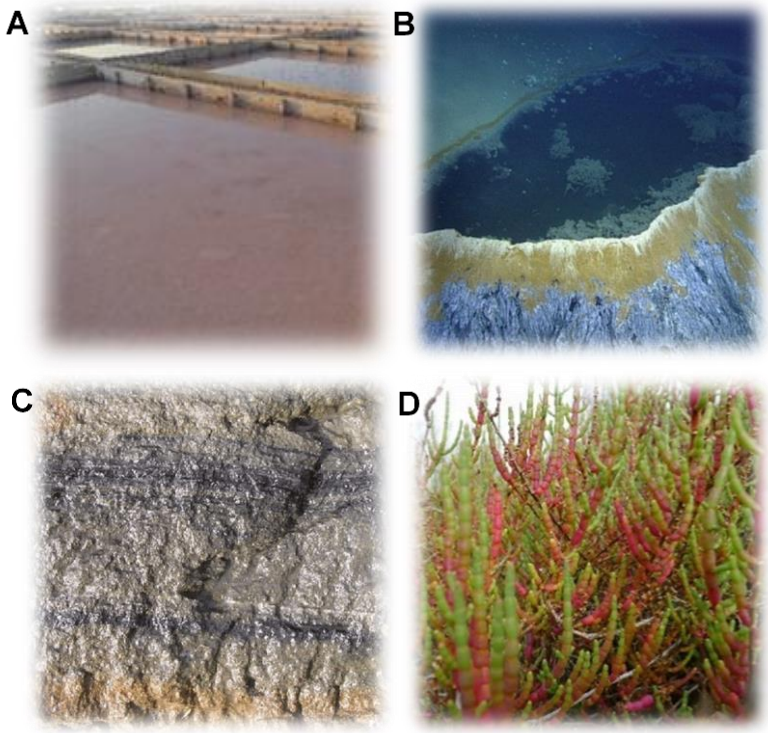

Figure I.1. Examples of hypersaline environments. **A**. Mediterranean solar salterns of Es Trenc in Campos (Spain). **B**. Deep-sea anoxic brine lakes in the Gulf of Mexico. **C**. Sediments from soda and salty lakes in Russia. **D**. Halophytes from s'Albufera of Alcúdia (Spain).

Microorganisms that live in salts concentrations above the seawater (≥ 3.5%) are classified as halophiles (Oren, 2002). These microorganisms, according to their tolerance to salt concentration, can be classified as halotolerant, moderate halophiles and extreme halophiles (Oren, 2008; Mcgenity, 2010; McGenity and Oren, 2012). Halotolerant microorganisms can thrive in salinities between 2% and 5% (actually do not require salt for growth), such as *Bacillus* spp. and *Micrococcus* spp. (Schneegurt, 2012; Oliveira *et al.*, 2015). Moderate halophiles survive in systems with saline concentrations from 4% to ~23%, as the *Salinicola* and *Halomonas* genera (Kaleem Sarwar *et al.*, 2015; Mora-Ruiz *et al.*, 2015; Oueriaghli *et al.*, 2018). Extreme halophiles, as *Salinibacter* spp. (Antón *et al.*, 2002; Viver *et al.*, 2018) and members of *Halobacteria* class (Youssef *et al.*, 2012; Oren, 2013; Sorokin, Kublanov, Yakimov, *et al.*, 2016), can thrive comfortably above the 20% until ~37% (close to saturation) of salinity (Schneegurt, 2012).

Besides the saline conditions, another important factor to consider in hypersaline environments is the concentration of oxygen. There is a large list of anaerobic natural habitats due to its absolute or almost complete absence of available oxygen. Thus, other relevant, naturally occurring hypersaline anaerobic environments appear to be globally scattered (McGenity and Oren, 2012), including deep-sea anoxic brine lakes of Gulf of Mexico (Joye *et al.*, 2009; Zhuang *et al.*, 2016; Nigro *et al.*, 2020), Red Sea (Eder *et al.*, 2001, 2002; Antunes *et al.*, 2011) and Mediterranean Sea (van der Wielen *et al.*, 2005; La Cono *et al.*, 2011; Yakimov *et al.*, 2013, 2015; Sorokin, Kublanov, Gavrilov, *et al.*, 2016; Sorokin, Kublanov, Yakimov, *et al.*, 2016); sediments from soda and salty lakes in Russia (Dimitry Y Sorokin *et al.*, 2017; Dimitry Y. Sorokin *et al.*, 2017; Vavourakis *et al.*, 2018), solar salterns of Eupatoria, Bari (Dimitry Y. Sorokin *et al.*, 2017) and Spain (López-López *et al.*, 2010, 2013), hypersaline microbial mats in Guerrero Negro (Mexico; Ley *et al.*, 2006), sediments from a permafrost Arctic spring in Canada (Lamarche-Gagnon *et al.*, 2015), hypersaline sediments in Orca Basin (Zhuang *et al.*, 2016; Nigro *et al.*, 2020) and a sea mud volcano in Napoli (Italy; Lazar *et al.*, 2011; Figure I.1).

These ecosystems have been widely studied by both culture-dependent and -independent analyses, the later especially based on 16S rRNA gene amplicon sequencing (Walsh *et al.*, 2005; Antunes *et al.*, 2011; La Cono *et al.*, 2011; Lazar *et al.*, 2011; Yakimov *et al.*, 2013, 2015; Lamarche-Gagnon *et al.*, 2015; Zhuang *et al.*, 2016), and more recently by the revolutionary and developing constantly "–omics" techniques, especially the metagenomics approach (Sorokin, Kublanov, Gavrilov, *et al.*, 2016; Sorokin, Kublanov, Yakimov, *et al.*, 2016; Dimitry Y Sorokin *et al.*, 2017; Dimitry Y. Sorokin *et al.*, 2017; Timmers *et al.*, 2018; Vavourakis *et al.*, 2018, 2019; Font-Verdera *et al.*, 2021).

2. Diversity and distribution of microbial communities in anaerobic hypersaline environments

Microbiota harbored in almost salt-saturated ecosystems has been widely studied, focusing to their diversity and correlating it with their biological adaptations to such extreme environmental conditions (Walsh *et al.*, 2005; Oren, 2008; López-López *et al.*, 2010, 2013; Lazar *et al.*, 2011; Vavourakis *et al.*, 2018). Nowadays, the knowledge on new taxa and their putative biogeochemical involvement is increasing (Eder *et al.*, 2002; van der Wielen *et al.*, 2005; Antunes *et al.*, 2011), principally for those discovered with next generation sequencing, as novel representatives of Candidate Phyla Radiation (chiefly fermenters; Vavourakis *et al.*, 2018), *Bathyarchaeota* and *Verstraetearchaeota* phyla (Evans *et al.*, 2015; Vanwonterghem *et al.*, 2016).

Brine microbial communities are mainly dominated by two major lineages, i.e., the archaeal *Halobacteria* class and the bacterial family of *Salinibacteraceae* of the class *Rhodothermia*, but with relatively high species richness within each class (Viver *et al.*, 2018, 2019). Most members of these taxons are known as strict aerobes, and only a few species exhibit a facultative anaerobic lifestyle, such as *Halalkaliarchaeum* and *Natrarchaeobaculum* (Oren, 2014; Sorokin *et al.*, 2021), or they are strict anaerobes, such as *Halodesulfurarchaeum* and *Halanaeroarchaeum* (Sorokin, Kublanov, Gavrilov, *et al.*, 2016; Sorokin, Kublanov, Yakimov, *et al.*, 2016; Dimitry Y Sorokin *et al.*, 2017; Dimitry Y. Sorokin *et al.*, 2017). On the other hand, extremely saline sediments are mostly dominated by unknown taxa (López-López *et al.*, 2010), and the majority of the cultivated extreme halophilic anaerobes are methanogenic members affiliating with other lineages of *Euryarchaeota*, as well as members of the bacterial domain with either fermentative, denitrifying or sulfate-reduction metabolisms (McGenity and Oren, 2012). Representatives of diverse methanogenic metabolisms have been described especially from the archaeal domain, such as the methylotrophic *Methanohalophilus* sp. and *Methanococcoides* sp. (Lazar *et al.*, 2011; Zhuang *et al.*, 2016), members of the *Methanonatronarchaeia* class involved in a newly discovered methyl-reducing pathway (Dimitry Y. Sorokin *et al.*, 2017), and putatively methanogenic representatives of the *Candidatus* MSBL1 (Mediterranean Sea Brine Lakes; van der Wielen *et al.*, 2005) lineage. However, whether this latter abundant uncultured monophyletic group within the phylum *Euryarchaeota* is involved in methanogenesis (McGenity and Sorokin, 2019) has remained largely unknown. Other relevant metabolic groups detected include anaerobic methanotrophs, such as ANME-1 (Lloyd *et al.*, 2006; Knittel and Boetius, 2009), and methylotrophs (Zhuang *et al.*, 2016; Nigro *et al.*, 2020), and also some anaerobic members of the class *Halobacteria* with sulfur-respiring metabolism classified as *Halodesulfurarchaeum* and *Halanaeroarchaeum* (Sorokin, Kublanov, Gavrilov, *et al.*, 2016; Sorokin, Kublanov, Yakimov, *et al.*, 2016; Dimitry Y Sorokin *et al.*, 2017; Dimitry Y. Sorokin *et al.*, 2017).

Conspicuously, some common members of the *Halobacteria* thriving abundantly in the overlying brines, and with predominantly aerobic metabolism, have been detected in the sediments where the availability of oxygen is limited (Walsh *et al.*, 2005; López-López *et al.*, 2010; Mora-Ruiz *et al.*, 2018). For some of the known aerobic members of the *Halobacteria* class, a denitrifying metabolism has been demonstrated (Torregrosa-Crespo *et al.*, 2016), but the diversity of the members of *Halobacteria* in the sediments is so large that their role, or even whether they are active, remains intriguing. Energetic contribution of *Halobacteria* members in ecosystems they inhabit is increasingly noticeable (Sorokin, Kublanov, Gavrilov, *et al.*, 2016; Sorokin, Kublanov, Yakimov, *et al.*, 2016), because of selective advantage with its competitors (Oren, 2013).

3. Metabolic inference in anaerobic and hypersaline sediments

Metabolisms described in marine and freshwater systems have also been encountered in hypersaline environments (McGenity and Oren, 2012). Hypersaline environments harbor a great amount of microorganisms related to complex carbohydrates degradation and synthesis, fermentation of saccharides and acetate, sulfur and nitrogen cycles and methanogenesis (Gottschalk, 1979), for which the high salinities are not an obstacle (McGenity and Sorokin, 2019), even thriving at a salt content of 400 g/L as in surface sediments of Siberian soda lakes (Vavourakis *et al.*, 2018).

In general, the associated sediments are characterized by a superposition of redox metabolic pathways, overlaid by aerobic respiration and transitioning in depth by less energetically favorable metabolisms, such as fermentation, nitrate, iron and manganese, and sulfate dissimilatory reductions (Schlegel, 1976; Fenchel *et al.*, 2012). The lowest energetically favorable reduction, occurring at the bottom of the superposed metabolisms is methanogenesis, which happens when the electron acceptors producing higher energetic yields (i.e. oxygen, nitrate, ferric iron and sulfate) have been depleted (Zengler *et al.*, 1999; Thamdrup *et al.*, 2000; Fenchel *et al.*, 2012; Petro *et al.*, 2017).

3.1. Methanogenesis

It is estimated that between 4 and 6 x 10^{30} prokaryotic cells (*Bacteria* and *Archaea* domains) thrive in the biosphere and only 10% of these would be colonizing water, air, soil and keeping contact with other living organisms (Whitman *et al.*, 1998). However, the remaining 90% is thought to be found in both ocean and land subsurface. Most of the microorganisms of these subsurfaces must have a sulphate-reducing or methanogenic

metabolism, and that is why methanogenesis is perhaps one of the most abundant metabolic processes in the biosphere (Mcgenity, 2010).

Methanogenesis requires primary and secondary fermenters to oxidize the complex organic matter into short-chain fatty acids and hydrogen, which are used by methanogens as substrates resulting in the production of methane via hydrogenotrophic, aceticlastic or methylotrophic pathways, the latter being the most common in salt-saturating environments (Zhuang *et al.*, 2016; McGenity and Sorokin, 2019), what is becoming questionable and might have been overestimated. Generally, syntrophy between secondary fermenters and methanogens is often needed for this process to occur, but a single methanogen is able to produce methane (Welte, 2018) and co-occurrence of methane synthesis and dissimilatory sulfur metabolism has also been reported, despite the competing metabolisms (McKay *et al.*, 2019). This syntrophy is essential for the conversion of organic matter such as polysaccharides, most aromatic compounds, proteins, nucleic acids and fatty acids to carbon dioxide and methane. This transformation is thermodynamically tight, and this is the main reason why it is very difficult to cultivate and isolate consortia of microorganisms (Mcinerney *et al.*, 2010; Sieber *et al.*, 2010; Lykidis, C. L. Chen, *et al.*, 2011; Morris *et al.*, 2013; Welte, 2018).

However, the anaerobic oxidation of methane (AOM) can occur in anoxic environments, coupled to metal reduction, as iron, manganese and sulphate. Anaerobic methanotrophic archaea (ANME) is the main consumer of this methane, by anaerobically oxidation (Cai *et al.*, 2018). Thus, the reversal canonical methanogenesis pathway has been described by means of metagenomics, single-cell genomics and metatranscriptomics analyses of bioreactors (Haroon *et al.*, 2013; Welte, 2018). In other cases, however, it seemed to be suppressed under hypersaline conditions found in brines and the underneath sediments (Nigro *et al.*, 2020). Besides, aerobic methane-oxidizing bacteria in general are also inhibited by high salt (McGenity and Sorokin, 2019).

Methanogens are essential contributors to the global carbon cycle and can work in three main different ways: through the reduction of carbon dioxide coupled with hydrogen as electrons donor (hydrogenotrophic), as an acetate decarboxylation to produce methane and carbon dioxide (aceticlastic), or using methylated substrates (methylotrophic; Thauer, 1998; Fenchel *et al.*, 2012). Besides using 16S rRNA gene to characterize the phylogenetic diversity of anaerobic digestion sludge (Manyi-loh *et al.*, 2013; Gao *et al.*, 2016), the description of key methanogenic genes, associated to hydrogenotrophic, aceticlastic and methylotrophic complete routes is essential to describe carbon mineralization. The specific genes related to the hydrogenotrophic pathway are *fdh/fwd*, *ftr*, *mch*, *mtd* and *mer*, *acs* or *ack* with *pta*, *cdhABCDE* for the aceticlastic; *mtaA* and *mtaB* (catalyzing the conversion of methanol to methyl-CoM) or *mtmBC, mtbBC, mttBC* (methyltransferase proteins involved in the conversion of methylamine, dimethylamine and trimethylamine into methyl-CoM) with *mtbA* for the methylotrophic routes (further details in Glossary of Appendix I). And the final and

common steps, involving the *mtr*, *mcrABC/mrtABC*, and *hdr* genes (Steinberg and Regan, 2009; Buriánková *et al.*, 2013; Costa and Leigh, 2014; Dziewit *et al.*, 2015; Gründger *et al.*, 2015; Wilkins *et al.*, 2015; Holmes and Smith, 2016; Mwirichia *et al.*, 2016). Conspicuously, Sorokin and cols. (2017) indicated a fourth methanogenic pathway employed by methanogens, known as "methyl reduction". In this route, C_1-methylated compounds are the electron acceptors and the hydrogen (H_2) is an external electron donor.

Hydrogenotrohic and aceticlastic methanogenesis have been detected mainly in members affiliated to the orders *Methanosarcinales* and *Methanomicrobiales* in deep aquifers of a coal-bearing sedimentary basin (Germany; Gründger *et al.*, 2015) or estuarine sediments (UK; Webster *et al.*, 2015). Also, methylotrophic methanogenesis seems to be more predominant in hypersaline ecosystems due to the high energetic requirement for conversion of compatible solutes, like *Methanohalophilus* and *Methanohalobium* spp. (McGenity and Sorokin, 2019), and *Methanococcoides* genus (Webster *et al.*, 2015). Members of *Methanosarcina* genus have initially been described as converters of trimethylamine, dimethylamine, methylamine and other methyl group containing compounds (Oren, 2014) to gas methane (with a yield ≥78.5%) and ammonia in anaerobic sediments, rumen or pure cultures (Hippe *et al.*, 1979; Patterson and Hespell, 1979). However, in more recent studies, this genus, together with the aceticlastic genus *Methanosaeta*, have been described to be able to utilize H_2/CO_2 or acetate as methanogenic substrates (Gründger *et al.*, 2015). It should be also highlighted the discovery of methane-metabolizing genes in members of new phyla, as *Bathyarchaeota* (Evans *et al.*, 2015) and *Verstraetearchaeota* (Vanwonterghem *et al.*, 2016), evidencing the genetic diversity of methanogenesis pathways.

The ability to perform complex fermentation coupled with methanogenesis in *Bathyarchaeota* phylum has been described (Evans *et al.*, 2015). Metabolic processes associated to simple or complex carbohydrates degradation to more reduced compounds in anoxic conditions have been widely reported (Fenchel *et al.*, 2012; Oren, 2017; McGenity and Sorokin, 2019; Sorokin *et al.*, 2021). Metabolic features related to fermentation are common in anaerobic sediments, even those with very high saline concentrations (McGenity and Oren, 2012). Members of the family *Halobacteriaceae*, still possessing an aerobic lifestyle in general, can grow anaerobically by arginine with ornithine fermentation (Oren, 2013). Moreover, energy can be obtained by fermentation of simple sugars, such as glycerol, as members of *Firmicutes* phylum and *Halanaerobiales* order can do (McGenity and Oren, 2012).

3.2. Nitrogen cycle: Denitrification, ammonification, nitrification, assimilatory and dissimilatory nitrate reduction, and nitrogen fixation

Metabolic pathways involved in nitrogen cycle have been described in hypersaline and anaerobic environments, where microorganisms capable of reducing nitrate, sulfate, dimethylsulfoxide have been largely described (Torregrosa-Crespo *et al.*, 2016). Nitrate can both be reduced to nitrite and to ammonium by the assimilatory and dissimilatory pathways. For the assimilatory route, genes *narGHI* and *napAB* are involved in the first step and *nirBD* and *nrfAH* in the second, while genes *narB*, *nasAB* and *nirA* are related to the dissimilatory nitrate reduction pathway (further details in Glossary of Appendix I). In the denitrification metabolism, nitrate is converted in nitrite (involving *narGHI* and *napAB* genes), which then is oxidized to nitric oxide (via *nirK* and *nirS* genes), the latter is transformed in nitrous oxide (*norBC*) and finally reduced to nitrogen (*nosZ*). The final conversion of nitrogen to ammonia is mediated by *nifDKH* genes. In the nitrification, the ammonium is converted to hydroxylamine (*amoAB* genes), *haoA* is coded in the transformation of the hydroxylamine to nitrite, and the latter in nitrate by *nxrAB* genes (Schlegel, 1976; Haroon *et al.*, 2013; Badhai *et al.*, 2015; Torregrosa-Crespo *et al.*, 2016).

Under anaerobic conditions, conversion of nitrate to molecular nitrogen or N_2O (denitrification) has been detected in *Haloferax* sp. and *Haloarcula* sp. (McGenity and Oren, 2012; Oren, 2013). Nitrite production has been detected by a novel lineage of anaerobic methanotrophic archaea (ANME-2d), that use the nitrate as the terminal electron acceptor (Haroon *et al.*, 2013). Genes encoding partial pathways of nitrification and denitrification have been detected in more recently described *Thaumarchaeota* and *Nitrospirae* phyla (Orellana *et al.*, 2018; Vavourakis *et al.*, 2018).

3.3. Sulfur cycle: Assimilatory and dissimilatory sulfate reduction and sulfur-oxidizing

Generally, hypersaline ecosystems are very rich in sulfates, being one of the main electron acceptors in both thalassohaline and athalassohaline environments.

The main pathways within sulfur cycle are the sulfate reduction, both assimilatory and dissimilatory routes, which uses the sulfate as substrate and the sulfide as final product; and the SOX (sulfur-oxidizing) system obtaining sulfate. Specifically, the dissimilatory sulfate reduction pathway comprises the reduction of sulfate to sulfite, also present in the assimilatory sulfate reduction. The *sat* and the *aprAB* genes encode this path for the dissimilatory route yielding sulfite, and the conversion of this substrate to sulfide is mediated for the *dsrAB* genes (further details in Glossary of Appendix I).

These genes have been normally encoded in members of the recently reclassified *Deltaproteobacteria* class (Waite *et al.*, 2020), e.g. the family *Desulfohalobiaceae* (McGenity and Oren, 2012). In hypersaline sediments from a soda lake, metagenome-assembled genomes (MAGs) affiliated to *Desulfonatronovibrio* and *Desulfonatronospira* were classified as lithoautotrophic sulfate-reducing bacteria and MAGs affiliated to *Desulfurivibrio* and *Dethiobacter* genera were classified as reducers of sulfur/thiosulfate (Vavourakis *et al.*, 2019).

4. Salinity patterns and ecological factors in prokaryotic communities

The specific microbial community assemblage living in a given ecosystem is a consequence interaction between biotic and abiotic forces. Amongst abiotic forces, salinity has been described as the major environmental factor driving microbial community structures in a wide range of environments (Lozupone and Knight, 2007). The microbial selective force applied by salinity has been studied in numerous habitats with temporal or spatial salinity gradients, such as estuaries, wetlands, salt marshes and coastal lagoons. In environmental ecosystems where salinity gradient exists, the abundance and activity of the prokaryotic communities is elevated, due to there is a high availability of electron acceptors and donors, nutrients and carbon sources (McGenity and Sorokin, 2019). Moreover, salt concentrations act as attenuators for some microbial and metabolic processes, and enhance others, affecting directly the biogeochemical cycles (McGenity and Oren, 2012).

Additionally to the salinity, total organic carbon is a another studied factor that would structure the microbial communities, for example the anoxic sediments of a California hypersaline lake (Salton Sea; Swan *et al.*, 2010). In surface and subsurface saline soils, total organic carbon and pH were the primary drivers in the prokaryotic community distribution along an ecological gradient of salinity (Xie *et al.*, 2017). Ecological factors as dilution, pH, alkalinity, (total) carbon availability, UV irradiation, and especially salinity, have been largely evaluated for their influence on microbial communities (Walsh *et al.*, 2005; Lozupone and Knight, 2007; Swan *et al.*, 2010; Sierocinski *et al.*, 2018; Viver *et al.*, 2020).

Therefore, the knowledge of the drivers or forces that structure community composition is essential for the understanding of the ecology of microbial communities. The information obtained from measurement of alpha- and beta-diversity indices, and the development of null-model approaches, have been frequently utilized to quantify how deterministic or stochastic factors are contributing in microbial community assembly processes (Chase *et al.*, 2011; Stegen *et al.*, 2012, 2013; Langenheder *et al.*, 2017; Liébana *et al.*, 2019). It is described that deterministic and stochastic factors appear simultaneously but with different relative importance. Usually, if stochastic processes (i.e. random birth, death,

colonization, extinction and speciation) prevail in determining microbial community composition in environments with similar abiotic conditions, it is expected a high variation in species composition within them. On the other hand, deterministic processes dominate when microbial communities differ between sites and these are tightly linked to differences in environmental conditions between them (i.e. salinity and irradiation).

5. Gas methane as alternative and renewable energetic resource, and the use *Posidonia oceanica* biomass

5.1. Clean and renewable energies. Biogas

Current societies are getting increasingly involved in the protection of the environment, so there is a need in the research and development of alternative clean energies in order to substitute fossil, scarce and nonrenewable resources (Manyi-loh *et al.*, 2013; Adekunle and Okolie, 2015). It is very necessary to find alternative sources of biomass for energy generation which is friendly to both the economy and the environment (Dębowski *et al.*, 2013; Gao *et al.*, 2016). Biogas is regarded as a versatile source of renewable energy that has been considered one of the most efficient energy processes in relation to its environmental benefits (Weiland, 2010; Manyi-loh *et al.*, 2013; Adekunle and Okolie, 2015). Biogas is a combustible gas composed of mainly methane (50-70%) and carbon dioxide (30-50%) and other minor gases. (Gao *et al.*, 2016; Holmes and Smith, 2016). The composition of the primary matter used, operation conditions of the reactor for the biogas generation and others are essential factors for the methane yield (Adekunle and Okolie, 2015).

A characterization of a hypersaline and mesophilic consortium using metagenomics already open the study of consortia in environments almost considered extremophiles (Lykidis, C.-L. Chen, *et al.*, 2011) or also the study of the effect of salt concentration in order to obtain the best methane yield rate from different suspensions at different salinities (Zhang *et al.*, 2017). However, it seems that there could be a huge potential in the understudied methanogenesis in extremophilia conditions (Brock, 1997; McGenity and Sorokin, 2019), especially in hypersaline environments, which perhaps could perform similar methane rates than the previously non-extremophile known processes. In fact, it is believed that all the methane generated in the biosphere is currently most likely biological origin (Zengler *et al.*, 1999; Haroon *et al.*, 2013; Gründger *et al.*, 2015; Holmes and Smith, 2016; Dimitry Y Sorokin *et al.*, 2017), and hypersalinity should not be an obstacle to methanogenesis (Mcgenity, 2010).

5.2. Anaerobic digestion for biogas (methane) production

In order to obtain a good rate of methane production, it is necessary an appropriate digestion of the primary compounds. Aerobic and anaerobic digestions have been studied and optimized in the last decades (Holmes & Smith, 2016), and the digestion in absence of oxygen almost always has presented the best results (Adekunle and Okolie, 2015; Gao *et al.*, 2016; Westerholm *et al.*, 2016). Anoxic digestion processes are not trivial, they have their complexities, which have to be analyzed in order to improve their products. The evaluation of the substrate composition, the potential syntrophy between the microorganisms, and the operating parameters, such as the pH, alkalinity, temperature, organic loading rate, mixing and incubation time is essential (Manyi-loh *et al.*, 2013; Adekunle and Okolie, 2015; Gao *et al.*, 2016; Westerholm *et al.*, 2016).

However, one of the main problems that reactors can have is the difficulty to digest some substrates due to their recalcitrance nature (Adekunle and Okolie, 2015), and even more considering this process performed by halophilic microorganisms (Zhang *et al.*, 2017). In general, anaerobic digestion occurs of four steps: hydrolysis (transformation of insoluble and complex organic compounds into soluble organic materials carried out by bacteria, protozoa and fungi), acidogenesis (simple carbohydrates are degraded by fermentative bacteria into short chain organic acids), acetogenesis (acetogenic bacteria transform short chain organic acids in methanogenic substrates, such as acetate, formate or CO_2 and H_2) and methanogenesis (methane and carbon dioxide are synthetized by methanogens from those methanogenic substrates; Manyi-loh *et al.*, 2013; Adekunle and Okolie, 2015; Gao *et al.*, 2016; Holmes and Smith, 2016).

5.3. *Posidonia oceanica* as a substrate in anaerobic digestion processes

Methane generation as combustible is mostly fed with products from agriculture or urban waste (Adekunle and Okolie, 2015), but recently the material of marine algae has been proposed as substrates in biogas technology (Dębowski *et al.*, 2013; Zhang *et al.*, 2017). In the Mediterranean there are large areas of underwater vegetated meadows which dead biomass could be used in the biogas industry.

Posidonia oceanica is a Mediterranean marine and endemic phanerogam (one of the approximately 50 species of *Potamogetonaceae*), which possess special characteristics that convert it to an important biological factor that is encompassed in the planning and integrated management of the Mediterranean coast (Marbà et al., 2014; Medina et al., 2001). *P. oceanica* meadows are the biggest plant component of Spanish Mediterranean coast, covering up to 60% of the sediments up to 40 meters deep (Montefalcone, 2009; Cocozza *et al.*, 2011; Mininni *et al.*, 2014). These plants produce an average of 38 tons of dry biomass per hectare and they are the major primary producers around the Mediterranean. Annually,

during the autumn, among 10 to 20% of the mature leaves of these prairies are deposited on the seabed and, because of the effect of currents and storms, they are transported and accumulated in coastal areas and beaches (Medina *et al.*, 2001). It is estimated that these accumulations are apparently recalcitrant to their degradation because they contain carbon compounds as phenols with difficulties for their metabolization (Medina *et al.*, 2001).

P. oceanica mostly protect the beaches from erosion but, due to tourist pressure, meadows are removed (Medina *et al.*, 2001). Removed biomass is disposed to landfill, and is used as agricultural fertilizer and to feed animals but it has also evaluated as a composting material or incineration power generation (Cocozza *et al.*, 2011; Mininni *et al.*, 2014). *P. oceanica* residues can be used for incineration for their heating values and for composting. However, rates of mineralization (CO_2 generation) are very important, until tripling those of the own submerged prairie (Mininni *et al.*, 2014), so this material is actively mineralized in probably anaerobic processes and therefore processes such as composting may not be the most suitable. However, one of the biggest problems in agricultural use or recycling these accumulations is the elevated content in NaCl that contain after seawater evaporation. That is why the leaching of salts prior to treatment is recommended (Cocozza *et al.*, 2011). Finding a microbial system that can grow with (at least) the proportion of salt contributed by *P. oceanica* leaf casts would simplify the biodegradation process and biogas generation as alternative energy.

6. Sediments from the solar salterns of S'Avall, a unique hypersaline and anaerobic ecosystem

Solar salterns are semi-artificial environments that represent unique ecosystems suitable for studies on how microbial community structures establish themselves under high-salt and strong irradiation conditions. Moreover, these habitats also allow the study of how microorganisms physiologically and genetically adapt to high ionic concentrations. These systems also constitute a source of microbial taxonomic novelty and underexplored virus-host interactions (Antón *et al.*, 2000; Oren, 2008; Santos *et al.*, 2012; Gomariz *et al.*, 2015; Mora-Ruiz *et al.*, 2015; Martin-Cuadrado *et al.*, 2019; Ramos-Barbero, Martin-Cuadrado, *et al.*, 2019; Viver *et al.*, 2019, 2020). In general, the aerobic brines that circulate through a system of ponds have largely been the focus of reported studies, especially for the effect of the salinity gradient on microbial composition and metabolic activity (McGenity and Oren, 2012). However, easily accessible hypersaline sediments underlying these brines can establish themselves, and they conform to an extreme halophilic anaerobic environment that has been scarcely examined using culture-dependent and -independent studies (e.g. López-López *et al.*, 2010, 2013; Munoz *et al.*, 2011; Dimitry Y. Sorokin *et al.*, 2017).

The S'Avall solar salterns (Figure I.2), located in Mallorca (Balearic Islands), have saline concentrations close to saturation (approximately 37% w/v). The anaerobic sediments underlying brines in S'Avall, which is a medium of high complexity level, contain an important population of putative methanogenic microorganisms (López-López *et al.*, 2010, 2013) and in especial some belonging to candidate taxa MSBL1, which it is hypothesized to be involved in methanogenesis at high salinities (van der Wielen *et al.*, 2005; Yakimov *et al.*, 2013, 2015; Fernandez *et al.*, 2016). The candidate division MSBL1 comprises an uncultured monophyletic group that had been thought to represent an abundant and novel order in methanogens within *Euryarchaeota* phylum, but their distinct phylogenetic affiliation in several studies leads to an uncertainty about its metabolic nature (Mwirichia *et al.*, 2016; McGenity and Sorokin, 2019). Furthermore, the lack of information about this archaeal group in the public gene repositories complicates its characterization even partially sequencing its genome (López-López et al. 2013; McGenity and Sorokin 2019).

In brief, the exhaustive knowledge concerning solar-saltern brine composition and dynamics, makes their underlying sediments unique for investigating their microbiome and for understanding possible interactions between both closely connected ecosystems.

Figure I.2. Images from S'Avall mediterranean solar salterns (**A** and **B**) and the particular ephemeral pond (**C**) where research was performed (López-López *et al.*, 2010, 2013).

II. OBJECTIVES

Hypersaline sediments underlying the solar salterns of S'Avall have been described as a source of an abundant metabolically diverse population of putative methanogenic microorganisms (López-López *et al.*, 2010, 2013), some of which especially belonged to candidate MSBL1 lineage. This taxon is the most abundant uncultivated in most deep-sea hypersaline brines (van der Wielen *et al.*, 2005; Yakimov *et al.*, 2013, 2015), but the metabolic role of this group remains uncertain (López-López *et al.*, 2010; Mwirichia *et al.*, 2016). Therefore, this research focuses on the characterization of the microbial communities from hypersaline anaerobic sediments of S'Avall, especially those involved in methanogenesis, by means of culture-independent analyses.

The effect of abiotic factors in structuring microbial communities have been largely described (Swan *et al.*, 2010; Sierocinski *et al.*, 2017; Xie *et al.*, 2017; Viver et al., 2019), even though salinity has been described as the major force in the assembly of microbial populations (Jiang *et al.*, 2007; Webster *et al.*, 2015; Xie *et al.*, 2017), but hypersaline anaerobic sediments have been scarcely studied. Hence, the sediments of S'Avall will be the basis of the study of possible disturbing factors, such as salinity, antibiotics and different substrate concentrations that could affect to microbial composition dynamics.

Taking aware the essential involvement of methanogenic communities in carbon cycle (Liu and Whitman, 2008; Zhang *et al.*, 2017; Nigro *et al.*, 2020) and the putative methanogenic potential of prokaryotic communities from sediments of S'Avall (López-López *et al.*, 2010, 2013), the generation and improvement of methanogenic consortia from these microbial hypersaline communities in order to obtain high methane yields is proposed.

Within this framework, three specific objectives were proposed:

1. To characterize genetically and taxonomically the hypersaline anaerobic sediments of S'Avall using metagenomics, metaviromics, 16S rRNA gene amplicon sequencing and geochemical parameters. The description includes the diversity, distribution and main phylogenetic and ecological characteristics of the prokaryotic communities thriving in the sediments.

This main objective can be divided in two subobjectives:

I) To evaluate the vertical stratification and the temporal stability of the microbial communities.

II) To describe the community composition by means of metagenomics and metaviromics.

2. To evaluate the discriminant factors as salinity, antibiotic (ampicillin) and *P. oceanica* leaves as substrate in the prokaryotic communities from hypersaline sediments of S'Avall.

3. To generate a halophilic methanogenic consortium, focusing on the best methanogenic yields modifying the conditions of salinity, substrate concentration and ampicillin; and genetically and taxonomically characterize this using metagenomics.

III. MATERIALS AND METHODS

1. Experimental site and samples' collection

Sediments from an ephemeral pond in the S'Avall Mediterranean solar salterns located on the southern coast of Majorca Island, Spain (39º19'28.5''N; 02º59'19.3''E) were sampled using methacrylate cores in order to collect the top 25 cm. The basin that accumulates rainwater in winter and desiccates in summer (Figures 1.1E and 1.1F) on a regular basis, collects brines resulting from the dissolution of the almost permanent adjacent salt deposit in use as storage for decades.

Sampling was performed on different occasions (Figure 1.1): twelve cores in December 2016 (Figure 1.1A) were homogenized and a fraction was selected (referred to as the S sample); one core in April 2017 (Figure 1.1B) was divided by depth into the sections 0-8.3 cm (U), 8.3-16.6 cm (M), 16.6-25 cm (L); and two cores (R1 and R2) separated by a distance of approximately 1 m in July 2016 (Figures 1.1C and 1.1D) were also divided by depth (R1_U, R1_M, R1_L; R2_U, R2_M and R2_L). The analyses referred to these samples are located in chapter 1.

Sediments from the same basin adjacent to the crystallizer ponds of the S'Avall Mediterranean solar salterns were sampled in December 2016 using methacrylate cores to collect the top 25 cm. Methacrylate cores were sealed and transported to the laboratory for further processing. Sediments were manipulated inside a rigid anaerobic chamber (Coy Laboratory Products Inc., USA), with controlled conditions of absence of oxygen (using a Lutron PO2-250 Oxygen Meter) and hydrogen (with an Anaerobic Monitor; Coy Laboratory Products Inc., USA). Brines on the top of twelve cores were discarded and all cores were homogenized, from which a fraction was selected (S sample, slurry) as time-zero of the experiment. A battery of sludge was prepared at eight different salinities (5%, 10%, 12%, 15%, 18%, 20%, 25% and 30%) from the S'Avall sediments at 34.4% of salinity, adjusting the salt content with seawater (4%) and brine at 25.4% of salinity, both previously bubbled with nitrogen gas to ensure the anaerobic conditions. Additionally, ~10 mg of sodium dithionite ($Na_2S_2O_4$; Sigma-Aldrich) were introduced in the seawater and the brine to reduce the redox potential of these reagents. Besides the basis of the cultures (sediments, seawater and brine), were amended with leaf casts of *Posidonia oceanica* (*Po*) at three distinct concentrations: 0.1% w/w, 1% w/w and 10% w/w as substrate. Additionally, half of the cultures were supplemented with ampicillin (5 mg/mL sediment) and introduced in previously sterilized bottles in duplicate, considering a final volume of 100 mL except for the lowest salinity with 200 mL of volume (ensuring half of the bottle space for gas production). The various permutations varying the eight salinities, the three *Po* concentrations, the antibiotic addition and the duplicates shaped a total number of ninety-six cultures. The nomenclature for these samples are W_XYZ, where W: salinity percentage (5%, 10%, 12%, 15%, 18%, 20%, 25% or 30%), X: *Po* percentage (0.1%, 1% or 10%), Y: Ampicillin (A) or not (_) and Z: duplicate (1 or

2). These microcosms were incubated at 30ºC (Figure 2.1A). Study associated to these samples are placed in the chapter 2.

Those microcosms that displayed higher detection of methane (CH_4) via gas chromatography (explained below) were subcultured. Twelve microcosms (englobing salinities from 5% to 25%, and amended with antibiotic and various *Po* abundances) were selected, and the same conditions of salinity, substrate concentration and the addition of ampicillin (if necessary) were reproduced in new cultures considering a final volume of 200 mL (half of the space for gas generation). Additionally, for helping in the degradation of complex lignin-carbohydrate *Po* added, this was previously minced and treated with a diluted inorganic base (NaOH 2% w/v in a ratio of 1:10 with H_2O Milli-Q), and after one hour at 100ºC, the corresponding quantity of acetic acid was used for its neutralization. Sediments were again manipulated in the anaerobic chamber at the same conditions describe above, and 1 mL of suspension from the original chosen cultures was transferred in the new prepared cultures. In order to enrich the cultures, these twelve cultures were prepared in duplicate and then one of them was amended with acetate at 10 mM (Gründger *et al.*, 2015), formate at 50 mM and trimethylamine at 10 mM (Dimitry Y Sorokin *et al.*, 2017). The total set of twenty-four new microcosms (twelve previously selected and twelve additionally amended with the cited supplements) were incubated at 30ºC. The two best subcultured and enriched microcosms were those of 5% of salinity, 10% of *Po* with ampicillin (5%_10%Po_Amp and 5%_10%Po_AmpATF, the second amended with acetate, trimethylamine and formate), which were analyzed in the third chapter.

2. Characterization of the geochemical properties of sediments and microcosms

Chemical parameters of sediments sampled in different occasions in triplicate and also of the amended microcosms were analyzed. Prior to the analysis of ionic concentration, samples were diluted 1:400 and filtered through 0.22 um hydrophilic PTFE filters. Concentrations of fluoride (F^-), chloride (Cl^-), bromide (Br^-), nitrate (NO_3^-), sulfate (SO_4^{2-}), sodium (Na^+), lithium (Li^+), potassium (K^+), ammonium (NH_4^+), magnesium (Mg^{2+}) and calcium (Ca^{2+}) were quantified by ion chromatography by Technical Research Services of Alicante University (Spain). Organic matter (OM) and carbonates (CO_3^{2-}) were measured with the loss on ignition method in a muffle furnace (Nabertherm). Salinity was calculated by a Sper Scientific Salt Refractometer. Microcosms' pH was measured from previously centrifuged samples at 13,200 rpm (Centrifuge 5415 R, Eppendorf) during 5 min, in two time-points, at time-zero (S, slurry) and in March 2021 (final time) with Whatman® Panpeha™ pH indicator strips (Sigma-Aldrich).

Gas chromatography was used for the measurement of methane (CH_4) in the sediment samples at the original collection site (S'Avall solar salterns). Throughout the isothermally and in darkness incubation, the gas methane potentially synthetized from the ninety-six cultures was quantified in different occasions during fifty-two months (from December 2016 to March 2021) by gas chromatography. Concentrations of CH_4 were determined with a Clarus 600 Gas Chromatograph (Perkin Elmer, USA) equipped with a Flame Ionization Detector (FID). A CH_4 pure standard (≥99.0%, Sigma-Aldrich) was used as a reference in order to determine the retention time of the CH_4 peak. For more detailed information, see the Supplementary materials and methods in the Appendix II.

3. Sample pre-processing and DNA extraction

Prior to DNA extraction, sediment pellets recovered from samples (S, U, M, L, R1_U, R1_M, R1_L, R2_U, R2_M and R2_L) were processed as previously described (López-López *et al.*, 2010, 2013; Mora-Ruiz *et al.*, 2018) but with some modifications (see Supplementary materials and methods in the Appendix II). For the ninety-six samples, 1 mL of homogenized biomass was extracted from all microcosms and time-zero slurry (S). Microbial DNA extraction was performed from 0.3 - 0.4 g of mixed biomass, using the kit DNAeasy® PowerSoil® Pro Kit (Qiagen, Germany), following the manufacturer's instructions. Extracted DNA was concentrated with a SpeedVac™ system (Thermo Scientific™ SPD121P-230) and was quantified with a Qubit HS DNA kit and Qubit 4.0 Fluorimeter (Invitrogen, Thermo Fisher Scientific). For the two subcultured and enriched microcosms (5%_10%Po_Amp and 5%_10%Po_AmpATF), 10 mL of mixed biomass were extracted and the prokaryotic DNA was obtained as the DNA extraction protocol previously reported (López-López *et al.*, 2010, 2013; Mora-Ruiz *et al.*, 2018), but slightly modified (Supplementary materials and methods in the Appendix II).

4. 16S rRNA gene amplification and sequencing

The hypervariable region of the 16S rRNA gene was amplified from the nucleic acid samples previously extracted from R1_U, R1_M, R1_L, R2_U, R2_M and R2_L. Amplifications for Bacteria and Archaea were executed with GM3 (5'-AGAGTTTGATCMTGGC-3') and 21F (5'-TTCCGGTTGATCCTGCCGGA-3'; Muyzer *et al.*, 1995) as forward primers and S (5'-GGTTACCTTGTTACGACTT-3') and 1492R (5'-TACGGYTACCTTGTTACG-3'; Turner *et al.*, 1999) as reverse primers, respectively. Amplicons were sent to Fisabio Inc. (Valencia, Spain) for Illumina MiSeq™ sequencing (see further details in the Supplementary materials and methods in the Appendix II).

The 16S rRNA gene was amplified in all ninety-six cultures and the S sample with the primer pair 515F (5'-GTGCCAGCMGCCGCGGTAA-3') and 806R (5'-GGACTACHVGGGTWTCTAAT-3'; Caporaso *et al.*, 2011), targeting the V4 region of the 16S SSU rRNA and designed to amplify both Bacteria and Archaea using paired-end 16S community sequencing on the Illumina platform to incorporate tags. PCR reaction mixtures and thermocycler conditions were performed as detailed by Caporaso *et al.* (2011), with the exception of using a DNA template of 10 µL for the reaction but acquiring a final volume of 50 µL for each sample. The bands were visualized in 1% (w/v) agarose gel electrophoresis in TAE 1X. Amplicons quality was checked with the Qubit 4.0 Fluorimeter and were sent to Fisabio Inc., Comunitat Valenciana, Spain for sequencing through Illumina Miseq™ technology.

5. 16S rRNA gene sequence processing and phylogenetic inference

Single-end raw reads of samples R1_U, R1_M, R1_L, R2_U, R2_M and R2_L were trimmed with Prinseq-lite program (Schmieder and Edwards, 2011) for quality assessment (minimum length 50, trimming quality 30, mean quality type and a quality window of 20), and then the forward and reverse reads were joined with FLASH software (Magoč and Salzberg, 2011). Due to the high number of sequences, these were clustered with the Swarm method (Mahé *et al.*, 2014), an algorithm that handles large sets of amplicons based on k-mers. Two consecutive swarms were performed and each individual aggrupation from the output of the second swarm was identified as an OTU (Operational Taxonomic Unit). Paired-end reads from Illumina amplicon sequencing of the ninety-six microcosms were processed with DADA2 R package, an implemented method consisting in filtering, dereplication, denoising, merging of paired-end reads and chimera removing (Callahan *et al.*, 2016). Quality profiles of forward and reverse reads were examined and the filtering and trimming parameters were adjusted accordingly. Amplicon Sequence Variants (ASVs) were obtained with DADA2 software. Additionally, short reads of the 16S rRNA gene from metagenomes S, U, M and L were cleaned and extracted with Parallel-meta v2.4 software (Su *et al.*, 2012).

All sequences were clustered in OTUs at a 99% identity using the UCLUST tool (Qiime; Caporaso *et al.*, 2010), and the longest representatives of the OTUs and ASVs were aligned with the SINA tool (Pruesse *et al.*, 2012) and inserted into the SILVA128 and LTP128 (Yarza *et al.*, 2010) databases using the ARB software package (Ludwig *et al.*, 2004). Closest reference species in both databases were selected and a set of supporting species was added (of high quality and covering all major phyla of Archaea and Bacteria domains) and used to build a Neighbor-Joining tree with the Jukes-Cantor correction. OTUs were inserted into this phylogenetic reconstruction and grouped into OPUs (Operational Phylogenetic Unit; França *et al.*, 2015) based on visual inspection of the final tree, as previously described (Mora-Ruiz

et al., 2015, 2016, 2018; Viver *et al.*, 2017). An OPU is the smallest monophyletic group of sequences containing ASV or OTU representatives and their closest reference sequence, including the type strain when possible and is the result of a phylogenetic inference by inserting the new sequences in a preexisting tree using the Parsimony tool implemented in the ARB program package (Ludwig *et al.*, 2004). This OPU approach allows 16S rRNA gene fragments of distinct length and position within the gene to be combined, in order to obtain comparable results between the amplicon and metagenome strategies.

The amplicon sequences of R1_U, R1_M, R1_L, R2_U, R2_M and R2_L were submitted to the European Nucleotide Archive (ENA) under study number PRJEB43308, and accession numbers ERS5883079, ERS5864944 and ERS5883078. The 16S rRNA gene amplicon sequences of the ninety-six microcosms and the sample S (slurry) will be submitted to ENA when results will be published.

6. Metagenome Sequencing, Trimming, Assembling and Binning

Samples U, M, L, MV_U, MV_M and MV_L were sequenced using the Illumina MiSeq™ system at Fisabio Inc. (Valencia, Spain). The S sample was sequenced through Illumina HiSeq™ technology, whilst microcosms 5%_10%Po_Amp and 5%_10%Po_AmpATF with the Nextera DNA XT + NovaSeq6000 150PE (150 x 2bp) technique (Illumina platform), and sent to Macrogen Inc. (Seoul, Korea). The different sequencing platforms were selected for the obtainment of the best quality metagenomes depending on the sampling year that were performed.

Metagenomic raw reads were trimmed with SolexaQA (Cox *et al.*, 2010) and cleaned with Prinseq-lite (S, U, M and L; Schmieder and Edwards, 2011) or Trimmomatic (5%_10%Po_Amp and 5%_10%Po_AmpATF; Bolger *et al.*, 2014) software, using a threshold quality of 20 and removing sequences shorter than 50 bp. The use of different software for cleaning sequences was due to the specific sequencing platform, since the coverage and the quality varied depending on them. Nonpareil analysis was undertaken to estimate the coverage of the community. Then the IDBA tool (Peng *et al.*, 2012) was used for assembly, performing *de novo* assemblies of reads with a pre-correction before. Binning of metagenomes was performed with MaxBin v2.2.4 (Wu *et al.*, 2014) and quality parameters were checked with the *HMM.essential.rb* script (http://enve-omics.ce.gatech.edu/enveomics/), MiGA (Microbial Genomes Atlas Online; http://microbial-genomes.org/) and the CheckM tool (Parks *et al.*, 2018). These MAGs (Metagenome-assembled genomes) contained contigs longer than 1,000 bp using default parameters. Statistical information for the best quality MAGs was collected with MiGA.

All raw sequences from S, U, M and L metagenomes were submitted to the European Nucleotide Archive (ENA) under the study number PRJEB43308, and accession numbers ERS5883080, ERS5883079, ERS5864944 and ERS5883078. Raw sequences from enriched microcosms (5%_10%Po_Amp and 5%_10%Po_AmpATF) will be submitted to ENA when results will be published.

7. Metagenome-assembled genome refinement and genome analysis

Highly contaminated and heterogeneous MAGs from S, U, M and L metagenomes were processed with consecutive rounds of binning in order to improve the recovered MAGs and separate the main populations (Ramos-Barbero *et al.*, 2019). Microcosms metagenomes' MAGs were checked and cleaned with the ANVI'O v7 software (https://merenlab.org/software/anvio/). Binned metagenome-assembled genomes (MAGs) and closest reference genomes were both used for ANI% (average nucleotide identity) and AAI% (average amino acid identity) calculations with scripts from Enve-omics scripts collection http://enve-omics.ce.gatech.edu/enveomics/ (Rodriguez-R and Konstantinidis, 2016).

For MAGs belonging to S, U, M and L, a phylogenetic reconstruction from essential genes according to similarity and their presence among MAGs was performed in order to refine MAGs taxonomic identification (for more details, see Supplementary materials and methods in the Appendix II). For MAGs retrieved from 5%_10%Po_Amp and 5%_10%Po_AmpATF, the taxonomic identification was achieved with MiGA and the GTDB-Tk tool, available in the public repository of GTDB (Genome Taxonomy DataBase; https://gtdb.ecogenomic.org/). The use of distinct methodologies for the taxonomic identification was performed in order to improve the robustness of the phylogenetic affiliation, employing effectively the available tools and complementing the information with more than one database. Metagenomes and MAGs were compared using BLASTn software (Basic Local Alignment Search Tool for nucleotides) with completely sequenced fosmids, as previously published (López-López *et al.*, 2013), and the ANI was calculated for all MAGs and fosmids. For MAGs from 5%_10%Po_Amp and 5%_10%Po_AmpATF, their comparison with the MAGs of S, U, M and L metagenomes was performed with the calculation of the AAI and ANI among them.

Abundance of all draft genomes was assessed by recruitment of metagenomic reads against the corresponding MAG sequence using 98% and 70% cutoffs for identity and coverage of a match, respectively. All MAGs from S, U, M and L were submitted to the European Nucleotide Archive (ENA) under the accession numbers ERZ1756676, ERZ1756679 - ERZ1756747. MAGs retrieved from 5%_10%Po_Amp and 5%_10%Po_AmpATF will be submitted to ENA when results will be published.

8. Metabolic inference from metagenomics data

Genes were predicted on large contigs with MetaGeneMark v2.8 (S, U, M and L; Zhu *et al.*, 2010) and Prodigal v2.6.3 (5%_10%Po_Amp and 5%_10%Po_AmpATF; Hyatt *et al.*, 2010), from which foretold functions were annotated with the RAST Server (Rapid Annotations using Subsystems Technology; Aziz *et al.*, 2008), the Uniprot Swiss-Prot available web server (https://www.uniprot.org/) and the MG-RAST metagenomics analysis server (https://www.mg-rast.org/) . Metabolic reconstructions were based on RAST, Uniprot Swiss-Prot annotations and KAAS-KEGG (Moriya *et al.*, 2007), as previously described (Viver *et al.*, 2017). Specific genes involved in methanogenesis, the nitrogen cycle and sulfate-reduction were detected, and closest and annotated reference genes (from Uniprot and KAAS-KEGG repositories) were compared using BLASTp software (Basic Local Alignment Search Tool for proteins) and BLAT (the BLAST-like assignment tool; Kent, 2002). Relative abundances of carbohydrate degradation, methanogenesis, fermentation, autotrophy and sulfur cycle as main metabolisms were also determined for metagenomes S, U, M and L and their associated MAGs. These were calculated from mapped reads of the S, U, M and L samples at 95% identity and 90% coverage, in reads per metagenome size in GB.

9. Characterization of virus communities

Virus-like particles (VLPs) in the U, M and L samples from April 2017 were purified from sediment suspensions after removing cells and virus concentrates. The concentrates were then used for pulsed-field gel electrophoresis (PFGE), transmission electron microscopy (TEM) and viral metagenomics (see Supplementary materials and methods in the Appendix II). Viral reads were filtered by quality and Illumina adapters were eliminated with Trimmomatic 0.36 (Bolger *et al.*, 2014). Assembly was performed with IDBA 1.1.1 and the resulting contigs were initially BLASTX-compared against the NCBI non-redundant (NR) database (Altschul *et al.*, 1990). Those contigs clearly associated with cells, and their corresponding reads, were removed. Cleaned viromes were then compared by BLASTN, using 10^6 randomly selected reads from each viral metagenome, in order to calculate the percentage of identical shared sequences (100% identity and coverage) and the percentage of similar sequences, or sequences associated with the same viral populations (≥95% identity and ≥70% read coverage). Cleaned reads were also re-assembled and contigs larger than 5 kb were selected and further studied. Initial sequence analyses included BLASTN (Basic Local Alignment Search Tool for nucleotides) alignments against the NCBI database and protein-level searches using Kaiju (Menzel *et al.*, 2016). Prediction of open reading frames (ORFs) in viral contigs was performed with VirSorter (Roux *et al.*, 2015) and predicted proteins were annotated using BLASTP against the NR NCBI database and searches against Pfam (Mistry *et al.*, 2021). Then, a manual exploration of *bona fide* viral contigs was carried out, selecting those where a clear

viral marker (terminase, integrase or caudoviral structural proteins) was confidently detected by BLASTP and Pfam and/or those contigs with BLASTP hits related to viruses. It was always checked that the gene context also contained other virus-associated genes, such as methyltransferases or nucleases, and was enriched in hypothetical proteins. In addition, to avoid redundancy in the analyses of very related viral contigs assembled from the U, M and L metaviromes, they were clustered in viral OTUs (vOTUs) at a 95% identity and 70% coverage using CD-HIT (Fu *et al.*, 2012). Fragment recruitments of *bona fide* vOTUs (those including a *bona fide* viral contig) against each metavirome and metagenome were performed using BLASTN (filtering by BlastTab.best_hit_sorted.pl (Rodriguez-R and Konstantinidis, 2016) and with a query coverage ≥70%) and plotted using enve.recplot2 (Rodriguez-R and Konstantinidis, 2016). Virus-host prediction was explored with the viral contigs using Phis-detector (Zhang *et al.*, 2020), Viral-Spacer BLAST in JGI IMG/VR (Roux *et al.*, 2021), the CRISPR database (Couvin *et al.*, 2018), tRNAScan (Chan and Lowe, 2019) and BLASTP ORFs taxonomy. A putative host for a given virus was only considered when at least two of the different tools mentioned coincided in the same taxa. Alternatively, virus-host predictions were also considered when a given viral contig was part of a given MAG. Metaviromic raw sequences were submitted to the European Nucleotide Archive (ENA) under the study number PRJEB43308, and accession numbers ERS5883079, ERS5864944 and ERS5883078.

10. Growth rate index for growth taxa in MAGs

Cellular replication activity of all recovered MAGs was measured by a microbial growth rate estimation using the software GRiD (Growth Rate inDex; Emiola and Oh, 2018). This estimates the *in situ* replication rates where GRiD scores >1 indicate genome replication that would reflect cell growth. This technique sorts all contigs of a MAG in a metagenome by coverage (≥ 0.2x), which are separated into ori-containing contigs at or near an arbitrary genome "start" and ter-containing contig near the mid-region of a MAG in order to estimate a synthetic circular genome. According to Emiola and Oh (2018), an approximate value of 1.00 for GRiD indicates that no growth is occurring, and the greater the value, the more cellular reproduction in the MAG. dnaA/ori and ter/dif coverage ratios must be close to each other and species heterogeneity should be lower than 0.3 to ensure the active behavior of a population.

11. Ecological insights and indices and Statistical analysis

The PAST (PAleontological STatistics) software v.2.23 (Hammer *et al.*, 2001) was used for calculating diversity indexes, richness estimators and rarefaction curves based on OPU abundances.

In the study presented in the chapter 1, the Shapiro-Wilk normality test (included in the 'mvnormtest' Package) was run in order to check the distribution of the populations, whilst stratification of sediments with regard to the U, M and L fractions was evaluated using non-metric multidimensional scaling (NMDS), performing clustering dendrograms with the Vegan Package (Oksanen *et al.*, 2018) in R v.3.4.4. (www.r-project.org) and applying the Mantel test (ape v5.3; based on Pearson's product-moment correlation and Monte-Carlo test, using 9,999 permutations) and DESeq2 in R v.3.6.0. Additionally, Bray-Curtis dissimilarity values were calculated, and the Mann-Whitney *U* non-parametric test and Permutation D-test were also applied in order to identify the biological replicates. Furthermore, Nonpareil curves were determined as a coverage estimation of the community sampled using default parameters (Rodriguez-R and Konstantinidis, 2016). Finally, Venn diagrams were created with the free on-line platform http://www.interactivenn.net/.

On the other hand, for the study presented in chapter 2, Bray-Curtis dissimilarity was calculated in order to study the dispersion and identify the differences among samples (in terms of ampicillin supplement, substrate concentration and salinity), and were evaluated using principal coordinates analysis (PCoA) and non-metric multidimensional scaling (NMDS) with the vegan package (Oksanen *et al.*, 2018) in R v.3.6.0. (www.r-project.org). The homogeneity of variances between groups of samples was assessed with PAST software v.2.23 (Hammer *et al.*, 2001). Additionally, Bray-Curtis data were also plotted employing the packages gplots and ggplot2, whilst DESeq2 was applied to discern patterns among salinities and in relation to the slurry. Permutation D-test, Kolmogorov-Smirnov (applying the Bonferroni correction) and T-test were performed to confirm the biological duplicates, and the Wilcoxon and the Mann-Whitney *U* non-parametric tests were applied in order to identify the salinity which caused the most relevant change in comparison to the original sediment in R v.3.6.0. Moreover, Nonpareil curves and Nd diversity index were determined as coverage estimators of the community sampled with default parameters (Rodriguez-R and Konstantinidis, 2014; Rodriguez-R *et al.*, 2018).

For the ninety-six microcosms and the S (slurry) sample, computational calculations based on Null Model Analysis to describe the ecology of the studied ecosystem were performed. Phylogenetic turnover was estimated with ß-nearest taxon index (ßNTI), as previously described by Stegen *et al.* (2012, 2013) and Liébana *et al.* (2019). Pairwise comparisons in relation to time zero sample (S) with $|ßNTI| > 2$ were considered statistically relevant and indicated that communities were governed by selection. Negative or positive values of ßNTI mean that samples are more phylogenetically similar than expected by chance or more phylogenetically distant from each other, respectively. Values comprised between -2 and 2 were not significantly different from the null expectation, which point that stochastic factors influenced the phylogenetic turnover (Stegen *et al.*, 2013). Taxonomic turnover was estimated through the modified method of Raup-Crick metric, based on Bray-Curtis

dissimilarities (RC_{bray}) as previously reported by Chase *et al.* (2011) and Stegen *et al.* (2013). The RC_{bray} values range between -1 (two communities are more similar, than expected by chance) and 1 (two communities are more dissimilar), while a value of 0 represents no difference in the dissimilarity from the null expectation. $|RC_{bray}| < 0.95$ was not considered statistically significant and so indicator of the high influence of the stochastic factors (Chase *et al.*, 2011; Zhou *et al.*, 2014). Therefore, combining the two indices in the pairwise comparison, and when $|ßNTI| < 2$, RC_{bray} index is defining to differentiate between the influence of dispersal limitation (above +0.95), homogenizing dispersal (below -0.95) or ecological drift (values ranging from -0.95 to 0.95; Stegen *et al.*, 2013). Additionally, to quantify ecological stochasticity in community assembly, the Normalized stochasticity ratio (NST; Ning *et al.*, 2019) was calculated using the NST package in R v.3.6.0. Values above the boundary point (50%) indicates that assembly is more stochastic and values < 50% more deterministic. Stochasticity ratio (ST; Zhou *et al.*, 2014), Standard effect size (SES; Kraft *et al.*, 2011) and Modified stochasticity ratio (MST; Liang *et al.*, 2020) were also measured to complement the hypotheses based on the different null model algorithms.

IV. RESULTS AND DISCUSSION

CHAPTER 1

Chapter 1. Inverted microbial community stratification and spatial–temporal stability in hypersaline anaerobic sediments from the S'Avall solar salterns

This chapter describes the characterization of the anaerobic and hypersaline microbial communities from S'Avall solar salterns. The stratification along a vertical profile, the temporal stability in different sampling time-points during the year and the metabolism of the prokaryotic communities are the main subjects explained. Due to the complexity of the environment, the investigation was complemented with its geochemical properties and the description of the viral communities. Metagenomics, metaviromics and 16S rRNA gene amplicon sequencing were applied in this research. All the analyses related to the study of the viral communities were enterely performed by the Microbiology Group, leaded by Dr. Josefa Antón, of the University of Alicante (UA; Spain). This study entails the discover of the inverted stratification of the microbial community and new taxa capable to perform methanogenesis in the anaerobic and hypersaline conditions of S'Avall solar salterns.

1. Experimental setup

The present study was conducted with the sediments of an ephemeral pond adjacent to the crystallizer ponds of the S'Avall salterns. The basin that accumulates rainwater in winter and desiccates in summer (Figures 1.1E and 1.1F) on a regular basis, collects brines resulting from the dissolution of the almost permanent adjacent salt deposit in use as storage for decades. During the three sampling dates (July 2016, December 2016 and April 2017), sediments always showed a muddy consistency, with a water content of 31.9 ± 2% in the pooled horizons of the winter samples (slurry), and ranging from 29.8 ± 0.9% to 30.9 ± 1.2% in the summer and from 24 ± 3.7% to 31.3 ± 3.4% in the spring. The sediments were dark-grey to black (Figures 1.1A, 1.1B and 1.1C), with small gas bubbles escaping from the surface after taking the cores (Figure 1.1G). A preliminary gas measurement of the accumulated bubbles indicated that they were formed by CH_4 together with other gases, with a concentration of 255.5 ± 24.7 mM for the collected gas. During the dates sampled, the major salts (Figure 1.1H) in decreasing concentrations were: sodium chloride (NaCl; 3.4 – 4 M), calcium carbonate ($CaCO_3$; 0.6 – 0.9 M), magnesium sulfate ($MgSO_4$; 0.4 – 1.2 M), magnesium chloride ($MgCl_2$; 0.07 – 0.5 M), potassium chloride (KCl; 0.1 – 0.2 M) and calcium chloride ($CaCl_2$; $3x10^{-3}$ – $7x10^{-3}$ M). The salt composition showed a temporal variability, especially for $MgSO_4$ and $CaCO_3$, displaying an opposite pattern for summer 2016 and spring 2017 (Figure 1.1H). In this case, the intermediate layer suffered the strongest variations with the lowest concentrations in July 2016, and the highest concentrations in April 2017 (Figure 1.1H), coinciding with the pond being overlaid with brine. The salinity of all samples ranged from a

minimum of ~31% and a maximum of ~36% w/v (Figure 1.1I). Organic matter was generally higher in the upper fraction (23.7% dry weight) and decreased with depth (23.7% - 18.6% dry weight), although the intermediate layer showed a lower value in spring 2017 (21.2% dry weight; Figure 1.1I).

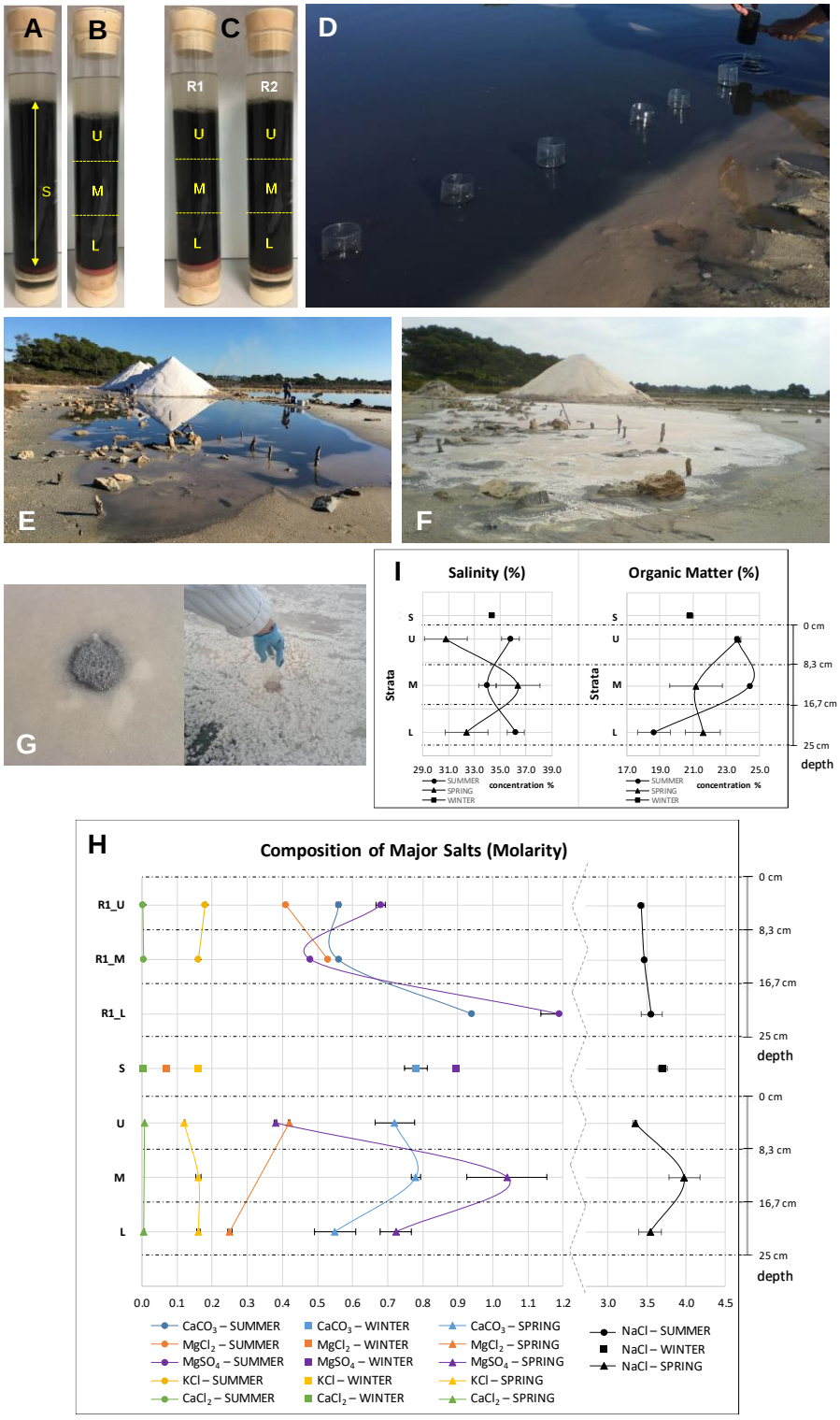

Figure 1.1. Image of one of the 12 homogenized cores of the sediment retrieved in December 2016 (**A**); the single core taken in April 2017 (**B**) with the three fractionated layers (U, M and L); and the two R1 and R2 cores with the three horizons of the July 2016 sampling (**C**), which were taken within a distance ≤1 m from each other (**D**). The view of the ephemeral pond that accumulates rainwater in winter (**E**) and desiccates in summer (**F**) is shown. Formation of bubbles accumulating on the brine surface when the cores have been extracted (**G**). Dynamics of the major salts (molarity) (**H**), with percentage salinity (w/v) and organic matter (w/w) (**I**). Salts are indicated in different colors, whereas circles and triangles represent the vertical profiles in summer and spring, respectively, and the squares are for the S data.

1.2. Microbial diversity based on 16S rRNA gene amplicons and their recruited metagenomic reads reveal spatial and temporal stability of the major prokaryotic components

Two samples were taken in July 2016 (Figure 1.1C) in order to evaluate the spatial stability and initial diversity measurements using 16S rRNA gene sequence amplicons. The cores were taken at a distance from each other of approximately 1 m (Figure 1.1D) and they were sliced into three 8.3 cm horizons (upper layer or U, intermediate layer or M, and lower layer or L). The OPU (equivalent to species; Viver *et al.*, 2019) abundance and diversity did not show any remarkable changes along the vertical profile (the full description is given in the Supplementary results in the Appendix III). Slight decreasing values could be detected with depth for the diversity measurements of the archaeal fraction in parallel with a slight increase of the bacterial counterpart (Table 1.1). Dendrograms based on Bray-Curtis dissimilarity showed that the community structures between the equivalent horizons in both cores were very similar (Supplementary Figure S1.1) and not statistically different (Mantel test, $p > 0.05$, $r = 0.433 - 0.618$) and, consequently, both cores could be treated as replicates (see Supplementary results in the Appendix III). On the other hand, the structures showed slight differences along the vertical profile, with the upper layer always being the most different (Supplementary Figures S1.1, S1.2 and S1.3). The phylogenetic analysis rendered a total of 1,334 unique OPUs, from which only 29 of the archaeal and 31 of the bacterial domains exhibited abundances >1% in at least one sample (Supplementary Table S1.1 and Supplementary results in the Appendix III).

To evaluate potential methanogenic metabolism in these sediments through cultivation, which will be published elsewhere, twelve cores from the same site in the same pond were collected in December 2016 and pooled to obtain a single slurry for culturing purposes (Font-Verdera, unpublished results). In general, all chemical properties of the slurry showed values that were close to the expected average of all parameters measured (Figure 1.1). The metagenome obtained from the slurry had a size of 42.2 million reads after trimming (read length average of S was 94.8 ± 14 bp) and 91,410 contigs with a length greater than 500 bp after assembly (Supplementary Table S1.2). The coverage of the metagenome was ~75% in accordance with the Nonpareil curves (Supplementary Figure S1.4). The reads recruited generated a total of 743 OPUs, from which 27 for the archaeal and 36 for the bacterial domains exhibited abundances >1% in at least one sample (Supplementary Table S1.3). Conspicuously, the archaeal community of the pooled horizons represented only ~26% of the 16S rRNA gene recruited reads, and therefore bacteria were dominant with relative abundances of ~74% (Table 1.1).

Table 1.1. Diversity indices based on OPUs derived from the 16S rRNA amplicon sequences (R1 and R2) or from the recruited reads from the metagenomes of the slurry (S) or the single core in April 2017 (A).

		Sequences				OPUs				Shannon				Chao-1				Evenness				Dominance			
	Samples	R1	R2	S	A	R1	R2	S	A	R1	R2	S	A	R1	R2	S	A	R1	R2	S	A	R1	R2	S	A
Archaea	U	44,843	44,751	4,117	980	389	385	197	77	4.122	4.061	4.031	2.476	440.2	438.1	266.2	110.5	0.159	0.151	0.286	0.155	0.036	0.046	0.045	0.241
	M	53,202	53,551		602	368	372		75	4.052	4.089		3.248	390.9	407		120.1	0.156	0.161		0.343	0.041	0.037		0.073
	L	41,405	42,793		479	363	361		80	4.034	3.975		3.489	393.4	381		109.1	0.156	0.148		0.409	0.042	0.045		0.064
Bacteria	U	6,873	6,960	11,573	610	371	345	546	105	3.023	2.915	4.214	3.547	699.8	631.1	739.6	194.4	0.055	0.053	0.124	0.331	0.163	0.156	0.045	0.072
	M	10,642	12,359		797	438	441		114	3.916	3.736		3.57	591	732.7		244.7	0.115	0.095		0.312	0.073	0.075		0.06
	L	7,524	6,047		929	397	387		126	4.015	4.321		3.417	576.4	593.9		256.1	0.14	0.195		0.242	0.063	0.032		0.083

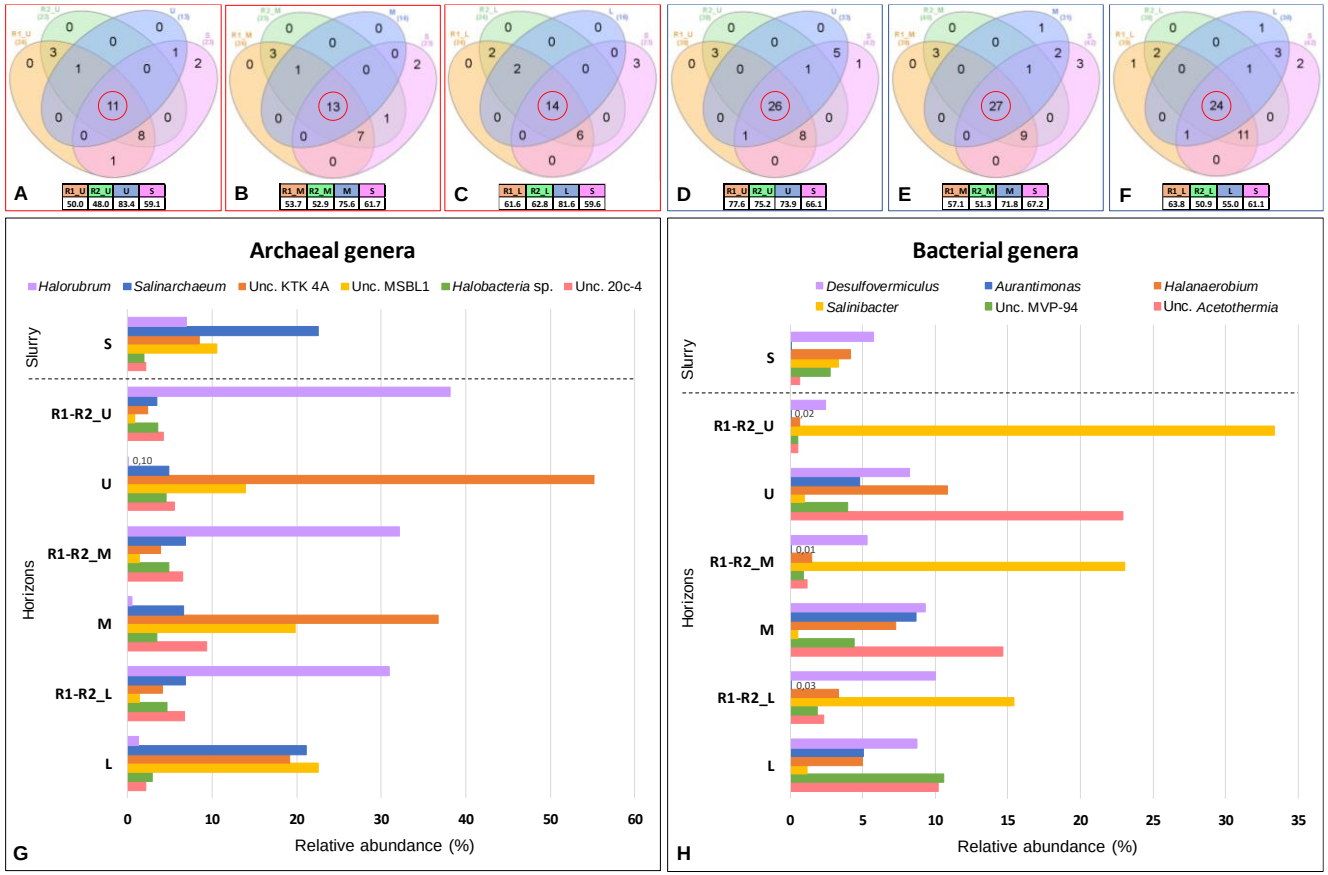

Figure 1.2. Venn diagrams based on genera from 16S rRNA sequence amplicons from the replicates R1 and R2 taken in July 2016 for the equivalent horizons from the recruited reads of the metagenomes of the April 2017 sampling, and slurry (S) from December 2016. The results shown are for the most abundant OPUs (≥1% relative abundance) at the genus level. The number of coinciding genera in all three samples for each horizon is circled in red and their relative abundance is given below each sample designation in each diagram. **A**, **B** and **C** correspond to the upper, intermediate and lower horizons (with the slurry), respectively for the archaeal domain and **D**, **E** and **F** to the same horizons but for the bacterial domain. Relative abundances of relevant core genera in the distinct fractions are shown in **G** and **H**, for the archaeal and bacterial domains, respectively. The *Aurantimonas/Aureimonas* genus does not belong to shared set of R1_L, R2_L and L, but it has been plotted for reference in all the other samples.

Finally, to evaluate the vertical taxa distribution based on metagenomes, and in the light of the previous results indicating that multiple cores could be treated as biological replicates, in April 2017, a single core was taken and sectioned into the same U, M and L horizons. We obtained three metagenomes with sizes of 2.89, 2.32 and 2.68 million reads after trimming (average read length of U, M and L was 278.3 ± 15.2 bp) and 42,418, 52,579 and 58,451 contigs longer than 500 bp after assembly for U, M and L, respectively (Supplementary Table S1.2). The coverage of the three metagenomes ranged between ~60 to ~68% in accordance with the Nonpareil curves (Supplementary Figure S1.4). Archaea were dominant with ~62% of the 16S rRNA gene recruited reads in the upper layer, but Bacteria dominated (>57%) the underlying horizons examined (Table 1.1), supporting the results for the dominance of this domain in the pooled slurry. The 16S rRNA gene reads recruited from the four metagenomes (U, M, L and S) affiliated with a total of 823 OPUs, from which 40 for the archaeal and 39 for the bacterial domains exhibited abundances >1% in at least one sample of these metagenomes (Supplementary Table S1.3). With both approaches (16S rRNA gene amplicon and metagenome recruited reads), the number of OPUs with abundances >1% was similar, and between 15 and 39 were identified as being the same or very closely related taxa.

The OPU approach allows each OPU to be identified down to the level of a single distinct species (Viver *et al.*, 2019), but for pragmatic reasons, and due to the low information content of the amplicons (mean length 422.4 ± 1.5) and reads (mean length 163.9 ± 56.3) that could lead to slight differences in the affiliation, we compiled the data at the genus level (i.e. all OPUs affiliating with the same branch that represented a single genus) for better interpretation. The three equivalent horizons (two from July 2016 and one from April 2017) and the slurry (S, from December 2016) shared the most abundant genera (relative abundances >1%) that we called the "core" of the prokaryotic community (Figure 1.2 and Supplementary Table S1.4). The archaeal "core genera" was represented by 11 to 14 taxa, while the bacterial domain was much more diverse, being formed by 24 to 27 taxa (Figure 1.2 and Supplementary Table S1.4). In both cases, the "core genera" together represented the majority of the 16S rRNA gene amplicons and reads of each domain, with values ranging from > 48% to ~84%. The most relevant archaea affiliated with *Halorubrum*, *Salinarchaeum*, and several uncultured taxa (i.e. *Candidatus* MSBL1 lineage, KTK 4A cluster, 20c-4 cluster) and from the bacterial domain with *Salinibacter*, *Desulfovermiculus* and *Halanaerobium* (Figure 1.2 and Supplementary Table S1.4). The statistically significant exclusive OPUs (abs(log2 fold change) > 2 and p-value < 0.05) in the upper layer (U) were from *Halobacteria* and *Thaumarchaeota* (for the archaeal domain), and *Salinibacter* and *Roseovarius* (for the bacterial domain; Supplementary Figures S1.2A and S1.2B); in the intermediate horizon (M) they were *Natronomonas*, *Halorubrum* and *Halopenitus* (for the archaeal domain), and *Truepera*, *Marinovum* and *Salinibacter* (for the bacterial domain; Supplementary Figures S1.3A and S1.3B); and in the deepest horizon (L), only halobacterial genera were statistically

relevant (Supplementary Figure S1.3C), whereas we did not find an OPU that dominated in abundance over the total bacterial OPUs.

The most representative archaeal OPUs shared among the samples affiliated with the genera *Halorubrum*, *Halapricum*, *Halodesulfurarchaeum* and *Salinarchaeum*, as well as the candidate lineages ST-12K10A, DHVEG-6, KTK4A and MSBL1 (Supplementary Tables S1.1 and S1.3 and spreadsheet Tables ST1.1 and ST1.2). The most representative bacterial OPUs shared among the samples affiliated with the genera *Roseovarius*, *Desulfovermiculus, Halanaerobium*, *Salinibacter*, *Aureimonas/Aurantimonas*, some unclassified genera of the families *Rhodobacteraceae*, *Marinilabiliaceae* and *Desulfobacteraceae*, and members of candidate lineages MVP-94, and uncultured *Acetothermia* (Supplementary Tables S1.1, S1.3, and spreadsheet Tables ST1.1 and ST1.2).

1.3. Diversity based on MAGs

The three metagenomes of the vertical profile collected in spring yielded a total of 34 MAGs, whilst the metagenome of the homogenized slurry from winter rendered 36 MAGs (Table 1.2 and Supplementary Table S1.5). Among the 70 MAGs, only one (S24) could be identified as a species with the validly published name *Salinibacter ruber* (Table 1.2), and the rest were identified to higher taxa. A total of 15 MAGs were identified at the genus rank and the rest were so distant from any classified taxon that they were only assigned to the order to phylum ranks (Table 1.2 and Supplementary Figure S1.5).

A total of eight species, represented by two or more MAGs with ANI values >99%, were retrieved from different samples of either the vertical profile and/or between seasons (grey shaded MAGs in Table 1.2 and Supplementary Tables S1.6 and S1.7). Especially, the MAGs representing an uncultured species of *Salinarchaeum* (U04, M04, L02 and S09), the three species affiliating with the deep-sea hydrothermal vent *Euryarchaeota* group 2 or DHVE2 (MAG pairs U01 and S02, and U05 and S05; and the four MAGs U03, M03, L03 and S23), or the three MAGs representing an uncultured species of the candidate division MSBL1 (U09, M10 and S13), were clear examples of the stable permanence of these taxa during the period sampled. Most of the archaeal MAGs (46 out of 53) only belonged to the four higher taxa *Halobacteria* (fourteen MAGs), the candidate DHVE2 (twenty MAGs), the candidate MSBL1 (seven MAGs), and *Thermococci* (four MAGs). The remaining MAGs affiliated with the classes *Archaeoglobi*, *Methanomicrobia*, *Methanobacteria* and *Thermoplasmata*, all of them from the phylum *Euryarchaeota.* On the other hand, the fewer bacterial MAGs (seventeen in total) were more diverse and with an even distribution between *Thermotogae* (three MAGs), *Alphaproteobacteria* (two MAGs), *Deltaproteobacteria* (two MAGs), *Planctomycetia* (two MAGs), *Gammaproteobacteria*, *Clostridia* and *Rhodothermia*, each with a single representative MAG.

Table 1.2. MAGs recovered from S, U, M and L and their most relevant features. From left to right, *D* indicates taxonomic domain (Archaea or Bacteria); *ID* indicates the MAG designation with the first letter indicating the metagenome of origin; *Id rank* indicates the lowest taxonomic rank to which the MAG could be assigned; *Category* indicates the taxonomic group to which the MAG could be assigned; the *closest reference* genome is the nearest genome or MAG available in the public repositories; *Comp.* indicates genome completeness; *Con.* indicates contamination, *ANI* indicates the average nucleotide identity with the closest genome or MAG; *AAI* indicates the average amino acid identity with the closest genome or MAG, *Prot.%* indicates the percentage of aligned proteins; *Mb* is the size in Mb of the binned MAG; S%, U%, M% and L% indicate the percentage of recruited reads of each MAG normalized by the MAG size and the metagenome size; the columns *u*, *m*, *l* and *s* indicate the degree of GRiD signal in where + is a positive replication signal, ~ indicates slight signal above 1 and · indicates absence of signal; *Putative metabolism* indicates the possible metabolic capabilities based on the annotated genes. MAGs sharing ANI > 96% identity and therefore identified as the same species are shaded in grey. i.h indicates the lack of sufficient hits to calculate ANI or AAI parameters. The MAGs recruiting reads > 0.7% of the total metagenome are highlighted in bold type. The sum of all abundances in each sample was: S: 17.7%; U: 24.4%; M: 19% and L: 15.7%. Sugar-fermenter means that the MAG showed annotations is being potentially able to ferment distinct types of sugars, such as saccarose, glucose, fructose, galactose, etc. The main sugars that each MAG degraded are shown in brackets. * indicates that the annotated genes were at a very low coverage, and the information was too scarce to hypothesize or to ensure the proposed metabolism.

D	ID	Id rank	Category	Closest reference sequence	Comp	Con	ANI	AAI	Prot%	Mb	S%	U%	M%	L%	u	m	l	s	Putative metabolism
A	**U04**	**Genus**	***Salinarchaeum***	***Salinarchaeum* sp. Harcht Bsk1 NC021313**	**96.2**	**7.7**	**76.7**	**58.8**	**49.1**	**2.58**	**3.60**	**1.38**	**1.65**	**2.84**	+	+	+	+	Sulfate-, nitrate- dissimilatory red
A	M04	Genus	*Salinarchaeum*	*Salinarchaeum* sp. Harcht Bsk1 NC021313	96.2	7.7	76.4	58.9	49.8	2.49					+	~	+	·	Sulfate-, nitrate- dissimilatory red
A	L02	Genus	*Salinarchaeum*	*Salinarchaeum* sp. Harcht Bsk1 NC021313	96.2	0.0	77.0	58.8	49.1	2.72					+	~	~	+	Sulfate-, nitrate- dissimilatory red
A	S09	Genus	*Salinarchaeum*	*Salinarchaeum* sp. Harcht Bsk1 NC021313	100.0	0.0	76.2	59.3	61.1	2.14					+	+	+	·	Sulfate-, nitrate- dissimilatory red
A	**U01**	**Class**	**DHVE2**	***Aciduliprofundum* sp. MAR08 339 NC019942**	**96.2**	**7.7**	**i.h.**	**43.0**	**62.0**	**2.60**	**0.87**	**8.12**	**0.59**	**0.16**	~	+	·	+	Acetic acid fermenter
A	S02	Class	DHVE2	*Aciduliprofundum* sp. MAR08 339 NC019942	98.4	2.8	i.h.	42.7	61.8	2.85					~	+	~	+	Acetic acid fermenter
A	S05	Class	DHVE2	*Aciduliprofundum* sp. MAR08 339 NC019942	84.6	7.7	i.h.	42.4	47.0	1.47	0.31	1.04	0.62	0.36	·	+	·	·	Chemoorganotroph *
A	U05	Class	DHVE2	*Aciduliprofundum* sp. MAR08 339 NC019942	96.2	3.8	i.h.	42.3	57.0	2.74					+	~	+	·	Chemoorganotroph *
A	**U03**	**Class**	**DHVE2**	***Aciduliprofundum* sp. MAR08 339 NC019942**	**96.2**	**7.7**	**i.h.**	**43.2**	**62.5**	**2.71**	**0.47**	**2.05**	**2.72**	**0.82**	+	+	+	+	Chemoorganotroph
A	M03	Class	DHVE2	*Aciduliprofundum* sp. MAR08 339 NC019942	96.2	7.7	i.h.	43.2	63.0	3.09					·	·	~	+	Chemoorganotroph *
A	L03	Class	DHVE2	*Aciduliprofundum* sp. MAR08 339 NC019942	73.1	7.7	i.h.	43.2	53.4	2.06					+	+	+	~	Chemoorganotroph *
A	S23	Class	DHVE2	*Aciduliprofundum* sp. MAR08 339 NC019942	69.6	4.3	i.h.	43.5	53.9	2.02					·	+	+	·	Chemoorganotroph *
A	U09	Class	MSBL1	candidate division MSBL1 SCGC-AAA382K21	88.5	7.7	68.7	55.0	46.5	2.17	0.29	0.83	0.97	0.35	+	+	+	+	Hydrogenotrophic methanogen
A	M10	Class	MSBL1	candidate division MSBL1 SCGC-AAA382K21	88.5	0.0	68.9	49.9	62.3	1.82					+	+	+	+	Hydrogenotrophic methanogen
A	S13	Class	MSBL1	candidate division MSBL1 SCGC-AAA382K21	88.5	7.7	67.9	47.5	63.4	1.64					+	+	+	+	Hydrogenotrophic methanogen
B	M05	Genus	*Aureimonas*	*Aureimonas altamirensis* DSM 21988	76.6	2.7	90.9	93.7	75.8	3.86	0.03	0.19	0.62	0.42	+	+	+	+	Alcohol fermenter, DMSO- diss. red
B	L06	Genus	*Aureimonas*	*Aureimonas altamirensis* DSM 21988	69.6	0.0	90.8	92.4	61.8	2.69					·	+	+	+	Alcohol fermenter, DMSO- diss. red
B	**M02**	**Class**	***Planctomycetia***	***Cand. Kuenenia stuttgartiensis* NZ LT934425**	**91.0**	**7.2**	**i.h.**	**39.3**	**36.0**	**5.48**	**0.17**	**0.17**	**1.32**	**2.21**	+	+	+	+	Anaerobic sugar-fermenter * (glucose, fructose, galactose)
B	L01	Class	*Planctomycetia*	*Cand. Kuenenia stuttgartiensis* NZ LT934425	91.9	0.9	i.h.	39.3	34.5	4.94					+	~	~	~	Anaerobic sugar-fermenter * (glucose, fructose, galactose)
B	M12	Phylum	*Kiritimatiellota*	*Kiritimatiella glycovorans* NZ CP010904^{T}	60.9	0.0	63.4	37.3	38.7	2.54	0.18	0.15	0.54	0.68	·	+	+	+	Denitrifying and fermenter bacteria *
B	L09	Phylum	*Kiritimatiellota*	*Kiritimatiella glycovorans* NZ CP010904^{T}	87.0	4.3	i.h.	39.5	44.0	4.01					+	+	+	+	Denitrifying and fermenter bacteria
A	S12	Genus	*Halodesulfurarchaeum*	*Halodesulfurarchaeum formicicum* NZ CP016070	88.0	5.6	79.3	74.4	75.2	1.81	0.36	0.10	0.11	0.05	+	+	+	+	Lithoheterotrophic sulfur- diss. red

A	S20	Genus	*Halodesulfurarchaeum*	*Halodesulfurarchaeum formicicum* NZ CP016070	43.5	8.7	79.3	68.6	71.0	0.42	0.23	0.07	0.10	0.04	+	·	+	+	Lithoheterotrophic sulfur- diss. red
A	S19	Genus	*Halorubrum*	*Halorubrum lacusprofundi* NC012029^T	50.0	0.0	83.7	73.9	50.5	2.42	0.34	0.02	0.04	0.05	·	+	+	+	Chemoorganotroph
A	S21	Genus	*Halomicrobium*	*Halomicrobium mukohataei* NC013202^T	61.5	3.8	75.0	58.7	54.0	1.60	0.24	0.03	0.03	0.01	+	·	~	+	Sugar-fermenter * (glucose, fructose)
A	S22	Genus	*Halomicrobium*	*Halomicrobium mukohataei* NC013202^T	34.6	3.8	75.4	57.5	54.9	1.17	0.20	0.03	0.05	0.02	+	~	+	+	Sugar-fermenter * (glucose)
A	S32	Genus	*Halorientalis*	*Halorientalis* sp. IM1011 NZ CP019067	19.2	0.0	i.h.	54.8	65.6	0.52	0.05	0.002	0.003	0.003	·	·	·	+	Sugar-fermenter * (glucose)
A	**S10**	**Genus**	***Salinarchaeum***	***Salinarchaeum* sp. Harcht Bsk1 NC021313**	**100.0**	**0.0**	**75.8**	**56.9**	**52.4**	**2.37**	**1.89**	**0.10**	**0.08**	**0.12**	·	+	·	~	Chemoorganotroph
A	**S01**	**Genus**	***Salinarchaeum***	***Salinarchaeum* sp. Harcht Bsk1 NC021314**	**96.5**	**5.4**	**i.h.**	**57.3**	**51.1**	**3.68**	**0.70**	**0.04**	**0.05**	**0.06**	·	+	·	+	**Chemoorganotroph, C_x-degrader**
A	S31	Genus	*Halorientalis*	*Halorientalis* sp. IM1011 NZ CP019067	46.2	7.7	75.7	56.9	62.3	0.51	0.11	0.01	0.01	0.01	·	·	·	+	Sugar-fermenter * (glucose)
A	S30	Order	*Haloferacales*	*Halorubrum lacusprofundi* NC012029^T	18.0	2.7	83.8	47.5	29.9	2.67	0.21	0.05	0.06	0.07	·	·	+	+	Nitrate-respiring (denitrifier)
A	U08	Class	DHVE2	*Aciduliprofundum boonei* T469 NC013926	50.0	3.8	i.h.	38.8	45.3	2.04	0.34	1.08	0.59	0.31	+	·	·	·	Hydrogenotrophic/Aceticlastic meth
A	**M01**	**Class**	**DHVE2**	***Aciduliprofundum boonei* T469 NC013926**	**73.1**	**7.7**	**i.h.**	**43.2**	**49.5**	**2.14**	**0.22**	**0.37**	**1.05**	**0.66**	+	~	+	~	**C_x-degrader, aceticlastic meth**
A	U10	Class	DHVE2	*Aciduliprofundum boonei* T469 NC013926	26.9	3.8	i.h.	39.0	36.3	1.65	0.15	0.51	0.46	0.29	+	+	+	·	Sugar-fermenter * (glucose, fructose)
A	L04	Class	DHVE2	*Aciduliprofundum boonei* T469 NC013926	53.8	3.8	i.h.	41.4	47.2	2.16	0.08	0.10	0.23	0.37	·	·	·	·	C_x-degrader, aceticlastic meth
A	L08	Class	DHVE2	*Aciduliprofundum boonei* T469 NC013926	46.2	3.8	i.h.	40.0	38.2	0.78	0.08	0.14	0.16	0.21	·	+	+	·	Acetic acid fermenter *
A	S25	Class	DHVE2	*Aciduliprofundum boonei* T469 NC013926	80.8	7.7	i.h.	42.6	51.2	0.94	0.07	0.09	0.09	0.08	~	+	+	·	Chemoorganotroph *
A	S03	Class	DHVE2	*Aciduliprofundum boonei* T469 NC013926	38.5	7.7	i.h.	42.6	43.7	1.72	0.06	0.08	0.12	0.09	+	·	+	~	Chemoorganotroph *
A	L07	Class	DHVE2	*Aciduliprofundum boonei* T469 NC013927	42.3	0.0	i.h.	40.3	37.1	1.40	0.04	0.08	0.18	0.20	+	+	+	·	Sugar-fermenter * (glucose, fructose)
A	**U02**	**Class**	**DHVE2**	***Aciduliprofundum* sp. MAR08 339 NC019942**	**88.5**	**0.0**	**i.h.**	**43.1**	**51.9**	**2.19**	**0.33**	**2.32**	**0.30**	**0.12**	~	~	·	·	**Acetic acid fermenter ***
A	U11	Class	DHVE2	*Aciduliprofundum* sp. MAR08 339 NC019942	34.6	3.8	i.h.	40.2	40.1	1.76	0.23	0.44	0.50	0.36	+	+	+	·	Acetic acid fermenter *
A	M07	Class	DHVE2	*Aciduliprofundum* sp. MAR08 339 NC019942	34.8	4.3	i.h.	39.6	48.9	2.36	0.13	0.18	0.54	0.33	·	~	·	~	Hydrogenotrophic methanogen
A	L10	Class	DHVE2	*Aciduliprofundum* sp. MAR08 339 NC019942	50.0	11.5	i.h.	41.7	41.2	1.09	0.09	0.13	0.14	0.18	·	·	+	·	Acetic acid fermenter *
A	S17	Class	*Archaeoglobi*	*Archaeoglobus fulgidus* DSM 4304 NC000917	69.6	4.3	i.h.	39.1	34.7	1.79	0.09	0.10	0.08	0.07	+	·	+	·	Acetic acid fermenter
A	M08	Class	MSBL1	candidate division MSBL1 SCGC-AAA259E19	50.0	3.8	70.2	43.8	35.2	1.84	0.21	0.16	0.57	0.42	·	+	·	·	Hydrogenotrophic/Aceticlastic meth
A	S36	Class	MSBL1	candidate division MSBL1 SCGC-AAA382A03	60.9	8.7	i.h.	40.2	47.0	0.56	0.06	0.03	0.03	0.03	·	+	·	+	Hydrogenotrophic methanogen *
A	L05	Class	MSBL1	candidate division MSBL1 SCGC-AAA382A20	50.0	3.8	68.0	36.9	42.8	1.48	0.16	0.10	0.33	0.59	·	·	~	·	Aceticlastic methanogen
A	U12	Class	MSBL1	candidate division MSBL1 SCGC-AAA382N08	50.0	11.5	72.1	40.7	58.9	1.78	0.31	0.51	0.31	0.19	·	·	+	+	Hydrogenotrophic methanogen
A	S18	Class	MSBL1	candidate division MSBL1 SCGC-AAA382N08	47.8	13.0	72.5	40.4	47.8	1.63	0.11	0.08	0.06	0.06	+	·	·	+	Hydrogenotrophic methanogen *
A	U07	Class	*Methanomicrobia*	*Methanohalophilus halophilus* NZ CP017921^T	57.7	7.7	i.h.	37.6	50.5	4.03	0.15	0.55	0.33	0.24	+	+	+	+	Methylotrophic/Aceticlastic meth
A	U06	Class	*Methanobacteria*	*Methanothermobacter* sp. EMTCatA1 AP018336	65.4	3.8	i.h.	39.7	39.5	1.20	0.27	0.56	0.44	0.34	+	+	+	·	Aceticlastic methanogen
A	S34	Class	*Thermococci*	*Pyrococcus furiosus* DSM 3638 NC003413^T	38.5	3.8	i.h.	39.3	31.9	1.34	0.15	0.09	0.05	0.04	·	·	·	+	Acetic acid fermenter
A	S08	Class	*Thermococci*	*Pyrococcus* sp. ST04 NC017946	42.3	15.4	i.h.	40.6	57.7	0.31	0.17	0.13	0.09	0.10	·	+	·	+	Anaerobic chemolithotroph *
A	M06	Class	*Thermococci*	*Thermococcus barophilus* MP NC014804^T	57.7	7.7	i.h.	40.5	47.1	3.85	0.07	0.13	0.33	0.19	+	+	+	·	Anaerobic sugar-fermenter (glucose, fructose)
A	S35	Class	*Thermococci*	*Thermococcus* sp. 5-4 NZ CP021848	30.4	4.3	i.h.	38.6	57.9	0.34	0.18	0.03	0.03	0.06	·	+	+	+	Anaerobic sugar-fermenter (glucose)
A	S28	Class	*Thermoplasmata*	*Thermoplasmatales* SCGC AB-540-F20	52.2	8.7	63.3	36.5	36.1	1.58	0.05	0.04	0.06	0.05	+	+	+	·	Sugar-fermenter * (glucose)
A	S06	Phylum	*Euryarchaeota*	*Halorhabdus tiamatea* SARL4B NC021921^T	34.6	7.7	i.h.	38.8	33.9	3.98	0.15	0.09	0.10	0.10	+	+	·	~	Chemolithotroph, sulfate-reducer
A	S33	Phylum	*Euryarchaeota*	*Methanothermobacter* sp. EMTCatA1 AP018336	30.4	4.3	i.h.	37.8	35.7	1.69	0.17	0.09	0.06	0.05	·	·	·	+	Hydrogenotrophic methanogen
A	M11	Domain	*Archaea*	*Methanothermobacter* sp. EMTCatA1 AP018336	34.6	7.7	i.h.	37.1	37.5	1.91	0.10	0.13	0.36	0.23	+	+	+	·	Sulfate-reducer/Fermenter *
B	S24	Species	*Salinibacter ruber*	*Salinibacter ruber* M8 NC014032	73.9	4.3	98.8	92.6	64.2	2.81	0.26	0.06	0.05	0.06	·	+	+	·	Aerobic heterotrophic
B	S16	Genus	*Halorhodospira*	*Halorhodospira halophila* SL1 NC008789^T	87.0	4.3	81.1	76.5	71.1	1.92	0.42	0.03	0.04	0.02	·	+	·	+	Photoautotrophic anaerobic
B	S04	Class	*Deltaproteobacteria*	*Desulfovibrio* sp. FW1012B NZ CM001368	64.0	6.3	73.9	46.4	39.7	2.93	0.24	0.09	0.09	0.11	~	·	·	·	Sulfate-reducer
B	S07	Class	*Deltaproteobacteria*	*Desulfovibrio vulgaris* NC002937^T	31.5	5.4	i.h.	37.7	36.0	4.23	0.18	0.08	0.08	0.09	+	+	·	+	Sulfate-reducer
B	S29	Class	*Clostridia*	*Moorella glycerini* NMP	46.8	6.3	61.7	39.2	34.4	1.91	0.14	0.07	0.11	0.09	·	~	+	~	Sugar-fermenter (glucose, fructose, galactose)

B	**S14**	**Class**	***Thermotogae***	***Thermotoga maritima* NZ CP011108**	**91.3**	**4.3**	**i.h.**	**38.6**	**48.0**	**2.57**	**0.88**	**0.30**	**0.33**	**0.23**	+	+	+	+	**Sulfate-, nitrate- dissimilatory red**
B	S15	Class	*Thermotogae*	*Thermotoga maritima* NZ CP011108	69.4	1.8	i.h.	38.9	41.8	1.99	0.55	0.50	0.39	0.24	+	+	+	+	Sulfate-, nitrate- dissimilatory red
B	S11	Class	*Thermotogae*	*Thermotoga maritima* NZ CP011108	87.0	4.3	i.h.	39.2	44.9	1.77	0.34	0.17	0.17	0.23	+	·	+	+	Sulfate-, nitrate- dissimilatory red
B	S27	Phylum	*Thermotogae*	*Defluviitoga tunisiensis* DSM 23805	8.7	0.0	i.h.	34.7	31.6	1.07	0.05	0.07	0.08	0.07	·	+	+	·	Sugar-fermenter * (glucose)
B	S26	Phylum	*Thermotogae*	*Petrotoga mobilis* SJ95 NC010003^{T}	17.4	4.3	59.8	34.2	42.2	0.85	0.11	0.13	0.11	0.10	+	+	+	·	Sugar-fermenter * (glucose)
B	M09	Domain	*Bacteria*	*Petrotoga mobilis* SJ95 NC010003^{T}	52.2	8.7	63.3	34.0	32.0	1.97	0.09	0.17	0.40	0.27	+	+	+	·	Sulfur-oxidizing bacteria, fermenter (glucose)

The complete set of 70 MAGs had read abundances that together ranged between ~15.7% to ~24.4% of the total metagenome reads (Table 1.2 and Supplementary Figure S1.6), with the upper horizon being the one with the highest MAG coverage, which was in good agreement with the lower diversity and richness of this horizon (Table 1.1). However, the complete set of 70 MAGs recruited between 8.2% to 45.8% of the total reads mapping to the assembled contigs. All 70 MAGs mapped relative abundances ≤3.04% in each metagenome (Table 1.2).

The most representative MAGs in our samples were conspicuously those retrieved in more than one sample. For instance, MAG U04 (equivalent to M04, L02 and S09) was identified as a new species of the genus *Salinarchaeum*, or MAGs U01 (equivalent to S02) and U03 (equivalent to M03, L03 and S23), both affiliating with members of the candidate lineage DHVE2, reached relative abundances >2% of the communities. The rest of the MAGs were always found in lower relative abundances. Despite being diverse, the members of DHVE2 together represented ~17% of the total reads in the upper layer and were prevalent throughout the column, and MSBL1 up to ~2.3% in the intermediate layer but with similar abundances in the other metagenomes. Similarly, the three detected species of the genus *Salinarchaeum* represented up to ~6% in the slurry with values ranging from ~1.5% in the upper layers increasing to ~3% in the lower horizon. Noticeably, genera *Halodesulfurarchaeum* and *Salinarchaeum*, classes *Deltaproteobacteria* and *Planctomycetia*, and the phylum *Kiritimatiellota*, showed an increase in abundance in the lower horizons, especially for the bacterial members. Contrarily, class *Thermotogae* was dominant in the superficial layers, which was a similar trend to the methanogenic MAGs (Table 1.2).

1.4. Inferred metabolisms

The metabolic screening based on the annotation of genes associated with carbohydrate utilization, methanogenesis, fermentation and the sulfur cycle indicated that all these pathways were relevantly present in all samples, with relative abundances ranging from 2.5 to 11% of the total metagenomic reads (Supplementary Figure S1.7). The subsystems annotated in the assembled contigs were mainly related to the metabolism of amino acids and derivatives, clustering-based subsystems (a subsystem in which there is functional coupling present among the proteins, but their exact roles in the metabolic pathways are still unknown), cofactors, vitamins, pigments, DNA and RNA metabolism, protein metabolism and respiration, ranging from 4.6% to 12% singly of total metagenomic reads. Hydrolysis and photosynthesis were of low relevance in all metagenomes (data not shown).

1.4.1. Methanogenesis

Genes associated with the hydrogenotrophic, methylotrophic and aceticlastic pathways were detected in all metagenomes, with a relative higher abundance in the upper layer of the sediment. Genes involved in the hydrogenotrophic pathway were the most abundant but decreased with depth, while genes from the methylotrophic and aceticlastic pathways were higher in the intermediate horizon (Figures 1.3A and 1.3B and Supplementary Figure S1.7). From all genes detected for this metabolism in all metagenomes, 67% were binned in one or several MAGs, whereas only 11.4% were for the hydrogenotrophic pathway, 6.8% for the aceticlastic, 2.2% for the methylotrophic with methanol as substrate, 3.9% for the methylotrophic with methylamines as substrate pathways, and 8.8% of genes in the final step of methane synthesis were not binned. These non-binned fractions represented 7.6%, 8.5%, 7.7% and 9.2% for metagenomes S, U, M and L respectively (Supplementary Table S1.8). The hydrogenotrophic pathway was the most represented in MAGs, with all genes of this pathway encoded in MAGs of the candidate division MSBL1 (MAG U09, and the same species as S13 and M10). In addition, both an unknown lineage within *Euryarchaeota* (MAG S33) and a member of the candidate lineage DHVE2 (U08) encoded for the almost complete pathway (Figure 1.3B; Supplementary Figure S1.8 and Glossary in the Appendix I). Genes encoding the aceticlastic route were detected in all metagenomes. The sub-pathway based on *ack* and *pta* was encoded by the candidate MSBL1 (M08), while *acs* was detected in members of *Methanomicrobia* (U07), *Methanobacteria* (U06), and the candidate lineages DHVE2 (MAGs U08, M01 and L04) and MSBL1 (MAGs U09-M10-S13: same species, and U12). Subunits of the *cdh* gene were also identified in the previously listed MAGs. Genes related to the methylotrophic pathway with methanol and/or amines as substrates were encoded by members of the candidate MSBL1 (MAGs U09, M08 and U12), the *Euryarchaeota* phylum (S33) and DHVE2 (U08). Noticeably, a MAG affiliating with the uncultivated *Methanomicrobia* (U07) lineage that had a methylotrophic metabolism using methanol as substrate, was the only MAG encoding for a complete pathway up to the last steps of methanogenesis (Figure 1.3B and Table 1.1; Supplementary Figure S1.8 and Glossary in the Appendix I). The three methanogenic pathways were detected in MAGs affiliated with the uncultured lineage MSBL1 (U09, M10 and S13). The MAGs associated with candidate division MSBL1 (U09-M10-S13, U12, M08, L05, S18 and S36), *Methanobacteria* (U06), *Methanomicrobia* (U07), DHVE2 lineage (U08, M07 and L04) and the *Euryarchaeota* phylum (S33) encoded for some genes of methanogenesis and, therefore, we can speculate that they also have such a metabolism. From among all the samples analyzed, the spring intermediate horizon M showed the highest salinity of ~36.4%. In this horizon, the MAGs encoding for the hydrogenotrophic pathway dominated in abundance (candidate lineage MSBL1 – MAGs U09, M10 and S13: 1%, M08: 0.6% and U12: 0.3%; candidate lineage DHVE2 – MAGs U08: 0.6%, M05: 0.5%), in the same way as that encoding for aceticlastic metabolism (DHVE2 – MAGs M01: 1.1% and L04: 0.2%;

candidate MSBL1 – MAG L05: 0.3%; *Methanomicrobia* – MAG U07: 0.3% and *Methanobacteria* – MAG U06: 0.4%).

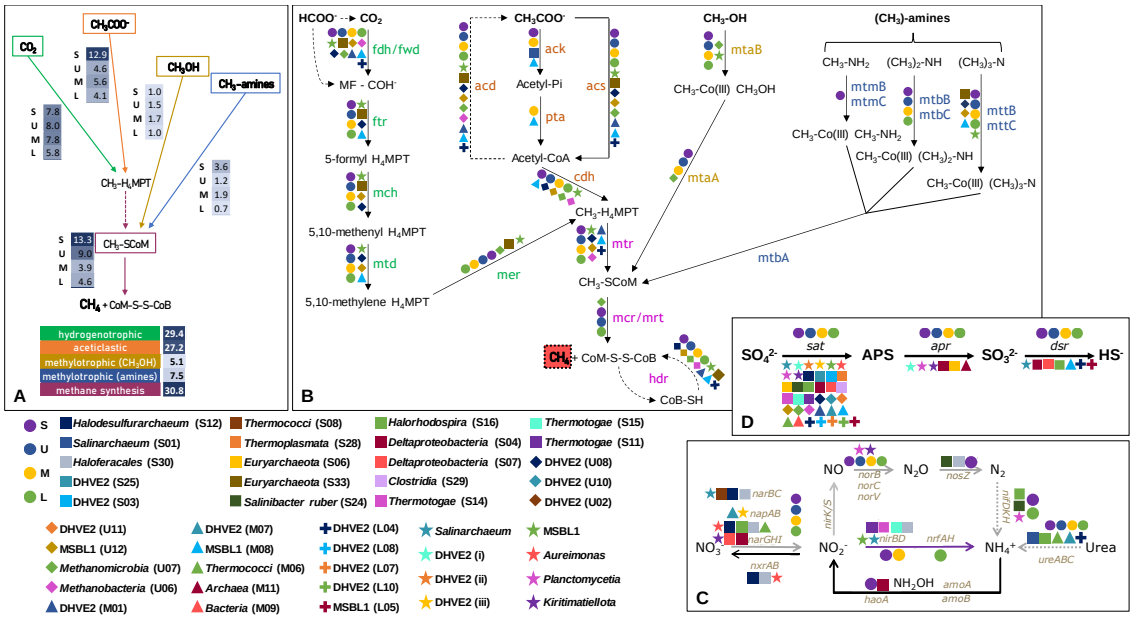

Figure 1.3. (**A**) Schema of the presence of the main general pathways of methanogenesis (green for hydrogenotrophic, orange for aceticlastic, yellow and blue for the methylotrophic routes) detected in S, U, M and L metagenomes. The number of gene copies implicated in a specific methanogenesis route related to total copies are represented by a blue scale bar (white for the lowest presence and dark blue for the largest) for the four metagenomes. (**B**) Methanogenesis superpathway encoded in the metagenomes and the MAGs (colored symbols with their designation indicated in the legend on the lower left side of the figure) encoding for each of the genes. Genes involved in hydrogenotrophic (CO_2), aceticlastic (CH_3COO^-) and methylotrophic (CH_3OH or CH_3-amines compounds) pathways are highlighted in green, orange and yellow-blue colors, respectively. Common intermediate and final routes are shown in pink. (**C**) Genes involved in the nitrogen cycle present in metagenomes and their MAGs. Black arrows represent nitrification, grey arrows show denitrification, the nitrogen fixation route is marked with dotted grey arrows, and dissimilatory nitrate reduction with purple arrows. (**D**) Dissimilatory sulfate reduction genes present in the metagenomes and their associated MAGs. Metagenomes are represented by circles and squares for MAGs from S, whereas rhombuses, triangles and crosses indicate the MAGs for U, M and L, respectively. The same species, comprising MAGs from the distinct metagenomes (see Table 1.2), are represented by stars.

1.4.2. Nitrogen cycle

Genes associated with anaerobic respiration, especially those for denitrification, were detected in all metagenomes. A total of 47.4% of the mentioned genes involved in the nitrogen metabolism did not bin, especially for denitrification and N_2-fixation (11.5%; Supplementary Table S8). Genes related to ammonification were detected in *Salinarchaeum* sp. (MAG S01), *Thermococci* (M06), the candidate lineage DHVE2 (MAGs M07 and L04) and the bacterial genus *Halorhodospira* (S16). The oxidation of ammonium to nitrite in the

nitrification pathway was detected in *Deltaproteobacteria* (S04), whilst *Halodesulfurarchaeum* sp. (S12), the *Haloferacales* order (S30) and *Aureimonas* sp. (M05) encoded for the oxidation of nitrite to nitrate (Figure 1.3C and Glossary in the Appendix I). The route of the pathway for dissimilatory nitrate reduction was encoded in the candidate lineage DHVE2 (MAGs M07 and L03). Subsequently, the nitrite reduction genes were detected in the bacterial MAGs of the *Thermotogae* class (S11, S14 and S15), and in the archaeal MAGs of candidate linage MSBL1 (S13), *Haloferacales* (S30), and those belonging to the *Salinarchaeum* genus (M04). On the other hand, the direct reduction of nitrite to ammonium was evaluated by the presence of the formate-dependent nitrite reductase (more details in the Glossary of the Appendix I), detected only in the metagenome of the intermediate horizon (L), and the contig could be affiliated with *Ignavibacteriaceae* (phylum *Chlorobi*).

Genes involved in nitrate reduction to nitrogen (N_2) were found in the archaeal MAGs affiliated to *Halodesulfurarchaeum* sp. (S12), *Halorhodospira* sp. (S16), a *Haloferacales* order archaeon (S30), *Thermococci* (M06); and in the bacterial MAGs affiliated to *Salinibacter* sp. (S24), *Aureimonas* sp. (M05), *Deltaproteobacteria* (S04 and S07), *Planctomycetia* (M02) and *Kiritimatiellota* (L09; Figure 1.3C and Glossary in the Appendix I). Finally, codification was also detected for nitrogen fixation genes, that could be found in the bacterial MAGs of *Halorhodospira* sp. (S16), *Salinibacter* sp. (S24) and a distant lineage within *Planctomycetia* (L01; Figure 1.3C and Table 1.1).

1.4.3. Sulfur cycle

Genes involved in the sulfur cycle were detected within a non-binned fraction of ~11%, of which 2.8%, 5.3% and 3.2% belonged to dissimilatory sulfate reduction, the assimilatory route and to sulfur oxidation, respectively (Supplementary Table S1.8). The first step in the reduction of sulfate to sulfite, shared by the assimilatory and dissimilatory routes, was widely represented in all metagenomes and MAGs (Figure 1.3D and Glossary in the Appendix I). The complete dissimilatory sulfate reduction pathway was detected only in the deltaproteobacterial MAG S04. It was partially detected in archaeal MAGs belonging to *Euryarchaeota* (S06), the candidate lineage DHVE2 (U05), the *Kiritimatiellota* phylum (L09) and an unclassified archaea (M11); and in the bacterial MAG of a divergent lineage within the *Planctomycetia* (M02), which encoded genes for the reduction of adenosine 5'-phosphosulfate to sulfite. Genes involved in the reduction of sulfite to hydrogen sulfide were encoded by the archaeal MAGs belonging to the *Salinarchaeum* genus (S09), the MSLB1 lineage (M08 and L05), the DHVE2 lineage (L04), and the bacterial MAGs of *Deltaproteobacteria* (S07), as well as those belonging to the genus *Halorhodospira* (S16; Figure 1.3D and Table 1.1).

1.4.4. Fermentation

Genes associated with fermentation were widely detected in all metagenomes. Alcoholic fermentation (ethanol) could be performed by a MAG of the *Aureimonas* genus (L06). Lactic acid fermentation could be inferred for the bacterial MAGs of the *Planctomycetia* (M02), the *Thermotogae* class (S14 and S15), the genus *Halorhodospira* (S16) and the class *Clostridia* (S29). For the archaeal MAG of the DHVE2 lineage (U01), both lactic acid and acetic acid fermentation could be inferred. Acetic acid fermentation for the MAGs of the candidate lineage DHVE2 (U03, U02, U11, and L10), *Archaeoglobi* (S17) and *Thermococci* (S34) could also be inferred.

1.4.5. Additional metabolic mechanisms of anaerobic respiration

The presence of DMSO reductase (DMSOR; catalyzes the reduction of DMSO to DMS under anaerobic respiration) was detected in the archaeal MAGs affiliating with the *Salinarchaeum* genus (S01 and S09), *Halodesulfurarchaeum* sp. (S12 and S20) and the candidate lineages MSBL1 (U09 and U12) and DHVE2 (S23 and U08). In addition, this gene was detected in the bacterial MAGs of the *Thermotogae* class (S15) and those affiliated with the genus *Aureimonas* (Table 1.1).

1.5. Replication rates of the MAGs

To evaluate the putative viability and replication of the MAGs we used the approach of Emiola and Oh (2018), which is based on the calculation of the Growth Rate InDex (GRiD). The GRiD ranged from 1.0 (no replication), for example *Haloferacales* (S30), to 3.1 for *Halomicrobium* sp. (S22). Almost all MAGs showed positive signals with the exception of those affiliated with uncultured lineages DHVE2 (L04) and MSBL1 (L05) and the *Deltaproteobacteria* (S04), and the rest showed positive GRiD rates in at least one metagenome. A total of 18 MAGs had positive signals in all of them, and 59 in at least two metagenomes (Table 1.2). The values diverged between MAGs and samples, and we could detect that the three horizons showed slightly different profiles for the most "active" MAGs (Figure 1.4). Alcohol fermenters affiliated with *Aureimonas* sp. (MAGs M05 and L06) showed GRiD values above 1.0 in all metagenomes, whilst acetic acid fermenters displayed higher ratios in the superficial fraction (DHVE2 – U11 and *Archaeoglobi* – S17) but more MAGs with a positive replication rate were detected in the deepest fraction, with the lineage DHVE2 and *Archaeoglobi* being the most representative. In general, among sugar-fermenters, there were positive GRiD rates, especially members of the *Halomicrobium* genus (S22 and S21), *Thermoplasmata* (S28) and *Thermococci* (M06). Chemoorganotrophs seemed to exhibit positive replication activity in the middle and lower fractions, especially for *Halorubrum* sp.

(S19) and DHVE2 (S23, U05, S05 and S25). Regarding methanogens, in general, members belonging to candidate lineages DHVE2 (M01) and MSBL1 (S18, S36 and U12), and to the *Methanobacteria* (U06) and *Methanomicrobia* (U07) classes displayed positive growth activity, with the aceticlastic methanogens being more GRiD active in the U, M and L layers, and the hydrogenotrophic in the slurry. Sulfate-reducers and other members associated with the metabolism of sulfur showed positive activity ratios, especially an unclassified archaeon (M11, specifically in U, M and L) and members of *Thermotogae* (S14, S15 and S11). Furthermore, the GRiD values of *Kiritimatiellota* (L09 and M10) and *Salinibacter* sp., with a denitrifying heterotrophic metabolism, showed positive replication rates, especially in the M and L fractions (Table 1.2 and Figure 1.4).

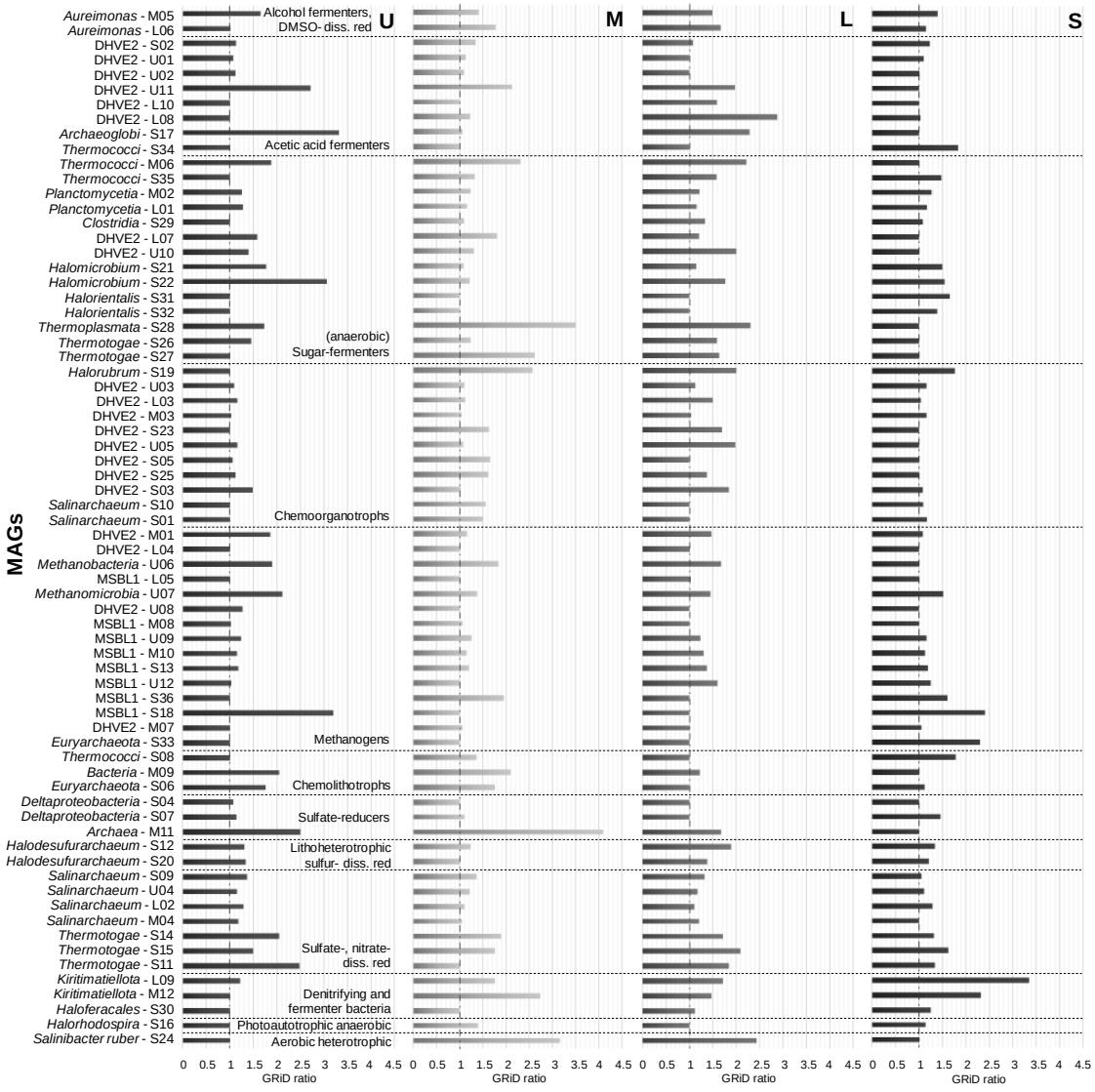

Figure 1.4. From left to right: Growth Rate inDex (GRiD) of MAGs, ordered by functional groups, in the U, M, L horizons, and the slurry (S) samples. GRiD growth ratios estimate the *in situ* genome replication rates in metagenomes. Dotted lines indicate the threshold for positive growth GRiD values (GRiD score > 1.0), where positive cell growth can be considered.

With regard to the inferred metabolisms, we could not observe any evident stratification that would respond to either the expected electron acceptor availability, or to a taxonomic segregation. In general, the most "GRiD active" in the upper and intermediate layers were also positive in the lower layer, and among these we could infer distinct anaerobic respiration types as well as distinct types of methanogenesis, but with dissimilar dominance. The lowest profile shifted the taxonomic diversity and maintained a metabolic redundancy. Therefore, vertical stratification could not be observed since almost all metabolisms, with similar "GRiD activity" measurements, were detected, all of which were compatible with this ecosystem. The slurry showed a smaller number of "GRiD active" MAGs that could have been related to the winter temperatures that slow down metabolisms (Figure 1.4).

Almost all MAGs were taxonomically congruent with the types of inferred metabolisms that thrive in this environment. However, there were some unexpected MAGs due to their identities, for instance, S21 and S22 identified as *Halomicrobium* sp., S31 as *Halorientalis* sp. and S30 from the order *Haloferacales* of the *Halobacteria*, S24 as *Salinibacter* sp. from the *Salinibacteraceae*, and M05 and L06 identified as *Aureimonas* sp. from the *Alphaproteobacteria*, all of which have strict aerobe metabolisms. However, except for the archaeon *Haloferacales* (S30), they were all "active" in one or various samples, and also for whom some putative anaerobic metabolisms could be inferred (see previous sections and Table 1.2).

1.6. Viral communities of S'Avall sediments

Virus-like particles (VLPs) in the upper, medium and lower horizons of the sediment core sampled in April 2017 were in the range of 10^{10} per gram, with a slight decrease in depth (from 1.9 x 10^{10}/g in U to 8.9 x 10^{9}/g in L). The predominant viral genome sizes, estimated by pulsed-field gel electrophoresis (PFGE), were approximately 40 kb and transmission electron microscopy (TEM) revealed the viral morphotypes commonly observed in salt-saturated brines: tailed, spindle-shaped, spherical and filamentous (Supplementary Figures S1.9A and S1.9B; Santos *et al.*, 2012; Martin-Cuadrado *et al.*, 2019). The three corresponding U, M and L viral metagenomes, or viromes, (Supplementary Table S1.9) were above the recommended threshold of 60% (Nonpareil analysis; Rodriguez-R and Konstantinidis, 2016) and showed <0.02% 16S rRNA gene reads, which is the established value for considering a viral metagenome as "clean" from cellular DNA (Roux *et al.*, 2013). A BLASTN-based comparison between the viromes, using randomly selected reads, showed, in concordance with the structure of the prokaryotic communities, a higher similarity between the viral assemblages from horizons M and L (with approximately 17% identical reads and approximately 67% with identities above 95%; Supplementary Figure S1.9C).

The virome assembly yielded a total of 818 contigs ≥5 kb, which were clustered in 190 viral OTUs (vOTUs) based on sequence identity (Supplementary Table S1.9). These contigs only recruited 5% of the total nucleotides from each virome (average), most likely as a consequence of high virus microdiversity that affected the assembly process (Ramos-Barbero, Martínez, *et al.*, 2019). However, they constituted a source of virus novelty, since the vast majority of vOTUs (95%) had no hits against the NCBI database and 77.5% of the predicted open reading frames (ORFs) were unknown. Regarding the viral genes with assigned functions in Pfam (530 ORFs), the category of "structural proteins" was the most abundant (31.13%), followed by "conserved hypothetical proteins" (14.91%). Three viral ORFs (0.57%) were related to reverse transcriptases, which have been associated with "diversity-generating" enzymes in dsDNA viruses (Liu *et al.*, 2002) and that were also found in the hypersaline chaotropic lake of Salar de Uyuni (Bolivia; Ramos-Barbero, Martínez, *et al.*, 2019). Noticeably, 9.8% of the total classified ORFs were annotated as integrases (Supplementary Table S1.3), a value which was higher than those previously found in metaviromes from other studied brines (Santos *et al.*, 2010; Martin-Cuadrado *et al.*, 2019; Ramos-Barbero, Martínez, *et al.*, 2019). As a consequence, 26% of the vOTUs might undergo a temperate lifestyle in S'Avall sediments. It was also relevant that most vOTUs were present in the three analyzed horizons and that 43% of the vOTUs were also detected in their corresponding cellular metagenomes (with a quarter carrying integrases). The highest percentage of shared vOTUs between two horizons was found, as expected, for M and L. In addition, for each horizon, there was a fraction of vOTUs that was not shared with the other two horizons. Not unexpectedly, this specific virome constituted a very small part of the transition horizon, whereas it was considerably higher for U and L (4.2% in U, 0.5% in M and 3.2% in L; Supplementary Figure S1.10 and Table S1.10).

With respect to the virus-host interactions, 12% of the vOTUs could be assigned to putative hosts. Most assignments were established with the class *Halobacteria*, which formed the most relevant archaeal "core" in the sediments. Remarkably, seven vOTUs corresponded to viruses likely integrated into the genomes of MAGs from class *Planctomycetia* (L01 and M02) and the candidate lineages MSBL1 (L05) and DHVE2 (U02; Figure 1.5 and Supplementary Table S1.10). This is the first report of viruses infecting these uncultured members of the so-called "microbial dark matter".

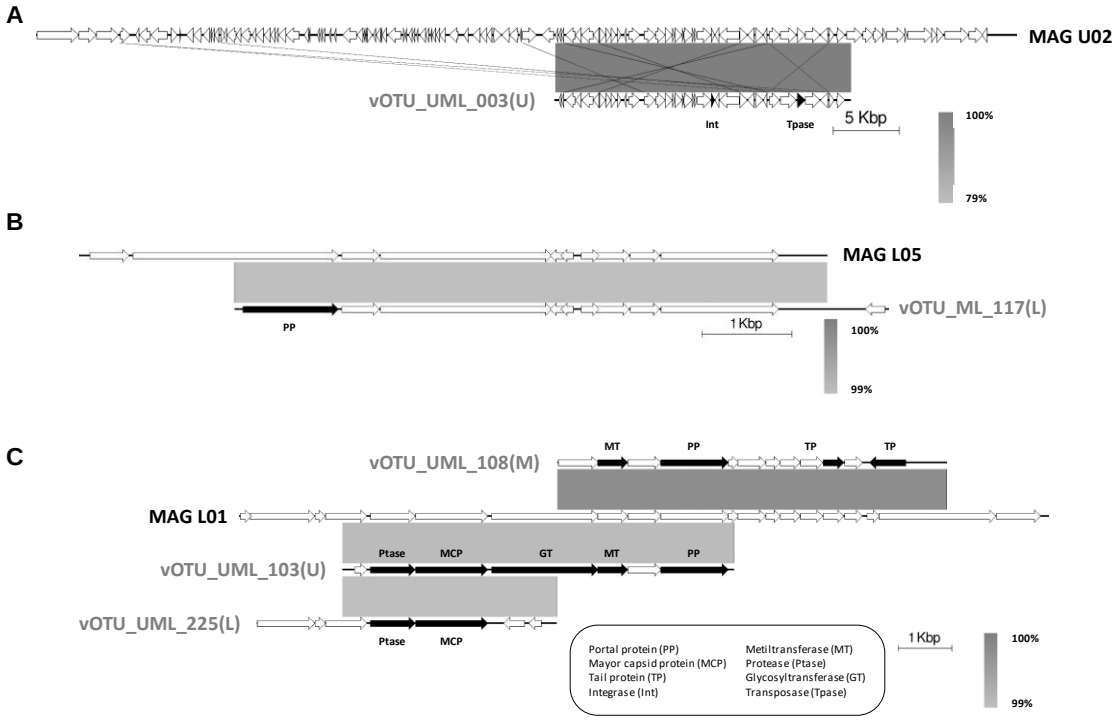

Figure 1.5. Alignments of certain selected viral OTUs, examples of the viral novelty retrieved from S'Avall sediments, against the corresponding MAGs where the viral sequences were detected. Predicted ORFs are indicated by horizontal arrows; black arrows indicate ORFs with assigned functions (see legend). The representation is based on Easyfig, where grey intensities are related to the identity percentages in the alignment. **A**: MAG U02 assigned to DHVE2 lineage. **B**: MAG L05 assigned to *Candidatus* MSBL1. **C**: MAG L01 assigned to *Planctomycetia* class.

1.7. Discussion

The hypersaline anaerobic sediments of an ephemeral pond from S'Avall had attracted our attention, since initial results indicated the presence of an exceptional microbial assemblage, where distinctive lineages detected in brines of some Mediterranean deep-sea anoxic hypersaline basins (DHABs; Joye *et al.*, 2009; Antunes *et al.*, 2011; Sorokin, Kublanov, Gavrilov, *et al.*, 2016; Sorokin, Kublanov, Yakimov, *et al.*, 2016) were easily accessible at only a few centimeters below the surface (López-López *et al.*, 2010, 2013). The prokaryotic community structures of the sediments, for which generation of methane gas was demonstrated in high quantities, appeared to be spatially and seasonally stable throughout the pond, as well as even in the years sampled (López-López *et al.*, 2010, 2013). In addition, the sediments had a vertically stratified community structure, similar to what has already been reported (Walsh *et al.*, 2005; Webster *et al.*, 2015; Vavourakis *et al.*, 2019), although in our case we could not link it to salinity and pH gradients, and ammonium was the only single statistically significant variable. In good agreement with what has also been observed for DHABs, viral abundance in S'Avall sediments decreased only slightly with depth. However, the number of VLPs in the sediments was up to three orders of magnitude higher than those previously reported for DHABs (Danovaro *et al.*, 2005; Corinaldesi *et al.*, 2014) or cold hypersaline Arctic sediments (Colangelo-Lillis *et al.*, 2016, 2017), which are, as far as we know, the only similar environments where virus quantification has been reported.

Metagenomics was applied in order to gain precision in the understanding of the prokaryotic and viral composition of the sediments and compare them with their described analogous anaerobic systems. It was remarkable that contrarily to what we expected (López-López *et al.*, 2010, 2013), the MAGs retrieved from the hypersaline sediments of S'Avall were an important source of taxonomic novelty, since almost all MAGs were distantly related to all the taxa detected in studies of comparable systems (Mwirichia *et al.*, 2016; Sorokin, Kublanov, Gavrilov, *et al.*, 2016; Sorokin, Kublanov, Yakimov, *et al.*, 2016; Baker *et al.*, 2020). The MAGs detected together represented a relative abundance comparable to other studies on hypersaline systems (Viver *et al.*, 2019) and were the most represented taxa in the sediments, despite the global diversity not being captured after binning. Conspicuously, the same MAG populations of six distinct taxa were binned in two or more samples with their independence reinforcing their stable presence in time and space.

At a depth of 25 cm, vertical stratification of microbial taxa that would mirror the expected gradient of electron acceptors characterizing marine sediments (Fenchel *et al.*, 2012) could not be detected. Contrarily, the metagenomes showed a vertical profile with a marked dominance of archaeal taxa in the overlaying horizons, with bacterial taxa in the deeper horizons. This vertical distribution was inverted compared to that expected in a classic sediment structure where methanogenic Archaea appear in the deeper horizons and Bacteria

appear in the upper layers where electron acceptors allow higher energetic yields (Fenchel *et al.*, 2012; Petro *et al.*, 2017). Different anaerobic metabolisms to the major taxa could be inferred, such as fermentation (e.g. members of the DHVE2 cluster), anaerobic respiration (e.g. *Salinarchaeum* sp.) and methanogenesis (e.g. *Methanobacteria* class and *Methanomicrobia* class). A large number of genes from interrelated pathways involving methane, sulfur and nitrogen were detected in the three layers of the sediments, indicating that complete cycles could be performed.

The analysis of the viral metagenome, which is the first reported to date for hypersaline anoxic sediments, also indicated a certain stratification of the viral assemblage, as well as a remarkable novelty. The vast majority of analyzed viral OTUs (considered as "viral species") and their predicted proteins did not produce matches against isolated haloviruses or haloviral sequences obtained by culture-independent approaches, which might be directly connected to the fact that their hosts had not been described previously. For instance, for the haloarchaea, the tools employed did not accurately assign viruses to hosts at the genus or species levels, most likely due to the scarce data on the anaerobic extremely halophilic members of class *Halobacteria*. However, for some reconstructed MAGs, including some conspicuous uncultured microbes, viruses were clearly assigned due to their presence as prophages. The high presence of viral sequences coding for integrases, which are hallmarks of a potential temperate lifestyle, was remarkable. Indeed, except for the athalassohaline sulfate-rich crust from Peñahueca lake (Martin-Cuadrado *et al.*, 2019), with a similar percentage of integrases, metaviromes from hypersaline brines have been typically considered as mainly dominated by lytic viruses (Santos *et al.*, 2012). In S'Avall sediments, lysogeny appears to gain significance, which has also been hypothesized for cold hypersaline oligotrophic sediments with low microbial growth (Colangelo-Lillis *et al.*, 2017) or has been proposed generally for freshwater and marine sediments. In these environments, lysogeny might be more important than the lytic cycle when the growth rates of the hosts are slowed down by the limitation of nutrients (Danovaro *et al.*, 2008).

From a metabolic perspective, the vertical profile of the microbial community showed only minor trends, as in general the inferred anaerobic metabolisms overlapped throughout the 25 cm horizon. The relative abundance of genes involved in methanogenesis was highest in the upper layer with the hydrogenotrophic route being the most representative. Interestingly, in the same layer, we detected abundant members of the genus *Acetothermia*, an acetogenic fermenter and competitor with aceticlastic methanogens for acetate (Youssef *et al.*, 2019), although the findings were only based on OPUs since these populations could not be binned. Bacterial MAGs affiliated to the *Thermotogae* class were dominant in the upper layer and they might thrive in syntrophy (Rathi *et al.*, 2018; Mand and Metcalf, 2019). The methanogen *Candidatus* MSBL1 lineage incremented in relative abundance with depth, although the opposite was found for the genes related to the aceticlastic methanogenesis

pathway, whereas putative competitors, such as the acetogenic fermenter *Acetothermia* sp., decreased in abundance.

There was a notable increase of taxa with putative fermentative metabolisms in the lower horizons, for instance, *Salinarchaeum* sp. richness increased with depth and was the dominant Archaea in the deepest fraction in spring. This genus exhibits a metabolism related to oxidation of sugars, using carbohydrates as carbon sources (Minegishi *et al.*, 2017). Other taxa with putative fermentative metabolisms, such as the phylum *Kiritimatiellota* (Spring *et al.*, 2016), the order *Thermoplasmatales* or the genus *Acetothermia,* were also abundant in this layer. This taxa stratification was mirrored by the prevalence of genes related to polymer degradation and fermentation, losing methanogenesis representativeness. Similarly, sulfur-related metabolisms increased in the lower layers, such as MAGs affiliating with *Halodesulfurarchaeum* sp. (Dimitry Y. Sorokin *et al.*, 2017) or with *Deltaproteobacteria*. Reinforcing the inverted vertical biogeochemical profile, a higher dominance of bacteria was detected with a putative anammox metabolism in the lowest horizons, represented by MAGs M02 and L01 affiliating with the *Planctomycetia* class (*Candidatus* Kuenenia stuttgartiensis was the closest reference), and with *Candidatus* Brocadiaceae for which this metabolism is still unreported (Speth *et al.*, 2012). In addition, other metabolisms related to the nitrogen cycle were more represented in the lowest horizons. Genes involved in the reduction of nitrate to ammonium were detected in abundant taxa in these layers, thus providing the necessary substrate to anammox bacteria. However, the oxidation of substrates, such as acetate, have been reported in some species of anammox bacteria (Oshiki *et al.*, 2016).

We especially detected members of two candidate lineages with scarce genomic information, as well as the first viruses associated with them. On the one side, the candidate lineage MSBL1 already observed in our previous studies (López-López *et al.*, 2010), which were present in all samples of the vertical profile with a decreasing trend in abundances and GRiD growth rates with depth. One of their associated MAGs (U02) harbored an integrated provirus that was ubiquitous in the three metaviromes analyzed. The candidate lineage MSBL1 detected is the most abundant uncultivated microorganisms in most deep-sea hypersaline brine lakes (van der Wielen *et al.*, 2005; Yakimov *et al.*, 2015). The metabolic role of this group remains uncertain, but a putative methanogenic metabolism was hypothesized by López-López *et al.* (2010, 2013). Genes involved in methanogenesis were detected among the MAGs, such as the complete hydrogenotrophic, the complete aceticlastic, or the methylotrophic pathways. Interestingly, the syntrophic interactions between candidate lineage MSBL1 and *Candidatus* Acetothermia, supporting the methylotrophic methanogenic activity of the former with trimethylamine produced by the metabolism of glycine-betaine of the latter, has been reported (Merlino *et al.*, 2018), and would agree with our observations on the assemblages. However, it should be noted that the core gene *mcr*, encoding for the key enzyme methyl-coenzyme M reductase, which catalyzes methane production, was not

found in any MAG. The members of the candidate lineage MSBL1 could produce methane using an alternative reductase or could possibly even contain different *mcr* gene homologs (Evans *et al.*, 2015; Mwirichia *et al.*, 2016; Hua *et al.*, 2019) that might not have been annotated. Additionally, some MAGs encoded for genes involved in dissimilatory sulfate reduction, dissimilatory nitrate reduction, CO_2 fixation and sugar fermentation, supporting the idea of a mixotrophic lifestyle in this lineage (Mwirichia *et al.*, 2016). No genes involved in the Embden-Meyerhof-Parnas pathway were detected.

Members of the Deep-sea Hydrothermal Vent *Euryarchaeota* 2 (DHVE2) lineage are globally distributed, especially at deep-sea hydrothermal vents. *Aciduliprofundum boonei* $T469^T$ is the only isolate of the thermoacidophilic group, and is described as a sulfur- or iron-reducing heterotroph capable of degrading proteins to obtain energy (Reysenbach *et al.*, 2006; Flores *et al.*, 2012; Baker *et al.*, 2020). In this study, twenty genomes were detected along the column and they were affiliated to DHVE2, highlighting their abundance and metabolic diversity. We recruited MAGs having their main role in sulfate-reduction, heterolactic fermentation, DMSO reduction to DMS, and even as hydrogenotrophic members, contrarily to that described elsewhere (Borrel *et al.*, 2014). Moreover, one of the DHVE2 MAGs (L05) was infected by a novel caudovirus circumscribed to horizons M and L, where L05 abundance was higher.

Besides the detection of a plausible anaerobic microbial assemblage, we could also observe the presence of microorganisms in relatively high numbers that were described as strict aerobes, such as the *Salinibacter* and *Salinivenus* genera (Viver *et al.*, 2018), or several members of the class *Halobacteria* (McGenity and Oren, 2012; Oren, 2013). The presence of these taxa, together with the detection of other strict aerobes, such as ammonium oxidizing archaea (*Candidatus* Nitrosoarchaeum, *Candidatus* Nitrosopumilus, *Candidatus* Nitrososphaera) and nitrite oxidizing bacteria (*Nitrospira* sp.) might indicate that either oxygen could be sporadically available especially in the lower horizons, or that these taxa could also perform anaerobic metabolism. The viable presence of these organisms was reinforced by the GRiD analysis that showed putative DNA replication of *Salinibacter* sp. and *Halorubrum* sp. in the deepest layers. Metabolism of anaerobic sulfur and carbon cycling, as well as another based on anaerobic nitrate respiration, have been reported for some members of the class (Oren, 2013). The putative anaerobic metabolism is reinforced by the presence of specific genes in the halobacterial MAGs involved in anaerobic fermentation, the reduction of dimethyl-sulfoxide to dimethyl-sulfide (Zhuang *et al.*, 2018; McGenity and Sorokin, 2019), the conversion of glycerol 3-phosphate to dihydroxyacetone phosphate in anaerobic conditions, and respiratory nitrate reductase genes (Oren, 2013). In light of these results, the biogeochemical role of halobacterial taxa should be thoroughly studied, since the metabolic diversity and ecological relevance of this clade in anaerobic systems may be higher than previously assumed (Sorokin, Kublanov, Gavrilov, *et al.*, 2016).

Another interesting finding was the presence of two MAGs affiliating with *Aureimonas* sp., which is described as a mesophile with strict aerobic metabolism. However, we could infer a putative metabolism so far not reported for this genus, since the MAGs encoded for genes related to sulfur-metabolism, potential anaerobic DMSO respiration and their ability to produce ethanol via alcoholic fermentation (only encoded in L06). The ability of different species of *Aureimonas* to survive in halophily and the detection of new species belonging to this genus in diverse environments have been described before (Jurado *et al.*, 2006; Anderson *et al.*, 2009; Guo *et al.*, 2017). These MAGs displayed a positive GRiD growth activity, especially in the lowest horizons, reinforcing that the underlying ecosystem could be a source of oxygenic or oxidized environments that would allow growth of aerobic or nitrate reducing bacteria. Derived from the very dark color of the sediments along the whole column, and also the dominance of anaerobic taxa in the lowest horizons, we could assume that these layers were reduced and anaerobic. However, we did not study the deeper underlying substrate. It should be noted that the pond in question was located at approximately 50 m from the seashore and the deeper substrate probably has a sandy consistency with a porosity that could contain marine oxygenated porewater that could influence the overlaying hypersaline sediments and be responsible for the inverted stratification, although this fact should be proven in future studies.

CHAPTER 2

Chapter 2. Study of the effect of salinity, antibiotic and carbon source concentration in structuring the microbial communities from S'Avall hypersaline sediments

This chapter details the characterization of methanogenic enrichment cultures with *P. oceanica* dead biomass as substrate. Here we describe the structure of the prokaryotic communities determined by salinity, ampicillin and substrate concentration. This study focuses on the changes that the microbial communities experience by means of 16S rRNA gene amplicon sequencing. This investigation supports the theory that salinity acts as selection force that determines the composition of microbial community structures. We also study the influence of ampicillin and substrate at different concentrations. Stochastic processes prevail on the dynamics of the community assemblies and the dilution applied to microbial communities of S'Avall, modifying their natural media, is a determinant ecological factor.

2.1. Microcosms enrichments from slurry and their chemical properties

A collection of 96 microcosms was prepared using a salt saturated slurry collected from hypersaline anaerobic sediments as inoculum as reported in chapter 1 (Font-Verdera *et al.*, 2021). The slurry was diluted to salinities ranging from 30% to 5% in order to obtain an optimal methanogenic production and to analyze the influence of the salinity concentration during community assembly. Additionally, the effect of ampicillin emendation and *Posidonia oceanica* dead biomass as substrate load were assessed at different concentrations (0.1, 1 and 10% w/w). The enrichments were compared with the original slurry (S), described in chapter 1 (Font-Verdera *et al.*, 2021). Permutation D-test, Kolmogorov-Smirnov (with Bonferroni correction) and Wilcoxon (parameters: $D \leq 1.36$ and $p > 0.05$) and T-test ($\alpha = 0.05$ and $|t| \leq 1$; Supplementary Table S2.1) showed no statistically significant differences between the duplicated enrichments. Therefore, microcosms under the same conditions were considered as duplicates.

The concentrations of the major salts were calculated from their ionic composition and they were linked to the increasing gradient of salinities of the ninety-six microcosms (from 5 to 30% w/v; Figure 2.1). Sodium chloride (NaCl) was the dominant salt and ranged from 0.5 M (5% salinity) to 3.7 M (30% salinity and S; Figure 2.1B). The same pattern was observed in magnesium sulfate ($MgSO_4$: 0.05 – 0.5 M; Figure 2.1C), magnesium chloride ($MgCl_2$: 0.1 – 0.35 M; Figure 2.1E) and potassium chloride (KCl: 0 – 0.16 M; Figure 2.1F). Conversely, calcium carbonate ($CaCO_3$) decreased as salinity increased (from 14 M at 5% of salinity to 0.5 M at 30%; Figure 2.1D) while calcium chloride ($CaCl_2$) did not differ between salinities (0 – 0.03 M; Figure 2.1G). Organic matter content (OM) was around 20% in all samples, (Figure 2.1H),

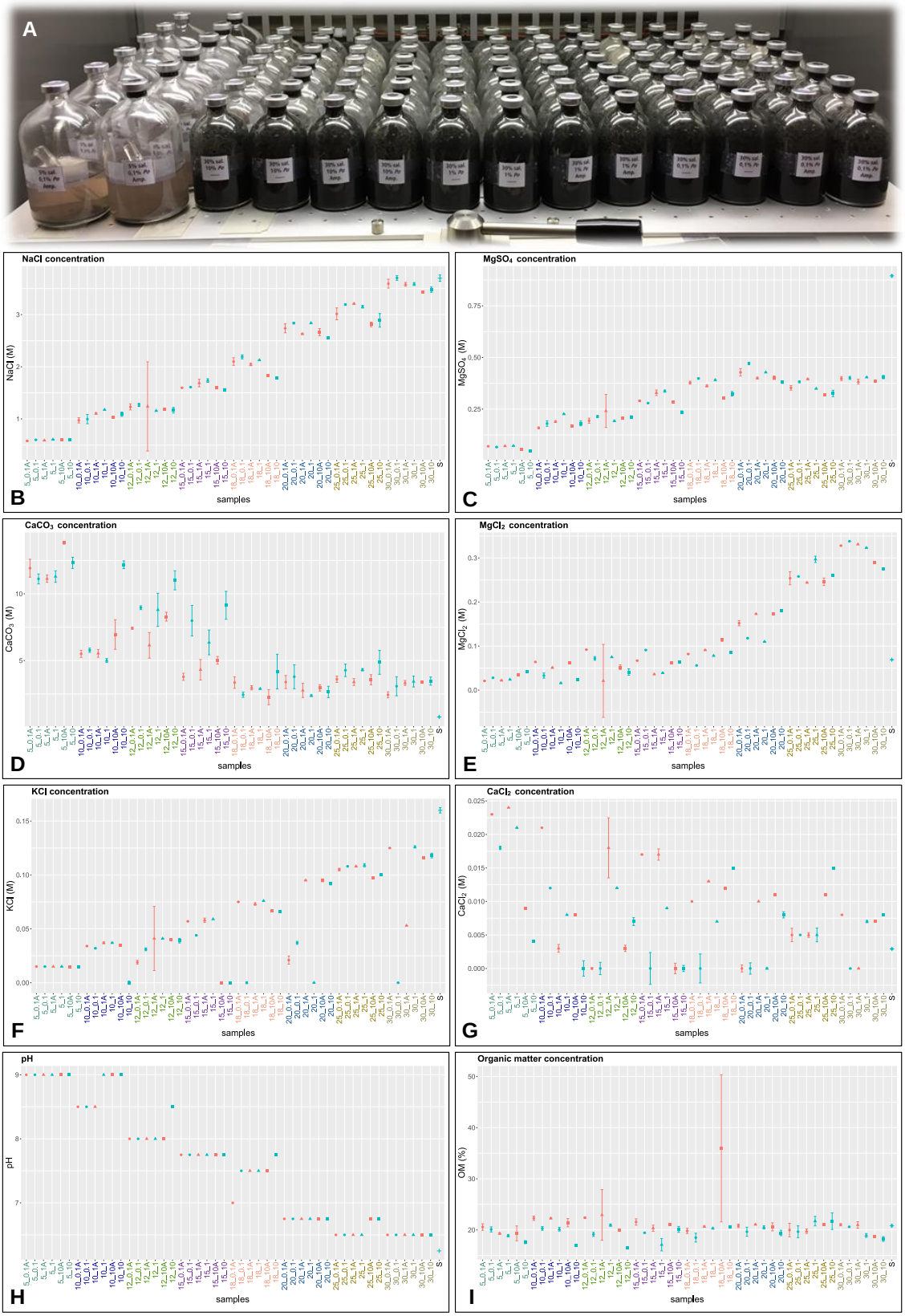

Figure 2.1. A. Image of the battery of ninety-six microcosms incubated at 30ºC. **B-G**. Concentrations of major salts in molarity: NaCl (**B**), $MgSO_4$ (**C**), $CaCO_3$ (**D**), $MgCl_2$ (**E**), KCl (**F**) and $CaCl_2$ (**G**) for the duplicate microcosms and S (slurry). Organic matter in percentage (w/w) (**H**) and pH (**I**). Samples with concentrations of 0.1%, 1% and 10% *Po* are represented in circles, triangles and squares, whereas those with or without ampicillin are shown in red and blue, respectively. Different salinities are colored in the x axis.

similar to the slurry (20.8%). Microcosms with ampicillin displayed slightly higher values (21.4±1.2% of OM) compared to the microcosms without antibiotic (19.4±0.5% of OM), except for those with 25% of salinity. The slurry had a pH of ~6.3, and microcosms displayed increasing pH with dilution, reaching 9.0 at 5% (Figure 2.1I).

2.2. Salinity as selection force determining the structure of microbial communities

A total of 6,223,459,746 total raw read bases, which read count ranged in length between 141.4 and 290.2 bp were sequenced from both the ninety-six microcosms and the slurry. After trimming and chimera removal a final set of 5,191,897 sequences were obtained, encompassing 1,632,127 for the archaeal and 3,559,770 for the bacterial domains (Supplementary Table S2.2). The dataset was rarified (sample size = 33,781) rendering 1,468 OPUs (210 and 1,258 for Archaea and Bacteria, respectively; Supplementary Table S2.2), with less than 10 species being removed per sample, thus not affecting total diversity. Diversity reached saturation for both domains, as the rarefaction curves indicated, with a sample sequence coverage between a minimum of 61.1% (sample 25_0.1A2) and 95.6% (sample 12_0.1A1).

Richness (Chao-1) values decreased as salinity increased (transitioning from a positive change to negative in relation to the inoculum, with values of Chao-1 of 39 and 116, for Archaea and Bacteria, respectively), displaying Bacteria higher index values (Figures 2.2A and 2.2B). With few exceptions, Shannon index in Archaea was overall lower in microcosms when compared to the inoculum (H=3.394; Figure 2.2B), with a drop in diversity ranging from -5.8% to -55.7%. Conversely, Shannon index in Bacteria was generally higher than the inoculum (H=2.988, Figure 2.2D), especially at 5% of salinity, ranging from 17.7% to 43.6% (Figures 2.2C and 2.2D and Supplementary Table S2.3). Dominance generally increased in Archaea with dilution, being highest at 5% (with a maximum of 479.2%), and with the exception of 12% salinity where the index decreased with regard to the inoculum. The opposite was observed for Bacteria, which displayed more dominant communities at high salinities (Figures 2.2E and 2.2F and Supplementary Table S2.3).

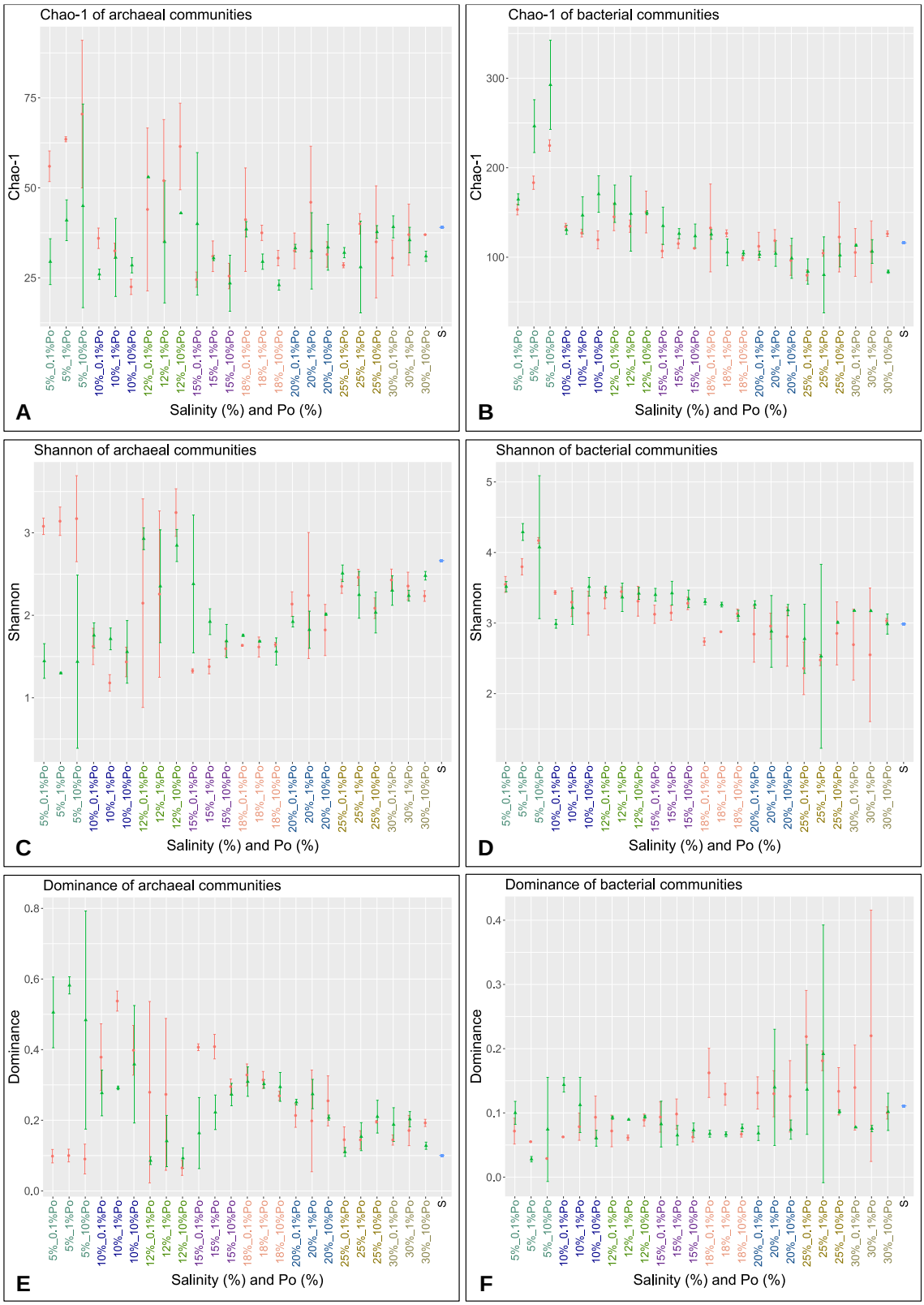

Figure 2.2. Diversity indices based on OPUs from 16S rRNA gene amplicons for archaeal (on the left) and bacterial (on the right) domains. Chao-1 (**A** and **B**), Shannon (**C** and **D**) and Dominance (**E** and **F**) data are shown in relation to the salinity and the *Posidonia oceanica* concentrations (in the x axes). Samples with or without ampicillin are marked in red and green, respectively, whereas the slurry (S) is colored in blue. Different salinities are colored in the x axis.

Aiming to evaluate the effect of salinity during community assembly, non-metric multidimensional scaling (NMDS) plot based on Bray-Curtis dissimilarity was obtained, grouping samples by salinity (Figure 2.3). Overall, as observed in the NMDS, samples grouped by salinity, being the dissimilarity highest within microcosms at 5% of salinity (from 0.6 to 0.93; Supplementary Figure S2.1A), observing statistically significant differences within communities at each salinity ($p < 0.05$, Wilcoxon and Mann-Whitney *U* non-parametric tests; Supplementary Figures S2.1B, S2.1C and S2.1D). Dissimilarity decreased as salinity increased, being lowest at 30% (from 0.3 to 0.5) and similar to the inoculum (with a Bray-Curtis dissimilarity average of 0.4). Comparisons between communities in the inoculum and at the different salinities at the end of the experiment showed that 5% of salinity experienced the most significant change (values of Bray-Curtis dissimilarity above 0.8), decreasing as salinity increased, being below 0.4 dissimilar to the inoculum (Figure 2.3 and Supplementary Figure S2.1).

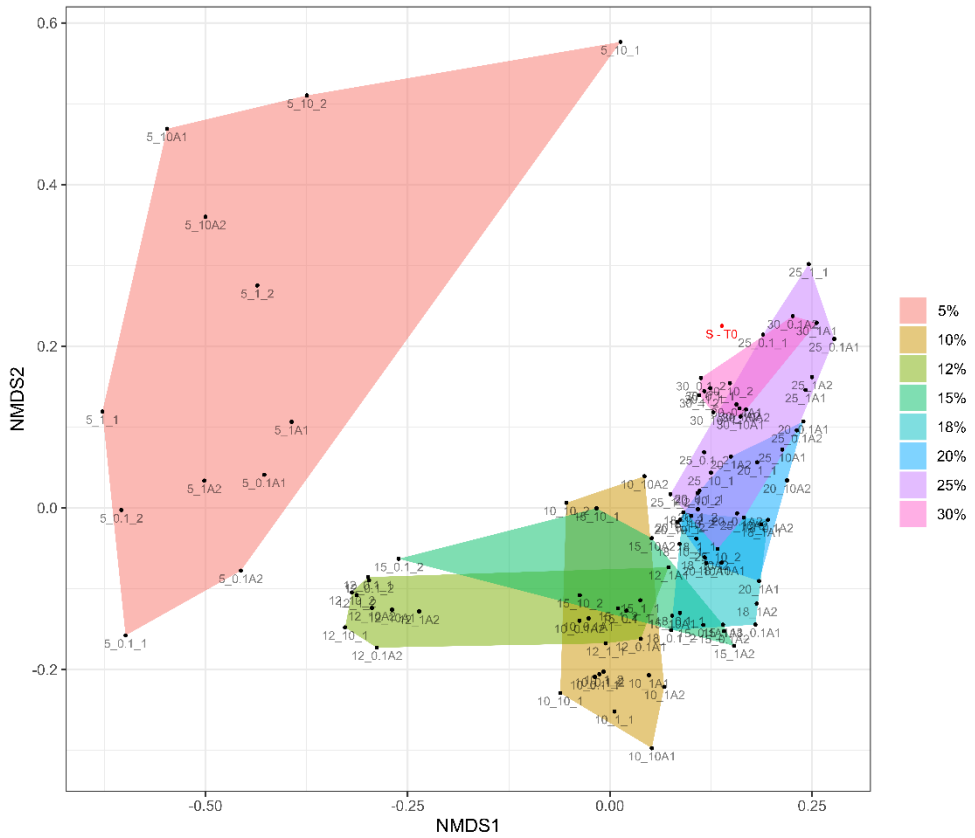

Figure 2.3. NMDS based on Bray-Curtis dissimilarity of 16S rRNA gene sequences from the ninety-six microcosms and the slurry sample (S - T0), marked in red. Samples grouped according to the salinity in different colored polygons, which legend is on the right-side of the plot.

Aiming to identify characteristic OPUs of a specific salinity, microcosms at 30% saline were considered to resemble the original conditions of the community since no statistically significant differences were found with the community of the inoculum (Kolmogorov-

Smirnov test and t-test; Supplementary Table S2.4), thus increasing robustness of statistical test. The number of OPUs with statistically significant differences (abs(log2 fold change) > 2 and p-value < 0.05) between the microcosms at the different salinities and 30% salinity increased as salinity decreased (Supplementary Figure S2.2), with 9 OPUs being statistically more abundant at salinity 25%, increasing to 300 at 5% salinity. When only the core community was considered (relative abundance ≥ 1%), the number of OPUs displaying statistically significant differences at a specific salinity is reduced by 30-40% (Supplementary Figure S2.2B and spreadsheet Tables ST2.1, ST2.2 and ST2.3). A total of 61 species were not detected in any of the twelve samples of 5%, 9 for Archaea and 52 for Bacteria (spreadsheet Tables ST2.1, ST2.2 and ST2.4).

Dominant species (≥ 5% relative sequence abundance) at each salinity, included OPUs affiliated to Unc. 20c-4, Unc. DHVEG-6, Unc. *Anaerolineaceae* and Unc. *Desulfovermiculus* sp. at 5%, Unc. MSBL1 and Unc. *Marinilabiliaceae* at 10-30% and Unc. *Halanaerobium* sp. and Unc. KTK 4A at salinity of 30%. No dominant OPU at the end of the experiment displayed a relative abundance higher than 5% in the inoculum (S; Table 2.1 and spreadsheet Table ST2.5).

Table 2.1. Major OPUs from 16S rRNA gene sequences analyzed from the ninety-six microcosms and S, with relative abundances ≥ 5% (at least in one sample) for Archaea (ARCH) and Bacteria (BACT). First column (from left to right) is the OPU number, the following five columns show the taxonomic affiliation of the closest relative sequence used as reference (phylum, class, order, family and genus/species, respectively). Those OPUs that are representatives of each salinity (statistically significant: abs(log2 fold change) > 2 and p-value < 0.05) are grey shaded in the last eight columns. Relative abundances data are shown in the spreadsheet Tables ST2.1 and ST2.2.

ARCH	phylum	class	order	family	genus - species	5%	10%	12%	15%	18%	20%	25%	30%
4	*Aenigmarchaeota*	-	-	-	Deep Sea Euryarchaeotic Group (DSEG)								
23	*Euryarchaeota*	-	-	-	Unc. KTK 4A								
25	*Euryarchaeota*	-	-	-	Unc. Marine Benthic Group D - DHVEG-1								
62	*Euryarchaeota*	*Halobacteria*	*Halobacteriales*	*Halobacteriaceae*	Unc. *Halobacteria* class								
136	*Euryarchaeota*	*Thermoplasmata*	*Thermoplasmatales*	-	Unc. 20c-4								
157	*Euryarchaeota i.s.*	-	-	-	Unc. MSBL1								
167	*Euryarchaeota i.s.*	-	-	-	Unc. MSBL1								
192	*Woesearchaeota*	-	-	-	Unc. DHVEG-6								
202	*Woesearchaeota*	-	-	-	Unc. DHVEG-6								
BACT	**phylum**	**class**	**order**	**family**	**genus - species**	**5%**	**10%**	**12%**	**15%**	**18%**	**20%**	**25%**	**30%**
18	-	-	-	-	Unc. TM6 (*Dependentiae*)								
24	-	-	-	-	Unc. WS1								
39	*Acetothermia*	-	-	-	Unc. *Acetothermia*								
156	*Bacteroidetes*	*Bacteroidia*	*Bacteroidales*	*Marinilabiliaceae*	Unc. *Marinilabiliaceae*								
157	*Bacteroidetes*	*Bacteroidia*	*Bacteroidales*	*Marinilabiliaceae*	Unc. *Marinilabiliaceae*								
165	*Bacteroidetes*	*Bacteroidia*	*Bacteroidales*	*Marinilabiliaceae*	Unc. *Marinilabiliaceae*								
276	*Chlamydiae*	*Chlamydiia*	*Chlamydiales*	*Simkaniaceae*	Unc. *Simkaniaceae*								
281	*Chlorobi*	*Chlorobia*	*Chlorobiales*	*Chlorobiaceae*	*Prosthecochloris vibrioformis*								
305	*Chloroflexi*	*Anaerolineae*	*Anaerolineales*	*Anaerolineaceae*	Unc. *Anaerolineaceae*								
318	*Chloroflexi*	*Anaerolineae*	*Anaerolineales*	*Anaerolineaceae*	Unc. *Anaerolineaceae*								
385	*Firmicutes*	*Bacilli*	*Bacillales*	*Bacillaceae*	*Halobacillus halophilus*								
386	*Firmicutes*	*Bacilli*	*Bacillales*	*Bacillaceae*	*Halobacillus mangrovi*								
409	*Firmicutes*	*Bacilli*	*Caryophanales*	*Bacillaceae*	*Paraliobacillus ryukyuensis*								
414	*Firmicutes*	*Bacilli*	*Caryophanales*	*Bacillaceae*	Unc. *Bacillus* sp.								
425	*Firmicutes*	*Bacilli*	*Caryophanales*	*Bacillaceae*	*Virgibacillus salarius*								
460	*Firmicutes*	*Clostridia*	*Eubacteriales*	-	Unc. MAT-CR-H4-C10								
469	*Firmicutes*	*Clostridia*	*Eubacteriales*	*Christensenellaceae*	Unc. *Christensenellaceae* R-7 group								
555	*Firmicutes*	*Clostridia*	*Halanaerobiales*	*Halanaerobiaceae*	Unc. *Halanaerobium* sp.								
559	*Firmicutes*	*Clostridia*	*Halanaerobiales*	*Halanaerobiaceae*	Unc. *Halanaerobium* sp.								
564	*Firmicutes*	*Clostridia*	*Halanaerobiales*	*Halanaerobiaceae*	Unc. *Halocella* sp.								
566	*Firmicutes*	*Clostridia*	*Halanaerobiales*	*Halanaerobiaceae*	Unc. *Halocella* sp.								
643	*Marinimicrobia*	-	-	-	Unc. SAR406 clade								
689	*Planctomycetes*	-	*Brocadiales*	*Brocadiaceae*	Unc. PB79								
1008	*Proteobacteria*	*Deltaproteobacteria*	*Desulfobacterales*	*Desulfobacteraceae*	Unc. *Desulfobacteraceae*								
1038	*Proteobacteria*	*Deltaproteobacteria*	*Desulfovibrionales*	*Desulfohalobiaceae*	Unc. *Desulfovermiculus* sp.								
1269	*Tenericutes*	*Mollicutes*	-	-	Unc. NB1-n								
1271	*Tenericutes*	*Mollicutes*	*Haloplasmatales*	*Haloplasmataceae*	*Haloplasma contractile*								

2.3. Ampicillin as effector on the prokaryotic communities

Ampicillin exerted an effect on alpha diversity. At low salinities Chao-1 for Archaea was higher in samples with ampicillin, increasing at 5% salinity in 80.8% with regard to the inoculum and only 35.9% without ampicillin. Bacteria displayed higher richness values at intermediate salinities (18%, 20% and 25%) when the antibiotic was present (Figures 2.2A and 2.2B and Supplementary Table S2.3). Interestingly, Shannon index increased from 15.6% to 19.1% in microcosms with 5% salinity and ampicillin, being especially higher than those at the same salinity but without ampicillin (-45.7% to -51.2%; Figures 2.2C and 2.2D and Supplementary Table S2.3). The addition of the antibiotic also caused changes in the dominance index (Figures 2.2E and 2.2F), decreasing at 5% of salinity for Archaea and increasing at 30% for Bacteria. As observed in the NMDS, samples grouped by the presence/absence of the antibiotic (dendrograms and NMDS based on Bray-Curtis dissimilarity, Figure 2.4 and Supplementary Figure S2.3) and at 5% salinity the effect of ampicillin was more notable. The communities assembled in the presence and absence of the antibiotic were statistically different (PCoA based in variance dispersion, Figure 2.5; clustering dendrograms based on Bray-Curtis dissimilarity applying the Mantel test ($p > 0.05$), Supplementary Figure S2.3; and betadisper multivariate analysis, Supplementary Figure S2.4).

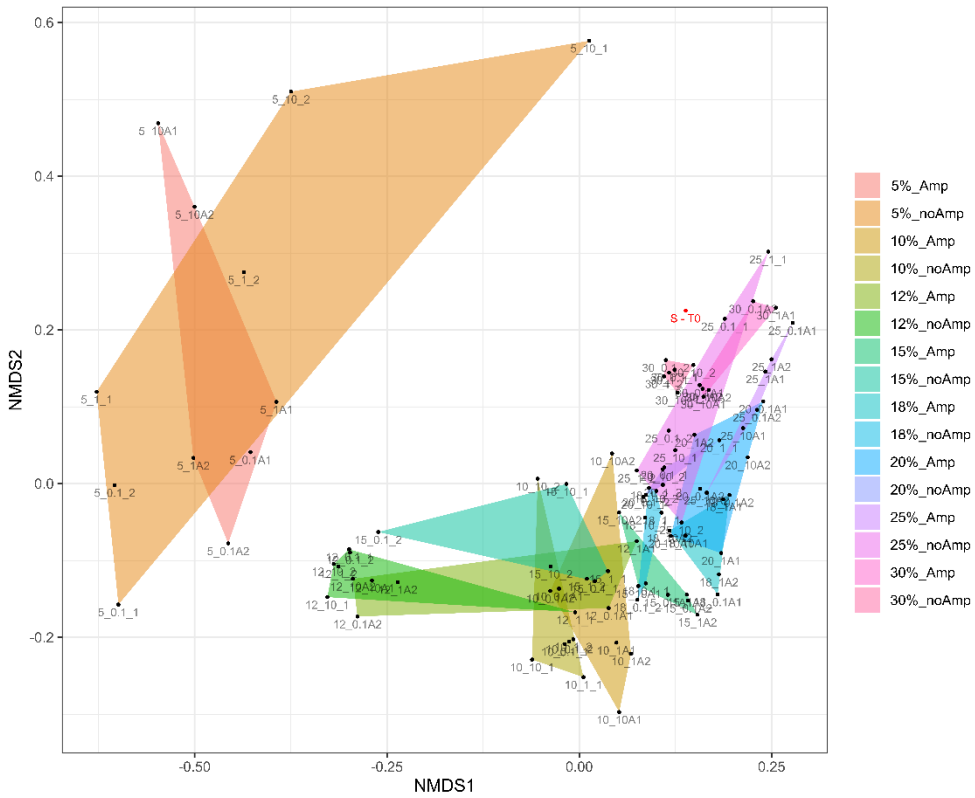

Figure 2.4. NMDS based on Bray-Curtis dissimilarity of 16S rRNA gene sequences from the ninety-six microcosms and the slurry sample (S - T0), marked in red. Samples grouped according to the salinity and ampicillin in different colored polygons, which legend is on the right-side of the plot. Polygons with ampicillin are defined with "_Amp", and without ampicillin with "_noAmp".

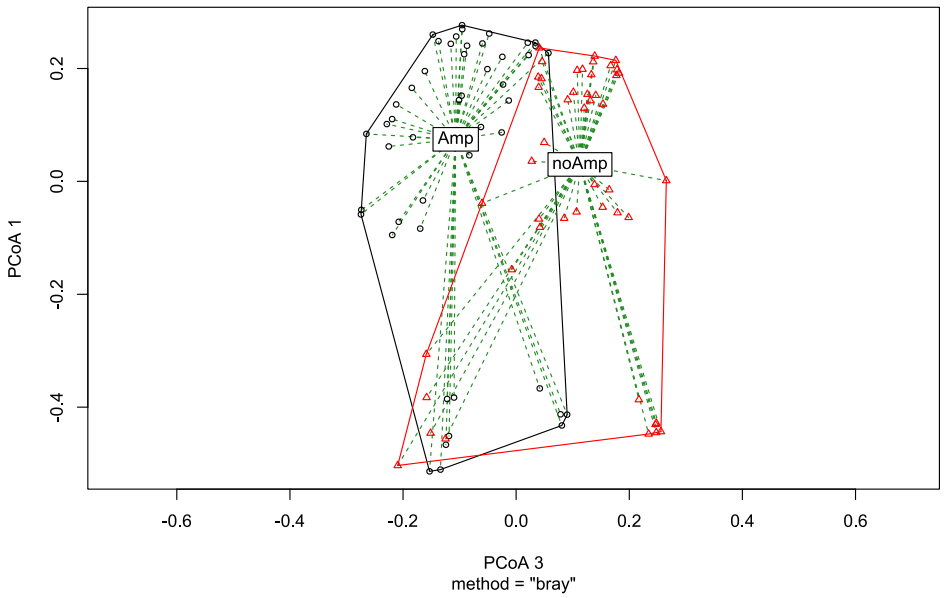

Figure 2.5. PCoA (Principal Coordinates Analysis) plot from analysis of multivariate homogeneity of groups dispersions (variances) applied to the ninety-six microcosms, attending to samples with ampicillin (in black) and without the antibiotic (in red).

When relative abundances of OPUs between the different salinities and the initial conditions (30% salinity) were compared, overall less OPUs were statistically more abundant in the presence of the antibiotic, especially at salinities below 15% (Supplementary Figure S2.2). *Sporosalibacterium* and *Brassicibacter* genera were not detected in microcosms with ampicillin at 5% salinity (spreadsheet Table ST2.6) while other species were not retrieved in samples amended with ampicillin at intermediate salinities, such as *Hydrogenedentes* at 10-15% salinity and the Marine Benthic Group D and DHVEG-1 at 15-18% salinity. The genus *Desulfovermiculus* and the family *Desulfobacteraceae* seemed to be affected for ampicillin. Whereas these taxa displayed lower abundances with ampicillin at salinities of 5-12%, no presence was detected at salinities of 15% and 30%. Some OPUs affiliated to the phylum *Acetothermia* displayed a different response to the presence of the antibiotic, with higher abundances with ampicillin at salinities of 5-10% for some species, while others were not detected with the antibiotic at 12-15% salinity (spreadsheet Table ST2.6). Contrarily, some taxa displayed higher abundances in samples with ampicillin, such as members associated to KTK 4A cluster at 5-20% salinity, *Salinibacter* genus at 5-15% salinity, taxa affiliated to MSBL1 as closest relative at all salinities but 10%, and *Christensenellaceae* R-7 group at 5, 10 and 12% salinity (spreadsheet Table ST2.7).

2.4. *Posidonia oceanica* influence on microbial community structures

Overall, the concentration of *Posidonia oceanica* substrate did not substantially affected alpha diversity. Clustering dendrograms based on Bray-Curtis distance (Supplementary Figures S2.3 and S2.5) showed the samples to cluster by substrate concentration, even being the effect of the antibiotic overall more important than the substrate (PCoA based in variance dispersion within groups, Figure 2.6). For salinities of 5, 10, 12 and 25%, the substrate concentration caused more compositional differences (with Bray-Curtis dissimilarities ranging from 0.5 to 0.8; Supplementary Figure S2.5). A high number of OPUs (reaching values of 85) was statistically significant of a single salinity and with a specific concentration of *Posidonia* (abs(log2 fold change) > 2 and p-value < 0.05) and, although there were relevant OPUs detected at the three substrate concentrations as statistically significant, high differences in number of OPUs was always observed between the tested concentrations (spreadsheet Table ST2.8).

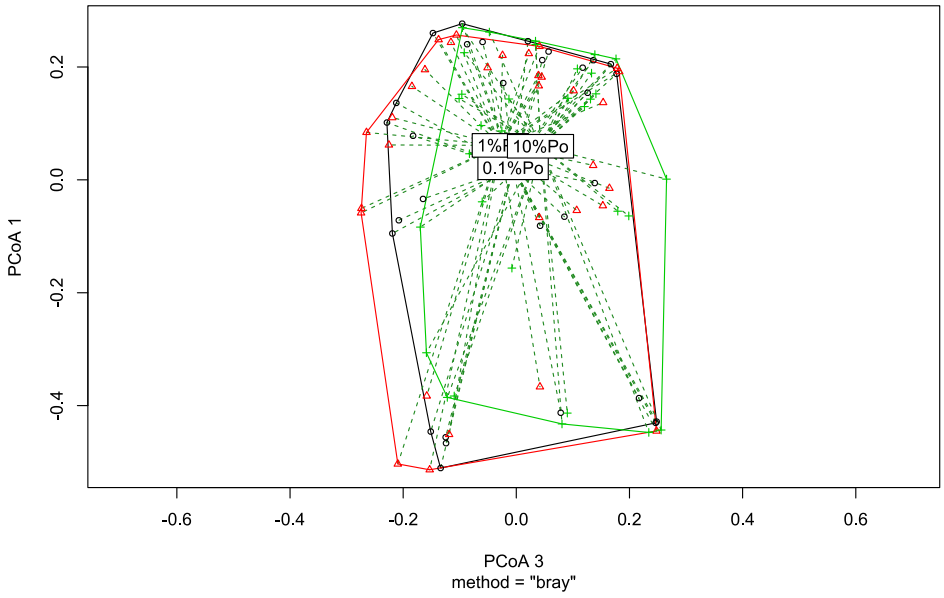

Figure 2.6. PCoA (Principal Coordinates Analysis) plot from analysis of multivariate homogeneity of groups dispersions (variances) applied to the ninety-six microcosms attending to the three substrate concentrations (0.1% Po, 1% Po and 10% Po), grouped in black, red and green colors.

2.5. Dilution effect in stochastic processes controlling the microbial ecosystem

Phylogenetic inference was evaluated taking into account the salinity, the presence or absence of ampicillin and substrate concentration. In general, beta-nearest taxon index (ßNTI) values from pairwise comparisons between the inoculum and the microcosms showed a nondiscriminatory distribution, where no data exceeded the statistically significant boundary

(|ßNTI| > 2). Overall, ßNTI in the Archaea domain showed that the phylogenetic turnover is close to the null expectation, being the community mainly influenced by stochastic factors (Figures 2.7A and 2.7B). The stochasticity decreased as salinity decreases since the replicates shows less dispersion in the index (Figure 2.7C). In Bacteria, the phylogenetic turnover is lower than in Archaea as ßNTI is closer to -1, with the exception of 5% salinity samples where a higher phylogenetic turnover is observed, being ßNTI > 1 for some of the samples. As for Archaea, and to a minor extent, the stochasticity seems to increase with salinity in Bacteria, as the dispersion between replicates increase with the exception of 5% salinity, where ßNTI of duplicates is also not reproducible (Figures 2.7A, 2.7B and 2.7C). Raup-Crick metric based on Bray-Curtis dissimilarities (RC_{bray}) showed a fairly defined pattern with a descending trend as salinity increased (Figures 2.7D, 2.7E and 2.7F). Therefore, there was a transition in taxonomic turnover from low to high as samples were diluted and salinity decreased from the initial condition of salt saturation. According to this index, Archaea was more influenced by stochasticity since, overall, RC_{bray} was closer to null expectation and the replicates were more dissimilar than in Bacteria.

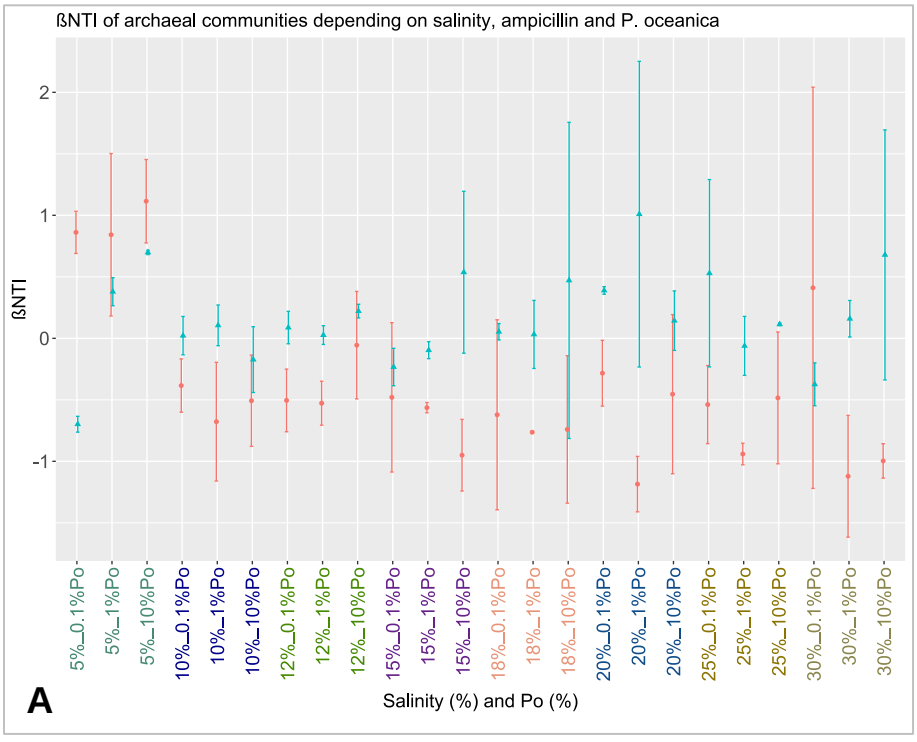

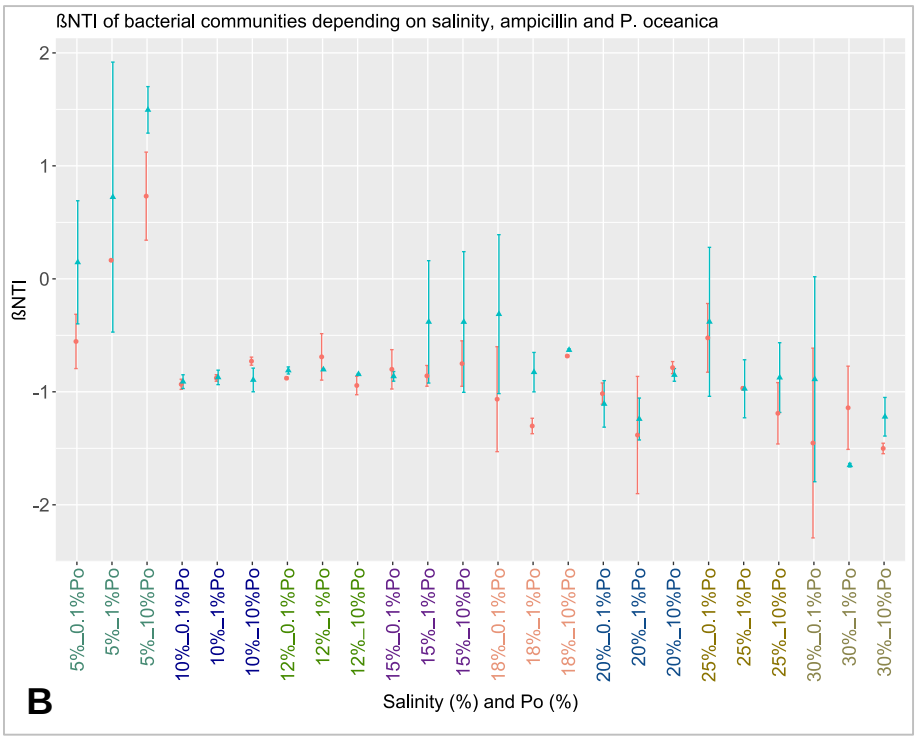
ßNTI of bacterial communities depending on salinity, ampicillin and P. oceanica
ßNTI
2
1
0
-1
-2
5%_0.1%Po
5%_1%Po
5%_10%Po
10%_0.1%Po
10%_1%Po
10%_10%Po
12%_0.1%Po
12%_1%Po
12%_10%Po
15%_0.1%Po
15%_1%Po
15%_10%Po
18%_0.1%Po
18%_1%Po
18%_10%Po
20%_0.1%Po
20%_1%Po
20%_10%Po
25%_0.1%Po
25%_1%Po
25%_10%Po
30%_0.1%Po
30%_1%Po
30%_10%Po
B
Salinity (%) and Po (%)

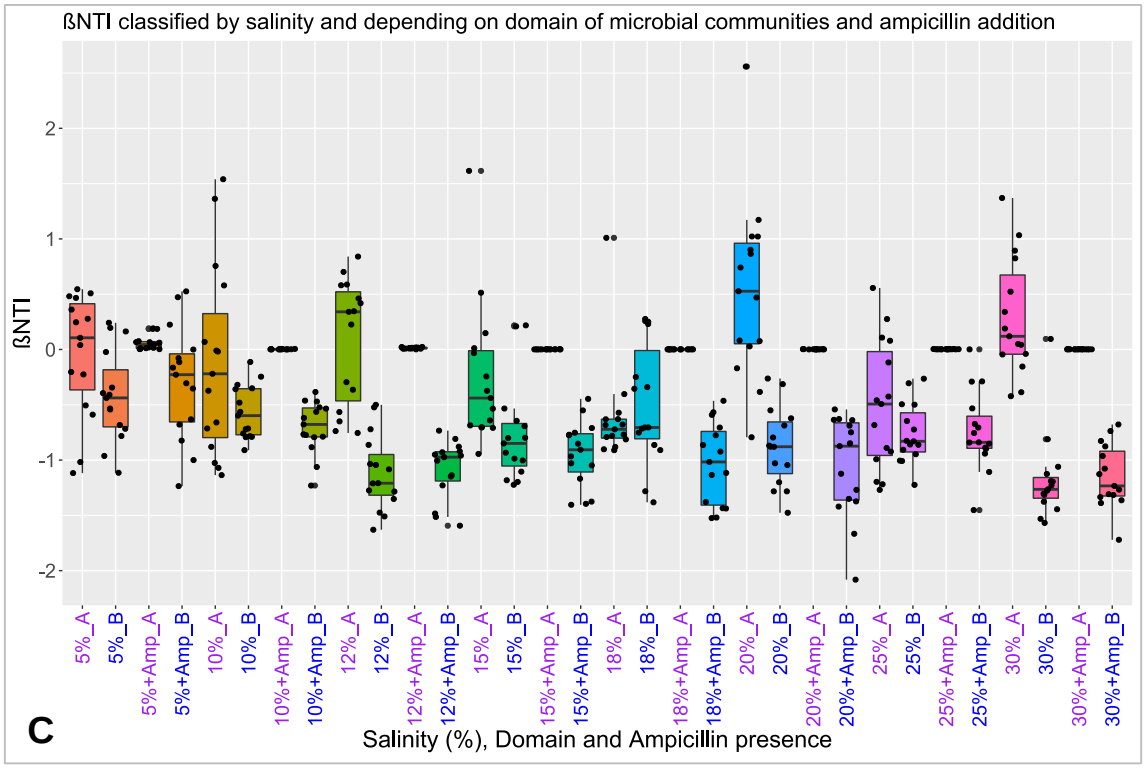
ßNTI classified by salinity and depending on domain of microbial communities and ampicillin addition
ßNTI
2
1
0
-1
-2
5%_A
5%_B
5%+Amp_A
5%+Amp_B
10%_A
10%_B
10%+Amp_A
10%+Amp_B
12%_A
12%_B
12%+Amp_A
12%+Amp_B
15%_A
15%_B
15%+Amp_A
15%+Amp_B
18%_A
18%_B
18%+Amp_A
18%+Amp_B
20%_A
20%_B
20%+Amp_A
20%+Amp_B
25%_A
25%_B
25%+Amp_A
25%+Amp_B
30%_A
30%_B
30%+Amp_A
30%+Amp_B
C
Salinity (%), Domain and Ampicillin presence

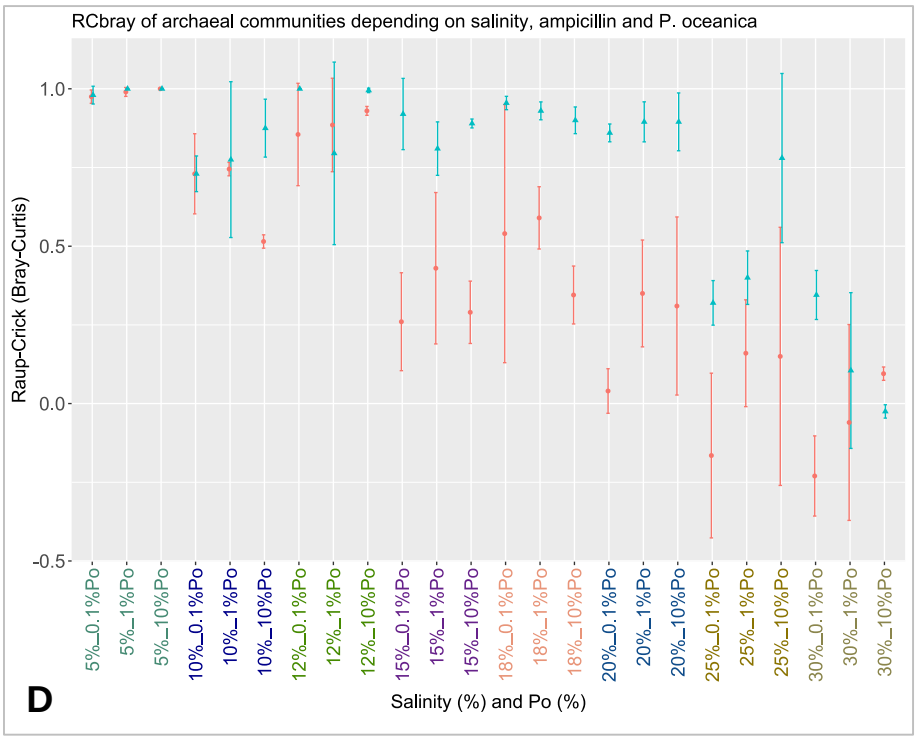
RCbray of archaeal communities depending on salinity, ampicillin and P. oceanica
Raup-Crick (Bray-Curtis)
1.0
0.5
0.0
-0.5
5%_0.1%Po
5%_1%Po
5%_10%Po
10%_0.1%Po
10%_1%Po
10%_10%Po
12%_0.1%Po
12%_1%Po
12%_10%Po
15%_0.1%Po
15%_1%Po
15%_10%Po
18%_0.1%Po
18%_1%Po
18%_10%Po
20%_0.1%Po
20%_1%Po
20%_10%Po
25%_0.1%Po
25%_1%Po
25%_10%Po
30%_0.1%Po
30%_1%Po
30%_10%Po
Salinity (%) and Po (%)
D

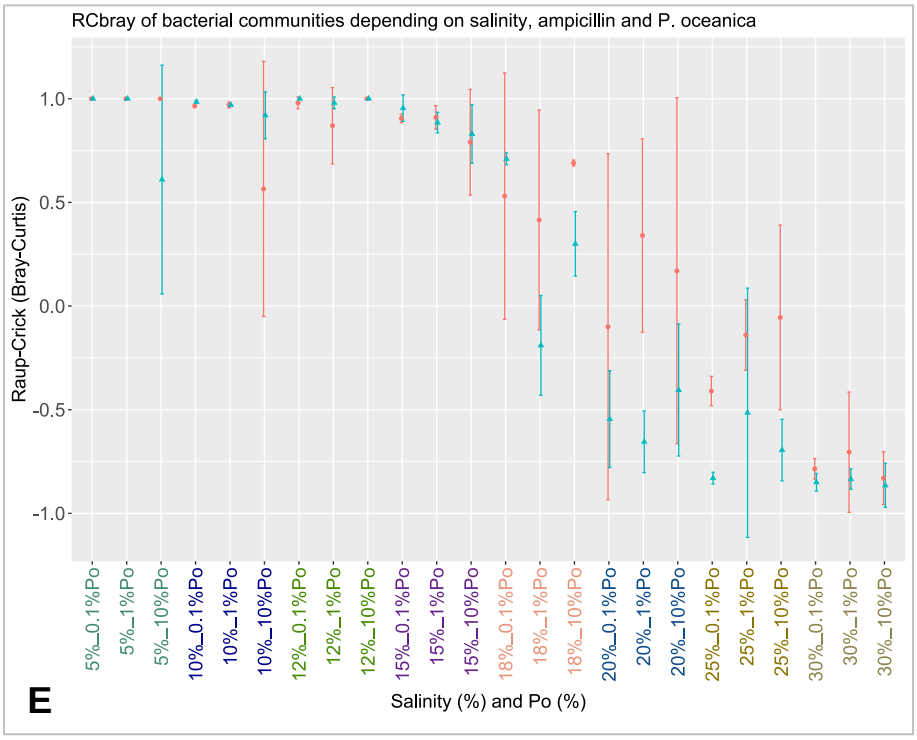
RCbray of bacterial communities depending on salinity, ampicillin and P. oceanica
Raup-Crick (Bray-Curtis)
1.0
0.5
0.0
-0.5
-1.0
5%_0.1%Po
5%_1%Po
5%_10%Po
10%_0.1%Po
10%_1%Po
10%_10%Po
12%_0.1%Po
12%_1%Po
12%_10%Po
15%_0.1%Po
15%_1%Po
15%_10%Po
18%_0.1%Po
18%_1%Po
18%_10%Po
20%_0.1%Po
20%_1%Po
20%_10%Po
25%_0.1%Po
25%_1%Po
25%_10%Po
30%_0.1%Po
30%_1%Po
30%_10%Po
Salinity (%) and Po (%)
E

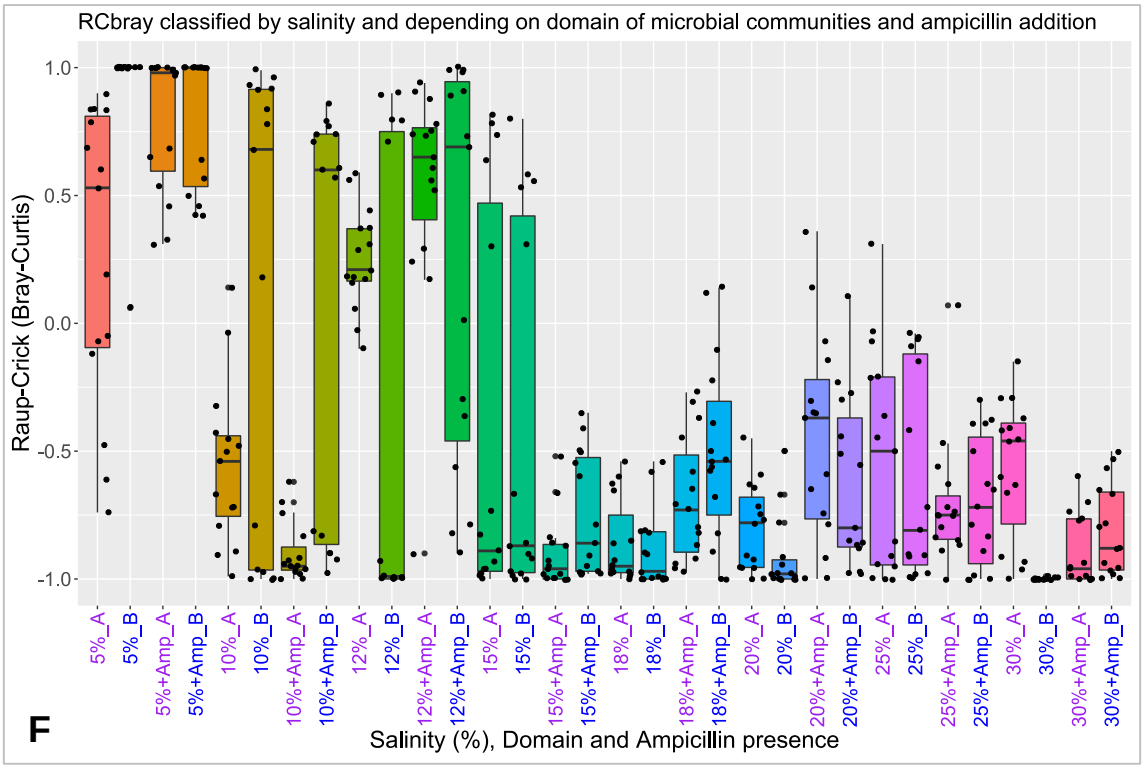

Figure 2.7. ßNTI values in relation to S of the microcosms depending on salinity (5% - 10% - 12% - 15% - 18% - 20% - 25% - 30%), ampicillin and *Posidonia oceanica* concentration (0.1% - 1% - 10%), for Archaea (**A**) and Bacteria (**B**). In the x axis, from left to right, the samples are ordered from lowest to highest salinity, whereas samples with and without ampicillin are shown in red circles and blue triangles, respectively. **C**. ßNTI values classified by salinity of the microcosms depending on domain (Archaea-A or Bacteria-B), salinity and ampicillin. In the x axis, from left to right, the samples are ordered from lowest to highest salinity, with the two domains colored in purple and blue, and separated according to ampicillin. Raup-Crick values based on Bray-Curtis dissimilarity in relation to S of the microcosms depending on salinity, ampicillin and *Posidonia oceanica* concentration for Archaea (**D**) and Bacteria (**E**). In the x axis, from left to right, the samples are ordered from lowest to highest salinity, whereas samples with and without ampicillin are shown in red circles and blue triangles, respectively. **F**. Raup-Crick values based on Bray-Curtis dissimilarity and classified by salinity of the microcosms depending on domain (Archaea or Bacteria), salinity and ampicillin. In the x axis, from left to right, the samples are ordered from lowest to highest salinity, whereas the two domains colored in purple and blue, and classified in accordance to the ampicillin presence.

To quantify ecological stochasticity between the different conditions applied in microcosms, stochasticity (ST) and normalized stochasticity (NST) ratios were calculated, displaying values >55% and indicating the stochasticity dominance either in Archaea or Bacteria domains (Supplementary Figures S2.6A and S2.6B). The ST and NST ratios were above 70% and 60%. In Archaea, NST ratio decreased with substrate concentration while the opposite was observed in Bacteria (Supplementary Figures S2.6C and S2.6D). Furthermore, when we compared the ampicillin effect in relation to the inoculum, in general stochasticity increased as salinity did, ranging from 54% to 100%, excepting few samples with 5 and 12% salinity which displayed values below the boundary of 50% in archaeal domain

(Supplementary Figure S2.6E). Modified stochasticity ratios (MST) exhibited a clear pattern of gradual transition of determinism dominance in the lowest salinities to stochasticity at those highest, denoting the differences between domains and especially among salinities. (Figure 2.8A). Accordingly, the standard effect size (SES), which measures the magnitude of the experimental effects, displayed decreasing values as salinity increased, being, therefore, at 5% of salinity where the effects of ampicillin were more relevant (Figure 2.8B).

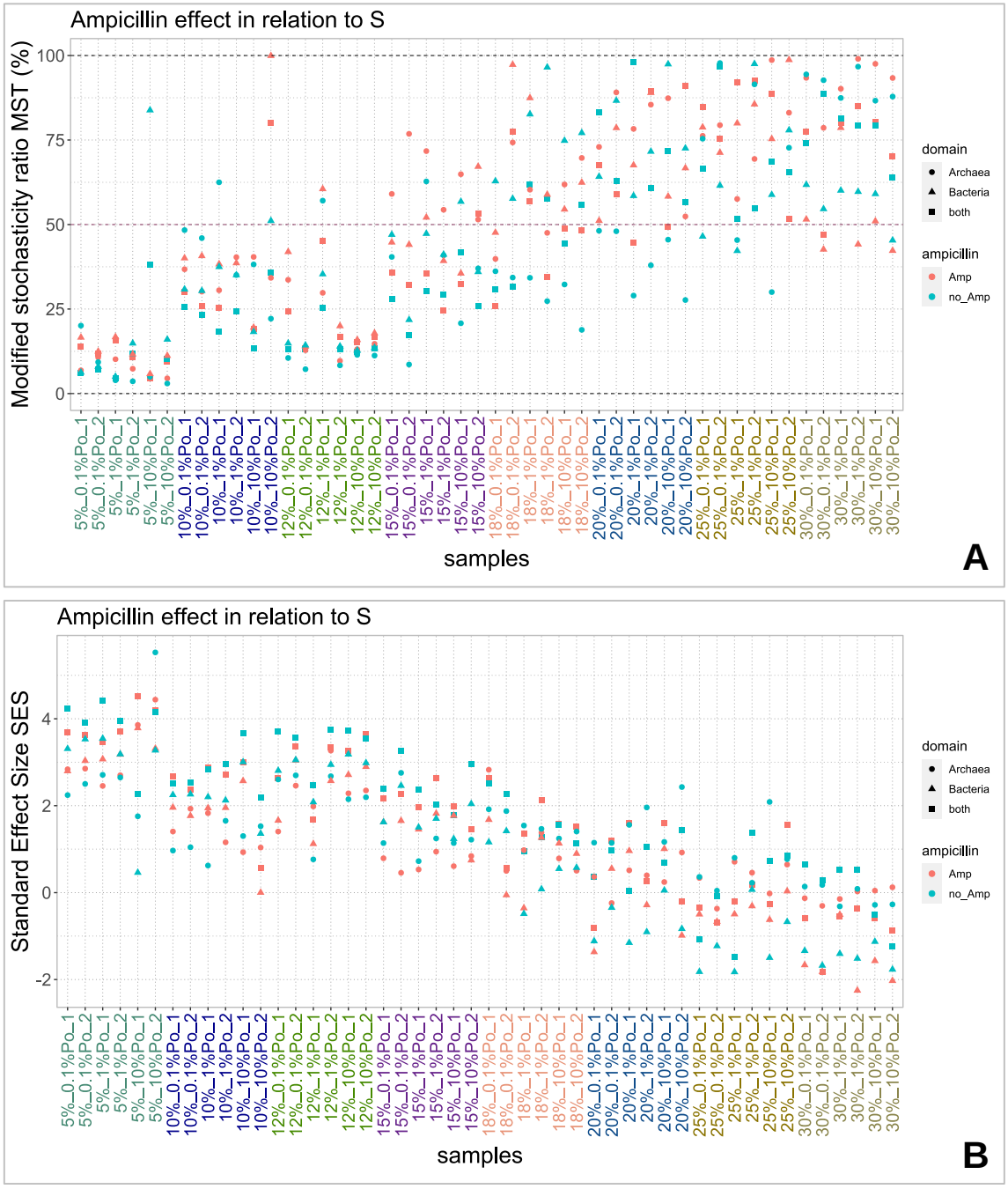

Figure 2.8. Modified stochasticity ratio (MST; **A**) in percentage, and Standard Effect Size (SES; **B**) regarding to the ampicillin effect in relation to S for the microcosms. Data from Archaea, Bacteria or both domains are represented in circles, triangles and squares, respectively, whereas samples with or without ampicillin are shown in red and blue, respectively.

2.6. Discussion

The hypersaline anaerobic sediments underlying brines from S'Avall solar salterns have been the focus of several related studies since initial results reported a highly diverse community thriving in this ecosystem (López-López *et al.*, 2010, 2013). Hypersaline anaerobic sediments have been scarcely studied and most investigations focused on the effect of salinity on microbial diversity, disregarding other factor that could be of great importance (Jiang *et al.*, 2007; Webster *et al.*, 2015; Xie *et al.*, 2017). Even though salinity has been reported as the main selective factor in hypersaline ecosystem, minor members of the community would also be affected by other factors, such as pH, total organic carbon, UV radiations or depth (Swan *et al.*, 2010; Sierocinski *et al.*, 2017; Xie *et al.*, 2017; Viver et al., 2019).

The effect of salt concentration was evaluated in a broad salinity gradient (5-30%) to study its effect both in halotolerant and extremophile microorganisms. The results here presented show that salinity acted as determinant factor during community assembly and, although the main diversity was conserved, a phylogenetic turnover was observed between microcosms at different salinities. The selective role of salinity has been reported before in saline soils (Xie *et al.*, 2017), hypersaline sediments from lakes (Jiang *et al.*, 2007) and hypersaline soda lakes (Vavourakis *et al.*, 2018), and sediment slurries of a solar saltern of Eilat (Israel; Sørensen *et al.* 2004) or a salt spring of British Columbia (Walsh *et al.*, 2005). Here, the salinity dilution affected community alpha diversity, especially in the archaeal domain. In the experiment, we progressively diluted brines to decrease the salinity, thus the lower is the salinity in the microcosms, the higher was the perturbation. Indeed, samples at 5% salinity displayed the highest compositional changes with regard to the inoculum. This is due to the fact that the sediments used to amend the microcosms had a salinity of 34.4% and the microbial community was adapted to salt saturation. At high salinities, communities are dominated by extreme halophilic Archaea, therefore decreasing the salt concentration would impact archaeal diversity to a higher extent. Accordingly, the increment of prokaryote cell number and the reduction of their diversity as salinity increases has been described along salinity gradients (Pedrós-Alió *et al.*, 2000; Benlloch *et al.*, 2002). Bacterial alpha diversity in turn, decreased with salinity, being highest at 5%. This would evidence the importance of rare taxa in maintaining community diversity, which would act as a seed bank increasing in relative abundance when the conditions are favorable. Salinity influences also nutrient availability, thus shaping microbial composition which, in turn, alter the microbial metabolic activity (Webster *et al.*, 2015; Zhang *et al.*, 2017). Here, core community OPUs affiliated with sulfate-reducers (e.g. *Desulfatiglans, Desulfovermiculus, Desulfobulbus* and *Sulfobacillus* genera) and microorganisms with inferred methanogenic metabolism (e.g. Uncultured MSBL1). These metabolic groups displayed, generally, an opposite relative abundance pattern, with sulfate-reducers decreasing with salinity and methanogens increasing as salt concentration did,

especially at 25% were only the putative methanogens dominated (Supplementary Table S2.5 and Figures S2.7 and S2.8; and spreadsheet Table ST2.3). It has been previously reported methanogens to be affected by sulfate-reduction at salinities below 18%, the latter displaying an optimum at 10-12% and being strongly inhibited at 21.5 (Sørensen *et al.*, 2004). OPUs affiliated with taxa involved in fermentative processes were retrieved at all salinities, however, a taxonomic turnover in the dominance of putative fermenters due to salinity was observed, with Unc. *Marinilabiliaceae*, Unc. 20c-4 and Unc. PB79 dominating at 5-12% and *Marinilabiliaceae* family, *Halanaerobium* genus, Unc. KTK 4A cluster and *Halobacteria* class dominating at 15-30%. This evidences a niche partitioning of fermenters in the different salinities, which belonged to the rare biosphere in the inoculum and increased in relative abundance due to the change of environmental conditions. Moreover, this rare biosphere, together with the importance of functional redundancy, ensures the maintenance of ecosystem functioning.

Aiming to study the effect of salinity dilution on communities with an additive perturbing factor, ampicillin was added to microcosms and compared to those without the antibiotic. This set-up allowed us to assess taxonomical changes at the different salinities and the ability to resist to the increasing perturbation caused by the dilution, when part of the community members had been eliminated. As far as we know, the study of antibiotic effects in hypersaline anoxic environments has never been performed. Previous studies have assessed the effect of this antibiotic in other ecosystems such as soils, wastewater or freshwater (Ye *et al.*, 2020), where ampicillin decreased the abundance of certain community members, hindering relevant ecosystem metabolic functions (Ferrer *et al.*, 2017; Baumgartner *et al.*, 2020; Ye *et al.*, 2020). In this study, the addition of ampicillin (5 mg/mL) in microcosms reduced community bacterial alpha diversity. Beta diversity between communities in microcosms with and without ampicillin displayed an increasing trend with dilution, although its real effect could be partially hidden by the salinity factor. The higher observed divergence between microcosms with and without antibiotic at lower salinities is related to the fact that ampicillin overall targets susceptible, usually gram-positive, bacteria, which are more abundant at lower salinities. Interestingly, archaeal alpha diversity at 5% salinity was higher in microcosms with ampicillin. This could be related to the emergence of new niches to be colonized due to the elimination of bacterial groups that are sensitive to the antibiotic, such as *Anaerolinea* and *Caldilinea* genera whose abundance decreased with ampicillin. Indeed, some taxa increased in abundance at low salinities when the antibiotic was added, i.e. members associated to KTK 4A, MSBL1, *Christensenellaceae* R-7 group, *Anaerolineaceae* and *Simkaniaceae* families or *Salinibacter* sp., the dominant bacterial taxa in hypersaline aerobic environments, for which high abundances in this anaerobic ecosystem were reported (Font-Verdera *et al.*, 2021). Overall, no growth has been detected below 15% of salinity (Antón *et al.*, 2002), and maybe this could be a new understudied species or genus. The effect of carbon substrate concentration was also assessed not observing an important effect on community

diversity nor affecting the organic carbon content of microcosms. This could be related with a low presence of microorganism able to hydrolyze *P. oceanica* which would make carbon available to fermenters. The weak observed effect of *P. oceanica* concentration on community structure might be linked to immigrant microbial populations present in the substrate leaves.

The effect of deterministic and/or stochastic factors on community assembly was assessed by means of null model analysis. In general, both phylogenetic and taxonomic turnover was low and overall not different from the null expectation, therefore, stochasticity generally prevailed. Salinity was the major ecological factor involved in community assembly, being higher the stochasticity and lower the effect size as the salinity increased. The original community belonged to a highly adapted microbiome to hypersaline and anaerobic conditions. In such ecological state, selection eventually had led to a stable community with low turnover where drift became the most relevant factor (Stegen *et al.*, 2012; Liébana *et al.*, 2019). Consequently, Archaea was more affected by stochasticity than Bacteria due to the dominance of the former at higher salinities. The environmental salt dilution exerted a selection of those community members able to thrive at lower salinities (Langenheder *et al.* (2017). Indeed, turnover between replicates decreased as salinity decreased, revealing determinism to gain relevance with dilution. Moreover, the importance of the substrate concentration and, more notably, by the ampicillin addition was also observed, exerting slightly different effects in the archaeal or bacterial communities. Salinity acted as a selection force and ampicillin applied a selective pressure that changed the structure of microbial populations, consistent with other studies (Ye *et al.*, 2020), whilst *P. oceanica* exerted a weak effect. The manipulation of natural and closed ecosystems applying a dilution gradient has its drawbacks. The loss of rare taxa and the overrepresentation of others influence the taxonomic structure and the metabolic processes associated to them (Sierocinski *et al.*, 2018). We should also be aware of the possible modulation of specific gene expression by microbial organisms to endure the changing conditions, rather than undergoing fluctuations in their abundances (Orellana *et al.*, 2018), an issue that might be explored in a future research.

CHAPTER 3

Chapter 3. Improvement and selection of methanogenic consortia. Description of the most efficient microcosms in methane generation

This chapter describes the selection of the most effective consortia in accordance with methanogenic yields, quantified by means of gas chromatography. The enrichment of the most efficient cultures, and the subsequently characterization of the selected halophilic methanogenic consortia using metagenomics are detailed. The research includes the description of microbial diversity, the main inferred metabolisms and the replication cellular activity of the enriched prokaryotic communities. This investigation entails the improvement of halophilic methanogenic consortia in laboratory conditions and the discover of putatively efficient anaerobic communities in generation of high yields of methane with the suitable conditions.

3.1. Enrichment and selection of the most productive microcosms in methane (CH_4) yield

This analysis was based on the hypersaline anaerobic sediments from the S'Avall solar salterns (Font-Verdera *et al.*, 2021), and specially focused on the evaluation of the potential generation of methane from the ninety-six microcosms previously described in Section IV. Chapter 2 (Figure 2.1A). These microcosms (Supplementary Figure S3.1) were incubated at 30ºC since December 2016 (time-zero conditions with no methane detection), and the CH_4 was quantified from October 2017 (287 days), to March 2021 (1539 days) in different time points (Figure 3.1).

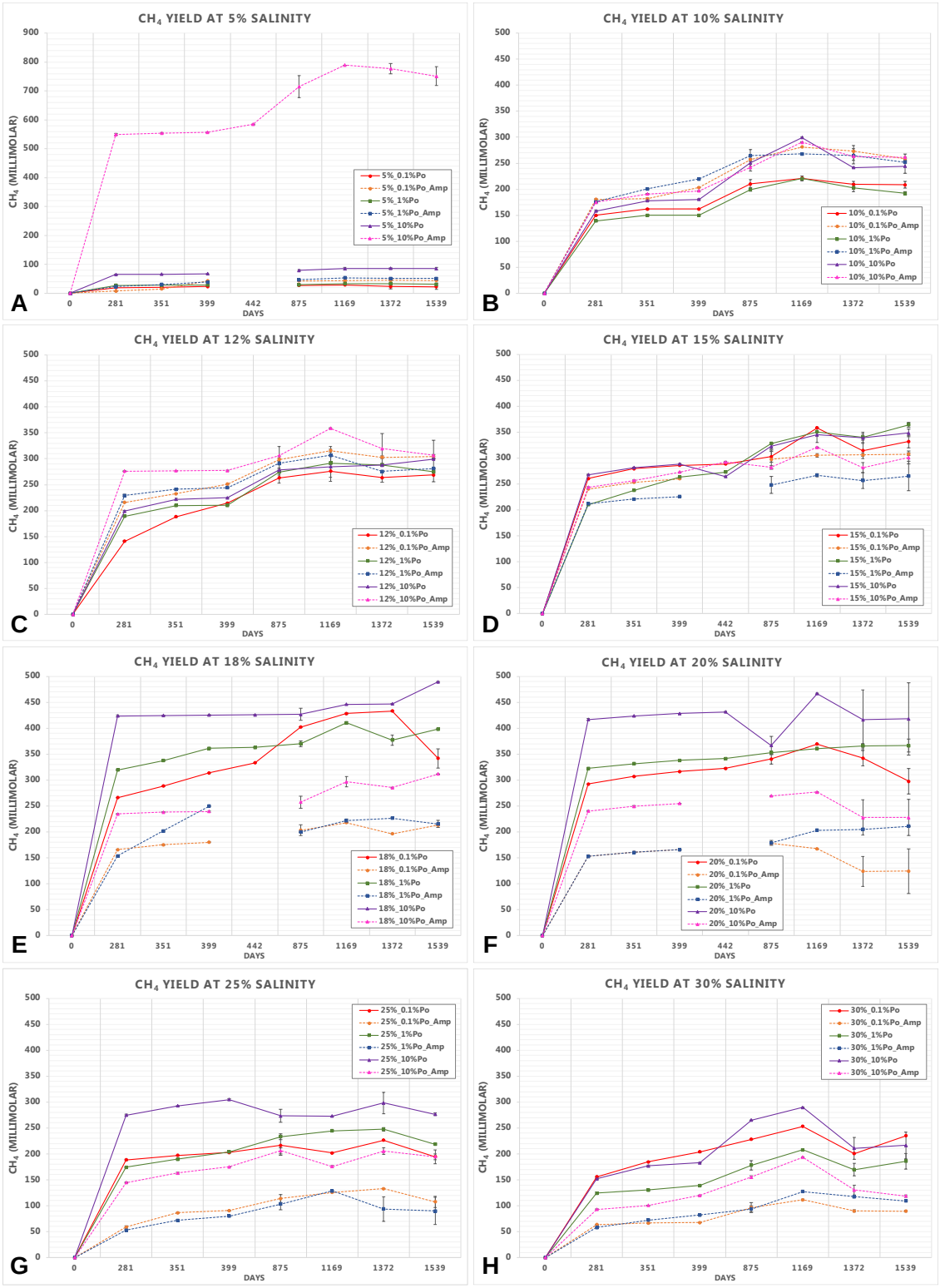

Figure 3.1. Methane yield of the ninety-six microcosms, divided in individual graphics (six in duplicate for each plot) for the eight salinities (**A**-**H**). In the x axis, the days when methane was measured, whereas in the y axis the molarity (in millimolar) of CH_4 are displayed. Different colors are used for the six samples, with dashed or continuous lines for microcosms with ampicillin or without it, and standard deviations for each duplicate are shown.

In general, the patterns in CH_4 production followed a logarithmic model for all salinities. In this type of model, the logarithm is always increasing, although its growth is very moderate as values increase in the x axis. In this case, methane concentration experienced a noticeable increment during the first year, whereas a more lineal trend was observed until the final measurement. Conspicuously, sample 5%_10%Po_Amp at 5% salinity (Figure 3.1A), displayed the highest molarity value (782.2 mM at 1169 days), well above the average regarding to the other samples (with a maximum of 85.8 mM at 1372 days). In the salinities of 10% and 12% (Figures 3.1B and 3.1C), all samples presented the same pattern and the microcosms with ampicillin displayed higher methane concentrations (~290 mM and ~359 mM for the 10% and 12% salinity, respectively). At salinity of 15% (Figure 3.1D), methane generation yields showed a moderate gain after 281 days, reaching the maximum of ~364 mM for 15%_1%Po, where the concentrations of other samples were overlapped but those with ampicillin on the top. On the other hand, the increase experienced after 281 days was more reduced for the salinities of 18%, 20%, 25% and 30% (Figures 3.1E, 3.1F, 3.1G and 3.1H), displaying the samples without antibiotic always higher concentrations with a maximum of ~489 mM for 18%_10%Po at 1539 days, and with lower CH_4 molarities as salinity increased. Microcosms with a substrate concentration of 10% *Po* exhibited the most elevated concentrations in all salinities (also depending on ampicillin), with the exception of 15% salinity, where those samples with 1% *Po* showed the highest molarities (Figure 3.1).

3.2. Selection and subculture of the most efficient methane production microcosms

To select those microcosms, which potentially could achieve high CH_4 yields, the most efficient was chosen in January 2018, after 399 days since their preparation (Supplementary Figure S3.1). These measurements indicated that, at that time point, the twelve microcosms that accumulated more gas methane were one at 5% of salinity (with 10% *Po* and ampicillin), four at 15% (the three concentrations of substrate without ampicillin, and one at 10% *Po* with ampicillin), three at 18% and 20% (each one with 0.1%, 1% and 10% *Po* without ampicillin) and one at 25% with 10% *Po* (Supplementary Table S3.1). The methane concentrations of this group ranged from 260 mM (15%_1%Po_Amp) to 560 mM (5%_10%Po_Amp).

For the purpose of obtaining the best methane consortium, two different cultivation conditions were applied to the selected microcosms (Supplementary Table S3.1). Acetate (10 mM), trimethylamine (10 mM) and formate (50 mM; designated as ATF) were added to a set of twelve new prepared microcosms (at same conditions of salinity, ampicillin and substrate concentration), whereas another set remained unamended (Supplementary Figure S3.1). Methane generation was estimated for these twenty-four microcosms, and no relevant peak signal was obtained for almost all samples, with the exception of microcosms at 5% of salinity

with 10% *Po* and ampicillin, either with or without ATF (Figure 3.2). CH_4 molarity was higher for supplemented sample (ATF), increasing up to 100 times the concentration obtained with the original microcosm, before subcultivation and enrichment (reaching a maximum molarity of ~69 M). The subcultured sample without ATF improved gas generation, but only in ~8 to ~19 M, after 86 days. The microbial communities of the two microcosms were assessed by means of metagenomics.

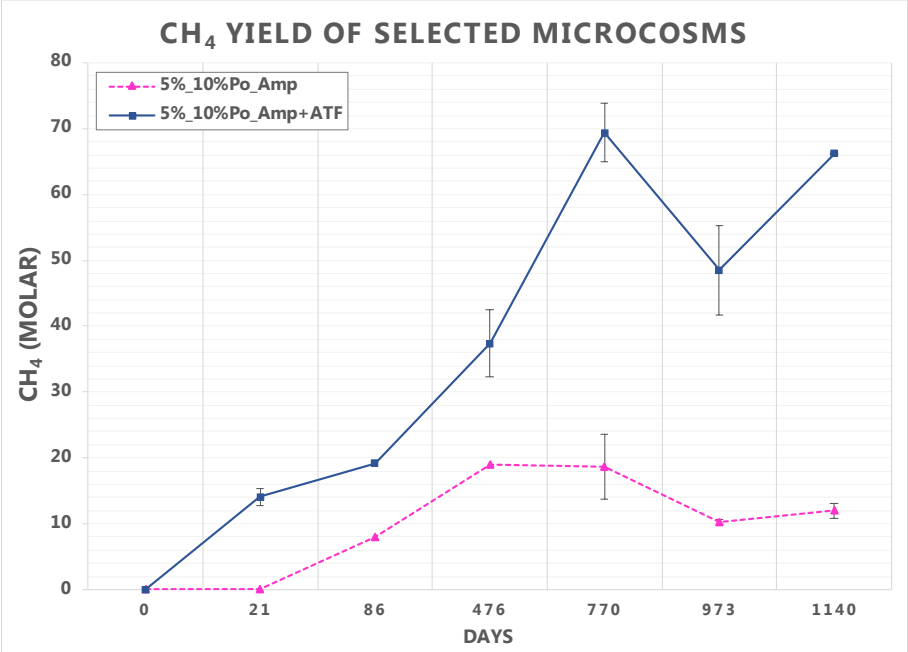

Figure 3.2. Methane yield of the two selected microcosms (5%_10%Po_Amp and 5%_10%Po_Amp+ATF). The time (in days) and the molarity (in molar) of CH_4 are displayed in the x and y axes, respectively. Microcosms with and without the supplement ATF are colored in blue and pink, respectively.

3.3. Metagenomic features and microbial diversity of the more efficient microcosms

The trimmed metagenomes, obtained from the two selected microcosms 5%_10%Po_Amp (designated as E) and 5%_10%Po_AmpATF (designated as ES), had a size of 64.6 and 70.7 million reads, respectively. The read length average of E was 120.5 ± 33.5 pb, whereas 127.4 ± 30.8 pb for ES, and 94,525 and 112,841 contigs with a length greater than 500 bp after assembly were obtained, respectively (Supplementary Table S3.2). The coverage of both metagenomes was ~92.3% and the Nonpareil diversity index ~18, according to Nonpareil analyses. The two metagenomes yielded a total of 97 MAGs, 46 from E and 51 for the supplemented ES. Among this set of 97 MAGs, 20 MAGs affiliated with archaeal domain whereas the rest were Bacteria (Table 3.1 and Supplementary Tables S3.3 and S3.4).

A total of 9 genomospecies (Gsp) could be assigned as described genera, 20 at family rank, 26 at order rank, 16 to a class and 5 to described phyla. Among those, 21

genomospecies, represented by 42 MAGs with ANI values >99%, were recovered equitably from E and ES (Table 3.1 and Supplementary Tables S3.3, S3.4 and S3.5). Among the species, the most relevant genomospecies were identified as members of genera *Brevefilum* (Gsp14) and *Methanosarcina* (Gsp65), and families *Desulfovibrionaceae* (Gsp36), *Desulfohalobiaceae* (Gsp37), *Anaerohalophaeraceae* (Gsp51) and DHVEG-1 (Gsp67). Additionally, some genomospecies were affiliated with orders *Desulfarculales* (Gsp33) and *Desulfatiglandales* (Gsp29), and classes *Bipolaricaulia* (Gsp60), *Gemmatimonadetes* (Gsp44) and *Bathyarchaeia* (Gsp71; Table 3.1 and Supplementary Tables S3.3, S3.4 and S3.5).

The sum of the read abundances of the 76 genomospecies ranged between 22.8% (E) to 36.1% (ES) of the total metagenome reads (Table 3.1). Moreover, the complete set of MAGs recruited between 72.3% to 81.2% of the total reads mapping to the assembled contigs for E and ES, respectively (Supplementary Table S3.2). A total of 15 genomospecies (11 represented by two MAGs) recruited >0.6% reads of the total metagenome, with a maximum of 6.3% for Gsp66 affiliated to DHVEG-1 family (*Thermoplasmatota;* Table 3.1 and Figure 3.3). Bacterial species were more dominant in E, whilst the archaeal species in ES. The archaeal species of E with higher relative abundances affiliated with *Thermoplasmatota*, with the family DHVEG-1 ranging from ~0.7 to ~1.4% (Gsp66, Gsp67, Gsp68 and Gsp69), and *Methanosarcina* (Gsp65; with ~2.4%). On the other hand, the bacterial taxa affiliated with the uncultured *Gemmatimonadetes* (Gsp44; with ~0.8%), *Bipolaricaulia* (Gsp60; with ~0.8%), *Planctomycetota* (*Anaerohalophaeraceae*, Gsp53; with ~1.9% of relative abundances) and *Desulfobacterota* (*Desulfarculaceae*, Gsp33; with the highest value of ~5.1%; Table 3.1 and Figure 3.3). The most representative species in ES were the family DHVEG-1 (with abundances ranging from 3.8% to 6.3%), the genera *Methanosarcina* (decreasing to ~0.8%) and *Methanoculleus* (Gsp64; ~0.8%) in Archaea, whereas bacterial species affiliated to *Chloroflexota* (*Brevefilum* genus in Gsp14 obtained ~0.7%), *Desulfobacterota* (values between 0.7% and 1.5%) and *Bipolaricaulota* (Gsp60) phyla, with 1.3% of the relative abundances (Table 3.1 and Figure 3.3).

To evaluate the selection of the microbial communities from the original sediments (S, U, M and L; Font-Verdera *et al*., 2021), an AAI comparison was performed with the MAGs described from S, U, M and L metagenomes (Supplementary Table S3.6). A total of six genomospecies obtained an AAI% above 45% (which is the boundary for the family rank; Konstantinidis *et al*., 2017), whilst the other AAI values were <45% and the similarity among them were only at higher taxa. No MAG of the same genomospecies was found to be shared in the metagenomes of the slurry and sediments with the methanogenic enrichments. The MAGs belonging to the same family and shared between datasets affiliated to *Deltaproteobacteria* class (S04), *Aureimonas* genus (M05-L06) and the candidade lineage DHVE2 (S05) were the most similar to the recruited MAGs from E and ES (Supplementary Table S3.6).

Table 3.1. MAGs recovered from E and ES metagenomes and their most relevant features. From left to right, *D* indicates taxonomic domain (Archaea or Bacteria); *ID* indicates the MAG designation; *Gsp* indicates the genomospecies designation; *Id rank* indicates the lowest taxonomic rank to which the genomospecies could be assigned; *Category* indicates the taxonomic group to which the genomospecies could be assigned; the *closest reference sequence* is the nearest genome or MAG available in the public repositories; *Comp.* indicates genome completeness; *Con.* indicates contamination; *AAI* indicates the average amino acid identity with the closest genome or MAG, *Prot%* indicates the percentage of aligned proteins; *contigs* indicates the number of assembled and binned contigs; *Mb* is the size in Mb of the binned MAG; *E%* and *ES%* indicate the percentage of recruited reads of each MAG normalized by the MAG size and the metagenome size, for E and ES, respectively. The highest quality MAG among the pair MAGs sharing ANI >99% identity and therefore identified as a genomospecies is shown. Light grey shaded in *E* and *ES* indicate the presence of genomospecies in metagenomes E and ES, respectively. The MAGs recruiting reads >0.6% of the total metagenome are highlighted in dark grey in *E* and *ES* columns. The sum of all abundances in each sample was 22.8% for E and 36.1% for ES.

D	Gsp	ID	Id rank	Category	Closest reference sequence	Comp	Con	AAI	Prot%	contigs	Mb	E%	ES%	E	ES
B	Gsp1	E27	Family	*Acholeplasmataceae*	*Acholeplasmatales* bacterium DTU056	100.0	0.0	42.8	64.9	696	3.05	0.14	0.23		
B	Gsp2	ES42	Phylum	*Firmicutes*	-	65.2	13.0	-	-	1,631	3.51	0.05	0.07		
B	Gsp3	E21	Genus	*Thermoclostridium*	*Clostridiales* bacterium DTU069	91.3	0.0	68.0	68.9	345	3.33	0.17	0.03		
B	Gsp4	ES36	Order	*Acetivibrionales*	-	43.5	13.0	-	-	580	2.86	0.02	0.04		
B	Gsp5	E39	Family	*Christensenellaceae*	WB7 2xB 045	87.0	26.1	43.6	12.6	956	2.55	0.09	0.08		
B	Gsp6	ES24	Family	*Christensenellaceae*	*Clostridiales* bacterium DTU074	100.0	0.0	45.5	45.3	86	2.50	0.08	0.20		
B	Gsp7	E36	Order	*Christensenellales*	*Clostridia* bacterium AD E	78.3	0.0	41.8	48.0	684	2.38	0.09	6.0E-03		
B	Gsp8	ES16	Genus	*Halanaerobium*	*Clostridia* bacterium DTU030	100.0	4.3	44.9	53.5	72	2.46	1.5E-02	0.32		
B	Gsp9	ES20	Order	*Halanaerobiales*	*Clostridia* bacterium DTU030	95.7	8.7	45.1	58.6	114	2.95	6.9E-04	0.25		
B	Gsp10	E29	Order	*Halanaerobiales*	*Halothermothrix* sp. DTU029	91.3	4.3	58.7	69.9	442	3.40	0.12	1.1E-02		
B	Gsp11	ES26	Order	*Halanaerobiales*	*Clostridia* bacterium DTU030	91.3	4.3	46.6	54.0	545	2.32	1.4E-03	0.16		
B	Gsp12	E32	Class	*Thermoleophilia*	AK5YR 15 metabat2 14 fa	78.3	8.7	41.9	36.8	525	2.27	0.10	0.02		
B	Gsp13	ES33	Phylum	*Actinobacteriota*	-	8.7	4.3	-	-	1,265	3.62	0.05	0.11		
B	Gsp14	ES11	Genus	*Brevefilum*	*Anaerolineaceae* bacterium	100.0	0.0	64.8	70.5	126	3.25	0.46	0.67		
B	Gsp15	ES22	Genus	*Pelolinea*	*Pelolinea submarina*	95.7	4.3	86.6	82.3	116	3.52	0.39	0.27		
B	Gsp16	E43	Order	*Anaerolineales*	-	34.8	0.0	-	-	1,488	3.21	0.07	0.04		
B	Gsp17	E42	Order	*Anaerolineales*	-	60.9	13.0	-	-	1,435	2.93	0.07	0.03		
B	Gsp18	ES47	Class	*Anaerolineae*	-	65.2	8.7	-	-	2,637	5.50	0.13	0.06		
B	Gsp19	E31	Class	*Anaerolineae*	-	95.7	21.7	-	-	1,013	4.57	0.13	0.10		
B	Gsp20	E34	Class	*Dehalococcoidia*	-	87.0	8.7	-	-	510	2.04	0.10	0.02		
B	Gsp21	ES41	Order	*Rhodospirillales*	TARA PSE MAG 00124	82.6	0.0	52.4	40.2	1,183	3.37	0.20	0.09		
B	Gsp22	ES45	Order	*Desulfobacterales*	AK5YR 20 metabat2 7 fa	82.6	8.7	44.8	50.6	1,322	3.49	6.4E-03	0.07		
B	Gsp23	E38	Order	*Desulfobacterales*	-	69.6	8.7	-	-	1,544	2.74	0.07	0.02		
B	Gsp24	E11	Order	*Desulfobacterales*	*Desulfobacteraceae* bacterium	47.8	0.0	62.9	54.0	271	6.56	0.30	0.04		
B	Gsp25	ES14	Order	*Desulfobacterales*	*Desulfobacteraceae* bacterium	100.0	4.3	60.7	53.6	287	3.50	0.03	0.54		
B	Gsp26	ES50	Class	*Desulfobacteria*	TARA PSW MAG 00126	65.2	0.0	42.0	29.8	2,246	4.11	0.12	0.06		
B	Gsp27	ES28	Order	*Desulfatiglandales*	-	91.3	4.3	-	-	340	4.18	1.1E-02	0.17		
B	Gsp28	ES38	Order	*Desulfatiglandales*	-	91.3	8.7	-	-	1,478	4.76	0.02	0.03		
B	Gsp29	ES08	Order	*Desulfatiglandales*	*Desulfobacteraceae* bacterium	100.0	4.3	63.2	66.3	289	5.64	0.03	0.78		
B	Gsp30	E26	Order	*Desulfatiglandales*	*Deltaproteobacteria* bacterium HGW-*Deltaproteobacteria*-15	65.2	4.3	56.3	43.6	1,055	5.97	0.12	0.04		
B	Gsp31	ES51	Order	*Desulfatiglandales*	TARA PSW MAG 00126	69.6	13.0	41.9	28.6	2,001	3.61	0.05	0.06		
B	Gsp32	ES06	Order	*Desulfatiglandales*	AK5YR 20 metabat2 7 fa	95.7	4.3	45.2	52.6	277	4.40	0.57	1.44		
B	Gsp33	ES15	Family	*Desulfarculaceae*	*Desulfarculus* sp. genome	100.0	8.7	67.6	71.4	85	4.39	5.10	0.44		

B	Gsp34	E37	Genus	*Desulforhopalus*	*Desulfopila* sp. IMCC35006	56.5	4.3	72.2	60.0	1,059	3.23	0.09	9.6E-03		
B	Gsp35	E33	Genus	*Desulforhopalus*	*Desulfopila* sp. IMCC35006	60.9	8.7	48.7	35.8	1,834	4.57	0.08	0.04		
B	Gsp36	ES37	Family	*Desulfovibrionaceae*	*Desulfovibrionaceae* bacterium UBA6814	95.7	0.0	59.0	61.3	669	3.12	0.09	0.10		
B	Gsp37	E12	Family	*Desulfohalobiaceae*	*Desulfovermiculus halophilus* DSM 18834	95.7	8.7	56.4	59.3	375	3.53	0.34	0.29		
B	Gsp38	E23	Family	*Desulfohalobiaceae*	*Desulfovermiculus halophilus* DSM 18834	73.9	13.0	55.0	50.3	480	2.61	0.14	0.07		
B	Gsp39	ES35	Family	*Desulfohalobiaceae*	*Desulfovermiculus halophilus* DSM 18834	82.6	4.3	53.5	48.3	967	3.00	0.05	0.04		
B	Gsp40	ES34	Order	*Bacteroidales*	*Bacteroidales* bacterium	21.7	0.0	46.3	42.2	341	3.12	0.22	0.11		
B	Gsp41	E13	Order	*Bacteroidales*	-	100.0	4.3	-	-	176	5.43	0.28	0.14		
B	Gsp42	E44	Family	*Melioribacteraceae*	*Ignavibacteriales* bacterium	58.5	1.9	69.0	67.1	1,653	3.47	0.07	0.02		
B	Gsp43	ES25	Phylum	SM23-31	candidate division KSB1 bacterium	100.0	4.3	49.3	60.4	91	4.43	5.5E-03	0.19		
B	Gsp44	ES17	Class	*Gemmatimonadetes*	TARA ION MAG 00042	100.0	0.0	52.5	63.2	128	4.38	0.81	0.34		
B	Gsp45	ES40	Phylum	*Aureabacteria*	PVC group bacterium	82.6	8.7	74.6	68.0	961	2.97	5.2E-03	0.03		
B	Gsp46	E24	Order	*Pirellulales*	TARA RED MAG 00100	82.6	4.3	48.1	39.1	1,296	5.09	0.16	0.12		
B	Gsp47	ES23	Order	*Pirellulales*	TARA RED MAG 00078	91.3	0.0	49.1	41.2	500	4.92	0.07	0.20		
B	Gsp48	ES21	Order	*Pirellulales*	TARA RED MAG 00050	100.0	0.0	45.0	39.8	188	6.97	0.09	0.26		
B	Gsp49	E19	Family	*Anaerohalophaeraceae*	-	100.0	0.0	-	-	232	4.86	0.17	0.00		
B	Gsp50	ES44	Family	*Anaerohalophaeraceae*	*Phycisphaerales* bacterium PLanc-01	65.2	17.4	70.6	55.9	2,736	5.78	0.05	0.06		
B	Gsp51	E22	Family	*Anaerohalophaeraceae*	*Phycisphaerales* bacterium PLanc-01	100.0	4.3	65.7	65.2	1,098	7.04	0.19	0.28		
B	Gsp52	ES29	Family	*Anaerohalophaeraceae*	*Phycisphaerales* bacterium PLanc-01	73.9	0.0	65.7	52.2	411	5.88	0.33	0.15		
B	Gsp53	E03	Family	*Anaerohalophaeraceae*	*Phycisphaerales* bacterium PLanc-01	100.0	0.0	66.7	64.1	315	6.59	1.86	0.18		
B	Gsp54	ES49	Family	*Anaerohalophaeraceae*	-	52.2	8.7	-	-	2,195	4.19	0.05	0.06		
B	Gsp55	E41	Order	*Sedimentisphaerales*	-	52.2	4.3	-	-	3,072	5.89	0.08	0.09		
B	Gsp56	E10	Phylum	*Planctomycetota*	*Planctomycetes* bacterium UBA4800	100.0	4.3	50.2	61.3	193	7.63	0.32	0.02		
B	Gsp57	E45	Family	*Sphaerochaetaceae*	-	100.0	0.0	-	-	26	3.15	0.63	0.65		
B	Gsp58	E46	Class	*Bipolaricaulia*	*Candidatus* Bipolaricaulota bacterium	100.0	0.0	76.7	85.0	83	2.71	0.20	1.3E-02		
B	Gsp59	E15	Class	*Bipolaricaulia*	*Candidatus* Atribacteria bacterium	100.0	4.3	71.7	76.7	165	3.20	0.24	1.0E-02		
B	Gsp60	E06	Class	*Bipolaricaulia*	*Candidatus* Atribacteria bacterium	100.0	0.0	66.7	70.9	107	2.67	0.77	1.26		
A	Gsp61	E35	Order	*Woesearchaeales*	archaeon GW2011_AR15	73.9	4.3	52.8	61.2	745	2.01	0.09	0.07		
A	Gsp62	ES12	Order	*Pacearchaeales*	*Candidatus* Pacearchaeota archaeon	91.3	8.7	57.2	81.4	141	1.17	0.04	0.55		
A	Gsp63	E16	Genus	*Methanoculleus*	*Methanoculleus* sp. DTU007	95.7	4.3	69.0	76.9	212	3.10	0.15	0.05		
A	Gsp64	ES07	Genus	*Methanoculleus*	*Methanoculleus* sp. DTU007	95.7	4.3	69.3	79.2	96	3.17	9.5E-03	0.81		
A	Gsp65	E02	Genus	*Methanosarcina*	*Methanosarcina* sp. DTU009	95.7	0.0	74.0	73.4	228	4.27	2.39	0.76		
A	Gsp66	ES01	Family	DHVEG-1	-	69.6	0.0	-	-	246	0.92	0.36	6.29		
A	Gsp67	E04	Family	DHVEG-1	-	69.6	0.0	-	-	284	1.62	1.35	3.81		
A	Gsp68	ES03	Family	DHVEG-1	-	17.4	0.0	-	-	192	0.95	0.15	5.41		
A	Gsp69	ES02	Family	DHVEG-1	*Thermoplasmatales* archaeon ex4572_165	100.0	0.0	60.2	77.3	54	2.55	0.73	5.81		
A	Gsp70	E28	Class	*Bathyarchaeia*	-	95.7	0.0	-	-	290	2.33	0.13	0.07		
A	Gsp71	ES13	Class	*Bathyarchaeia*	*Candidatus* Bathyarchaeota archaeon	95.7	8.7	71.9	62.0	208	1.90	0.28	0.76		
A	Gsp72	ES27	Class	*Bathyarchaeia*	*Candidatus* Bathyarchaeota archaeon	73.9	8.7	72.3	56.5	666	1.50	0.06	0.15		
A	Gsp73	E25	Class	*Bathyarchaeia*	-	91.3	4.3	-	-	386	2.43	0.13	0.07		
A	Gsp74	E07	Class	*Bathyarchaeia*	-	91.3	0.0	-	-	126	2.94	0.64	0.07		
A	Gsp75	ES48	Class	*Lokiarchaeia*	*Candidatus* Lokiarchaeota archaeon CR_4	52.2	0.0	44.2	44.9	2,423	5.46	0.05	0.06		
A	Gsp76	ES31	Class	*Lokiarchaeia*	*Candidatus* Lokiarchaeota archaeon	95.7	0.0	42.1	60.5	266	4.20	1.2E-03	0.12		

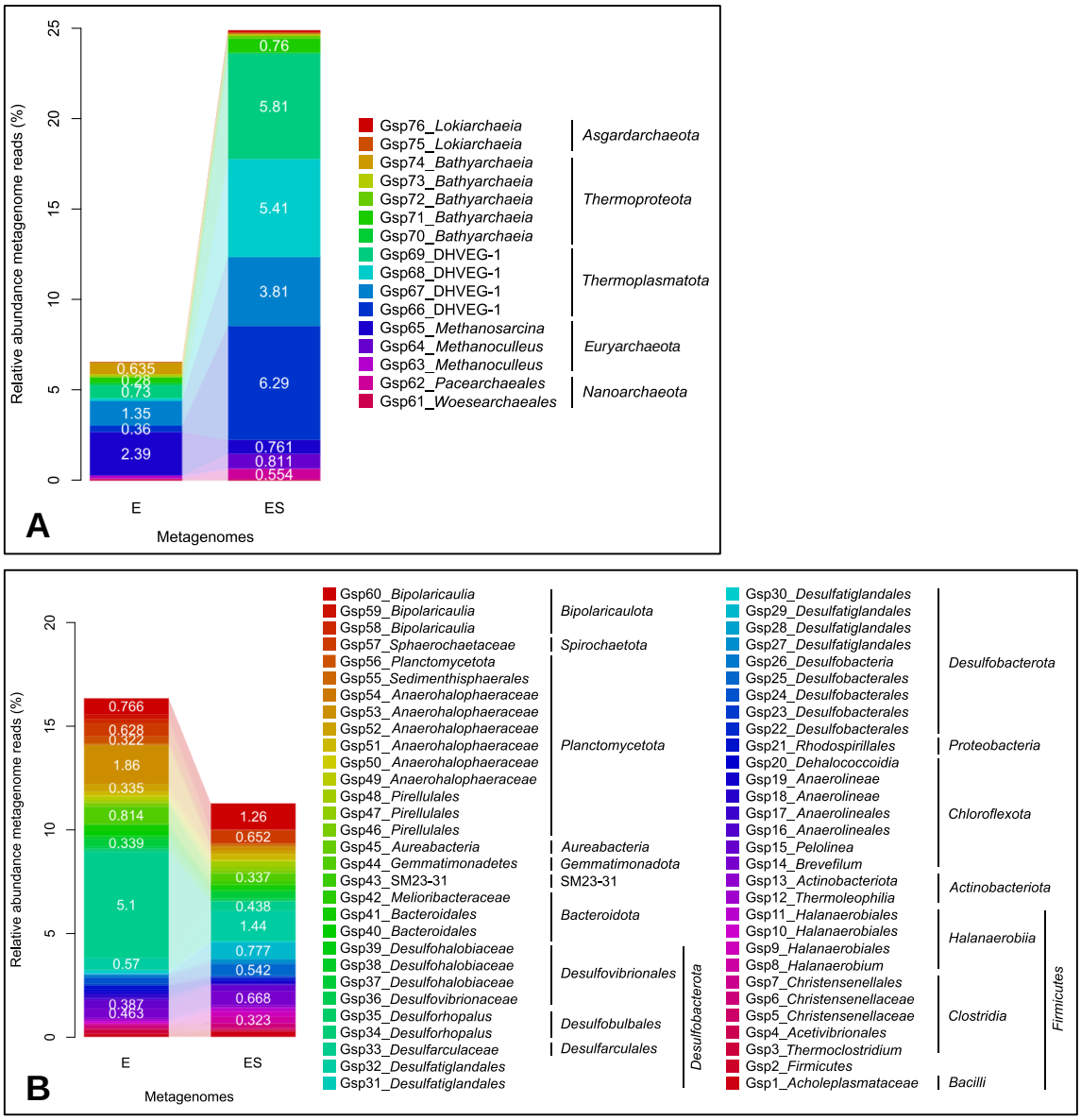

Figure 3.3. Relative abundance of mapped reads (%) at 98% identity and 70% coverage for the genomospecies against the two metagenomes (E and ES). Taxonomic categories of genomospecies are shown in the legend (Supplementary Table 3.3.). Relative abundances of metagenome reads above 0.2% for Archaea (**A**) and 0.3% for Bacteria (**B**) are indicated with a blank over the bars.

3.4. Inferred metabolisms and cellular replication activity (GRiD) of the MAGs

The metabolic screening based on annotated genes related to methanogenesis pathways, sulfur and nitrogen cycles was performed in both metagenomes and all recruited MAGs (Figure 3.4). Genes associated with hydrogenotrophic, aceticlastic and both methylotrophic (from methanol or methylamine compounds) pathways were encoded in the two metagenomes (Figure 3.4A). The complete or almost complete hydrogenotrophic route was detected in genera affiliated to *Bathyarchaeia* (Gsp71, Gsp72 and Gsp70)*, Euryarchaeota* (*Methanosarcina* with Gsp65; *Methanoculleus* with Gsp64 and Gsp63) and *Lokiarchaeia* (Gsp75). Genes encoding either via *acs* or *ack* and *pta* in the aceticlastic pathway were widely detected in both metagenomes and their associated MAGs, such as those affiliated to *Methanosarcina* (Gsp65) genus, being the most retrieved methanogenic route. Otherwise, genes involved in methylotrophic route from methanol and methylamine substrates for the three subpathways were encoded in *Methanosarcina* genus (Gsp65; Figure 3.4A, Table 3.1 and Supplementary Table S3.3).

Genes associated with the nitrogen cycle were detected in both metagenomes. No MAGs with the complete pathways were retrieved. The less representative route was nitrification, with the only detection of genes associated to nitrite oxidation in MAGs mainly belonging to *Planctomycetota* (Gsp48, Gsp55 and Gsp51) and *Firmicutes* (*Halanaerobiales* with Gsp9 and *Christensenellaceae* with Gsp6) phyla. Genes encoding denitrification were detected in *Methanoculleus* (Gsp64), *Sphaerochaetaceae* (Gsp57), *Bacteroidales* (Gsp41), *Desulfobacteria* (Gsp26), *Gemmatimonadetes* (Gsp44) and *Planctomycetota* (Gsp55). Besides, species affiliated to *Rhodospirillales* (Gsp21) was the only involved in the conversion of nitrous oxide to nitrogen. Genes belonging to dissimilatory nitrate reduction, were detected in *Methanosarcina* (Gsp65), *Bacteroidales* (Gsp41), *Desulfovibrionaceae* (Gsp36) and *Planctomycetota* (*Anaerohalophaeraceae*, Gsp51; Figure 3.4B, Table 3.1 and Supplementary Table S3.3). Sulfate dissimilatory reduction was detected in both E and ES. The complete sulfate dissimilatory reduction was mainly detected in *Gemmatimonadetes* (Gsp44), and *Desulfobacterota* phylum, such as *Desulfobacterales* (Gsp24), *Desulfatiglandales* (Gsp28), *Desulfarculaceae* (Gsp33), *Desulfohalobiaceae* (Gsp37) and the genus *Desulforhopalus* (Gsp34). Almost complete pathway was also encoded in other members of *Desulfobacterota* (Gsp30, Gsp35, Gsp32, Gsp25, Gsp27, Gsp22 and Gsp26), *Rhodospirillales* (Gsp21) and *Planctomycetota* (*Anaerohalophaeraceae*, Gsp54; Figure 3.4C, Table 3.1 and Supplementary Table S3.3).

With the aim to evaluate the growth activity of the recruited genomes, the replication rates of the MAGs were calculated using the software GRiD (Growth Rate inDex; Figure 3.5). The GRiD ranged from 1.0 (no replication activity) to ~12.0 (MAG E14-Gsp14; Figure 3.5, Table

3.1 and Supplementary Table S3.3). In the E metagenome, among methanogenic MAGs, those affiliated to *Bathyarchaeia*, such as Gsp71, Gsp72 and Gsp70 achieved a GRiD ratio between 1.2 and 2.5, whereas both *Methanoculleus* genus (Gsp64) and *Lokiarchaeota* (Gsp75) ~1.9. Among sulfate-reducers and within *Desulfobacterota*, MAGs affiliated with *Desulfohalobiaceae* obtained a ratio of 2.3 (Gsp38), whereas *Desulfatiglandales* displayed 1.6 (E09-Gsp32) and *Desulforhopalus* genus ranged from 1.5 to 2.4 (Gsp35 and Gsp34). Additionally, members of *Planctomycetota* showed GRiD ratios between 2.7-3.3 (Gsp52 and Gsp50) and 4.4 for *Sedimenthisphaerales* (Gsp55), whereas *Thermoplasmatota* displayed a range between 1.2 and 2.5 for DHVEG-1 family (Gsp67, E08-Gsp69, Gsp66, Gsp68 and ES05-Gsp67). On the other hand, in the ES, methanogenic *Methanoculleus* (Gsp63) displayed a GRiD of ~1.9, whilst *Bathyarchaeia* (Gsp70) 1.7 and *Lokiarchaeota* (Gsp76 and Gsp75) ~1.5. *Desulfatiglandales* (Gsp32, Gsp28, Gsp30, Gsp29, Gsp27 and Gsp31) ranged from 1.1 to 1.7, *Desulfohalobiaceae* (Gsp39 and Gsp38) from 2.7 to 6.1, and *Desulforhopalus* (Gsp35 and Gsp34) 1.1-1.8. Taxa affiliated to *Firmicutes* (Gsp2 – GRiD of 2.7; *Christensenellaceae*, Gsp5 – 5.6)*, Chloroflexota* (*Brevefilum*, E14-Gsp14 – 11.9; Gsp16 – 2.4)*, Planctomycetota* (Gsp46 and ES39-Gsp46 – 2.4; Gsp54 – 2.9) and *Thermoplasmatota* (DHVEG-1, ES05-Gsp67 – 2.7) exhibited high replication activity (Figure 3.5, Table 3.1 and Supplementary Table S3.3).

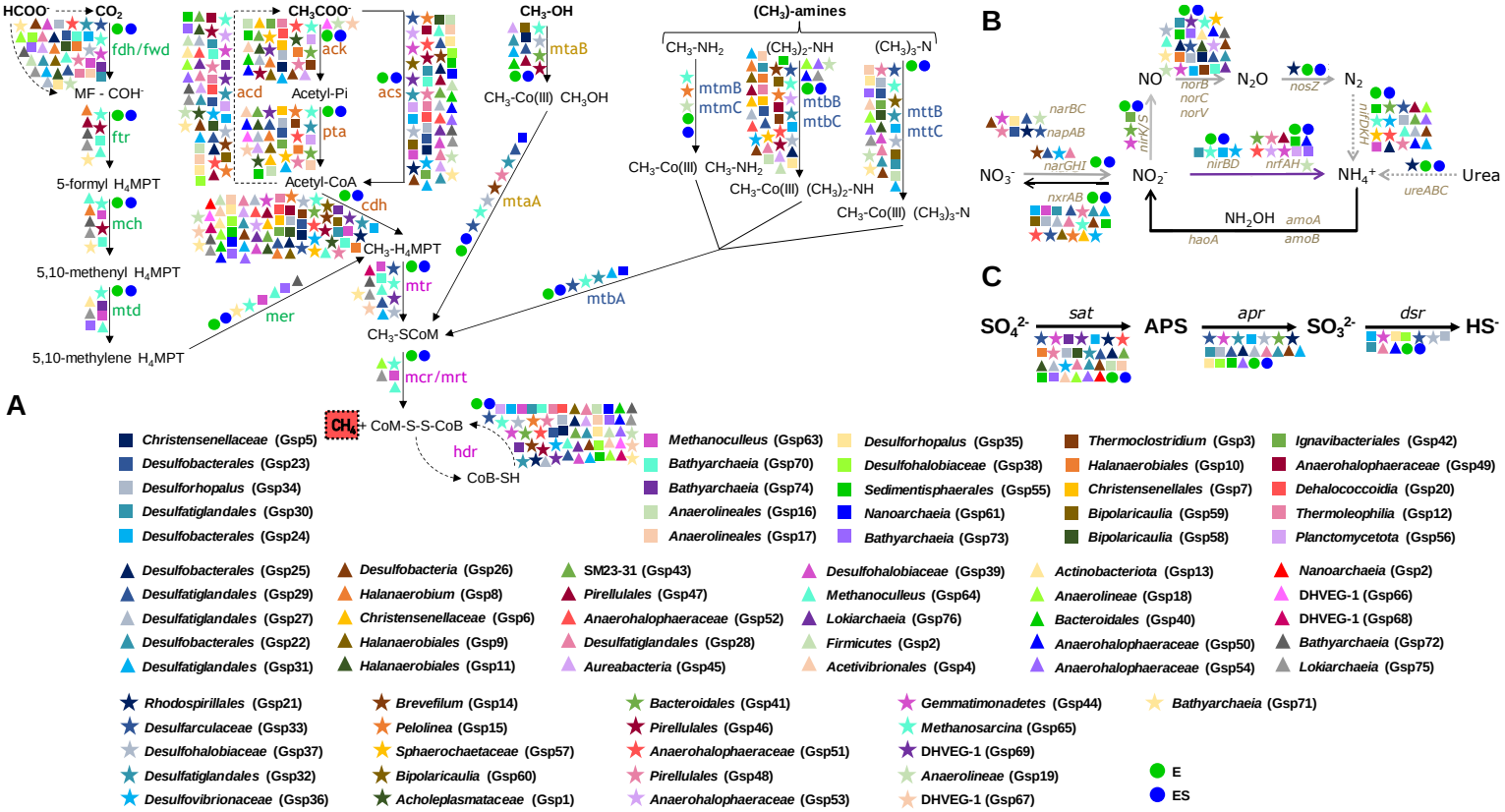

Figure 3.4. A. Methanogenesis superpathway detected in E and ES metagenomes and the genomospecies (colored symbols with their designation indicated in the legend on the figure) encoding for each of the genes. Genes involved in hydrogenotrophic (CO_2), aceticlastic (CH_3COO^-) and methylotrophic (CH_3OH or CH_3-amine compounds) pathways are highlighted in green, orange and yellow-blue colors, respectively. Common intermediate and final routes are shown in pink. **B**. Genes involved in the nitrogen cycle present in metagenomes and their MAGs. Black arrows represent nitrification, grey arrows show denitrification, the nitrogen fixation route is marked with dotted grey arrows, and dissimilatory nitrate reduction with purple arrows. **C**. Dissimilatory sulfate reduction genes present in the metagenomes and their associated MAGs. Metagenomes are represented by circles, squares for genomospecies only from E and triangles for genomospecies only from ES. The genomospecies, comprising MAGs from the distinct metagenomes (see Table 3.1 and Supplementary Table S3.3), are represented by stars.

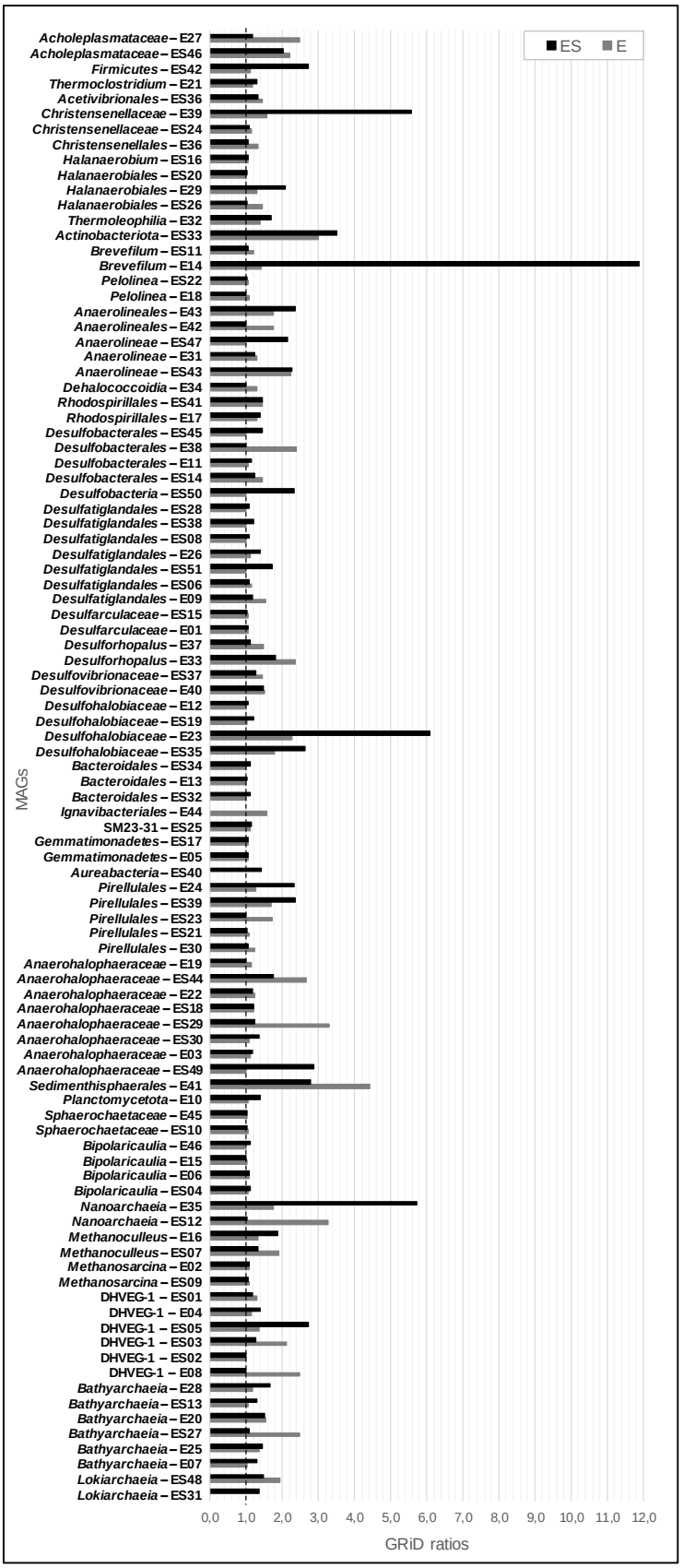

Figure 3.5. Growth Rate inDex (GRiD) of all MAGs in the E and ES metagenomes and ordered by taxonomy. GRiD growth ratios estimate the *in situ* genome replication rates in metagenomes. Dashed line in 1.0 indicates the threshold for positive growth GRiD values (GRiD score > 1.0), where a positive cell growth can be considered.

3.5. Discussion

Taking aware the essential involvement of methanogenic communities in carbon cycle and their contribution to biotechnological processes, the aim to cultivate and describe the microbial populations, understanding their role in the ecosystem and the potential syntrophic behavior among them has always prevailed (Thauer, 1998; Sieber *et al.*, 2010; Kaleem Sarwar *et al.*, 2015). However, it has always been a problem to isolate and culture these communities, so the attempts to composition's description are based in consortia (Lykidis, C. L. Chen, *et al.*, 2011; Rathi *et al.*, 2018; Timmers *et al.*, 2018). Enrichment cultures to improve the cultivability and consequently to select microbial communities have been tested (Lamarche-Gagnon *et al.*, 2015; Laso-Pérez *et al.*, 2018). With the aim to include the possible broadest range in cultivability requirements, eight different salinities (from 5% to 30%), the addition of ampicillin (5 mg/mL) and the different substrate concentrations (0.1%, 1% and 10%Po) were analyzed first. Then, the subculture of the most efficient microcosms with the supplement of ATF (Acetate, Formate and Trimethylamine) was also assessed.

As described in chapter 2, the salinity acts as a strong selection force, but the ampicillin also influences microbial communities, since in salinities up to 12%, methane rates are greater with ampicillin. This could be due to the fact that the antibiotic inhibited some bacterial microorganisms, such as sulfate-reducers, which probably stop competing and allowed methanogenic Archaea to generate more methane. Conversely, at salinities of 15% and above, samples without ampicillin produced more methane which could be due to the stablished syntrophy between Archaea and halophilic Bacteria which would enhance the methane generation. In fact, sulfate-reduction generally co-exists with methanogenesis in several environments, and methanogenesis would benefit from the reduction of this metabolic process (Sela-Adler *et al.*, 2017). For instance, slurry experiments from a microbial mat in a saltern pond in Eilat revealed high methane production rates only between 15% and 25% of salinity. However, when molybdate was added to prevent sulfate-reduction, sulfate-reducers were partially inhibited, allowing methanogens to increment the methane yield in salinities from 5% to 15% (Sørensen *et al.*, 2004).

The maximum methane rates obtained for the first set (from 5% to 12% of salinity) were more different among microcosms at each salinity (specially the 5%), whereas the divergence was lower for the highest salinities (15%-30%). The variability within each group with the same salinity caused by the different culture conditions evidenced its important influence in gas production. It should be noted that the methane concentrations here obtained were remarkably higher (up to a thousand times) when compared to the retrieved methane rates in previous studies of hypersaline sediments and slurries at low salinity (Sørensen *et al.*, 2004; Mcgenity, 2010; Lazar *et al.*, 2011; Gründger *et al.*, 2015; Webster *et al.*, 2015; Nigro *et al.*, 2020). Additionally, the supplement with ATF (at 5% of salinity with

ampicillin and 10% w/w *Po*) seemed to improve in the methane generation, reaching average values up to 69.4 M in the accumulated methane concentrations. Conspicuously, Giani and cols. (1989) described the enhancement of methanogenesis by the addition of methylated amines and methanol but not by acetate and formate, but at salinities from 20% to 30%.

Previous studies based on the estimation of methanogenesis have reported positive correlations between methane production and the diversity of methanogens (Sierocinski *et al.*, 2018). Indeed, here we found a higher methane production rate in the enriched microcosms, which displayed novel diversity in retrieved MAGs compared to the original sediments S, U, M and L (Font-Verdera *et al.*, 2021). A taxonomic turnover was observed among *Methanomicrobia* members depending on the supplement availability, with taxa affiliated with the genera *Methanosarcina* and *Methanoculleus* more abundant in E and ES, respectively. Moreover, hydrogenotrophic *Methanoculleus* exhibited high replication activity in comparison to *Methanosarcina*, a metabolically versatile taxon which can produce methane using any of the methanogenesis pathways (Patterson and Hespell, 1979; Satish Kumar *et al.*, 2011; Gründger *et al.*, 2015; Mand and Metcalf, 2019). Additionally, new members of *Bathyarchaeia* and *Lokiarchaeia* were also able to produce methane, specially *Bathyarchaeia* in no supplemented enrichment and *Lokiarchaeia* taxa in the supplemented one. Methanogenesis was performed mainly via aceticlastic route, with members of *Methanomicrobia* and *Bathyarchaeia* as examples of contributing species in methane generation, as described previously (Evans *et al.*, 2015; Zhang *et al.*, 2017). Rare species have been described to include high density of acetoclastic methanogens, in a syntrophic process where methane-producing Archaea and acetate-producing Bacteria worked together (Satish Kumar *et al.*, 2011), so the aceticlastic pathway is presumably still underrepresented.

The use of acetate and formate as supplement of cultures have been widely analyzed (Timmers *et al.*, 2018). The understudied anaerobic oxidation of acetate has not been assessed away from their presence in methanogenic processes influenced or conditioned by high temperatures, organic acid and ammonia concentrations, with exception of a study of Sorokin, Kublanov, Gavrilov, *et al.* (2016). Therefore, the consideration of the potential participation of microbial communities carrying out this metabolism in hypersaline habitats would be really interesting for this contribution in carbon cycling (Karakashev *et al.*, 2006; Sorokin, Kublanov, Gavrilov, *et al.*, 2016). Conspicuously, the supplemented enrichment displayed high presence of methanogens, affiliated with *Bathyarchaeia* and *Euryarchaeota* phyla, in addition to the higher cellular replication activity for the methanogenic (such as *Methanoculleus* and *Thermoplasmatota*). These altogether could be the main diversity involved in the improvement of methane generation with ATF. In fact, the supplement based on addition of acetate, trimethylamine and formate could be metabolized by the *Methanomicrobia* members (*Methanoculleus* performing the aceticlastic route and *Methanosarcina* capable to produce methane from any substrate) and the *Lokiarchaeia* class,

capable to achieve methane through the conversion of formate via hydrogenotrophic route. Sulfate-reduction was detected mainly in *Desulfobacterota* phylum, with *Desulfatiglandales, Desulfobacterales, Desulfarculales, Desulfohalobiaceae* and *Desulforhopalus* as the most abundant and active representatives in both metagenomes. Besides, taxa related to *Thermoplasmatota, Planctomycetota* and *Chloroflexota* were highly retrieved in E and ES metagenomes, specially the family *Anaerohalophaeraceae* (*Planctomycetota*) in E (with a high replication activity), and the family DHVEG-1 (described as protein and carbohydrates degrader; Fan and Xing, 2016) in both E and ES. Similar diversity has been retrieved in hypersaline sediments from a permafrost spring (Lamarche-Gagnon *et al.*, 2015) and from soda lakes (Vavourakis *et al.*, 2018, 2019). Conspicuously, the genus *Brevefilum* (*Chloroflexota*), presumably involved in fermentation (McIlroy *et al.*, 2017), was really abundant and exhibited the highest growth activity in supplemented enrichment. Normally, methanogenic communities are dominated by the phyla *Firmicutes, Bacteroidota* (formerly *Bacteroidetes*) and *Proteobacteria* (Sierocinski *et al.*, 2018). We recovered four MAGs belonging to *Bacteroidota,* two of *Proteobacteria* and twelve MAGs belonging to *Firmicutes*, with five taxa of the latter affiliated to *Clostridia*, described as key players in the hydrolysis step during biogas production in anaerobic digesters (Nelson *et al.*, 2011). In fact, some of these species showed a positive replication growth, especially in the supplemented enrichment (ES).

It should be noted that a diluted system as the one used here, can imply the loss of rare taxa and, consequently, the overrepresentation of major diversity. The metabolic efficiency has been reported elsewhere to decrease up to 50% due to the loss of half of the rare fraction of the community (Sierocinski *et al.*, 2018). However, here we found microcosms at 5%, where the highest dilution was applied, to be the most efficient in terms of methane production. This could be related to inhibition of methanogenesis caused by salinity. Zhang *et al.* (2017) reported the methanogenesis to be hindered at salinities greater than 5.5%, especially some hydrogenotrophic and aceticlastic methanogens.

V. GENERAL DISCUSSION

Discussion of the main findings

In this thesis, I have characterized the hypersaline anaerobic sediments underlying the solar salterns of S'Avall, along a vertical stratification and in different seasons of the year, by means of metagenomics and 16S rRNA gene sequencing, coupled with metaviromics. Besides, we observed how several important environmental factors (salinity, ampicillin and substrate) influence the microbial community structure and dynamics in the sediments, analyzing the response of prokaryotic populations through 16S rRNA gene sequencing. To finalize the work, we have achieved efficient microbial consortia in methane generation from hypersaline and anaerobic sediments as a basis, and these have been characterized by means of metagenomics.

The hypersaline and anaerobic sediments of S'Avall are unique environments, suitable for the research about their extremely halophilic community structure. With the aim in elucidate their physiological and genetic adaptation needed to thrive in these extremely halophilic conditions and to shed light to the understudied metabolic interrelation among them, this doctoral thesis focused in the study of the sediments underlying the solar salterns of S'Avall, following the previous published investigations (López-López *et al.*, 2010, 2013). At the starting point of this thesis, the main goal to achieve was the characterization of the hypersaline sediments from S'Avall, which would be the basis of microcosms for the evaluation of the putative methane generation, following with the initial hypothesis of López-López and cols. (2010, 2013).

In general, hypersaline and anaerobic environments are globally scattered, including deep-sea anoxic brine lakes (DHABS; Antunes *et al.*, 2011; Yakimov *et al.*, 2013, 2015; Zhuang *et al.*, 2016; Nigro *et al.*, 2020), sediments from soda and salty lakes (Lamarche-Gagnon *et al.*, 2015; Dimitry Y Sorokin *et al.*, 2017; Dimitry Y. Sorokin *et al.*, 2017; Vavourakis *et al.*, 2018) and solar salterns (López-López *et al.*, 2010, 2013; Dimitry Y. Sorokin *et al.*, 2017), among others. However, these studies normally focused in the description of the community structure, the ecosystem dynamics and the biogeochemical role that developed the prokaryotic communities. Therefore, we wanted to explore further in metabolic potential of the communities and their capability to generate a kind of renewable and clean energy, taking the microbial characterization as a basis and then to investigate and deepen in the potential of the microorganisms in the ecosystem. Thus we demonstrated that these sediments were a source of novel taxa involved in interrelated metabolisms, such as fermentation, nitrate- and sulfate-reduction, and especially in methanogenesis (Chapter 1). Altogether, the results of this study indicated that the combination of distinct next sequencing techniques could shape a good taxonomic characterization of the ecosystem, by means of OPU design (Mora-Ruiz *et al.*, 2015; Viver *et al.*, 2019). This OPU approach allowed 16S rRNA gene fragments of distinct length and position within the gene to be combined, in order to obtain comparable results between the amplicon and metagenome strategies, since

the comparison among the distinct seasonal time-points of sampling could be an issue due to the use of different sequencing methodologies.

Although the stratification that was expected would be distinguish by the gradient of electron acceptors characterizing marine sediments (Fenchel *et al.*, 2012), the metagenomes showed a vertical profile with the dominance of archaeal taxa in the overlying horizons and the bacterial taxa prevailing in the deepest. Therefore, the prokaryotic community structured the sediments and showed an inverted stratification, when in a classic sediment the methanogenic Archaea appear in the deeper layers and Bacteria in the upper horizons where electron acceptors allow higher energetic yields (Fenchel *et al.*, 2012; Petro *et al.*, 2017). In fact, the dominance of methanogenic and sulfate-reducers has been reported in deep layers of DHABS (Yakimov *et al.*, 2015), whereas in 0 – 3 m deep sediments displayed a very low detection of methanogenesis (Walsh *et al.*, 2005). Thus, similar ecosystems in terms of environmental factors showed very different patterns along a vertical profile, reinforcing the uniqueness and the need of research about them. Metaviromics were applied in order to gain precision in understanding the viral composition of the sediment. Metaviromics showed that viral abundance decreased slightly with depth, but the VLPs were indeed higher than those observed for DHABS (Danovaro *et al.*, 2005; Corinaldesi *et al.*, 2014).

A few previous studies have hypothesized on how a fairly stable bacterial and archaeal communities remained in analyzed sediments of different seasonal time-points (Lamarche-Gagnon *et al.*, 2015). So that, a spatial-temporal stability was detected throughout the ephemeral pond from S'Avall, as well as even the years sampled (López-López *et al.*, 2010, 2013). The novelty of species retrieved not only occasionally by means of metagenomics in this environment (Viver *et al.*, 2019), reinforced their stable presence in time (as previously described by Orellana *et al.*, 2018) and space.

Although a clear division among the inferred anaerobic metabolisms could be expected, these overlapped throughout the 25 cm horizon. The inverted vertical distribution was characterized by methanogenic hydrogenotrophic populations and acetogenic fermenters in the most superficial layer. In this regard, besides the involvement of members of *Methanobacteria* and *Methanomicrobia* classes in methanogenesis, the most predominant candidate taxon was MSBL1. In this study, we demonstrated its involvement in methane generation, previously hypothesized due to its high retrieval in hypersaline environments as DHABs and solar salterns (van der Wielen *et al.*, 2005; López-López *et al.*, 2010; Mwirichia *et al.*, 2016). The detected genetic inferences allow to discern its metabolic activity, classifying it mainly as a hydrogenotrophic methanogen, and supporting the hypothesis of a mixotrophic lifestyle of this lineage (Mwirichia *et al.*, 2016), since some of the retrieved MAGs also encoded for genes involved in dissimilatory sulfate reduction, dissimilatory nitrate reduction, CO_2 fixation and sugar fermentation. This novel lineage has demonstrated a high adaptation to hypersaline and anoxic environments, and both aerobic and anaerobic conditions in high

concentrations of magnesium ($MgCl_2$; Yakimov *et al.*, 2013, 2015). Moreover, metagenomics allowed to achieve more robust genetic information about these taxa, since the only attempt to describe these microorganisms was performed using the single-cell genomics technique, where the acquired genomes were only partially complete (Mwirichia *et al.*, 2016).

Once the microbial composition of the hypersaline sediments from S'Avall was characterized, these prokaryotic communities were subjected to selective pressures through modifying their natural media conditions, aiming to discern the possible disturb that could experience (Chapter 2). We hoped to get new insights into how the communities respond to distinct environmental factors. The results addressed several relevant questions, whether salt concentration, ampicillin and substrate concentration act as deterministic or stochastic forces selecting for the community composition. The implementation of cultures at the broadest salinity range (diluting the inoculum at 34.4% of salts, from 30% to 5%), with the addition of ampicillin and various substrate concentrations opened multiple lines of culture requirements, undescribed until now (Jiang *et al.*, 2007; Webster *et al.*, 2015; Xie *et al.*, 2017). Certainly, major diversity recovered in these modified conditions was determined by the salinity, acting as the major selection force to structure the microbial communities, as previously described (Sørensen *et al.*, 2004; Jiang *et al.*, 2007; Vavourakis *et al.*, 2018; Viver *et al.*, 2019). Certainly, sediments from S'Avall were governed by stochastic factors, with more similar microbial communities and higher stochasticity as salinity increased. This resulted in the theory that microcosms are more comfortable and adapted at salinity of 30% (close to the inoculum), since in their natural media the stochasticity governs the prokaryotic community (Stegen *et al.*, 2012). The dilution of the original media diminished the stochasticity of the community assembly, even transitioning to be governed by determinism in the lowest salinities, behavior that has been previously reported by Langenheder *et al.* (2017).

The ampicillin conferred a slightly distinct taxonomic structure, acting as selective pressure and affecting overall bacterial populations at elevated salinities (above 15%). The shift in the sediment microbial community due to the exposure to different antibiotics has been largely described (Yu *et al.*, 2019; Ye *et al.*, 2020; Zarei-Baygi *et al.*, 2020), although not focused in the possible inhibition of methanogenic microorganisms in an anaerobic ecosystem. Nevertheless, a large list of antibiotics have been described to influence the prokaryotic communities, even causing only an acute inhibitory impact and focused on a specific pathway, as aceticlastic methanogenic activity (Cetecioglu *et al.*, 2012). Besides, the putative emerging of free new niches after the reducing diversity caused by ampicillin addition still remains unknown and further investigation is needed.

Furthermore, the novel use of the *Posidonia oceanica* as a substrate (Bonet Aracil *et al.*, 2019; Kohn *et al.*, 2020) did not provoke relevant shifts in the dynamics of prokaryotic communities, even though the putatively immigrant microbial populations that were added

to the sediment's microbial communities. To our knowledge, this is the first time that this Mediterranean marine and endemic phanerogam is considered as substrate for methanogenic microbial populations, even their recalcitrance to degradation because they contain carbon compounds as phenols with difficulties for their metabolization (Medina *et al.*, 2001). However, rates of mineralization of this dead biomass are very important (Mininni *et al.*, 2014), still the elevated content in NaCl that contain after seawater evaporation (Cocozza *et al.*, 2011). But this encouraged us to use this normally discarded dead biomass to give an added value and benefit of its potential in biogas generation as alternative energy. However, the use of different concentrations of *Posidonia oceanica* seemed not to be determinant neither in the general structure of the community nor in the methane yields.

We could not observe any remarkable influence of the ampicillin for the obtainment of high methane yields, although ampicillin at specific salinity was decisive to select the most efficient microcosms for gas methane production (Chapter 3). Several studies have been focused in the assessment of methane rates from hypersaline sediments and slurries (Sørensen *et al.*, 2004; Mcgenity, 2010; Lazar *et al.*, 2011; Gründger *et al.*, 2015; Webster *et al.*, 2015; Nigro *et al.*, 2020). However, starting from a different biomass, following with the distinct techniques of enrichment applied, and the variations among the experimental useful time, the difficulty to compare and catalogue the more efficiency in a process is enormous. Definitely, microcosms with ampicillin and 10% w/w of *Posidonia oceanica* at 5% were the most suitable conditions in the methane generation, obtaining methane yields well above those reported (Sørensen *et al.*, 2004; Mcgenity, 2010; Lazar *et al.*, 2011; Gründger *et al.*, 2015; Webster *et al.*, 2015; Nigro *et al.*, 2020).

We could distinguish between the microbial structure of subcultured and amended with an organic supplement of acetate, formate and trimethylamine, and those without the supplement. This specific supplementation was added with the aim to enhance even more the methane yield, in accordance to the individual or coupled improvement of these compounds as reported by Gründger *et al.* (2015) and Dimitry Y Sorokin *et al.* (2017). The supplement with ATF (at 5% of salinity with ampicillin and 10% w/w *Po*) seemed to improve in the methane generation, reaching average values up to 69 M in the accumulated methane concentrations. To our knowledge, the study of these specified conditions to generate methane have not been assessed, and even less with hypersaline sediments as basis. Contrarily to our results, for instance Giani and cols. (1989) described the enhancement of methanogenesis by the addition of methylated amines and methanol but not by acetate and formate, but at salinities from 20% to 30%.

Beyond the scope of the precise description of all microbial consortia capable to generate gas methane, due to the difficulty in the individual cultivation of methanogenic populations (Lykidis, C. L. Chen, *et al.*, 2011; Rathi *et al.*, 2018; Timmers *et al.*, 2018), the characterization of the two most effective consortia was performed through metagenomics.

The research included the description of the main microbial diversity retrieved by MAGs, their genetic information regarding to the involvement in methanogenesis, sulfate-reduction and nitrogen cycling, and the replication cellular activity through the growth rate index (GRiD), as we did in Chapter 1. Enriched microcosms displayed novel diversity compared to the original sediments S, U, M and L analyzed in Chapter 1, denoting the shift and therefore adaptation of microbial communities at the modified ecosystem.

Euryarchaeota members have been considered as one of the most relevant taxa capable to perform methanogenesis, and had normally affiliated to the orders *Methanosarcinales* and *Methanomicrobiales* (Oren, 2014; Gründger *et al.*, 2015; Webster *et al.*, 2015; McGenity and Sorokin, 2019), although at present there is an emerging of new lineages involved in methanogenesis, such as the *Bathyarchaeota* (Evans *et al.*, 2015) and *Verstraetearchaeota* (Vanwonterghem *et al.*, 2016) phyla. We also recovered novel and understudied methanogenic taxa, affiliated to lineages that initially were not considered as methanogenic. For instance, members affiliated to *Thermoplasmatota*, a phylum that has evolved and highly increased in recent years, and still remains uncharacterized in most of its sublineages (Borrel *et al.*, 2014). Besides, *Thermoplasmatota* lineages (capable to reduce methanol and methylamines with hydrogen) were previously detected in hypersaline environments as DHABS by Yakimov *et al.* (2015) and soda lakes by Timmers *et al.* (2018) and Vavourakis *et al.* (2018). Additionally, new retrieved members of *Bathyarchaeota* and *Lokiarchaeota* seemed to be able to produce methane, due to encode a high extent of methanogenic genes. *Bathyarchaeota* was already reported as methanogenic phylum (Evans *et al.*, 2015), whereas *Lokiarchaeia* has been only described to syntrophically grow with methanogens or sulfate-reducing bacteria while degrading amino acids (Imachi *et al.*, 2020; Yin *et al.*, 2021). Altogether the putative hydrogenotrophic *Lokiarchaeia* class and members of *Methanomicrobia* (capable of methane generation from any substrate) could be the main metabolizers of the supplement based on acetate, trimethylamine and formate.

Additionally, no presence of the hydrogenotrophic *Candidatus* MSBL1 lineage (Font-Verdera *et al.*, 2021) was detected in these enriched microcosms at 5% of salinity, coherently with its extreme halophilia, even though the high concentration of formate (50 mM) added to the system, suitable for the hydrogenotrophic methanogens. Since methane yield was enhanced with the supplement of acetate, formate and trimethylamine, this enriched culture also highlighted by the high contribution of the species via the methanogenic aceticlastic route, such as those affiliated *Methanomicrobia* and *Bathyarchaeia* (Evans *et al.*, 2015; Zhang *et al.*, 2017). Thus, acetate is a very versatile substrate to use in methanogenic metabolisms in anoxic salt-saturated ecosystems, even with the addition of a ß-lactam such ampicillin.

The results of this thesis showed that sediments from S'Avall solar salterns are characterized by their inverted microbial structure and spatial-temporal stability, with prokaryotic communities capable to resist and thrive in an environment subjected to a

selection force as salinity, even the antibiotics and the different substrate concentrations in a lesser degree. Conspicuously, sediments underlying the solar salterns of S'Avall constitute an outstanding source of microbial novelty (Antón *et al.*, 2000; Mora-Ruiz *et al.*, 2015, 2016, 2018; Viver *et al.*, 2018, 2019; Font-Verdera *et al.*, 2021), and particularly the awesome halophilic and methanogenic microorganisms, that, in the suitable conditions, are capable to generate a clean and renewable energy (gas methane) using a novel substrate for this purpose, as *Posidona oceanica*. Further investigation could be performed in the research of the specific culture requirements for the enriched microcosms thriving, with this study as a basis, and to take the chance of using these consortia in a medium- or large-scale biodigesters, fed with *Posidonia oceanica* and seawater as main operating conditions.

VI. CONCLUSIONS

∞ Prokaryotic communities from the hypersaline and anaerobic sediments from S'Avall solar salterns showed an inverted stratification, and a spatial-temporal taxonomic structure stability. Hypersaline anaerobic sediments are a source of taxonomic novelty, with prokaryotes involved in fermentative (such as those belonging to *Salinarchaeum* sp., DHVE2 cluster and *Thermotogae* class), sulfate-reducing (*Halodesulfurarchaeum* sp. and *Deltaproteobacteria* class), acetogenesis (*Acetothermia* phylum), nitrogen cycle and predominantly methanogenic (*Candidatus* MSBL1 lineage, *Methanobacteria* and *Methanomicrobia* classes) metabolisms.

∞ Relevant species with scarce genomic information were binned, highlighting members of the candidate DHVE2 lineage and the *Candidatus* MSBL1 lineage, especially in the most superficial horizons within the vertical stratification. These microorganisms have been observed to be putative hydrogenotrophic methanogens, highly adapted to hypersaline and anoxic environments.

∞ Microbial communities affiliated to the class *Halobacteria* were detected in the deepest fraction of the sediment, with active cellular replication, and evidencing their metabolic involvement in hypersaline sediments, especially in fermentation and carbohydrates degradation.

∞ Salinity acts as the major selection force in the assembly of the microbial communities, in where at high salinities, communities were dominated by extreme halophilic Archaea, whereas bacterial alpha diversity decreased with salinity increase, being highest at 5%.

∞ The community structures of hypersaline sediments of S'Avall were governed by stochastic factors at high salinities as the community was already adapted to 30% salinity. As the salinity of the sediments was diluted, selection became more important as a result of the environmental change. The present findings conclude that dilution applied to the slurry (initial conditions), ranging from 30% to 5% of salinity (at which the highest compositional changes were detected), was the most relevant ecological factor structuring the microbial communities of S'Avall.

∞ The ampicillin exerted a selective pressure in the taxonomic structures, whereas the addition of different concentrations of *Posidonia oceanica* as a substrate did not cause relevant shifts in the microbial composition.

∞ Microcosms with ampicillin, 10% of *Posidonia oceanica* at 5% of salinity showed the highest methane yields, with the supplemented enrichment (ATF) as most efficient culture for methane generation. *Methanomicrobia* and *Bathyarchaeia* were identified as the main methane producers via methanogenic aceticlastic route.

∞ Sediments underlying the solar salterns of S'Avall constituted an outstanding source of microbial novelty, and particularly of halophilic and methanogenic microorganisms, capable to generate a clean and renewable energy (CH_4) using *Posidonia oceanica* as substrate for this purpose, in the suitable conditions of ampicillin and salinity.

REFERENCES

Adekunle, K.F. and Okolie, J.A. (2015) A review of biochemical process of anaerobic digestion. *Adv Biosci Biotechnol* **6**: 205–212.

Altschul, S.F., Gish, W., Miller, W., Myers, E.W., and Lipman, D.J. (1990) Basic local alignment search tool. *J Mol Biol* **215**: 403–410.

Anderson, C.R., Dick, G.J., Chu, M., Cho, J., Davis, R.E., Bräuer, S.L., et al. (2009) *Aurantimonas manganoxydans*, sp. nov. and *Aurantimonas litoralis*, sp. nov.: Mn(II) oxidizing representatives of a globally distributed clade of *alpha-Proteobacteria* from the order *Rhizobiales*. *Geomicrobiol J* **26**: 189–198.

Antón, J., Oren, A., Benlloch, S., Rodrı, F., and Amann, R. (2002) *Salinibacter ruber* gen . nov ., sp . nov ., a novel , extremely halophilic member of the Bacteria from saltern crystallizer ponds. *Int J Syst Evol Microbiol* **52**: 485–491.

Antón, J., Rosselló-Mora, R., Rodríguez-Valera, F., and Amann, R. (2000) Extremely halophilic Bacteria in crystallizer ponds from solar salterns. *Appl Environ Microbiol* **66**: 3052–3057.

Antunes, A., Ngugi, D.K., and Stingl, U. (2011) Microbiology of the Red Sea (and other) deep-sea anoxic brine lakes. *Environ Microbiol Rep* **3**: 416–433.

Aziz, R.K., Bartels, D., Best, A.A., Dejongh, M., Disz, T., Edwards, R.A., et al. (2008) The RAST Server: Rapid Annotations using Subsystems Technology. *BMC Genomics* **9**: 1–15.

Badhai, J., Ghosh, T.S., and Das, S.K. (2015) Taxonomic and functional characteristics of microbial communities and their correlation with physicochemical properties of four geothermal springs in Odisha, India. *Front Microbiol* **6**: 1–15.

Baker, B.J., De Anda, V., Seitz, K.W., Dombrowski, N., Santoro, A.E., and Lloyd, K.G. (2020) Diversity, ecology and evolution of Archaea. *Nat Microbiol* **5**: 887–900.

Baumgartner, M., Bayer, F., Pfrunder-Cardozo, K.R., Buckling, A., and Hall, A.R. (2020) Resident microbial communities inhibit growth and antibiotic-resistance evolution of Escherichia coli in human gut microbiome samples. *PLoS Biol* **18**: 1–30.

Benlloch, S., López-López, A., Casamayor, E.O., Øvreås, L., Goddard, V., Daae, F.L., et al. (2002) Prokaryotic genetic diversity throughout the salinity gradient of a coastal solar saltern. *Environ Microbiol* **4**: 349–360.

Bolger, A.M., Lohse, M., and Usadel, B. (2014) Trimmomatic: A flexible trimmer for Illumina sequence data. *Bioinformatics* **30**: 2114–2120.

Bonet Aracil, M., Gisbert Payá, J., Bou Belda, E., Montava, I., and Díaz García, P. (2019) Fibers of the

seagrass *Posidonia oceanic*a as substrate for germination of lentil seeds. *SN Appl Sci* **1**: 1–6.

Borrel, G., Parisot, N., Harris, H.M.B., Peyretaillade, E., Gaci, N., Tottey, W., et al. (2014) Comparative genomics highlights the unique biology of *Methanomassiliicoccales*, a *Thermoplasmatales*-related seventh order of methanogenic archaea that encodes pyrrolysine. *BMC Genomics* **15**: 679–701.

Boujelben, I., Yarza, P., Almansa, C., Villamor, J., Maalej, S., Antón, J., and Santos, F. (2012) Virioplankton community structure in Tunisian solar salterns. *Appl Environ Microbiol* **78**: 7429–7437.

Brock, T.D. (1997) The value of basic research: Discovery of *Thermus aquaticus* and other extreme thermophiles. *Genetics* **146**: 1207–1210.

Buriánková, I., Brablcová, L., Mach, V., Dvořák, P., and Chaudhary, P.P. (2013) Identification of methanogenic archaea in the hyporheic sediment of Sitka stream. *PLoS One* **8**: 1–10.

Cai, C., Leu, A.O., Xie, G.J., Guo, J., Feng, Y., Zhao, J.X., et al. (2018) A methanotrophic archaeon couples anaerobic oxidation of methane to Fe(III) reduction. *ISME J* **12**: 1929–1939.

Callahan, B.J., McMurdie, P.J., Rosen, M.J., Han, A.W., Johnson, A.J.A., and Holmes, S.P. (2016) DADA2: High resolution sample inference from Illumina amplicon data. *Nat Methods* **13**: 581–592.

Caporaso, J., Kuczynski, J., Stombaugh, J., Bittinger, K., Bushman, F., Costello, E., et al. (2010) QIIME allows analysis of high-throughput community sequencing data. *Natl Inst Heal* **7**: 1–12.

Caporaso, J.G., Lauber, C.L., Walters, W.A., Berg-Lyons, D., Lozupone, C.A., Turnbaugh, P.J., et al. (2011) Global patterns of 16S rRNA diversity at a depth of millions of sequences per sample. *Proc Natl Acad Sci U S A* **108**: 4516–4522.

Cetecioglu, Z., Ince, B., Orhon, D., and Ince, O. (2012) Acute inhibitory impact of antimicrobials on acetoclastic methanogenic activity. *Bioresour Technol* **114**: 109–116.

Chan, P.P. and Lowe, T.M. (2019) tRNAscan-SE: Searching for tRNA genes in genomic sequences. *Methods Mol Biol* **1962**: 1–14.

Chase, J.M., Kraft, N.J.B., Smith, K.G., Vellend, M., and Inouye, B.D. (2011) Using null models to disentangle variation in community dissimilarity from variation in α-diversity. *Ecosphere* **2**: 1–11.

Cocozza, C., Parente, A., Zaccone, C., Mininni, C., Santamaria, P., and Miano, T. (2011) Comparative management of offshore posidonia residues: Composting vs. energy recovery. *Waste Manag*

31: 78–84.

Colangelo-Lillis, J., Wing, B.A., Raymond-Bouchard, I., and Whyte, L.G. (2017) Viral induced microbial mortality in arctic hypersaline spring sediments. *Front Microbiol* **7**: 1–15.

Colangelo-Lillis, J., Wing, B.A., and Whyte, L.G. (2016) Low viral predation pressure in cold hypersaline Arctic sediments and limits on lytic replication. *Environ Microbiol Rep* **8**: 250–260.

La Cono, V., Smedile, F., Bortoluzzi, G., Arcadi, E., Maimone, G., Messina, E., et al. (2011) Unveiling microbial life in new deep-sea hypersaline Lake Thetis. Part I: Prokaryotes and environmental settings. **13**: 2250–2268.

Corinaldesi, C., Tangherlini, M., Luna, G.M., and Dell'Anno, A. (2014) Extracellular DNA can preserve the genetic signatures of present and past viral infection events in deep hypersaline anoxic basins. *Proc R Soc B Biol Sci* **281**: 1–10.

Costa, K.C. and Leigh, J.A. (2014) Metabolic versatility in methanogens. *Curr Opin Biotechnol* **29**: 70–75.

Couvin, D., Bernheim, A., Toffano-Nioche, C., Touchon, M., Michalik, J., Néron, B., et al. (2018) CRISPRCasFinder, an update of CRISRFinder, includes a portable version, enhanced performance and integrates search for Cas proteins. *Nucleic Acids Res* **46**: W246–W251.

Cox, M.P., Peterson, D.A., and Biggs, P.J. (2010) SolexaQA: At-a-glance quality assessment of Illumina second-generation sequencing data. *BMC Bioinformatics* **11**: 485–490.

Danovaro, R., Bongiorni, L., Corinaldesi, C., Giovannelli, D., Damiani, E., Astolfi, P., et al. (2008) Sunscreens cause coral bleaching by promoting viral infections. *Environ Health Perspect* **116**: 441–447.

Danovaro, R., Corinaldesi, C., Dell'Anno, A., Fabiano, M., and Corselli, C. (2005) Viruses, prokaryotes and DNA in the sediments of a deep-hypersaline anoxic basin (DHAB) of the Mediterranean Sea. *Environ Microbiol* **7**: 586–592.

Dębowski, M., Zieliński, M., Grala, A., and Dudek, M. (2013) Algae biomass as an alternative substrate in biogas production technologies - Review. *Renew Sustain Energy Rev* **27**: 596–604.

Dziewit, L., Pyzik, A., Romaniuk, K., and Sobczak, A. (2015) Novel molecular markers for the detection of methanogens and phylogenetic analyses of methanogenic communities. *Front Microbiol* **6**: 1–12.

Eder, W., Jahnke, L.L., Schmidt, M., and Huber, R. (2001) Microbial diversity of the brine-seawater interface of the Kebrit Deep, Red Sea, studied via 16S rRNA gene sequences and cultivation methods. *Appl Environ Microbiol* **67**: 3077–3085.

Eder, W., Schmidt, M., Koch, M., Garbe-Schönberg, D., and Huber, R. (2002) Prokaryotic phylogenetic diversity and corresponding geochemical data of the brine-seawater interface of the Shaban Deep, Red Sea. *Environ Microbiol* **4**: 758–763.

Emiola, A. and Oh, J. (2018) High throughput in situ metagenomic measurement of bacterial replication at ultra-low sequencing coverage. *Nat Commun* **9**: 1–8.

Evans, P.N., Parks, D.H., Chadwick, G.L., Robbins, S.J., Orphan, V.J., Golding, S.D., and Tyson, G.W. (2015) Methane metabolism in the archaeal phylum *Bathyarchaeota* revealed by genome-centric metagenomics. *Science (80-)* **350**: 434–438.

Fan, X. and Xing, P. (2016) Differences in the composition of archaeal communities in sediments from contrasting zones of Lake Taihu. *Front Microbiol* **7**: 1–11.

Fenchel, T., King, G.M., and Blackburn, T.H. (2012) Bacterial metabolism. In *Bacterial Biogeochemistry: The ecophysiology of mineral cycling*. USA: Academic Press, pp. 1–34.

Fernandez, A.B., Rasuk, M.C., Visscher, P.T., Contreras, M., Novoa, F., Poire, D.G., et al. (2016) Microbial diversity in sediment ecosystems (evaporites domes, microbial mats, and crusts) of Hypersaline Laguna Tebenquiche, Salar de Atacama, Chile. *Front Microbiol* **7**: 1–18.

Ferrer, M., Méndez-García, C., Rojo, D., Barbas, C., and Moya, A. (2017) Antibiotic use and microbiome function. *Biochem Pharmacol* **134**: 114–126.

Flores, G.E., Wagner, I.D., Liu, Y., and Reysenbach, A.L. (2012) Distribution, abundance, and diversity patterns of the thermoacidophilic "deep-sea hydrothermal vent euryarchaeota 2." *Front Microbiol* **3**: 1–17.

Font-Verdera, F., Liébana, R., Aldeguer-Riquelme, B., Gangloff, V., Santos, F., Viver, T., and Rosselló-Móra, R. (2021) Inverted microbial community stratification and spatial–temporal stability in hypersaline anaerobic sediments from the S'Avall solar salterns. *Syst Appl Microbiol* **44**: 126231.

França, L., Lopéz-Lopéz, A., Rosselló-Móra, R., and Costa, M.S. (2015) Microbial diversity and dynamics of a groundwater and a still bottled natural mineral water. *Environ Microbiol* **17**: 577–593.

Fu, L., Niu, B., Zhu, Z., Wu, S., and Li, W. (2012) CD-HIT: Accelerated for clustering the next-

generation sequencing data. *Bioinformatics* **28**: 3150–3152.

Gao, J., Liu, G., Li, H., Xu, L., Du, L., and Yang, B. (2016) Predictive functional profiling using marker gene sequences and community diversity analyses of microbes in full-scale anaerobic sludge digesters. *Trends Microbiol* **20**: 251–258.

Giani, D., Jannsen, D., Schostak, V., and Krumbein, W.E. (1989) Methanogenesis in a saltern in the Bretagne (France). *FEMS Microbiol Lett* **62**: 143–149.

Gomariz, M., Martínez-García, M., Santos, F., Rodriguez, F., Capella-Gutiérrez, S., Gabaldón, T., et al. (2015) From community approaches to single-cell genomics: The discovery of ubiquitous hyperhalophilic *Bacteroidetes* generalists. *ISME J* **9**: 16–31.

Gottschalk, G. (1979) Bacterial Metabolism, 1st Editio. Microbiology, S. series in (ed) United States: New York: Springer-Verlag, c1979.

Gründger, F., Jiménez, N., Thielemann, T., Straaten, N., Lüders, T., Richnow, H.H., and Krüger, M. (2015) Microbial methane formation in deep aquifers of a coal-bearing sedimentary basin, Germany. *Front Microbiol* **6**: 1–17.

Guo, B., Liu, Y., Gu, Z., Shen, L., Liu, K., Xing, T., et al. (2017) *Aureimonas glaciei* sp. nov., isolated from ice core. *Int J Syst Evol Microbiol* **67**: 485–488.

Hammer, Ø., Harper, D.A.T., and Ryan, P.D. (2001) PAST: Paleontological statistics software package for education and data analysis. *Palaeontol Electrónica* **4**: 1–9.

Haroon, M.F., Hu, S., Shi, Y., Imelfort, M., Keller, J., Hugenholtz, P., and Yuan, Z. (2013) Anaerobic oxidation of methane coupled to nitrate reduction in a novel archaeal lineage. *Nature* **0**: 2–8.

Hippe, H., Caspari, D., Fiebig, K., and Gottschalk, G. (1979) Utilization of trimethylamine and other N methyl compounds for growth and methane formation by *Methanosarcina barkeri*. *Proc Natl Acad Sci U S A* **76**: 494–498.

Holmes, D.E. and Smith, J.A. (2016) Biologically produced methane as a renewable energy source. *Adv Appl Microbiol* **97**: 1–61.

Hua, Z.S., Wang, Y.L., Evans, P.N., Qu, Y.N., Goh, K.M., Rao, Y.Z., et al. (2019) Insights into the ecological roles and evolution of methyl-coenzyme M reductase-containing hot spring Archaea. *Nat Commun* **10**: 1–11.

Hyatt, D., Chen, G.L., LoCascio, P.F., Land, M.L., Larimer, F.W., and Hauser, L.J. (2010) Prodigal: Prokaryotic gene recognition and translation initiation site identification. *BMC*

Bioinformatics **11**: 1–11.

Imachi, H., Nobu, M.K., Nakahara, N., Morono, Y., Ogawara, M., Takaki, Y., et al. (2020) Isolation of an archaeon at the prokaryote–eukaryote interface. *Nature* **577**: 519–525.

Jiang, H., Dong, H., Yu, B., Liu, X., Li, Y., Ji, S., and Zhang, C.L. (2007) Microbial response to salinity change in Lake Chaka, a hypersaline lake on Tibetan plateau. *Environ Microbiol* **9**: 2603–2621.

Joye, S.B., Samarkin, V.A., Orcutt, B.N., MacDonald, I.R., Hinrichs, K.U., Elvert, M., et al. (2009) Metabolic variability in seafloor brines revealed by carbon and sulphur dynamics. *Nat Geosci* **2**: 349–354.

Jurado, V., Gonzalez, J.M., Laiz, L., and Saiz-jimenez, C. (2006) *Aurantimonas altamirensis* sp. nov., a member of the order *Rhizobiales* isolated from Altamira Cave. *Int J Syst Evol Microbiol* **56**: 2583–2585.

Kaleem Sarwar, M., Azam, I., and Iqbal, T. (2015) Biology and applications of halophilic Bacteria and Archaea: A review. *Electron J Biol* **11**: 98–103.

Karakashev, D., Batstone, D.J., Trably, E., and Angelidaki, I. (2006) Acetate oxidation is the dominant methanogenic pathway from acetate in the absence of *Methanosaetaceae*. *Appl Environ Microbiol* **72**: 5138–5141.

Kent, W.J. (2002) BLAT---The BLAST-Like Alignment Tool. *Genome Res* **12**: 656–664.

Knittel, K. and Boetius, A. (2009) Anaerobic oxidation of methane: Progress with an unknown process. *Annu Rev Microbiol* **63**: 311–334.

Kohn, T., Rast, P., Kallscheuer, N., Wiegand, S., Boedeker, C., Jetten, M.S.M., et al. (2020) The Microbiome of *Posidonia oceanica* seagrass leaves can be dominated by *Planctomycetes*. *Front Microbiol* **11**: 1–14.

Konstantinidis, K.T., Rosselló-Móra, R., and Amann, R. (2017) Uncultivated microbes in need of their own taxonomy. *ISME J* **11**: 2399–2406.

Kraft, N.J.B., Comita, L.S., Chase, J.M., Sanders, N.J., Swenson, N.G., Crist, T.O., et al. (2011) Disentangling the drivers of β diversity along latitudinal and elevational gradients. *Science (80-)* **333**: 1755–1758.

Lamarche-Gagnon, G., Comery, R., Greer, C.W., and Whyte, L.G. (2015) Evidence of in situ microbial activity and sulphidogenesis in perennially sub-0 °C and hypersaline sediments of a high Arctic permafrost spring. *Extremophiles* **19**: 1–15.

Langenheder, S., Wang, J., Karjalainen, S.M., Laamanen, T.M., Tolonen, K.T., Vilmi, A., and Heino, J. (2017) Bacterial metacommunity organization in a highly connected aquatic system. *FEMS Microbiol Ecol* **93**: 1–9.

Laso-Pérez, R., Krukenberg, V., Musat, F., and Wegener, G. (2018) Establishing anaerobic hydrocarbon-degrading enrichment cultures of microorganisms under strictly anoxic conditions. *Nat Protoc* **13**: 1310–1330.

Lazar, C.S., Parkes, R.J., Cragg, B.A., L'Haridon, S., and Toffin, L. (2011) Methanogenic diversity and activity in hypersaline sediments of the centre of the Napoli mud volcano, Eastern Mediterranean Sea. *Environ Microbiol* **13**: 2078–2091.

Ley, R.E., Harris, J.K., Wilcox, J., Spear, J.R., Miller, S.R., Bebout, B.M., et al. (2006) Unexpected diversity and complexity of the Guerrero Negro hypersaline microbial mat. *Appl Environ Microbiol* **72**: 3685–3695.

Liang, Y., Ning, D., Lu, Z., Zhang, N., Hale, L., Wu, L., et al. (2020) Century long fertilization reduces stochasticity controlling grassland microbial community succession. *Soil Biol Biochem* **151**: (108023) 1-9.

Liébana, R., Modin, O., Persson, F., Szabó, E., Hermansson, M., and Wilén, B.M. (2019) Combined deterministic and stochastic processes control microbial succession in replicate granular biofilm reactors. *Environ Sci Technol* **53**: 4912–4921.

Liu, M., Deora, R., Doulatov, S.R., Gingery, M., Eiserling, F.A., Preston, A., et al. (2002) Reverse transcriptase-mediated tropism switching in *Bordetella* bacteriophage. *Science (80-)* **295**: 2091–2094.

Liu, Y. and Whitman, W.B. (2008) Metabolic, phylogenetic, and ecological diversity of the methanogenic archaea. *Ann N Y Acad Sci* **1125**: 171–189.

Lloyd, K.G., Lapham, L., and Teske, A. (2006) An anaerobic methane-oxidizing community of ANME-1b Archaea in hypersaline Gulf of Mexico sediments. *Appl Environ Microbiol* **72**: 7218–7230.

López-López, A., Richter, M., Peña, A., Tamames, J., and Rosselló-Móra, R. (2013) New insights into the archaeal diversity of a hypersaline microbial mat obtained by a metagenomic approach. *Syst Appl Microbiol* **36**: 205–214.

López-López, A., Yarza, P., Richter, M., Suárez-Suárez, A., Antón, J., Niemann, H., and Rosselló-Móra, R. (2010) Extremely halophilic microbial communities in anaerobic sediments from a

solar saltern. *Environ Microbiol Rep* **2**: 258–271.

Lozupone, C.A. and Knight, R. (2007) Global patterns in bacterial diversity. *Proc Natl Acad Sci U S A* **104**: 11436–11440.

Ludwig, W., Strunk, O., Westram, R., Richter, L., Meier, H., Yadhukumar, A., et al. (2004) ARB: A software environment for sequence data. *Nucleic Acids Res* **32**: 1363–1371.

Lykidis, A., Chen, C.-L., Tringe, S.G., McHardy, A.C., Copeland, A., Kyrpides, N.C., et al. (2011) Multiple syntrophic interactions in a terephthalate-degrading methanogenic consortium authors inadvertently ommitted from the original version of the paper. *ISME J* **5**: 122–130.

Lykidis, A., Chen, C.L., Tringe, S.G., McHardy, A.C., Copeland, A., Kyrpides, N.C., et al. (2011) Multiple syntrophic interactions in a terephthalate-degrading methanogenic consortium. *ISME J* **5**: 122–130.

Magoč, T. and Salzberg, S.L. (2011) FLASH: Fast length adjustment of short reads to improve genome assemblies. *Bioinformatics* **27**: 2957–2963.

Mahé, F., Rognes, T., Quince, C., de Vargas, C., and Dunthorn, M. (2014) Swarm: Robust and fast clustering method for amplicon-based studies. *PeerJ* **2014**: 1–13.

Mand, T.D. and Metcalf, W.W. (2019) Energy conservation and hydrogenase function in methanogenic Archaea, in particular the genus *Methanosarcina*. *Microbiol Mol Biol Rev* **83**: 1–22.

Manyi-loh, C.E., Mamphweli, S.N., Meyer, E.L., and Okoh, A.I. (2013) Microbial anaerobic digestion (Bio-Digesters) as an approach to the decontamination of animal wastes in pollution control and the generation of renewable energy. *Int J Environ Res Public Health* **10**: 4390–4417.

Marbà, N., Díaz-almela, E., and Duarte, C.M. (2014) Mediterranean seagrass (*Posidonia oceanica*) loss between 1842 and 2009. *Biol Conserv* **176**: 183–190.

Martin-Cuadrado, A.B., Senel, E., Martínez-García, M., Cifuentes, A., Santos, F., Almansa, C., et al. (2019) Prokaryotic and viral community of the sulfate-rich crust from Peñahueca ephemeral lake, an astrobiology analogue. *Environ Microbiol* **21**: 3577–3600.

Mcgenity, T.J. (2010) Chapter 53 - Methanogens and methanogenesis in hypersaline environments. In *Handbook of hydrocarbon and lipid microbiology*. pp. 665–680.

McGenity, T.J. and Oren, A. (2012) Hypersaline environments. In *Life at extremes: Environments. Organisms and strategies for survival*. Bell, E.M. (ed). UK, pp. 402–437.

McGenity, T.J. and Sorokin, D.Y. (2019) Methanogens and methanogenesis in hypersaline environments. In *Biogenesis of hydrocarbons, Handbook of hydrocarbon and lipid microbiology*. A., S. and D., S. (eds). Springer, Cham, pp. 283–309.

McIlroy, S.J., Kirkegaard, R.H., Dueholm, M.S., Fernando, E., Karst, S.M., Albertsen, M., and Nielsen, P.H. (2017) Culture-independent analyses reveal novel anaerolineaceae as abundant primary fermenters in anaerobic digesters treating waste activated sludge. *Front Microbiol* **8**: 1–10.

Mcinerney, M.J., Sieber, J.R., and Gunsalus, R.P. (2010) Syntrophy in anaerobic global carbon cycles. *Curr Opin Biotechnol* **20**: 623–632.

McKay, L.J., Dlakić, M., Fields, M.W., Delmont, T.O., Eren, A.M., Jay, Z.J., et al. (2019) Co-occurring genomic capacity for anaerobic methane and dissimilatory sulfur metabolisms discovered in the Korarchaeota. *Nat Microbiol* **4**: 614–622.

Medina, J.R., Tintoré, J., and Duarte, C.M. (2001) Las praderas de *Posidonia oceanica* y la regeneración de playas. *Rev Obras Publicas* **148**: 31–43.

Menzel, P., Ng, K.L., and Krogh, A. (2016) Fast and sensitive taxonomic classification for metagenomics with Kaiju. *Nat Commun* **7**: 1–9.

Merlino, G., Barozzi, A., Michoud, G., Ngugi, D.K., and Daffonchio, D. (2018) Microbial ecology of deep-sea hypersaline anoxic basins. *FEMS Microbiol Ecol* **94**: 1–15.

Minegishi, H., Enomoto, S., Echigo, A., Shimane, Y., Kondo, Y., Inoma, A., et al. (2017) *Salinarchaeum chitinilyticum* sp. nov., a chitin-degrading haloarchaeon isolated from commercial salt. *Int J Syst Evol Microbiol* **67**: 2274–2278.

Mininni, C., Grassi, F., Traversa, A., Cocozza, C., Parente, A., and Santamaria, P. (2014) *Posidonia oceanica* (L .) based compost as substrate for potted basil production. *J Sci Food Agric*.

Mistry, J., Chuguransky, S., Williams, L., Qureshi, M., Salazar, G.A., Sonnhammer, E.L.L., et al. (2021) Pfam: The protein families database in 2021. *Nucleic Acids Res* **49**: D412–D419.

Montefalcone, M. (2009) Ecosystem health assessment using the Mediterranean seagrass *Posidonia oceanica*: A review. *Ecol Indic* **9**: 595–604.

Mora-Ruiz, M. del R., Cifuentes, A., Font-Verdera, F., Pérez-Fernández, C., Farias, M.E., González, B., et al. (2018) Biogeographical patterns of bacterial and archaeal communities from distant hypersaline environments. *Syst Appl Microbiol* **41**: 139–150.

Mora-Ruiz, M. del R., Font-Verdera, F., Díaz-Gil, C., Urdiain, M., Rodríguez-Valdecantos, G., González, B., et al. (2015) Moderate halophilic bacteria colonizing the phylloplane of

halophytes of the subfamily *Salicornioideae* (*Amaranthaceae*). *Syst Appl Microbiol* **38**: 406–416.

Mora-Ruiz, M.D.R., Font-Verdera, F., Orfila, A., Rita, J., and Rosselló-Móra, R. (2016) Endophytic microbial diversity of the halophyte *Arthrocnemum macrostachyum* across plant compartments. *FEMS Microbiol Ecol* **92**: 1–10.

Moriya, Y., Itoh, M., Okuda, S., Yoshizawa, A.C., and Kanehisa, M. (2007) KAAS: an automatic genome annotation and pathway reconstruction server. *Nucleic Acids Res* **35**: 182–185.

Morris, B.E.L., Henneberger, R., Huber, H., and Moissl-Eichinger, C. (2013) Microbial syntrophy: Interaction for the common good. *FEMS Microbiol Rev* **37**: 384–406.

Munoz, R., López-López, A., Urdiain, M., Moore, E.R.B., and Rosselló-Móra, R. (2011) Evaluation of matrix-assisted laser desorption ionization-time of flight whole cell profiles for assessing the cultivable diversity of aerobic and moderately halophilic prokaryotes thriving in solar saltern sediments. *Syst Appl Microbiol* **34**: 69–75.

Muyzer, G., Teske, A., Wirsen, C.O., and Jannasch, H.W. (1995) Phylogenetic relationships of *Thiomicrospira* species and their identification in deep-sea hydrothermal vent samples by denaturing gradient gel electrophoresis of 16S rDNA fragments. *Arch Microbiol* **164**: 165–172.

Mwirichia, R., Intikhab, A., Rashid, M., Vinu, M., Ba-, W., Kamau, A.A., et al. (2016) Metabolic traits of an uncultured archaeal lineage -MSBL1- from brine pools of the Red Sea. *Nat Sci Reports* **6**: 1–14.

Nelson, M.C., Morrison, M., and Yu, Z. (2011) A meta-analysis of the microbial diversity observed in anaerobic digesters. *Bioresour Technol* **102**: 3730–3739.

Nigro, L.M., Elling, F.J., Hinrichs, K.U., Joye, S.B., and Teske, A. (2020) Microbial ecology and biogeochemistry of hypersaline sediments in Orca Basin. *PLoS One* **15**: 1–25.

Ning, D., Deng, Y., Tiedje, J.M., and Zhou, J. (2019) A general framework for quantitatively assessing ecological stochasticity. *Proc Natl Acad Sci U S A* **116**: 16892–16898.

Oksanen, A.J., Blanchet, F.G., Friendly, M., Kindt, R., Legendre, P., Mcglinn, D., et al. (2018) vegan: Community Ecology Package. R package version 2.4-4. 298.

Oliveira, L.C.G., Ramos, P.L., Marem, A., Kondo, M.Y., Rocha, R.C.S., Bertolini, T., et al. (2015) Halotolerant bacteria in the São Paulo Zoo composting process and their hydrolases and bioproducts. *Brazilian J Microbiol* **46**: 347–354.

Orellana, L.H., Chee-Sanford, J.C., Sanford, R.A., Löffler, F.E., and Konstantinidis, K.T. (2018) Year-round shotgun metagenomes reveal stable microbial communities in agricultural soils and novel ammonia oxidizers responding to fertilization. *Appl Environ Microbiol* **84**:.

Oren, A. (2002) Diversity of halophilic microorganisms: Environments, phylogeny, physiology, and applications. *J Ind Microbiol Biotechnol* **28**: 56–63.

Oren, A. (2017) Glycerol metabolism in hypersaline environments. *Environ Microbiol* **19**: 851–863.

Oren, A. (2013) Life at high salt and low oxygen: How do the *Halobacteriaceae* cope with low oxygen concentrations in their environment? *Polyextremophiles Life Under Mult Forms Stress* **27**: 531–548.

Oren, A. (2008) Microbial life at high salt concentrations: phylogenetic and metabolic diversity. *Saline Systems* **4**: 1–13.

Oren, A. (2014) Taxonomy of halophilic Archaea: current status and future challenges. *Extremophiles* **18**: 825–834.

Oshiki, M., Satoh, H., and Okabe, S. (2016) Ecology and physiology of anaerobic ammonium oxidizing bacteria. *Environ Microbiol* **18**: 2784–2796.

Oueriaghli, N., Castro, D.J., Llamas, I., Béjar, V., and Martínez-Checa, F. (2018) Study of bacterial community composition and correlation of environmental variables in Rambla Salada, a hypersaline environment in South-Eastern Spain. *Front Microbiol* **9**: 1–17.

Parks, D.H., Chuvochina, M., Waite, D.W., Rinke, C., Skarshewski, A., Chaumeil, P.A., and Hugenholtz, P. (2018) A standardized bacterial taxonomy based on genome phylogeny substantially revises the tree of life. *Nat Biotechnol* **36**: 996.

Patterson, J.A. and Hespell, R.B. (1979) Trimethylamine and methylamine as growth substrates for rumen bacteria and *Methanosarcina barkeri*. *Curr Microbiol* **3**: 79–83.

Pedrós-Alió, C., Calderón-Paz, J.I., MacLean, M.H., Medina, G., Marrasé, C., Gasol, J.M., and Guixa-Boixereu, N. (2000) The microbial food web along salinity gradients. *FEMS Microbiol Ecol* **32**: 143–155.

Peng, Y., Leung, H.C.M., Yiu, S.M., and Chin, F.Y.L. (2012) IDBA-UD: a de novo assembler for single-cell and metagenomic sequencing data with highly uneven depth. *Bioinformatics* **28**: 1420–1428.

Petro, C., Starnawski, P., Schramm, A., and Kjeldsen, K.U. (2017) Microbial community assembly in marine sediments. *Aquat Microb Ecol* **79**: 177–195.

Pruesse, E., Peplies, J., and Glöckner, F.O. (2012) SINA: Accurate high-throughput multiple sequence alignment of ribosomal RNA genes. *Bioinformatics* **28**: 1823–1829.

Ramos-Barbero, M.D., Martin-Cuadrado, A.B., Viver, T., Santos, F., Martinez-Garcia, M., and Antón, J. (2019) Recovering microbial genomes from metagenomes in hypersaline environments: The Good, the Bad and the Ugly. *Syst Appl Microbiol* **42**: 30–40.

Ramos-Barbero, M.D., Martínez, J.M., Almansa, C., Rodríguez, N., Villamor, J., Gomariz, M., et al. (2019) Prokaryotic and viral community structure in the singular chaotropic salt lake Salar de Uyuni. *Environ Microbiol* **21**: 2029–2042.

Rathi, R., Lavania, M., Kukreti, V., and Lal, B. (2018) Evaluating the potential of indigenous methanogenic consortium for enhanced oil and gas recovery from high temperature depleted oil reservoir. *J Biotechnol* **283**: 43–50.

Reysenbach, A.L., Liu, Y., Banta, A.B., Beveridge, T.J., Kirshtein, J.D., Schouten, S., et al. (2006) A ubiquitous thermoacidophilic archaeon from deep-sea hydrothermal vents. *Nature* **442**: 444–447.

Richter, M., Rosselló-Móra, R., Glockner, F.O., and Peplies, J. (2016) JSpeciesWS: a web server for prokaryotic species circumscription based on pairwise genome comparison. *Bioinformatics* **32**: 929–931.

Rodriguez-R, L.M., Gunturu, S., Tiedje, J.M., Cole, J.R., and Konstantinidis, K.T. (2018) Nonpareil 3: Fast estimation of metagenomic coverage and sequence diversity. *mSystems* **3**: 1–9.

Rodriguez-R, L.M. and Konstantinidis, K.T. (2014) Nonpareil: A redundancy-based approach to assess the level of coverage in metagenomic datasets. *Bioinformatics* **30**: 629–635.

Rodriguez-R, L.M. and Konstantinidis, K.T. (2016) The enveomics collection: a toolbox for specialized analyses of microbial genomes and metagenomes microbial genomes and metagenomes. *PeerJ Prepr* **4**:.

Roux, S., Enault, F., Bronner, G., Vaulot, D., Forterre, P., and Krupovic, M. (2013) Chimeric viruses blur the borders between the major groups of eukaryotic single-stranded DNA viruses. *Nat Commun* **4**: 1–10.

Roux, S., Enault, F., Hurwitz, B.L., and Sullivan, M.B. (2015) VirSorter: Mining viral signal from microbial genomic data. *PeerJ* **2015**: 1–20.

Roux, S., Páez-Espino, D., Chen, I.M.A., Palaniappan, K., Ratner, A., Chu, K., et al. (2021) IMG/VR v3: An integrated ecological and evolutionary framework for interrogating genomes of

uncultivated viruses. *Nucleic Acids Res* **49**: D764–D775.

Santos, F., Yarza, P., Parro, V., Briones, C., and Antón, J. (2010) The metavirome of a hypersaline environment. *Environ Microbiol* **12**: 2965–2976.

Santos, F., Yarza, P., Parro, V., Meseguer, I., Rosselló-Móra, R., and Antón, J. (2012) Culture-independent approaches for studying viruses from hypersaline environments. *Appl Environ Microbiol* **78**: 1635–1643.

Satish Kumar, V., Ferry, J.G., and Maranas, C.D. (2011) Metabolic reconstruction of the archaeon methanogen *Methanosarcina Acetivorans*. *BMC Syst Biol* **5**: 1–10.

Schlegel, H.G. (1976) Microbiología General, Georg Thieme Verlag, Stuttgart: 1997 Ediciones Omega, S.A., Barcelona.

Schmieder, R. and Edwards, R. (2011) Quality control and preprocessing of metagenomic datasets. *Bioinformatics* **27**: 863–864.

Schneegurt, M.A. (2012) Media and conditions for the growth of halophilic and halotolerant Bacteria and Archaea. In *Advances in Understanding the Biology of Halophilic Microorganisms, Chapter 2*. pp. 35–58.

Sela-Adler, M., Ronen, Z., Herut, B., Antler, G., Vigderovich, H., Eckert, W., and Sivan, O. (2017) Co-existence of methanogenesis and sulfate reduction with common substrates in sulfate-rich estuarine sediments. *Front Microbiol* **8**: 1–11.

Sieber, J.R., Mcinerney, M.J., Plugge, C.M., Schink, B., and Gunsalus, R.P. (2010) Methanogenesis: Syntrophic Metabolism, Chapter 12. In *Handbook of Hydrocarbon and Lipid Microbiology*. pp. 337–355.

Sierocinski, P., Bayer, F., Yvon-Durocher, G., Burdon, M., Großkopf, T., Alston, M., et al. (2018) Biodiversity–function relationships in methanogenic communities. *Mol Ecol* **27**: 4641–4651.

Sierocinski, P., Milferstedt, K., Bayer, F., Großkopf, T., Alston, M., Bastkowski, S., et al. (2017) A single community dominates structure and function of a mixture of multiple methanogenic communities. *Curr Biol* **27**: 3390-3395.e4.

Sievers, F., Wilm, A., Dineen, D., Gibson, T.J., Karplus, K., Li, W., et al. (2011) Fast, scalable generation of high-quality protein multiple sequence alignments using Clustal Omega. *Mol Syst Biol* **7**: 1–6.

Sørensen, K.B., Canfield, D.E., and Oren, A. (2004) Salinity responses of benthic microbial communities in a solar saltern (Eilat, Israel). *Appl Environ Microbiol* **70**: 1608–1616.

Sorokin, D.Y., Kublanov, I. V., Gavrilov, S.N., Rojo, D., Roman, P., Golyshin, P.N., et al. (2016) Elemental sulfur and acetate can support life of a novel strictly anaerobic haloarchaeon. *ISME J* **10**: 240–252.

Sorokin, D.Y., Kublanov, I. V., Yakimov, M.M., Rijpstra, W.I.C., and Sinninghe Damsté, J.S. (2016) *Halanaeroarchaeum sulfurireducens* gen. nov., sp. nov., the first obligately anaerobic sulfur-respiring haloarchaeon, isolated from a hypersaline lake. *Int J Syst Evol Microbiol* **66**: 2377–2381.

Sorokin, Dimitry Y, Makarova, K.S., Abbas, B., Ferrer, M., Golyshin, P.N., Galinski, E.A., et al. (2017) Discovery of extremely halophilic, methyl-reducing euryarchaea provides insights into the evolutionary origin of methanogenesis. *Nat Microbiol* **2**: 1–11.

Sorokin, D.Y., Messina, E., Smedile, F., La Cono, V., Hallsworth, J.E., and Yakimov, M.M. (2021) Carbohydrate-dependent sulfur respiration in halo(alkali)philic archaea. *Environ Microbiol* **00**: 1–20.

Sorokin, Dimitry Y., Messina, E., Smedile, F., Roman, P., Sinninghe Damsté, J.S., Ciordia, S., et al. (2017) Discovery of anaerobic lithoheterotrophic haloarchaea, ubiquitous in hypersaline habitats. *ISME J* **11**: 1245–1260.

Speth, D.R., Hu, B., Bosch, N., Keltjens, J.T., Stunnenberg, H.G., and Jetten, M.S.M. (2012) Comparative genomics of two independently enriched "*Candidatus* Kuenenia stuttgartiensis" anammox bacteria. *Front Microbiol* **3**: 1–7.

Spring, S., Bunk, B., Spröer, C., Schumann, P., Rohde, M., Tindall, B.J., and Klenk, H.P. (2016) Characterization of the first cultured representative of *Verrucomicrobia* subdivision 5 indicates the proposal of a novel phylum. *ISME J* **10**: 2801–2816.

Stegen, J.C., Lin, X., Fredrickson, J.K., Chen, X., Kennedy, D.W., Murray, C.J., et al. (2013) Quantifying community assembly processes and identifying features that impose them. *ISME J* **7**: 2069–2079.

Stegen, J.C., Lin, X., Konopka, A.E., and Fredrickson, J.K. (2012) Stochastic and deterministic assembly processes in subsurface microbial communities. *ISME J* **6**: 1653–1664.

Steinberg, L.M. and Regan, J.M. (2009) mcrA -Targeted real-time quantitative PCR method to examine methanogen communities. *Appl Environ Microbiol* **75**: 4435–4442.

Su, X., Xu, J., and Ning, K. (2012) Parallel-META: Efficient metagenomic data analysis based on high-performance computation. *BMC Syst Biol* **6**: S16.

Swan, B.K., Ehrhardt, C.J., Reifel, K.M., Moreno, L.I., and Valentine, D.L. (2010) Archaeal and bacterial communities respond differently to environmental gradients in anoxic sediments of a california hypersaline lake, the Salton Sea. *Appl Environ Microbiol* **76**: 757–768.

Thamdrup, B., Rosselló-Mora, R., and Amann, R. (2000) Microbial manganese and sulfate reduction in Black Sea shelf sediments. *Appl Environ Microbiol* **66**: 2888–2897.

Thauer, R.K. (1998) Biochemistry of methanogenesis: a tribute to Marjory Stephenson. *Microbiology* **144**: 2377–2406.

Timmers, P.H.A., Vavourakis, C.D., Kleerebezem, R., Sinninghe Damsté, J.S., Muyzer, G., Stams, A.J.M., et al. (2018) Metabolism and occurrence of methanogenic and sulfate-reducing syntrophic acetate oxidizing communities in haloalkaline environments. *Front Microbiol* **9**: 1–18.

Torregrosa-Crespo, J., Martínez-Espinosa, R.M., Esclapez, J., Bautista, V., Pire, C., Camacho, M., et al. (2016) Anaerobic metabolism in *Haloferax* genus: Denitrification as case of study. *Adv Microb Physiol* **68**: 41–85.

Turner, S., Pryer, K.M., Miao, V.P.W., and Palmer, J.D. (1999) Investigating deep phylogenetic relationships among *Cyanobacteria* and plastids by small subunit rRNA sequence analysis. *J Eukaryot Microbiol* **46**: 327–338.

Vanwonterghem, I., Evans, P.N., Parks, D.H., Jensen, P.D., Woodcroft, B.J., Hugenholtz, P., and Tyson, G.W. (2016) Methylotrophic methanogenesis discovered in the archaeal phylum *Verstraetearchaeota*. *Nat Microbiol* **1**: 1–9.

Vavourakis, C.D., Andrei, A.S., Mehrshad, M., Ghai, R., Sorokin, D.Y., and Muyzer, G. (2018) A metagenomics roadmap to the uncultured genome diversity in hypersaline soda lake sediments. *Microbiome* **6**: 168–185.

Vavourakis, C.D., Mehrshad, M., Balkema, C., van Hall, R., Andrei, A.Ş., Ghai, R., et al. (2019) Metagenomes and metatranscriptomes shed new light on the microbial-mediated sulfur cycle in a Siberian soda lake. *BMC Biol* **17**: 1–20.

Ventosa, A. and Arahal, D.R. (2009) Physico-chemical characteristics of hypersaline environments and their biodiversity. In *Extremophiles*. p. 16.

Villamor, J., Ramos-Barbero, M.D., González-Torres, P., Gabaldón, T., Rosselló-Móra, R., Meseguer, I., et al. (2018) Characterization of ecologically diverse viruses infecting co-occurring strains of cosmopolitan hyperhalophilic *Bacteroidetes*. *ISME J* **12**: 424–437.

Viver, T., Conrad, R.E., Orellana, L.H., Urdiain, M., González-Pastor, J.E., Hatt, J.K., et al. (2020) Distinct ecotypes within a natural haloarchaeal population enable adaptation to changing environmental conditions without causing population sweeps. *ISME J.*

Viver, T., Orellana, L., González-Torres, P., Díaz, S., Urdiain, M., Farías, M.E., et al. (2018) Genomic comparison between members of the Salinibacteraceae family, and description of a new species of *Salinibacter* (*Salinibacter altiplanensis* sp. nov.) isolated from high altitude hypersaline environments of the Argentinian Altiplano. *Syst Appl Microbiol* **41**: 198–212.

Viver, T., Orellana, L.H., Díaz, S., Urdiain, M., Ramos-Barbero, M.D., González-Pastor, J.E., et al. (2019) Predominance of deterministic microbial community dynamics in salterns exposed to different light intensities. *Environ Microbiol* **21**: 4300–4315.

Viver, T., Orellana, L.H., Hatt, J.K., Urdiain, M., Díaz, S., Richter, M., et al. (2017) The low diverse gastric microbiome of the jellyfish *Cotylorhiza tuberculata* is dominated by four novel taxa. *Environ Microbiol* **19**: 3039–3058.

Waite, D.W., Chuvochina, M., Pelikan, C., Parks, D.H., Yilmaz, P., Wagner, M., et al. (2020) Proposal to reclassify the proteobacterial classes *Deltaproteobacteria* and *Oligoflexia*, and the phylum *Thermodesulfobacteria* into four phyla reflecting major functional capabilities. *Int J Syst Evol Microbiol* **70**: 5972–6016.

Walsh, D.A., Papke, R.T., and Doolittle, W.F. (2005) Archaeal diversity along a soil salinity gradient prone to disturbance. *Environ Microbiol* **7**: 1655–1666.

Webster, G., O'Sullivan, L.A., Meng, Y., Williams, A.S., Sass, A.M., Watkins, A.J., et al. (2015) Archaeal community diversity and abundance changes along a natural salinity gradient in estuarine sediments. *FEMS Microbiol Ecol* **91**: 1–18.

Weiland, P. (2010) Biogas production: current state and perspectives. *Appl Microbiol Biotechnol* **85**: 849–860.

Welte, C.U. (2018) Revival of archaeal methane microbiology. *mSystems* **3**: 1–4.

Westerholm, M., Moestedt, J., and Schnürer, A. (2016) Biogas production through syntrophic acetate oxidation and deliberate operating strategies for improved digester performance. *Appl Energy* **179**: 124–135.

Whitman, W.B., Coleman, D.C., and Wiebe, W.J. (1998) Prokaryotes: the unseen majority. *Proc Natl Acad Sci* **95**: 6578–6583.

van der Wielen, P.W., Bolhuis, H., Borin, S., Daffonchio, D., Corselli, C., Giuliano, L., et al. (2005) The

enigma of prokaryotic life in deep hypersaline anoxic basins. *Science (80-)* **307**: 121–123.

Wilkins, D., Lu, X., Shen, Z., Chen, J., and Lee, P.K.H. (2015) Pyrosequencing of mcrA and archaeal 16S rRNA genes reveals diversity and substrate preferences of methanogen communities in anaerobic digesters. *Appl Environ Microbiol* **81**: 604–613.

Wu, Y.-W., Tang, Y.-H., Tringe, S.G., Simmons, B.A., and Singer, S.W. (2014) MaxBin: an automated binning method to recover individual genomes from metagenomes using. *Microbiome* **2**: 1–18.

Xie, K., Deng, Y., Zhang, S., Zhang, W., Liu, J., Xie, Y., et al. (2017) Prokaryotic community distribution along an ecological gradient of salinity in surface and subsurface saline soils. *Sci Rep* **7**: 1–10.

Yakimov, M.M., La Cono, V., Slepak, V.Z., La Spada, G., Arcadi, E., Messina, E., et al. (2013) Microbial life in the Lake Medee, the largest deep-sea salt-saturated formation. *Sci Rep* **3**: 1–9.

Yakimov, M.M., La Cono, V., Spada, G.L., Bortoluzzi, G., Messina, E., Smedile, F., et al. (2015) Microbial community of the deep-sea brine Lake Kryos seawater-brine interface is active below the chaotropicity limit of life as revealed by recovery of mRNA. *Environ Microbiol* **17**: 364–382.

Yarza, P., Ludwig, W., Euzéby, J., Amann, R., Schleifer, K.H., Glöckner, F.O., and Rosselló-Móra, R. (2010) Update of the all-species living tree project based on 16S and 23S rRNA sequence analyses. *Syst Appl Microbiol* **33**: 291–299.

Ye, M.Q., Chen, G.J., and Du, Z.J. (2020) Effects of antibiotics on the bacterial community, metabolic functions and antibiotic resistance genes in mariculture sediments during enrichment culturing. *J Mar Sci Eng* **8**: 1–26.

Yin, X., Cai, M., Liu, Y., Zhou, G., Richter-Heitmann, T., Aromokeye, D.A., et al. (2021) Subgroup level differences of physiological activities in marine *Lokiarchaeota*. *ISME J* **15**: 848–861.

Youssef, N.H., Ashlock-Savage, K.N., and Elshahed, M.S. (2012) Phylogenetic diversities and community structure of members of the extremely halophilic Archaea (order *Halobacteriales*) in multiple saline sediment habitats. *Appl Environ Microbiol* **78**: 1332–1344.

Youssef, N.H., Farag, I.F., Rudy, S., Mulliner, A., Walker, K., Caldwell, F., et al. (2019) The Wood–Ljungdahl pathway as a key component of metabolic versatility in candidate phylum *Bipolaricaulota* (*Acetothermia*, OP1). *Environ Microbiol Rep* **11**: 538–547.

Yu, N., Zhao, C., Ma, B., Li, S., She, Z., Guo, L., et al. (2019) Impact of ampicillin on the nitrogen

removal, microbial community and enzymatic activity of activated sludge. *Bioresour Technol* **272**: 337–345.

Zarei-Baygi, A., Harb, M., Wang, P., Stadler, L.B., and Smith, A.L. (2020) Microbial community and antibiotic resistance profiles of biomass and effluent are distinctly affected by antibiotic addition to an anaerobic membrane bioreactor. *Environ Sci Water Res Technol* **6**: 724–736.

Zengler, K., Richnow, H.H., Rosselló-Mora, R., Michaelis, W., and Widdel, F. (1999) Methane formation from long-chain alkanes by anaerobic microorganisms. *Nature* **401**: 266–9.

Zhang, F., Zhou, F., Gan, R., Ren, C., and Yuqiang, J. (2020) PHISDetector: a tool to detect diverse in silico phage-host interaction signals for virome studies. 1–20.

Zhang, Y., Alam, M.A., Kong, X., Wang, Z., Li, L., Sun, Y., and Yuan, Z. (2017) Effect of salinity on the microbial community and performance on anaerobic digestion of marine macroalgae. *J Chem Technol Biotechnol* **92**: 2392–2399.

Zhou, J., Deng, Y., Zhang, P., Xue, K., Liang, Y., Van Nostrand, J.D., et al. (2014) Stochasticity, succession, and environmental perturbations in a fluidic ecosystem. *Proc Natl Acad Sci U S A* **111**: E836–E845.

Zhu, W., Lomsadze, A., and Borodovsky, M. (2010) Ab initio gene identification in metagenomic sequences. *Nucleic Acids Res* **38**: e132:1-15.

Zhuang, G.C., Elling, F.J., Nigro, L.M., Samarkin, V., Joye, S.B., Teske, A., and Hinrichs, K.U. (2016) Multiple evidence for methylotrophic methanogenesis as the dominant methanogenic pathway in hypersaline sediments from the Orca Basin, Gulf of Mexico. *Geochim Cosmochim Acta* **187**: 1–20.

Zhuang, G.C., Heuer, V.B., Lazar, C.S., Goldhammer, T., Wendt, J., Samarkin, V.A., et al. (2018) Relative importance of methylotrophic methanogenesis in sediments of the Western Mediterranean Sea. *Geochim Cosmochim Acta* **224**: 171–186.

APPENDICES

Appendix I. Glossary

acd = ADP-forming acetyl-CoA synthetase.

ack = Acetate kinase.

acs = Acetyl-coenzyme A synthethase.

amoA/amoB = Ammonia monooxigenase; subunits A and B.

apr = Adenylyl-sulfate reductase.

APS: Adenosine 5'-phosphosulfate.

cdh = Acetyl-coenzyme A: corrinoid protein coenzyme-methyltransferase.

CH_3-Co(III) = Methyl-coenzyme III.

CoA = Coenzyme A.

CoB-SH = Coenzyme B (7-mercaptoheptanoylthreoninephosphate).

CoM-S-S-CoB = Coenzyme M (7-mercaptoheptanoylthreonine-phosphate heterodisulfide).

DMS: Dimethyl sulfide.

DMSO: Dimethyl sulfoxide.

dsr = Dissimilatory sulfite reductase.

F_{420} = Coenzyme 8-hydroxy-5-deazaflavin.

fdh/fwd = Formate / formylmethanofuran dehydrogenases.

ftr = Formylmethanofuran-tetrahydromethanopterin N-formyltransferase.

haoA = NH_2OH (hydroxylamine) oxidoreductase.

hdr = Coenzyme B-Coenzyme M heterodisulfide reductase.

H_4MPT = Tetrahydromethanopterin.

mch = N(5), N(10)-methenyltetrahydromethanopterin cyclohydrolase.

mcr/mrt = Methyl coenzyme M reductase I/II.

mer = F_{420}-dependent N(5),N(10)-methylenetetrahydromethanopterin reductase.

MF = Methanofuran.

mtaA = Methanol-corrinoid protein:coenzyme methyltransferase.

mtaB = Methanol: mtaC protein coenzyme-methyltransferase.

mtbA = Methylated corrinoid protein:coenzyme M methyltransferase.

mtbB/mtbC = Dimethylamine methyltransferases.

mtd = F_{420}-dependent methylenetetrahydromethanopterin dehydrogenase.

mtmB/mtmC = Monomethylamine methyltransferases.

mtr = N5-methyltetrahydromethanopterin: coenzyme M methyltransferase.

mttB/mttC = Trimethylamine methyltransferases.

napAB = Nitrate reductase (cytochrome).

narGHI/narBC = Respiratory nitrate reductases.

nifDKH = Nitrogenase molybdenum-iron protein alpha, beta chain.

nirBD = Nitrite reductase (NADH); large and small subunits.

nirK/S = Nitrite reductases.

norB/norC/norV = Nitric oxide reductases.

nosZ = Nitrous-oxide reductase.

nrfAH = Formate-dependent nitrite reductase cytochrome c-552.

nxrA = Nitrite oxidoreductase; subunit alpha.

pta = Phosphotransacetylase.

sat = Sulfate adenylyltransferase.

ureABC = Urea amidohydrolase; subunits alpha, beta and gamma.

Appendix II. Supplementary materials and methods

Sampling procedures

Fifty grams of each fraction were washed using 50 mL seawater at a salt concentration of 25%, mixed by vortex and treated to ultrasound for 5 min at 50 W, 230 V, 50 Hz. The supernatants from five consecutive washes were recovered until a clean supernatant was obtained and then mixed. One mL was fixed with 4% (v/v) formaldehyde for viral counts. Volumes of 250 mL were centrifuged in two successive steps of 13,500 and 20,000 rpm for 15-20 min at room temperature, and the final supernatants and both pellets were kept. The pellets were stored at -20 ºC for subsequent DNA extractions. The supernatants from the U, M and L samples from April 2017 were filtered through 0.22 µm filters (Sterivex) and concentrated to approximately 40 mL. Viruses were ultracentrifuged at 286,000 x g, for 4 hours at 20 ºC in a Beckman Coulter® optimaTM Max-XP ultracentrifuge with a SW Ti 41 rotor. Viral pellets were subsequently used for transmission electron microscopy, DNA extraction and pulsed field gel electrophoresis (PFGE), as explained below.

Gas collection and chemical analysis

Gas samples were collected from the sampling locations as sediment cores in order to analyze the CH_4 production. The gas harvest was transferred into glass bottles previously bubbled with nitrogen gas to remove all oxygen and ensure anaerobic conditions. Concentrations of CH_4 were measured with a Clarus 600 Gas Chromatograph (Perkin Elmer, USA) equipped with one channel connected to a flame ionization detector (FID). The FID was used for measurements with an Elite-Plot Q packed column (Perkin Elmer, 30 meter, 0.25 mm ID, 0.25 um; Crossbond 5% diphenyl – 95% dimethylpolysiloxane). Helium was used as a carrier gas at a flow rate of 5 mL min^{-1}, and oven and detector temperatures were set at 50 and 200 ºC, respectively. The gas chromatograph was calibrated using ≥99% pure methane gas (Sigma-Aldrich). A total of 300 uL of the headspace were injected into the gas chromatograph at 200 ºC with a GT 1750RN syringe for methane quantification.

Microbial DNA extraction

Pellets obtained from the centrifugations were mixed with 2 mL extraction buffer containing, per liter: 100 mM Tris-HCl at pH 8, 20 mM EDTA at pH 8, 1.4 M NaCl, 2% CTAB (hexadecyltrimethylammonium bromide 99%, Sigma-Aldrich), and 2% PVP (polyvinylpirrolidone K90, Fluka). The suspensions were divided into two 2 mL Eppendorf tubes, adding 16 µL proteinase K at 10 mg mL^{-1} (Roche), 20 µL mutanolysin at 1,000 units mL^{-1} (Roche), 20 µL lysozyme at 300 mg mL^{-1} (Roche) and 10 µL RNase A/T1 Mix (mix of RNase A at 2 mg mL^{-1} and RNase T1 at 5,000 units mL^{-1}, Thermo Fisher Scientific). The samples were

incubated at 37 ºC for 2 h in an Oven/Skaker SI 20H (Stuart Scientific). Thereafter, 250 µL sodium dodecyl sulfate (10% w/v; Panreac) were added to each tube, which were incubated at 55 ºC for 30 min. The DNA was extracted with a phenol:chloroform:isoamyl alcohol (25:24:1, v/v/v, pH 6.7/8) solution (VWR). Phenol wastes were removed with a chloroform:isoamyl alcohol (24:1, v/v) solution (Scharlau and Panreac, respectively), washing the samples until the supernatant was clear. After centrifugation at 13,000 rpm for 15 min (Eppendorf 5415 R centrifuge), the DNA was precipitated with 0.2 (v/v) sodium acetate 3M (Panreac) and 0.8 (v/v) isopropyl alcohol (Scharlau) for 3 h at -20 ºC. Samples were centrifuged at 13,000 rpm for 30 min (Eppendorf 5415 R centrifuge) and each one was rinsed with 200 µL 70% (v/v) ethanol. Another centrifugation (13,000 rpm for 15 min) was performed and the DNA was air-dried and resuspended with 100 µL sterile nuclease-free water (Sigma-Aldrich). Extracted DNA quality was checked through visualization in 0.8% agarose gel electrophoresis run in 1X TAE buffer and library concentrations were quantified by fluorescence using a Qubit HS DNA kit and Qubit 4.0 Fluorimeter (Invitrogen, Thermo Fisher Scientific). DNA samples were frozen at -20 ºC for further processing.

PCR amplification of samples (R1_U, R1_M, R1_L, R2_U, R2_M and R2_L)

Extracted DNA quality was checked through visualization in 0.8% agarose gel electrophoresis run in 1X TAE buffer, and library concentrations were quantified by fluorescence using a Qubit HS DNA kit and Qubit 4.0 Fluorimeter (Invitrogen, Thermo Fisher Scientific). 16S rRNA genes were amplified for R1_U, R1_M, R1_L, R2_U, R2_M and R2_L. Amplifications for Bacteria and Archaea were executed with GM3 and 21F, and S and 1492R, respectively. The PCR reactions were performed as detailed by Mora-Ruiz *et al.* (2018). As a result, a second PCR was performed as described in Mora-Ruiz *et al.* (2016), in a final volume of 25 µL in triplicate using specific primers (5'-TCGTCGGCAGCGTCAGATGTGTATAAGAGACAGCCTACGGGNGGCWGCAG-3' and 5'-GTCTCGTGGGCTCGGAGATGTGTATAAGAGACAGGACTACHVGGGTATCTAATCC-3' as forward and reverse primers for Bacteria, respectively, and 5'-TCGTCGGCAGCGTCAGATGTGTATAAGAGACAGGYGCASCAGKCGMGAAW-3' and 5'-GTCTCGTGGGCTCGGAGATGTGTATAAGAGACAGGGACTACVSGGGTATCTAAT-3' for Archaea, respectively) in order to incorporate tags, using the same conditions as the first PCR but reducing the number of cycles to 7. The bands were visualized in 1% (w/v) agarose gel electrophoresis in TAE 1X at 25 V for 50 min, excised and eluted with the Zymoclean™ Gel DNA Recovery Kit (Zymo Research, California, USA) following the manufacturer's instructions. The concentration was measured with a NanoDrop™ and the MassRuler™ Express Forward DNA Ladder mix, from which an equimolar mixture of amplicons was sent to sequencing.

Identification of metagenome-assembled genomes

Once metagenome-assembled metagenomes were trimmed, assembled and binned, the closest relative nucleotide and amino acid genome sequences were selected from the JSpecies WS online program (Richter *et al.*, 2016) and MiGA. The ANI and AAI calculations between them were performed. Reciprocal best matches (RBM) between MAGs were also calculated, orthologous genes were identified and together with ANI% and AAI% permitted the same and/or similar MAGs (i.e. same genus, order…) to be recognized. ANI%, AAI% and RBM were calculated with available scripts from http://enve-omics.ce.gatech.edu/enveomics (Rodriguez-R and Konstantinidis, 2016). A phylogenetic reconstruction from essential genes was executed in order to refine the identification of the retrieved MAGs. Groups of MAGs according to their similarity and presence of their essential or own genes of the relative closest genomes were formed, and the selected genes were aligned with clustalo v1.2.1 (Sievers *et al.*, 2011) and concatenated in order to be inserted into the ARB software. A Neighbor-Joining tree with Kimura correction was created with all genomes for the final taxonomic affiliation of MAGs.

Analysis of viral assemblages and DNA extraction

Fixed samples from the U, M and L horizons were stained with SybrGold, as previously described (Boujelben *et al.*, 2012), and virus-like particles (VLPs) were counted under a Leica DM 4000B epifluorescence microscope using a 100X fluorescence oil-immersion objective. To determine the viral morphologies, 5 µL of ultracentrifuged viruses (see above) were stained with 2% (w/v) uranyl acetate following the protocol previously described (Villamor *et al.*, 2018) and they were visualized in a Jeol JEM-2010 transmission electron microscope (JEOL Manufacturer, Tokyo, Japan). Ultracentrifuged viruses were mixed with equal volumes of 1.6% (w/v) low-melting-point agarose (Pronadisa), dispensed into 100 µL molds, and allowed to solidify at 4 ºC. The plugs were incubated with 3 units of Turbo DNase (Ambion), for 1 hour at 37 ºC, in order to remove dissolved DNA, and incubated overnight at 50 ºC in ESP to disrupt the viral capsids. Viral DNA was extracted as described in Santos *et al.* (2010) and quantified using Qubit® (Invitrogen). Cellular DNA contamination was checked by PCR amplification of 16S rRNA genes, as described by Ramos-Barbero *et al.* (2019), and the viral DNA was sequenced at Fisabio Inc. (Valencia, Spain) using an Illumina Mi-Seq Nextera XT 2x300 bp paired-end run. Some plugs were also used for the analysis of viral genome sizes by PFGE, as previously described (Santos *et al.*, 2010).

Appendix III. Supplementary results

Chapter 1. Inverted microbial community stratification and spatial–temporal stability in hypersaline anaerobic sediments from the S'Avall solar salterns

OPU grouping of short metagenomic reads and 16S rRNA amplified genes

After sequence trimming, OTU clustering using the program UCLUST (Qiime; Caporaso *et al.*, 2010) and the Swarm method (Mahé *et al.*, 2014), one representative of each OTU was used for a phylogenetic tree reconstruction using the ARB software package. The representative sequences of each OTU were inserted into a pre-calculated tree using the parsimony insertion tool implemented in ARB, and they were grouped in OPUs (França *et al.*, 2015) based on visual inspection of the tree, as previously described (Mora-Ruiz *et al.*, 2016, 2018). An OPU is the smallest monophyletic group of sequences containing OTU representatives and their closest reference sequence, including the type strain when possible.

Archaeal and bacterial diversity and abundance based on 16S rRNA gene amplicons

A set of 342,129 raw sequences, 290,341 for the archaeal and 51,788 for the bacterial domains, were obtained from the R1 and R2 cores taken in July 2016. The reads ranged in length between 375.9 and 418.2 bp for the archaeal (average 417.9 ± 0.2 for R1 and 379.2 ± 2.5 for R2, respectively) and from 434.8 to 453.6 bp for the bacterial (439.2 ± 3.2 and 453.4 ± 0.2 for R1 and R2, respectively) sequenced amplicons. Sequences were trimmed, chimeras removed and a final set of 330,950 sequences were grouped into OTUs. A total of 130,442 OTUs were obtained for the archaeal and 23,430 for the bacterial sequences. Archaea rendered a total of 447 OPUs where 389 (summing 44,843 sequences), 368 (summing 53,202 sequences) and 363 (summing 41,405 sequences) corresponded to the U, M and L fractions of R1, respectively; and 385 (summing 44,751 sequences), 372 (summing 53,551 sequences) and 361 (summing 42,793 sequences) to the U, M and L fractions of R2. On the other hand, a total of 887 OPUs were obtained for the bacterial community, distributed in 371 (summing 6,873 sequences) and 345 (summing 6,960 sequences) for the upper fractions R1_U and R2_U, respectively, 438 (summing 10,642 sequences) and 441 (summing 12,359 sequences) for R1_M and R2_M, and finally 397 (summing 7,524 sequences) and 387 (summing 6,047 sequences) for the deepest horizon R1_L and R2_L (Table 1.1). The diversity based on OPUs reached close to saturation only for the archaeal domain, based on rarefaction curves. The Shannon index showed a decrease for Archaea and an increase for Bacteria with depth, whereas richness was always highest in the upper layers (Table 1.1). The Evenness and

Dominance indices were similar in all horizons for both domains. The average sequencing coverage, calculated with the k-mer kernel algorithm (Nonpareil curves), of the microbial community in R1 samples was 93.8 ± 1.4 and 49.9 ± 2.4 for R2.

The most representative archaeal OPUs (≥ 2.5% relative sequence abundance) affiliated with the phylum *Euryarchaeota* (Supplementary Table S1.1A). The most abundant OPUs were OPUs 1, 14, 26 and 28, which were closest to *Halorubrum* species, whereas OPUs 60 and 63 were closest to an uncultured *Halonotius*, OPU 219 affiliated with an uncultured *Salinarchaeum*, OPU 299 affiliated with an uncultured *Halobacteria*, OPU 313 with an uncultured KTK 4A and OPU 317 with an uncultured 20c-4. The genera *Halorubrum*, *Halonotius*, *Haloarcula* and *Salinarchaeum* (OPUs 1, 3, 14, 19, 26, 28, 60, 63, 71, 131, 132, 181, 190, 219, 387) compiled most of the sequences of the class *Halobacteria*, which included the great majority (350 out of 447) of the archaeal OPUs. Six OPUs affiliated with the *Methanomicrobia* class with different profiles. The ones affiliating with the uncultured ST-12K10A (OPUs 293, 294 and 319) showed increasing abundance with depth, whereas two that affiliated with *Methanohalobium evestigatum* (OPUs 318 and 322) were more characteristic of the L layer, and *Methanohalophilus* species (OPU 323) that was only present in the upper fraction. A total of 19 OPUs affiliated with the uncultured/candidate division MSBL1, predominantly present in all fractions but with higher abundance in the M and L layers. Eleven OPUs affiliated with the *Nanohaloarchaeota* phylum and decreased significantly with depth, whereas four OPUs affiliating with the uncultured KTK 4A lineage exhibited an increase with depth. Twenty-two OPUs affiliated with the *Woesearchaeota* phylum and were identified as members of the candidate lineage DHVEG-6 (11 were exclusive to the U fraction and the other was predominantly more abundant in the L layer). *Thaumarchaeota* was represented by 21 OPUs, where the three OPUs affiliating with the *Candidatus* Nitrosopumilus and the six affiliating with the uncultured Marine Group were more present in the superficial layer of sediment (Supplementary Table S1.1A and spreadsheet Table ST1.1).

The most representative bacterial OPUs (with ≥ 2% of the relative sequence abundances) were OPU 1 affiliating with an uncultured *Roseovarius*, OPU 521 affiliating with *Salinibacter ruber*, OPU 522 affiliating with *Salinivenus iranica* and OPU 523 affiliating with *Salinivenus lutea*, which all had decreasing abundances with depth (Supplementary Table S1.1B and spreadsheet Table ST1.2). OPU 304 affiliating with an uncultured *Desulfovermiculus* and OPU 746 affiliating with an uncultured *Acetothermia* increased with depth. OPU 88 affiliating with an uncultured *Rhodobacteraceae* and OPU 520 affiliating with an uncultured *Truepera* were also abundant. *Roseovarius*, *Salinibacter*, *Salinivenus*, *Desulfovermiculus*, *Bacillus* and *Halanaerobium* were the most abundant genera. The families *Rhodobacteraceae*, *Desulfobacteraceae* and *Marinilabiliaceae* accumulated a high number of sequences (i.e. OPUs 1, 7, 10, 27, 88 – 300, 301, 304, 313 – 531, 538, respectively). *Methylobacterium* spp. (OPUs 151, 152, 153 and 578), *Aureimonas/Aurantimonas* spp. (OPUs 133, 134 and 359) and

members of the *Planctomycetia* (twenty-one; OPUs 457, 719 - 729, 730 - 737, 768 and 769) and *Thermotogae* classes (two; OPUs 718 and 885) were also detected but with lower abundances. A total of 13 OPUs of some uncultured *Acetothermia* (OPUs 713, 714, 741 – 750, 886) were observed, summing 3.4 ± 0.1% for the U fraction, 7.7 ± 0.3% for the intermediate and 13.9 ± 0.8% for the deepest section (Supplementary Table S1.1B and spreadsheet Table ST1.2).

Microbial diversity based on metagenome-assembled genomes (MAGs)

The three metagenomes of the vertical profile taken in spring yielded a total of 34 MAGs (Table 1.2 and Supplementary Table S1.5), 17 of which had good quality (≥ 70% completeness and < 7.7% contamination). The metagenome of the homogenized slurry taken in winter rendered 36 MAGs of acceptable quality, 26 of which affiliated with the archaeal and ten with the bacterial domains, and from these, 15 were of good quality (Table 1.2 and Supplementary Table S1.5). From among the 70 MAGs, only one (S24) could be identified up to the species level, and the rest were identified to higher taxa. The accurate identification to the lowest possible rank (Table 1.2) was carried out by reconstructing phylogenies using the sets of shared conserved genes available for each MAG (Supplementary Figure S1.5).

The complete set of 70 MAGs summed read abundances that ranged between ~15.7% to ~24.4% of the total metagenome reads (Table 1.2 and Supplementary Figure S1.6). However, taking into account that the assembly rendered between 42,418 to 91,410 contigs with sizes ≥500 bp, which recruited between 47.8% and 58.9% (using 95% identity and 70% coverage), the 70 MAGs recruited between 8.2% to 45.8% of the total reads mapped to the assembled contigs (Supplementary Table S1.2).

The most representative MAGs in our samples were conspicuously those retrieved in more than one sample. In addition, the members of the *Halobacteria* known as aerobes (except for *Salinarchaeum* and *Halodesulfurarchaeum*; Table 1.2) could account for up to ~1.2% in the slurry, and ~0.2% along the column in the April sampling. MAGs affiliating with known methanogenic lineages (i.e. *Methanobacteria* and *Methanomicrobia*) were prevalent along the column with sums of ~0.2% and up to ~1% in the slurry, which was similar to the sulfate reducing *Deltaproteobacteria* of the bacterial domain. Noticeably, two MAGs representing a unique species and associated with the *Aureimonas* genus (M05 and L06) were retrieved from the deepest horizons and accounted for up to 0.62% along the column. Additionally, this genus (likewise found under its basonym *Aurantimonas*) was also detected in amplicon sequences from R1 and R2, which ranged from 0.01% to 0.05%, and the 16S recruited reads from S, U, M and L, varying from 0.01% to 8.7% (M) in relative abundance.

Archaeal and bacterial diversity and abundance based on 16S rRNA gene read recruitment from metagenomes

A total of 16,387 16S rRNA gene sequence reads were extracted from metagenome S taken in December 2016. The read length ranged between 42 and 100 nucleotides (average 89.7 ± 12.6). The sequences were clustered in 3,507 OTUs and grouped into 743 OPUs, 197 (4,117 sequences) for the archaeal and 546 (11,573 sequences) for the bacterial domains, respectively. The diversity of OPUs did not reach saturation, but the occurrence of archaeal reads was closest to saturation based on rarefaction. The Shannon index showed agreement with that observed for the amplicon data (Table 1.1), and ranged from 4.031 to 4.214 for both domains. On the other hand, the richness estimations using the Chao-1 index for this pooled set of winter samples showed lower values for Archaea (266.2) and higher values for Bacteria (739.6) than in the summer sample. Evenness was higher for the archaeal fraction and lower for the bacterial fraction than the values obtained in the summer sample. Dominance indices were similar for both domains (Table 1.1). The coverage of the population provided by S was 75.4%.

The most representative archaeal OPUs from S (≥ 2.4% relative sequence abundance) affiliating with *Euryarchaeota* were OPU 1, which affiliated with *Halorubrum arcis*, OPU 222 affiliating with an uncultured *Salinarchaeum*, OPU 273 affiliating with an uncultured *Haloferacaceae*, OPUs 314 and 315 affiliating with an uncultured KTK 4A, and OPU 437 affiliating with an uncultured *Halodesulfurarchaeum*. However, there were four OPUs affiliating with an uncultured *Candidatus* MSBL1 that ranged between 1.4 and 2.9% relative abundances (Supplementary Table S1.3A and spreadsheet Table ST1.1). *Halorubrum*, *Salinarchaeum* and *Halodesulfurachaeum* were the most abundant genera within class *Halobacteria*. Other minor but significant OPUs affiliated with the *Methanomicrobia* class (OPUs 293, 294 and 319 – affiliating with the ST-12K10A lineage), *Nanohaloarchaeota* phylum (eleven OPUs: 296, 298, 306 to 312, 474 and 497), uncultured DHVEG-6 from the *Woesearchaeota* phylum (nine OPUs: 304, 407, 409, 412, 413, 420, 422, 425 and 426) and 25 OPUs (OPUs 347 to 352, 354, 378 to 385, 435, 476 to 483 and 485) from the uncultured/candidate division MSBL1 (Supplementary Table S1.3A and spreadsheet Table ST1.1).

The most representative bacterial OPUs from S were OPU 256 affiliating with an uncultured *Halorhodospira*, OPU 294 affiliating with an uncultured *Desulfovermiculus*, OPU 521 affiliating with *Salinibacter ruber*, OPU 566 affiliating with an uncultured MVP-94, OPUs 736, 742, 745, 748 and 750 affiliating with uncultured *Acetothermia*, and OPU 640 affiliating with uncultured PB79 (*Brocadiaceae*). *Halorhodospira*, *Desulfovermiculus* and *Halanaerobium* were the most detected genera, together with a very high presence of members of the families *Rhodobacteraceae*, *Desulfobacteraceae* and *Marinilabiliaceae* (Supplementary Table S1.3B and spreadsheet Table ST1.2). Genera *Aurantimonas/Aureimonas* and

Methylobacterium were detected in one (OPU 133) and two OPUs (153 and 578), respectively, whilst OPUs 718, 1025 to 1027, 1152 and 1153 affiliated with class *Thermotogae* and OPUs 728 to 731, 735, 737 and 1098 with class *Planctomycetia* (spreadsheet Table ST1.2).

The 16S rRNA gene reads recovered from the three metagenomes of the April samples, showed 1,605, 1,415 and 1,425 sequences from the U, M and L layers, respectively. The read length average of the 4,445 reads was 238 ± 99.9 (ranging from 43 to 531 nucleotides). Sequences were grouped into 1,354 OTUs and 327 OPUs, 121 OPUs (summing 2,061 sequences) for the archaeal and 206 OPUs (summing 2,336 sequences) for the bacterial domains, respectively. In the horizons, the archaeal OPUs were distributed in 77 OPUs (summing 980 sequences), 75 OPUs (summing 602 sequences) and 80 OPUs (summing 479 sequences) in the L, U, M and L layers, respectively. On the other hand, the bacterial OPUs were distributed in 105 OPUs (summing 610 sequences), 114 OPUs (summing 797 sequences) and 126 OPUs (summing 929 sequences) for the U, M and L layers, respectively. None of the individual rarefaction curves showed saturation based on diversity of OPUs, but the archaeal fraction was closest to saturation. The Shannon index was similar for all bacterial layers (ranging from 3.42 to 3.57), while the archaeal upper section presented a minor diversity (2.48) compared to the underlying horizons (Table 1.1), and these values were lowest for the three seasons tested. The Chao-1 estimator indicated higher richness for Bacteria that increased with depth (194.4, 244.7 and 256.1 for U, M and L, respectively), while the archaeal richness did not differ much along the vertical profile. Similar trends were observed for the Evenness and Dominance indices, with Archaea only showing a higher dominance in the U fraction from the April sample in contrast to the other sampling dates. The remaining values were in accordance with those obtained for the summer and winter samples. The average sequence coverage of the microbial community in each sample was 68.7%, 63.6% and 60.37% for the U, M and L samples, respectively.

The most representative archaeal OPUs (≥ 2% relative sequence abundance) affiliated with the phylum *Euryarchaeota*, with OPU 219 affiliating with an uncultured *Salinarchaeum*, OPU 475 affiliating with a member of the uncultured 20c-4 lineage, and OPUs 313 to 315 affiliating with a member of the uncultured KTK 4A lineage (Supplementary Table S1.3A). *Salinarchaeum*, *Halorubrum* and *Halodesulfurarchaeum* (OPUs 1, 219, 222, 437 and 448) were the most abundant genera detected in the class *Halobacteria* (more than 50 OPUs). Finally, the presence of 27 OPUs (347, 349, 352, 353, 380, 384, 441, 478, 479, 480 and 486, among others) affiliating with the candidate division MSBL1 was remarkable; OPUs 293, 294 and 319 affiliated with the class *Methanomicrobia* closest to an uncultured member of the ST-12K10A lineage; all five OPUs affiliating with *Woesearchaeota* were members of the uncultured DHVEG-6 lineage, and the uncultured DSEG group was detected in four OPUs (Supplementary Table S1.3A and spreadsheet Table ST1.1).

The most representative bacterial OPUs (≥ 2% of the relative total abundance) were OPU 133 affiliating with *Aurantimonas coralicida / A. manganoxydans*, OPUs 294 and 300 affiliating with an uncultured *Desulfovermiculus*, OPU 481 affiliating with an uncultured *Halanaerobium*, OPUs 736, 741, 744, 745, 747 and 749 affiliating with an uncultured *Acetothermia* and OPU 640 affiliating with a member of the uncultured PB79 lineage. The most detected genera were *Desulfovermiculus*, *Halanaerobium*, and *Salinibacter* but with lower values for the latter. Additionally, the families *Rhodobacteraceae*, *Desulfobacteraceae* and *Marinilabiliaceae* accumulated high abundances (Supplementary Table S1.3B and spreadsheet Table ST1.2).

Ecological and statistical approaches: Venn diagrams and shared OPUs

The OPU approach allows each OPU to be identified up to the level of a single distinct species (Viver *et al.*, 2019), but for pragmatic reasons we compiled the data at the genus level to allow for a better interpretation.

A total of 73 genera comprised the main community (OPUs with relative abundances > 1%), with 27 archaeal and 46 bacterial genera. The archaeal "core genera" was represented by 11 (upper horizon, U) to 14 (lower horizon, L) taxa, and these summed > 48% of the sequences in the upper layer and > 53% in the intermediate and lower horizons (Figure 1.2 and Supplementary Table S1.4). On the other hand, the bacterial domain was much more diverse, being formed by 24 (lower horizon, L) to 27 (middle horizon, M) "core genera", as well as also representing > 51% of the relative sequence abundances. Therefore, in both cases, the "core genera" summed the majority of the 16S rRNA gene amplicons and reads of each domain, with values up to 84% and 74% for the upper fractions in the Archaea and Bacteria domains, respectively. The most relevant archaea were those affiliated with *Halorubrum* (relative abundances up to 38.2%), *Salinarchaeum* (21.1%), and several uncultured taxa (i.e. *Candidatus* MSBL-1 lineage – 22.6%, KTK 4A cluster – 55.2%, 20c-4 cluster – 9.3%) and those from the bacterial domain with *Salinibacter* (relative abundances up to 34.1%), *Desulfovermiculus* (10.9%) and *Halanaerobium* (10.8%; Figure 1.2 and Supplementary Table S1.4).

Shared diversity based on 16S rRNA gene amplicons (July 2016) and read recruitment (December 2016 and April 2017)

A total of 23 of the archaeal and 37 of the bacterial OPUs were shared among all samples (six from July 2016, one from December 2016 and three from April 2017). These archaeal OPUs summed > 16% and up to 68% of the relative sequence abundances, whilst the bacterial community abundance ranged from 38% to 68.2% (spreadsheet Tables ST1.1

and ST1.2). The most representative shared OPUs were those that affiliated with *Halorubrum* and *Salinarchaeum*, within the class *Halobacteria*. Members of uncultured ST-12K10A (*Methanomicrobia* class), uncultured DHVEG-6 (*Woesearchaeota* phylum), the uncultured KTK4A lineage and the *Candidatus* MSBL1 lineage were also detected (Supplementary Tables S1.1 and S1.3 and spreadsheet Table ST1.1). In the bacterial domain, the most abundant and shared OPUs were those that affiliated with *Roseovarius*, *Desulfovermiculus*, *Halanaerobium* and *Salinibacter* genera. OPUs assigned to the *Rhodobacteraceae*, *Marinilabiliaceae* and *Desulfobacteraceae* families, and members of the uncultured MVP-94 cluster, *Aureimonas/Aurantimonas* genus and *Acetothermia* phylum were present in all samples (Supplementary Tables S1.1 and S1.3 and spreadsheet Table ST1.2).

Nevertheless, for pragmatic reasons, we grouped the data from the three samplings according to seasons: summer (R1_U, R2_U, R1_M, R2_M, R1_L and R2_L; July 2016), winter (S; December 2016) and spring (U, M and L; April 2017) to allow for better interpretation of the results. Thus, a total of 75 of the archaeal and 113 of the bacterial OPUs were shared between all three seasons. These archaeal OPUs ranged from 28.7% to 45.7% in the summer samples, whilst abundances of 63.4% and 88.1% were obtained for winter and spring, respectively. In the bacterial domain, the summer samples summed up to 70.4%, the winter sample displayed 76.3%, and the spring sampling > 90% (spreadsheet Tables ST1.1 and ST1.2). The most representative shared OPUs were those affiliated with *Halorubrum* sp., *Halapricum* sp., *Halodesulfurarchaeum* sp. and *Salinarchaeum* sp., within the class *Halobacteria*. Members of uncultured ST-12K10A, uncultured DHVEG-6, the uncultured KTK4A lineage and the *Candidatus* MSBL1 lineage were also detected (Supplementary Tables S1.1 and S1.3 and spreadsheet Table ST1.1). In the bacterial domain, the most abundant and shared OPUs were those that affiliated with the *Roseovarius*, *Desulfovermiculus*, *Halanaerobium* and *Salinibacter* genera. OPUs assigned to the *Rhodobacteraceae*, *Marinilabiliaceae* and *Desulfobacteraceae* families, and members of the uncultured MVP-94 cluster, *Aureimonas / Aurantimonas* genus and *Acetothermia* phylum were present in all seasons (Supplementary Tables S1.1 and S1.3 and spreadsheet Table ST1.2).

Appendix IV. Supplementary Figures and Tables

Supplementary data to this thesis can be found online in the document designated as Supplementary_spreadsheet.xlsx.

Chapter 1. Inverted microbial community stratification and spatial–temporal stability in hypersaline anaerobic sediments from the S'Avall solar salterns

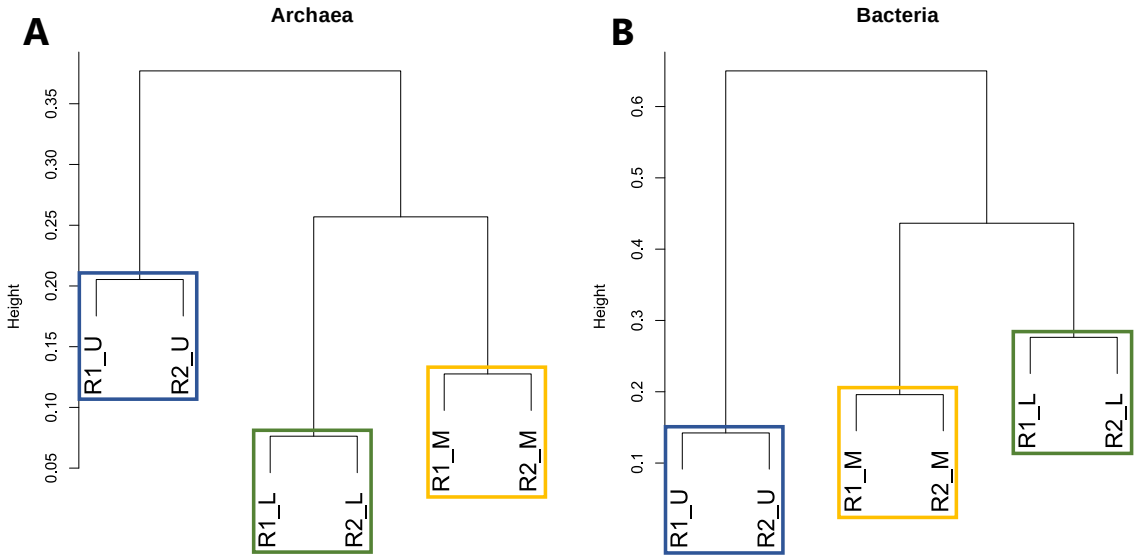

Supplementary Figure S1.1. Dendrograms based on Bray-Curtis dissimilarity using OPUs based on 16S rRNA gene amplicons from the July 2016 samples. Dendrogram for the archaeal domain (**A**) and bacterial domain (**B**). Replicates (R1 and R2) are marked with blue, yellow and green rectangles for the Upper, Middle and Lower layers, respectively.

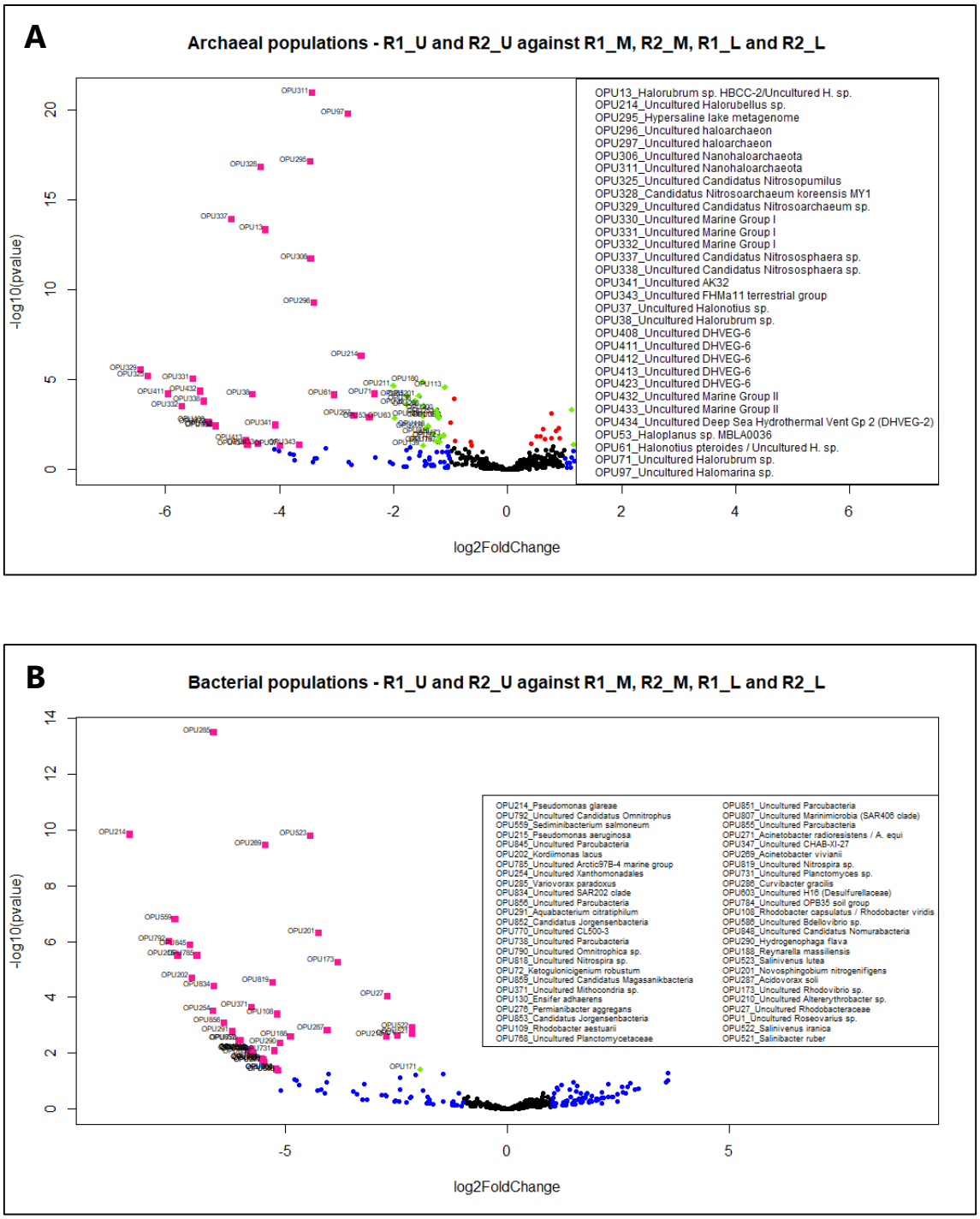

Supplementary Figure S1.2. Volcano plots performed from Log2Foldchange values obtained from the DESeq2 function comparing the Upper (U) sections (R1_U and R2_U) against M (R1_M and R2_M) and L (R1_L and R2_L) for the archaeal (**A**) and bacterial (**B**) sequences, respectively. Colored points: red if p-value < 0.05, blue if absolute Log2Foldchange > 1, green if both, and pink if p-value < 0.05 and absolute Log2Foldchange > 2. On the right, taxonomic affiliation of the statistically significant pink-marked OPUs is indicated.

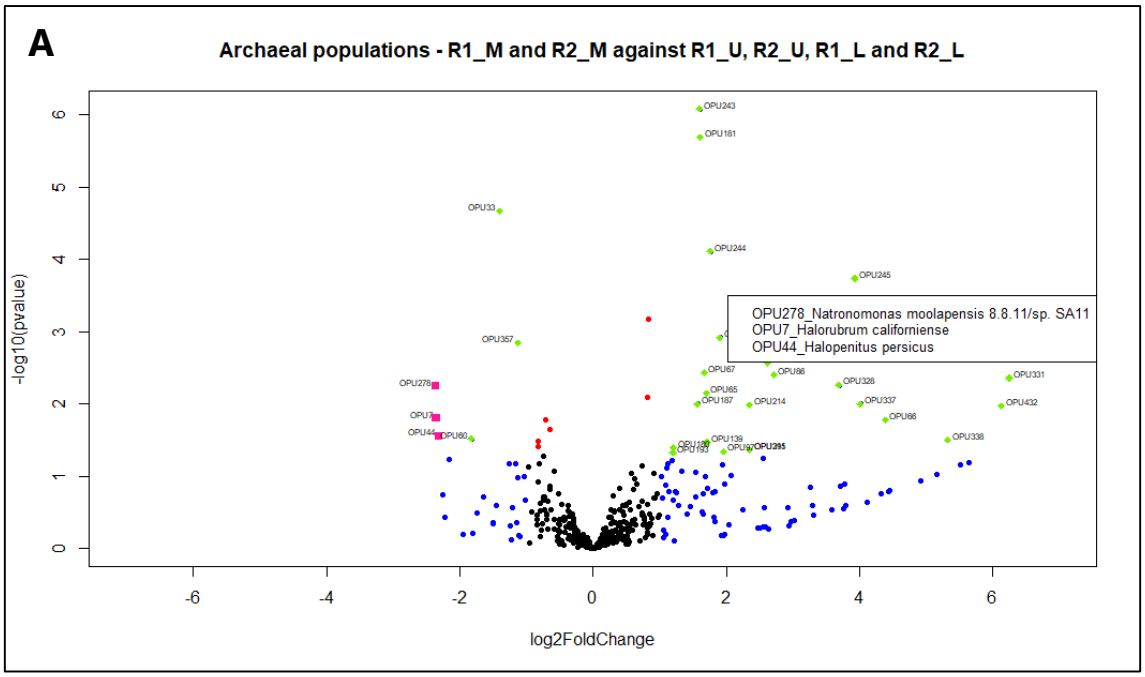
A
Archaeal populations - R1_M and R2_M against R1_U, R2_U, R1_L and R2_L
-log10(pvalue)
log2FoldChange
OPU278_Natronomonas moolapensis 8.8.11/sp. SA11
OPU7_Halorubrum californiense
OPU44_Halopenitus persicus

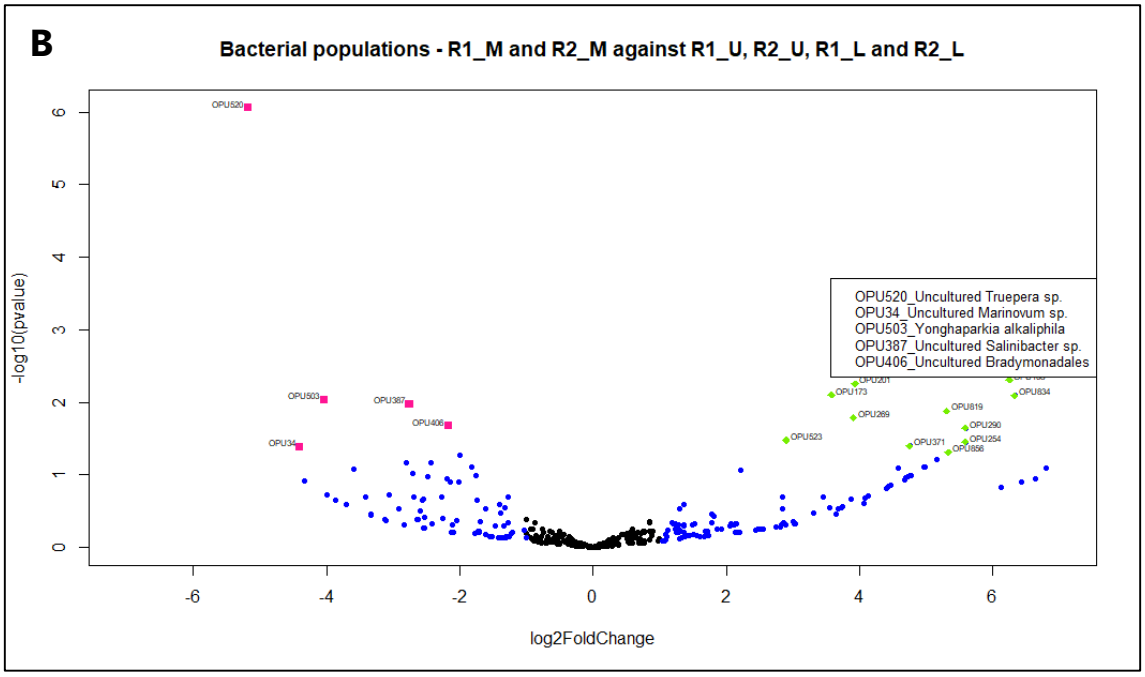
B
Bacterial populations - R1_M and R2_M against R1_U, R2_U, R1_L and R2_L
-log10(pvalue)
log2FoldChange
OPU520_Uncultured Truepera sp.
OPU34_Uncultured Marinovum sp.
OPU503_Yonghaparkia alkaliphila
OPU387_Uncultured Salinibacter sp.
OPU406_Uncultured Bradymonadales

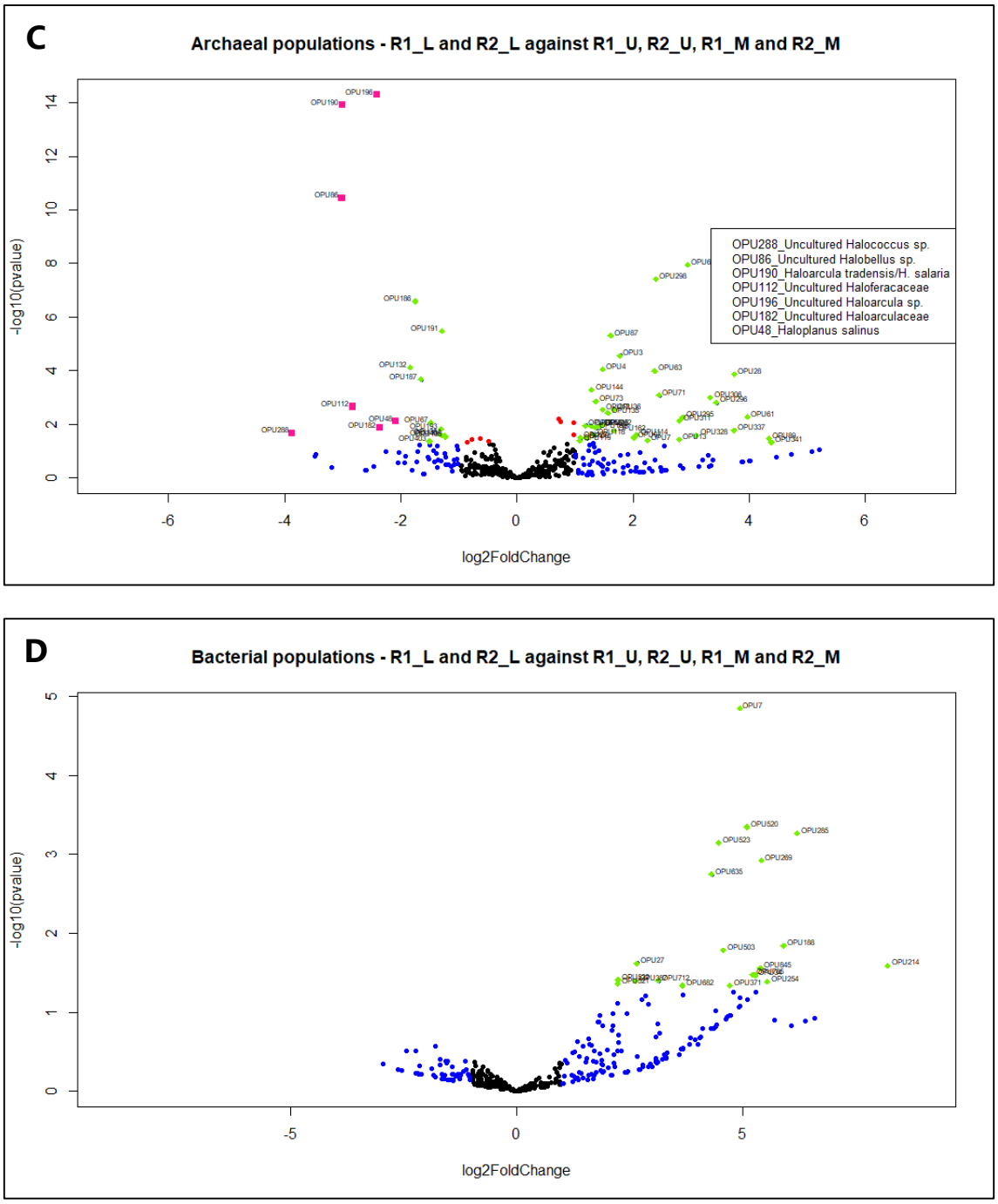

Supplementary Figure S1.3. Volcano scatterplots showing statistical significance (p-value) against Log2Foldchange obtained from the DESeq2 function comparing the Middle-M (R1_M and R2_M) fractions against U and L (**A** and **B**) and R1_L and R2_L horizons against R1_U, R2_U, R1_M and R2_M for the archaeal and bacterial sequences (**C** and **D**), respectively. Legend of colored points: red if p-value < 0.05, blue if absolute Log2Foldchange > 1, green if both, and pink if p-value < 0.05 and absolute Log2Foldchange > 2. On the right, taxonomic affiliation of the statistically significant pink-marked OPUs is shown.

Supplementary Table S1.1. Most relevant OPUs (29 for the archaeal (**A**) and 31 for the bacterial (**B**) domains) accumulating sequence abundances above 1% at least in one sample obtained from the 16S rRNA gene amplicons (R1 and R2). Columns (from left to right): OPU indicates the OPU number; taxonomic affiliation at the phylum, class and/or order, family and genus and/or species levels depending on the distance to the closest relative sequence; accession number of the closest relative. The subsequent columns show the percentage relative abundance of each OPU referenced to the total number of sequences for each sample.

A. Major OPUs of Archaea

OPU	Phylum	Class-Order	Family	Genus-Species	Accession number	R1_U	R2_U	R1_M	R2_M	R1_L	R2_L	ALL
1	*Euryarchaeota*	*Halobacteria - Haloferacales*	*Halorubraceae*	*Halorubrum arcis*	DQ355793	8.31	7.08	10.98	11.00	10.98	9.99	9.78
26	*Euryarchaeota*	*Halobacteria - Haloferacales*	*Halorubraceae*	*Halorubrum* sp. AV_13S15 / *H. orientale*	AM235786/LN649924	5.96	16.46	9.98	3.08	11.19	13.05	9.70
317	*Euryarchaeota*	*Thermoplasmata - Thermoplasmatales*	-	Unc. 20c-4	DQ103669	4.23	4.16	6.51	6.60	6.76	6.76	5.86
299	*Euryarchaeota*	*Halobacteria - Halobacteriales*	*Halobacteriaceae*	Unc. *Halobacteriaceae*	FJ536516	2.97	4.14	4.96	4.76	4.76	4.60	4.39
28	*Euryarchaeota*	*Halobacteria - Haloferacales*	*Halorubraceae*	Unc. *Halorubrum* sp.	HQ157594	10.93	2.60	0.63	7.28	0.42	0.46	3.80
219	*Euryarchaeota*	*Halobacteria - Natrialbales*	*Natrialbaceae*	Unc. *Salinarchaeum* sp.	EF459703	1.62	0.53	5.04	4.97	4.77	4.36	3.62
14	*Euryarchaeota*	*Halobacteria - Haloferacales*	*Halorubraceae*	*Halorubrum* sp. S5a-2 / *H.* sp. AV_12S85	JN196465/LN649909	3.91	4.26	2.14	2.62	2.73	2.66	3.02
313	-	-	-	Unc. KTK 4A	HE604525/AJ133621	2.03	2.02	3.27	3.47	3.41	3.60	2.98
60	*Euryarchaeota*	*Halobacteria - Haloferacales*	*Halorubraceae*	Unc. *Halonotius* sp.	AM947464/FN391228	2.42	1.60	5.51	5.17	0.50	0.46	2.82
63	*Euryarchaeota*	*Halobacteria - Haloferacales*	*Halorubraceae*	Unc. *Halonotius* sp.	KC465589/AM947475	4.40	4.81	1.72	2.53	0.91	0.52	2.49
39	*Euryarchaeota*	*Halobacteria - Haloferacales*	*Halorubraceae*	Unc. *Halorubrum* sp.	AM947501	0.94	2.47	2.40	2.24	2.55	2.60	2.20
387	*Euryarchaeota*	*Halobacteria - Natrialbales*	*Natrialbaceae*	Unc. *Salinarchaeum* sp. MSP1	AB012049/EF459703	3.28	1.38	1.86	1.80	2.27	2.28	2.12
19	*Euryarchaeota*	*Halobacteria - Haloferacales*	*Halorubraceae*	*Halorubrum salinum* / *H.* sp. Q5A	HM063951/KR150746	2.12	2.26	2.86	1.85	1.64	1.79	2.11
48	*Euryarchaeota*	*Halobacteria - Haloferacales*	*Haloferacaceae*	*Haloplanus salinus*	JQ237126	0.13	1.23	1.44	1.38	4.56	4.30	2.08
47	*Euryarchaeota*	*Halobacteria - Haloferacales*	*Haloferacaceae*	*Haloplanus natans* DSM 17983	ATYM01000002	2.33	2.18	1.61	1.86	1.28	2.67	1.98

3	*Euryarchaeota*	*Halobacteria - Haloferacales*	*Halorubraceae*	*Halorubrum xinjiangense*	AY510707	1.80	1.12	2.50	3.08	0.72	0.55	1.72
181	*Euryarchaeota*	*Halobacteria - Halobacteriales*	*Haloarculaceae*	Unc. *Haloarculaceae*	JN714439/LN649992	1.17	1.49	0.64	0.66	1.94	2.46	1.33
131	*Euryarchaeota*	*Halobacteria - Halobacteriales*	*Haloarculaceae*	Unc. *Haloarcula* sp.	AB766180/KC465611	1.44	1.36	0.85	1.12	1.86	1.47	1.32
156	*Euryarchaeota*	*Halobacteria - Halobacteriales*	*Haloarculaceae*	Unc. *Halapricum* sp.	CU467265/FN391257	0.81	0.97	1.37	1.24	1.41	1.49	1.22
132	*Euryarchaeota*	*Halobacteria - Halobacteriales*	*Haloarculaceae*	Unc. *Haloarcula* sp.	KF673170/EU722673	0.73	0.74	0.45	0.43	2.37	2.14	1.08
71	*Euryarchaeota*	*Halobacteria - Haloferacales*	*Halorubraceae*	Unc. *Halorubrum* sp.	CU467131/CU467138	2.46	1.84	1.00	0.50	0.31	0.27	1.06
324	*Euryarchaeota i.s.*	-	-	Unc. MSBL1	FJ536509/KJ881758	0.66	0.59	1.15	1.20	1.00	1.13	0.97
87	*Euryarchaeota*	*Halobacteria - Haloferacales*	*Haloferacaceae*	Unc. *Halobellus* sp.	JN714459	1.23	1.30	1.15	1.14	0.53	0.31	0.96
32	*Euryarchaeota*	*Halobacteria - Haloferacales*	*Halorubraceae*	Unc. *Halonotius* sp.	CU467178	1.74	1.47	0.53	0.71	0.28	0.74	0.90
295	*Nanohaloarchaeota*	-	-	Unc. *Nanohaloarchaeota*	APHM01002808	2.06	2.04	0.30	0.23	0.13	0.23	0.81
113	*Euryarchaeota*	*Halobacteria - Haloferacales*	*Halorubraceae*	*Halolamina rubra / H.* sp. YJ-41	KF314044/KJ689297	1.14	1.07	0.73	0.61	0.66	0.49	0.78
99	*Euryarchaeota*	*Halobacteria - Haloferacales*	*Haloferacaceae*	Unc. *Haloquadratum* sp.	HQ157618	0.51	1.29	0.47	1.06	0.36	0.55	0.72
190	*Euryarchaeota*	*Halobacteria - Halobacteriales*	*Haloarculaceae*	*Haloarcula tradensis / H. salaria*	KF962648/KF962645	0.07	0.11	0.19	0.12	0.97	1.07	0.40
38	*Euryarchaeota*	*Halobacteria - Haloferacales*	*Halorubraceae*	Unc. *Halorubrum* sp.	FN391244	1.74	0.02	0.05	0.05	0.05	0.05	0.32

i.s. = *incertae sedis*

B. Major OPUs of Bacteria

OPU	Phylum	Class-Order	Family	Genus-Species	Accession number	R1_U	R2_U	R1_M	R2_M	R1_L	R2_L	ALL
521	*Bacteroidetes*	*Rhodothermaeota - Rhodothermales*	*Salinibacteraceae*	*Salinibacter ruber*	CP000159	33.86	32.41	24.07	19.44	21.61	9.01	23.25
523	*Bacteroidetes*	*Rhodothermaeota - Rhodothermales*	*Salinibacteraceae*	*Salinivenus lutea*	HQ197983	19.19	18.20	3.06	2.27	1.71	1.32	6.75
1	*Proteobacteria*	*Alphaproteobacteria - Rhodobacterales*	*Rhodobacteraceae*	Unc. *Roseovarius* sp.	EU592378/HM128277	8.31	8.79	2.08	5.74	6.31	1.01	5.26
520	*Deinococcus-Thermus*	*Trueperales - Deinococci*	*Trueperaceae*	Unc. *Truepera* sp.	JN119225	0.26	0.17	4.75	15.80	0.35	0.18	5.01
88	*Proteobacteria*	*Alphaproteobacteria - Rhodobacterales*	*Rhodobacteraceae*	Unc. *Rhodobacteraceae*	DQ103618	0.36	7.23	6.39	5.39	1.59	8.45	4.97

304	*Proteobacteria*	*Deltaproteobacteria - Desulfovibrionales*	*Desulfohalobiaceae*	Unc. *Desulfovermiculus* sp.	KF814554/KF234383	1.76	1.25	3.57	2.61	5.89	7.89	3.63
522	*Bacteroidetes*	*Rhodothermaeota - Rhodothermales*	*Salinibacteraceae*	*Salinivenus iranica*	HQ197982	4.54	5.20	3.35	3.04	1.82	2.84	3.40
746	*Acetothermia*	-	-	Unc. *Acetothermia*	AJ133618/HQ530528	1.05	0.83	2.33	2.11	3.71	4.47	2.36
410	*Firmicutes*	*Bacilli - Bacillales*	*Bacillaceae*	*Bacillus zhanjiangensis / B. cohnii*	HM460884/X76437	0.58	0.75	2.05	1.42	2.87	3.72	1.84
531	*Bacteroidetes*	*Bacteroidia - Marinilabiliales*	*Marinilabiliaceae*	Unc. *Marinilabiliaceae*	FJ536452/KP174652	0.81	0.49	1.48	1.27	2.50	2.81	1.51
743	*Acetothermia*	-	-	Unc. *Acetothermia*	JX883738/JX883799	0.55	0.43	1.70	1.33	2.66	1.65	1.41
456	*Firmicutes*	*Bacilli - Bacillales*	*Bacillaceae*	*Bacillus isabeliae*	AM503357	0.29	1.11	1.39	1.03	1.97	2.30	1.31
741	*Acetothermia*	-	-	Unc. *Acetothermia*	HQ425220	0.44	0.63	1.12	1.17	2.14	2.41	1.28
525	*Balneolaeota*	*Balneolia - Balneolales*	*Balneolaceae*	*Aliifodinibius halophilus*	JR559733	1.56	0.07	1.69	1.62	0.17	1.87	1.23
7	*Proteobacteria*	*Alphaproteobacteria - Rhodobacterales*	*Rhodobacteraceae*	*Roseovarius litoreus*	JQ390520	1.63	2.11	1.44	1.32	0.12	0.17	1.18
406	*Proteobacteria*	*Deltaproteobacteria - Bradymonadales*	-	Unc. *Bradymonadales*	JX884186/JX883895	0.22	0.30	2.28	1.80	0.65	0.53	1.15
538	*Bacteroidetes*	*Bacteroidia - Marinilabiliales*	*Marinilabiliaceae*	Unc. *Marinilabiliaceae*	EF105954	0.60	0.40	1.05	0.95	2.06	1.92	1.13
10	*Proteobacteria*	*Alphaproteobacteria - Rhodobacterales*	*Rhodobacteraceae*	Unc. *Roseovarius* sp.	HM128371/HM128290	0.33	0.53	1.25	0.54	2.34	1.60	1.06
745	*Acetothermia*	-	-	Unc. *Acetothermia*	EU246019/HQ425219	0.41	0.43	0.97	0.97	1.59	2.08	1.05
301	*Proteobacteria*	*Deltaproteobacteria - Desulfovibrionales*	*Desulfohalobiaceae*	Unc. *Desulfovermiculus* sp.	JX883933/FJ536437	0.49	0.27	1.21	1.13	1.57	1.31	1.03
566	*Lentisphaerae*	-	-	Unc. MVP-94	HQ425193/FJ536428	0.48	0.42	0.73	0.83	1.57	1.80	0.93
394	*Firmicutes*	*Clostridia - Eubacteriales*	*Clostridiaceae*	Unc. *Hydrogenispora* sp.	EF558966	0.81	0.27	1.34	1.26	0.96	0.12	0.90
300	*Proteobacteria*	*Deltaproteobacteria - Desulfovibrionales*	*Desulfohalobiaceae*	Unc. *Desulfovermiculus* sp.	KP174429/HQ425221	0.48	0.27	0.95	0.57	1.28	1.09	0.77
27	*Proteobacteria*	*Alphaproteobacteria - Rhodobacterales*	*Rhodobacteraceae*	Unc. *Rhodobacteraceae*	AF513933/KP174548	1.57	1.02	0.61	0.51	0.37	0.46	0.72
635	*Bacteroidetes*	*Rhodothermaeota - Rhodothermales*	*Salinibacteraceae*	Unc. *Salinibacter* sp.	JX884506/JN484616	0.28	0.24	1.48	1.16	0.00	0.17	0.69
481	*Firmicutes*	*Clostridia - Halanaerobiales*	*Halanaerobiaceae*	Unc. *Halanaerobium* sp.	EF106374/DQ103656	0.25	0.27	0.59	0.43	1.08	1.64	0.66
748	*Acetothermia*	-	-	Unc. *Acetothermia*	KM278839/KM278906	0.35	0.29	0.49	0.71	0.82	1.22	0.63
313	*Proteobacteria*	*Deltaproteobacteria - Desulfobacterales*	*Desulfobacteraceae*	Unc. *Desulfobacteraceae*	KP174597/DQ103668	0.17	0.13	0.52	0.43	0.88	1.17	0.53
747	*Acetothermia*	-	-	Unc. *Acetothermia*	KM019052	0.13	0.27	0.42	0.53	0.74	1.12	0.52
269	*Proteobacteria*	*Gammaproteobacteria - Pseudomonadales*	*Moraxellaceae*	*Acinetobacter vivianii*	KT997477	1.41	1.36	0.07	0.12	0.11	0.00	0.44
285	*Proteobacteria*	*Betaproteobacteria - Burkholderiales*	*Comamonadaceae*	*Variovorax paradoxus*	AJ420329	0.86	1.02	0.02	0.03	0.03	0.02	0.28

Supplementary Table S1.2. Metagenomic sequencing features of the four metagenomes S, U, M and L.

	S	***U***	***M***	***L***
Number of raw reads	48,053,586	3,347,558	2,746,676	3,122,107
Raw reads mean length (bp)	86.74	243.59	266.43	247.53
Number of trimmed and merged reads	42,167,940	2,895,160	2,324,012	2,684,585
Trimmed reads mean length (bp)	94.75	267.99	295.75	271.2
Number of assembled contigs	193,470	92,453	111,237	120,982
Number of contigs >500 bp	91,410	42,418	52,579	58,451
Total size contigs >500 bp	121,667,984	59,602,441	72,159,574	72,761,649
N50 (assembled contigs)	1,041	1,060	1,085	956
N50 (contigs >500 bp)	1,641	1,735	1,676	1,393
G+C mol%	51.1	44.9	46.9	46.8
Longer contig size (bp)	65,457	139,815	110,450	112,248
Number of gene contigs >500 bp	184,093	95,200	114,169	117,664
% reads assembled to contigs >500 bp	48.99%	58.87%	50.94%	47.82%
% reads mapping to trimmed reads*	41.03%	58.35%	47.92%	42.56%
% reads of MAGs mapping to trimmed reads*	19.95%	45.79%	18.06%	8.17%

*At 98% identity and 70% coverage.

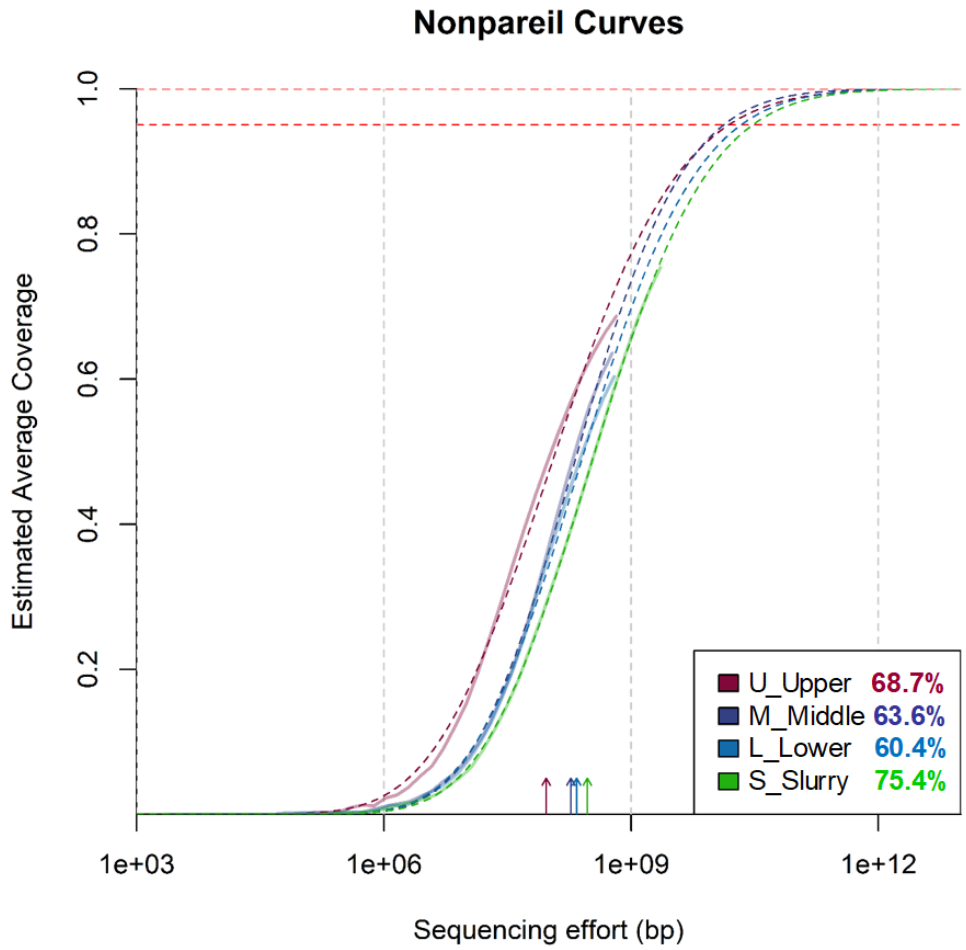

Supplementary Figure S1.4. Nonpareil curves of the four metagenomes (S, U, M and L).

Supplementary Table S1.3. Most relevant OPUs with relative sequence abundances ≥ 1% (at least in one of the layers) for Archaea (**A**) and Bacteria (**B**) from the 16S rRNA gene sequences recruited from the S, U, M and L metagenomes. First column (from left to right): OPU number; from second to fifth columns: the taxonomic affiliation of the closest relative sequence used as a reference (phylum, class and/or order, family and genus/species); sixth column: accession number of the reference sequence; seventh to tenth columns: the percentage relative abundance of each OPU per sample.

A. Major OPUs of Archaea

OPU	Phylum	Class-Order	Family	Genus-Species	Accession number	S	U	M	L
219	*Euryarchaeota*	*Halobacteria - Natrialbales*	*Natrialbaceae*	Unc. *Salinarchaeum* sp.	EF459703	17.59	4.49	6.63	19.21
273	*Euryarchaeota*	*Halobacteria - Haloferacales*	*Haloferacaceae*	Unc. *Haloferacaceae*	AM947491/DQ432537	4.30	0.41	0.66	1.46
315	*Euryarchaeota*	-	-	Unc. KTK 4A	HE604545	3.79	47.35	15.59	6.68
384	*Euryarchaeota i.s.*	-	-	Unc. MSBL1	KJ882144	2.87	0.51	0.66	0.63
314	*Euryarchaeota*	-	-	Unc. KTK 4A	DQ103675	2.65	1.63	5.47	2.30
1	*Euryarchaeota*	*Halobacteria - Haloferacales*	*Halorubraceae*	*Halorubrum arcis*	DQ355793	2.60	0.10	0.17	0.84
222	*Euryarchaeota*	*Halobacteria - Natrialbales*	*Natrialbaceae*	Unc. *Salinarchaeum* sp.	EF690598	2.60	0.00	0.00	0.00
349	*Euryarchaeota i.s.*	-	-	Unc. MSBL1	KJ881758	2.55	5.20	3.48	4.80
437	*Euryarchaeota*	*Halobacteria - Halobacteriales*	*Halobacteriaceae*	Unc. *Halodesulfurarchaeum* sp.	KC465610/HQ425150	2.43	0.00	0.00	0.00
406	*Euryarchaeota*	*Halobacteria - Halobacteriales*	*Halobacteriaceae*	Unc. *Halobacteriaceae*	HQ400437	2.33	0.00	0.17	0.00
448	*Euryarchaeota*	*Halobacteria - Haloferacales*	*Halorubraceae*	Unc. *Halorubrum* sp.	AJ969858	2.31	0.00	0.33	0.21
96	*Euryarchaeota*	*Halobacteria - Haloferacales*	*Haloferacaceae*	Unc. *Halobellus* sp.	FN391236/KF591570	2.28	0.00	0.00	0.00
475	*Euryarchaeota*	*Thermoplasmata - Thermoplasmatales*	-	Unc. 20c-4	DQ103669	2.11	5.51	9.29	2.09
313	*Euryarchaeota*	-	-	Unc. KTK 4A	HE604525/AJ133621	2.04	6.22	15.59	10.23
464	*Euryarchaeota*	*Halobacteria - Natrialbales*	*Natrialbaceae*	Unc. *Natrialbaceae*	HQ400437	2.02	0.00	0.00	0.00
299	*Euryarchaeota*	*Halobacteria*	-	Unc. *Halobacteria*	FJ536516	1.97	4.59	3.48	2.92
463	*Euryarchaeota*	*Halobacteria - Natrialbales*	*Natrialbaceae*	Unc. *Salinarchaeum* sp.	AB012054	1.87	0.31	0.00	1.88
450	*Euryarchaeota*	*Halobacteria - Haloferacales*	*Halorubraceae*	*Halorubrum* sp. s1-1 / Unc. *H.* sp.	FJ042667/AJ969863	1.87	0.00	0.00	0.00
479	*Euryarchaeota i.s.*	-	-	Unc. MSBL1	FJ536511	1.72	1.63	3.15	2.92
347	*Euryarchaeota i.s.*	-	-	Unc. MSBL1	FJ536512	1.43	0.51	1.16	1.04
245	*Euryarchaeota*	*Halobacteria - Halobacteriales*	*Halobacteriaceae*	Unc. *Halanaeroarchaeum* sp.	HQ425150	1.38	0.00	0.00	0.00
291	*Euryarchaeota*	*Halobacteria - Halobacteriales*	*Halococcaceae*	Unc. *Halococcus* sp.	HQ157635	1.31	0.00	0.00	0.00
293	*Euryarchaeota*	*Methanomicrobia*	-	ST-12K10A	AJ347786	1.19	1.33	1.99	2.51
241	*Euryarchaeota*	*Halobacteria - Halobacteriales*	*Halobacteriaceae*	Unc. *Salinirubrum* sp.	HQ400450	1.17	0.10	0.00	0.00
268	*Euryarchaeota*	*Halobacteria - Haloferacales*	*Haloferacaceae*	Unc. *Haloquadratum* sp	AM947446/CU467264	1.17	0.00	0.00	0.00
441	*Euryarchaeota i.s.*	-	-	Unc. MSBL1	HE604509	1.14	0.00	0.17	0.00
469	*Euryarchaeota*	*Halobacteria - Haloferacales*	*Haloferacaceae*	Unc. *Haloferacaceae*	FN391292	1.02	0.00	0.00	0.00
380	*Euryarchaeota i.s.*	-	-	Unc. MSBL1	HE604509	0.41	0.00	0.50	1.04
269	*Euryarchaeota*	*Halobacteria - Haloferacales*	*Haloferacaceae*	Unc. *Haloferacaceae* (MSP23)	FN994982	0.24	1.12	1.00	2.30
478	*Euryarchaeota i.s.*	-	-	Unc. MSBL1	FJ536509/KJ881758	0.22	3.06	4.64	2.09
477	*Euryarchaeota i.s.*	-	-	Unc. Candidate division MSBL1	AY226367	0.17	0.51	1.16	1.67

480	*Euryarchaeota i.s.*	-	-	Unc. MSBL1	FJ536508	0.17	0.41	0.66	1.04
407	*Woesearchaeota*	-	-	Unc. DHVEG-6	EU731442	0.15	0.31	0.83	1.25
428	*Aenigmarchaeota*	-	-	Unc. DSEG	AGBK01001752	0.12	0.51	2.16	1.67
442	*Euryarchaeota*	*Halobacteria - Halobacteriales*	*Halobacteriaceae*	Unc. *Halodesulfurarchaeum* sp.	CP016804	0.12	0.82	1.16	1.25
378	*Euryarchaeota i.s.*	-	-	Candidate division MSBL1 archaeon SCGC-AAA382C18	LHYF01000011	0.10	0.82	1.99	0.84
352	*Euryarchaeota i.s.*	-	-	Unc. MSBL1	KJ882122/KJ882121	0.02	0.82	1.16	2.92
409	*Woesearchaeota*	-	-	Unc. DHVEG-6	AB243808/EU181722	0.02	0.10	0.33	3.13
353	*Euryarchaeota i.s.*	-	-	Unc. MSBL1	KJ881757	0.00	0.31	0.50	1.04
486	*Euryarchaeota i.s.*	-	-	Unc. MSBL1	KJ882194/KJ882043	0.00	0.20	0.50	2.51

i.s. = *incertae sedis*

B. Major OPUs of Bacteria

OPU	Phylum	Class-Order	Family	Genus-Species	Accession number	S	U	M	L
750	*Acetothermia*	-	-	Unc. *Acetothermia*	HE604704	16.67	0.82	1.13	0.22
742	*Acetothermia*	-	-	Unc. *Acetothermia*	HE604684/HE604747	6.95	0.82	1.26	0.86
745	*Acetothermia*	-	-	Unc. *Acetothermia*	EU246019/HQ425219	4.31	2.62	2.01	2.26
256	*Proteobacteria*	*Gammaproteobacteria - Chromatiales*	*Ectothiorhodospiraceae*	Unc. *Halorhodospira* sp.	FN393473	4.18	0.49	0.38	0.00
748	*Acetothermia*	-	-	Unc. *Acetothermia*	KM278839/KM278906	3.95	0.16	0.50	0.43
521	*Bacteroidetes*	*Rhodothermaeota - Rhodothermales*	*Salinibacteraceae*	*Salinibacter ruber*	CP000159	3.32	0.82	0.50	1.18
640	*Planctomycetes*	*Candidatus* Brocadiales	*Brocadiaceae*	Unc. PB79	HE604774	3.08	5.90	13.82	23.47
566	*Lentisphaerae*	-	-	Unc. MVP-94	HQ425193/FJ536428	2.77	2.30	3.39	8.29
736	*Acetothermia*	-	-	Unc. *Acetothermia*	AJ133618/HQ530528	2.75	4.10	4.15	2.69
294	*Proteobacteria*	*Deltaproteobacteria - Desulfovibrionales*	*Desulfohalobiaceae*	Unc. *Desulfovermiculus* sp.	KF814554/KF234383	2.15	4.10	4.40	4.74
749	*Acetothermia*	-	-	Unc. *Acetothermia*	HE604693/HE604707	1.89	1.48	1.38	1.51
300	*Proteobacteria*	*Deltaproteobacteria - Desulfovibrionales*	*Desulfohalobiaceae*	Unc. *Desulfovermiculus* sp.	KP174429/HQ425221	1.88	3.44	2.01	2.26
399	-	-	-	Unc. TM6 (*Dependentiae*)	JX881376/JN524548	1.61	1.80	0.25	0.11
714	*Acetothermia*	-	-	Unc. *Acetothermia*	AJ133618/HE604707	1.52	0.16	0.00	0.00
991	-	-	-	Unc. WS1	AB177145/JN480620	1.41	0.16	0.00	0.22
494	*Firmicutes*	*Clostridia - Halanaerobiales*	*Halanaerobiaceae*	Unc. *Halarsenatibacter* sp.	FJ536430/EU245490	1.32	0.33	0.38	0.43
167	*Proteobacteria*	*Alphaproteobacteria - Rhodospirillales*	*Rhodovibrionaceae*	Unc. *Rhodovibrio* sp.	DQ103604/DQ103605	1.30	0.00	0.38	0.43
744	*Acetothermia*	-	-	Unc. *Acetothermia*	KP174520	1.28	3.44	3.39	2.15
302	*Proteobacteria*	*Deltaproteobacteria - Desulfovibrionales*	*Desulfohalobiaceae*	Unc. *Desulfovermiculus* sp.	FJ536445	1.27	0.33	0.63	0.43
481	*Firmicutes*	*Clostridia - Halanaerobiales*	*Halanaerobiaceae*	Unc. *Halanaerobium* sp.	EF106374/DQ103656	1.24	2.30	2.51	1.83
670	*Firmicutes*	*Bacilli - Bacillales*	*Bacillaceae*	*Bacillus oleronius*	X82492	1.18	0.00	0.00	0.00
646	*Firmicutes*	*Clostridia - Halanaerobiales*	*Halanaerobiaceae*	Unc. *Halanaerobium* sp.	EU869420/DQ103656	1.09	0.49	0.13	0.32
969	*Firmicutes*	*Clostridia - Halanaerobiales*	*Halanaerobiaceae*	*Halothermothrix orenii*	L22016	0.99	0.49	0.13	0.65
567	*Lentisphaerae*	-	-	Unc. MVP-94	KP174606/JX883575	0.67	1.64	1.01	2.26
563	*Marinimicrobia*	-	-	Unc. SAR406 clade	JX883021	0.65	1.48	2.26	2.05

741	*Acetothermia*	-	-	Unc. *Acetothermia*	HQ425220	0.65	22.95	14.70	10.23
484	*Firmicutes*	*Clostridia - Halanaerobiales*	*Halanaerobiaceae*	Unc. *Halanaerobium* sp.	JX684094	0.64	2.30	1.01	0.97
1131	*Parcubacteria*	-	-	Unc. *Parcubacteria*	HE604802	0.61	2.95	1.26	1.51
533	*Bacteroidetes*	*Bacteroidia - Marinilabiliales*	*Marinilabiliaceae*	Unc. *Marinilabiliaceae*	DQ330523/EU245987	0.55	1.80	2.01	0.54
740	*Parcubacteria*	-	-	Unc. *Candidatus* Falkowbacteria	AJ347768/HQ691934	0.45	1.15	1.13	1.08
301	*Proteobacteria*	*Deltaproteobacteria - Desulfovibrionales*	*Desulfohalobiaceae*	Unc. *Desulfovermiculus* sp.	JX883933/FJ536437	0.30	0.16	1.01	0.97
747	*Acetothermia*	-	-	Unc. *Acetothermia*	KM019052	0.27	0.66	1.63	2.58
491	*Firmicutes*	*Clostridia - Halanaerobiales*	*Halanaerobiaceae*	Unc. *Halanaerobium* sp.	JX882984/JX883106	0.00	0.98	1.25	1.18
493	*Firmicutes*	*Clostridia - Halanaerobiales*	*Halanaerobiaceae*	Unc. *Halanaerobium* sp.	EU245191/KC465643	0.22	4.10	1.63	0.32
933	*Proteobacteria*	*Deltaproteobacteria - Desulfovibrionales*	*Desulfohalobiaceae*	Unc. *Desulfovermiculus* sp.	JN518340	0.10	0.16	1.26	0.32
313	*Proteobacteria*	*Deltaproteobacteria - Desulfobacterales*	*Desulfobacteraceae*	Unc. *Desulfobacteraceae*	KP174597/DQ103668	0.04	0.16	1.76	0.43
133	*Proteobacteria*	*Alphaproteobacteria - Hyphomicrobiales*	*Aurantimonadaceae*	*Aurantimonas coralicida / A. manganoxydans*	AJ786361/U53824	0.01	4.75	8.67	5.06
531	*Bacteroidetes*	*Bacteroidia - Marinilabiliales*	*Marinilabiliaceae*	Unc. *Marinilabiliaceae*	FJ536452/KP174652	0.01	0.98	1.00	0.43
1161	*Proteobacteria*	*Deltaproteobacteria - Desulfobacterales*	*Desulfobacteraceae*	Unc. *Desulfococcus* sp.	KM278909/AJ937690	0.00	0.00	0.88	1.08

Supplementary Table S1.4. Relative abundance of core OPUs (abundances ≥1%) grouped at a genus level and shared by replicates R1 and R2 sampled in July 2016 (R1_U, R1_M, R1_L, R2_U, R2_M, R2_L) obtained from the 16S rRNA gene amplicons, and from 16S rRNA gene reads of the metagenomes sampled in April 2017 (U, M, L) and December 2016 (S). Shared genera for archaeal (**A**) and bacterial (**B**) domains between horizons are marked with blue, yellow, green and violet for U, M, L and S, respectively. Shared genera among all samples are marked in bold, and red color when one horizon and slurry (S) co-occur. Species grouping according to the genus level (**C**) are shown for Archaea (orange) and Bacteria (blue) for the shared genera, respectively.

A. Archaea	**%R1_U**	**%R2_U**	**%U**	**%R1_M**	**%R2_M**	**%M**	**%R1_L**	**%R2_L**	**%L**	**%S**
1-*Halorubrum*	**38.17**	**38.11**	**0.10**	**32.53**	**31.72**	**0.50**	**30.59**	**31.41**	**1.25**	**6.97**
2-*Halonotius*	8.56	7.89	0.00	7.77	8.41	0.00	1.69	1.72	0.63	0.05
3-*Haloplanus*	2.46	3.41	0.00	3.05	3.24	0.17	5.84	6.97	0.21	0.24
6-*Haloarcula*	2.24	2.22	0.00	1.49	1.67	0.00	5.20	4.68	0.21	0.15
7-*Salinarchaeum*	**4.90**	**1.92**	**4.90**	**6.89**	**6.77**	**6.64**	**7.04**	**6.66**	**21.09**	**22.54**
8-Unc. KTK 4A	**2.37**	**2.41**	**55.20**	**3.78**	**3.99**	**36.71**	**3.96**	**4.20**	**19.21**	**8.48**
9-Unc. MSBL1	**0.84**	**0.73**	**13.98**	**1.45**	**1.41**	**19.77**	**1.28**	**1.47**	**22.55**	**10.59**
10-Unc. DHVEG-6	**4.5E-03**	**0.01**	**0.41**	**0.02**	**0.02**	**1.16**	**0.03**	**0.01**	**4.38**	**0.17**
11-*Halodesulfurarchaeum*	**0.06**	**0.02**	**0.82**	**0.08**	**0.08**	**1.16**	**0.07**	**0.07**	**1.25**	**2.55**
17-*Haloferacaceae*	**0.04**	**0.03**	**1.12**	**0.12**	**0.06**	**1.00**	**0.09**	**0.04**	**2.30**	**0.24**
18-*Haloferacaceae*	**2.2E-03**	**4.5E-03**	**0.41**	**0.01**	**1.9E-03**	**0.66**	**0.01**	**0.01**	**1.46**	**4.30**
20-Unc. ST-12K10A	**0.59**	**0.56**	**1.33**	**0.76**	**0.78**	**1.99**	**0.94**	**0.90**	**2.51**	**1.19**
21-*Nanohaloarchaeota*	2.06	2.04	0.00	0.30	0.23	0.00	0.13	0.23	0.42	0.00
22-*Halobacteriaceae*	**2.97**	**4.14**	**4.59**	**4.96**	**4.76**	**3.49**	**4.76**	**4.60**	**2.92**	**1.97**
23-Unc. 20c-4	4.23	4.16	5.51	6.51	6.60	9.30	6.76	6.76	2.09	0.00
24-*Halobacteriaceae*	2.2E-03	0.00	0.00	1.9E-03	1.9E-03	0.17	2.4E-03	2.3E-03	0.00	2.33
25-Unc. DSEG	**0.05**	**0.03**	**0.51**	**0.06**	**0.08**	**2.16**	**0.06**	**0.07**	**1.67**	**0.12**
HORIZON SHARED SEQS%	**54.21**	**52.12**	**88.88**	**60.22**	**59.51**	**84.88**	**68.46**	**69.78**	**84.13**	
HORIZON+S SHARED SEQS%	**49.99**	**47.96**	**83.37**	**53.71**	**52.91**	**75.58**	**61.58**	**62.79**	**81.63**	
U-M-L-S SHARED SEQS%			**83.37**			**75.25**			**80.58**	**59.12**
TOTAL SEQS%	**69.54**	**67.67**	**88.88**	**69.77**	**69.83**	**84.88**	**68.47**	**69.78**	**84.13**	**61.89**

B. Bacteria	**%R1_U**	**%R2_U**	**%U**	**%R1_M**	**%R2_M**	**%M**	**%R1_L**	**%R2_L**	**%L**	**%S**
1-*Roseovarius*	**10.27**	**11.44**	**0.66**	**4.76**	**7.61**	**0.75**	**8.77**	**2.78**	**0.22**	**0.21**
2-*Halorhodospira*	0.01	0.01	0.49	0.02	0.02	0.38	0.03	0.03	0.00	5.11
3-*Desulfovermiculus*	**2.87**	**2.00**	**8.20**	**6.05**	**4.58**	**9.28**	**9.16**	**10.85**	**8.72**	**5.71**
6-*Rhodobacteraceae*	0.13	0.06	0.16	0.39	0.40	0.00	0.60	0.84	0.00	0.78
8-*Aurantimonas*	0.01	0.03	4.75	0.01	0.01	8.66	0.05	0.00	5.06	0.01
9-*Rhodovibrio*	0.03	0.06	0.00	0.14	0.13	0.38	0.16	0.18	0.43	1.30
11-*Halanaerobium*	**0.64**	**0.69**	**10.82**	**1.66**	**1.32**	**7.28**	**2.70**	**3.99**	**4.95**	**4.15**
13-*Salinivenus*	23.73	23.41	0.82	6.42	5.32	0.25	3.54	4.17	0.00	0.92
14-*Salinibacter*	**34.13**	**32.66**	**0.98**	**25.55**	**20.60**	**0.50**	**21.61**	**9.18**	**1.18**	**3.33**
15-Unc. MVP-94	**0.54**	**0.47**	**3.93**	**0.84**	**1.00**	**4.39**	**1.74**	**1.97**	**10.55**	**2.77**
16-*Desulfobacteraceae*	**0.17**	**0.13**	**0.16**	**0.52**	**0.43**	**1.76**	**0.88**	**1.17**	**0.43**	**0.04**
18-Unc. TM6	0.06	0.00	1.80	0.12	0.12	0.25	0.13	0.21	0.11	1.61
20-*Halarsenatibacter*	**0.07**	**0.07**	**0.33**	**0.24**	**0.22**	**0.38**	**0.35**	**0.63**	**0.43**	**1.32**
23-Unc. *Marinilabiliaceae*	**0.81**	**0.49**	**0.98**	**1.48**	**1.27**	**1.00**	**2.50**	**2.81**	**0.43**	**8.6E-03**

24-Unc. *Marinilabiliaceae*	**0.12**	**0.04**	**1.80**	**0.19**	**0.23**	**2.01**	**0.49**	**0.69**	**0.54**	**0.55**
25-Unc. *Marinilabiliaceae*	**0.60**	**0.40**	**0.33**	**1.05**	**0.95**	**0.13**	**2.06**	**1.92**	**0.43**	**0.17**
26-Unc. SAR406 clade	**0.10**	**0.01**	**1.48**	**0.18**	**0.15**	**2.26**	**0.32**	**0.21**	**2.05**	**0.65**
27-Unc. PB79	0.00	0.00	5.90	0.00	0.02	13.80	0.00	0.07	23.47	3.08
28-Unc. *Acetothermia*	0.07	0.07	0.16	0.16	0.11	0.00	0.27	0.26	0.00	1.52
29-Unc. *Cand.* Falkowbacteria	0.00	0.01	1.15	0.01	0.02	1.13	0.05	0.02	1.08	0.45
30-Unc. *Acetothermia*	**0.44**	**0.63**	**22.95**	**1.12**	**1.17**	**14.68**	**2.14**	**2.41**	**10.23**	**0.65**
31-Unc. *Acetothermia*	**0.07**	**0.11**	**0.82**	**0.18**	**0.15**	**1.25**	**0.36**	**0.33**	**0.86**	**6.95**
32-Unc. *Acetothermia*	**0.55**	**0.43**	**0.82**	**1.70**	**1.33**	**0.88**	**2.66**	**1.65**	**0.54**	**0.17**
33-Unc. *Acetothermia*	**0.22**	**0.14**	**3.44**	**0.31**	**0.15**	**3.39**	**0.47**	**0.58**	**2.15**	**1.28**
34-Unc. *Acetothermia*	**0.41**	**0.43**	**2.62**	**0.97**	**0.97**	**2.01**	**1.59**	**2.08**	**2.26**	**4.31**
35-Unc. *Acetothermia*	**1.05**	**0.83**	**4.10**	**2.33**	**2.11**	**4.14**	**3.71**	**4.47**	**2.69**	**2.75**
36-Unc. *Acetothermia*	**0.13**	**0.27**	**0.66**	**0.42**	**0.53**	**1.63**	**0.74**	**1.12**	**2.58**	**0.27**
37-Unc. *Acetothermia*	**0.35**	**0.29**	**0.16**	**0.49**	**0.71**	**0.50**	**0.82**	**1.22**	**0.43**	**3.95**
38-Unc. *Acetothermia*	**0.07**	**0.04**	**1.48**	**0.19**	**0.15**	**1.38**	**0.25**	**0.36**	**1.51**	**1.89**
39-Unc. *Acetothermia*	**0.04**	**0.01**	**0.82**	**0.11**	**0.04**	**1.13**	**0.11**	**0.08**	**0.22**	**16.67**
41-*Halothermothrix*	0.00	0.00	0.49	0.00	0.00	0.13	0.00	0.00	0.65	0.99
44-Unc. *Parcubacteria*	0.00	0.00	2.95	0.00	0.00	1.25	0.00	0.00	1.51	0.61
HORIZON SHARED SEQS%	**77.62**	**75.19**	**73.93**	**57.07**	**51.28**	**71.77**	**63.77**	**50.93**	**55.01**	
HORIZON+S SHARED SEQS%	**77.62**	**75.19**	**73.93**	**57.07**	**51.28**	**71.77**	**63.77**	**50.93**	**55.01**	
U-M-L-S SHARED SEQS%			**84.59**			**85.95**			**85.25**	**64.53**
TOTAL SEQS%	**77.71**	**75.26**	**86.23**	**57.61**	**51.82**	**86.95**	**68.25**	**56.31**	**85.68**	**74.16**

C. Species group

GROUP	OPU	Species	%R1_U	%R2_U	%U	%R1_M	%R2_M	%M	%R1_L	%R2_L	%L	%S
species group - 1	1	*Halorubrum arcis*	8.30	7.08	0.10	10.98	11.00	0.17	10.98	9.99	0.84	2.60
	3	*Halorubrum xinjiangense*	1.80	1.12	0.00	2.50	3.08	0.00	0.72	0.55	0.00	0.00
	14	*Halorubrum* sp. S5a-2	3.91	4.26	0.00	2.14	2.62	0.00	2.73	2.66	0.00	0.00
	19	*Halorubrum salinum*	2.12	2.26	0.00	2.86	1.85	0.00	1.64	1.79	0.00	0.00
	26	*Halorubrum orientale*	5.96	16.46	0.00	9.98	3.08	0.00	11.19	13.05	0.21	0.00
	28	*Halorubrum* sp.	10.93	2.60	0.00	0.63	7.28	0.00	0.42	0.46	0.00	0.07
	38	*Halorubrum* sp.	1.74	0.02	0.00	0.05	0.05	0.00	0.05	0.05	0.00	0.10
	39	*Halorubrum* sp.	0.94	2.47	0.00	2.40	2.24	0.00	2.55	2.60	0.00	0.02
	71	*Halorubrum* sp.	2.46	1.84	0.00	1.00	0.50	0.00	0.31	0.27	0.00	0.00
	448	*Halorubrum* sp.	0.00	0.00	0.00	0.00	0.00	0.33	0.00	0.00	0.21	2.31
	450	*Halorubrum* sp. s1-1	0.00	0.00	0.00	0.00	0.00	0.00	0.00	0.00	0.00	1.87
sp.gr.-2	32	*Halonotius* sp.	1.74	1.47	0.00	0.53	0.71	0.00	0.28	0.74	0.63	0.05
	60	*Halonotius* sp.	2.42	1.60	0.00	5.51	5.17	0.00	0.50	0.46	0.00	0.00
	63	*Halonotius* sp.	4.40	4.81	0.00	1.72	2.53	0.00	0.91	0.52	0.00	0.00
sp.gr.-3	47	*Haloplanus natans* DSM 17983	2.33	2.18	0.00	1.61	1.86	0.00	1.28	2.67	0.00	0.00
	48	*Haloplanus salinus*	0.13	1.23	0.00	1.44	1.38	0.17	4.56	4.30	0.21	0.24
sp.gr.-6	131	*Haloarcula* sp.	1.44	1.36	0.00	0.85	1.12	0.00	1.86	1.47	0.00	0.00
	132	*Haloarcula* sp.	0.73	0.74	0.00	0.45	0.43	0.00	2.37	2.14	0.21	0.15
	190	*Haloarcula tradensis / H. salaria*	0.07	0.11	0.00	0.19	0.12	0.00	0.97	1.07	0.00	0.00
sp.gr.-7	219	*Salinarchaeum* sp.	1.62	0.53	4.49	5.04	4.97	6.64	4.77	4.36	19.21	17.59
	222	*Salinarchaeum* sp.	0.00	0.00	0.10	0.00	0.00	0.00	0.00	0.01	0.00	2.60
	387	*Salinarchaeum* sp. MSP1	3.28	1.38	0.00	1.86	1.80	0.00	2.27	2.28	0.00	0.49
	463	*Salinarchaeum* sp.	0.00	0.00	0.31	0.00	0.00	0.00	0.00	0.00	1.88	1.87
sp.gr.-8	313	Unc. KTK 4A	2.03	2.02	6.22	3.27	3.47	15.61	3.41	3.60	10.23	2.04
	314	Unc. KTK 4A	0.25	0.31	1.63	0.31	0.36	5.48	0.45	0.44	2.30	2.65
	315	Unc. KTK 4A	0.09	0.08	47.35	0.20	0.15	15.61	0.10	0.15	6.68	3.79
sp.gr.-9	324	Unc. MSBL1	0.66	0.59	3.06	1.15	1.20	4.65	1.00	1.13	2.09	0.00
	347	Unc. MSBL1	0.03	0.02	0.51	0.05	0.03	1.16	0.03	0.04	1.04	1.43
	349	Unc. MSBL1	0.05	0.04	5.20	0.09	0.05	3.49	0.06	0.10	4.80	2.55
	352	Unc. MSBL1	0.02	0.03	0.82	0.04	0.04	1.16	0.03	0.04	2.92	0.02
	353	Unc. MSBL1	0.00	2.2E-03	0.31	0.01	1.9E-03	0.50	0.02	0.01	1.04	0.00
	378	Unc. MSBL1	0.05	0.04	0.82	0.07	0.05	1.99	0.08	0.10	0.84	0.10
	380	Unc. MSBL1	0.01	0.00	0.00	0.02	0.01	0.50	0.03	0.03	1.04	0.41
	384	Unc. MSBL1	0.01	0.01	0.51	0.02	0.02	0.66	0.03	0.02	0.63	2.87
	477	Unc. MSBL1	0.00	0.00	0.51	0.00	0.00	1.16	0.00	0.00	1.67	0.17
	479	Unc. MSBL1	0.00	0.00	1.63	0.00	0.00	3.16	0.00	0.00	2.92	1.72
	480	Unc. MSBL1	0.00	0.00	0.41	0.00	0.00	0.66	0.00	0.00	1.04	0.17
	483	Unc. MSBL1	0.00	0.00	0.00	0.00	0.00	0.17	0.00	0.00	0.00	1.14

	486	Unc. MSBL1	0.00	0.00	0.20	0.00	0.00	0.50	0.00	0.00	2.51	0.00
sp.gr.-10	407	Unc. DHVEG-6	2.2E-03	2.2E-03	0.31	0.02	0.01	0.83	0.02	4.7E-03	1.25	0.15
	409	Unc. DHVEG-6	2.2E-03	0.01	0.10	1.9E-03	0.01	0.33	0.01	2.3E-03	3.13	0.02
sp.gr.-11	437	*Halodesulfurarchaeum* sp.	0.06	0.02	0.00	0.08	0.08	0.00	0.07	0.07	0.00	2.43
	442	*Halodesulfurarchaeum* sp.	0.00	0.00	0.82	0.00	0.00	1.16	0.00	0.00	1.25	0.12
sp.gr.-17	269	Unc. *Haloferacaceae*	0.04	0.03	1.12	0.12	0.06	1.00	0.09	0.04	2.30	0.24
sp.gr.-18	273	Unc. *Haloferacaceae*	2.2E-03	4.5E-03	0.41	7.5E-03	1.9E-03	0.66	0.01	0.01	1.46	4.30
sp.gr.-20	293	Unc. ST-12K10A	0.59	0.56	1.33	0.76	0.78	1.99	0.94	0.90	2.51	1.19
sp.gr.-21	295	*Nanohaloarchaeota*	2.06	2.04	0.00	0.30	0.23	0.00	0.13	0.23	0.42	0.00
sp.gr.-22	299	Unc. *Halobacteriaceae*	2.97	4.14	4.59	4.96	4.76	3.49	4.76	4.60	2.92	1.97
sp.gr.-23	317	Unc. 20c-4	4.23	4.16	5.51	6.51	6.60	9.30	6.76	6.76	2.09	0.00
sp.gr.-24	406	Unc. *Halobacteriaceae*	2.2E-03	0.00	0.00	1.9E-03	1.9E-03	0.17	2.4E-03	2.3E-03	0.00	2.33
sp.gr.-25	428	Unc. DSEG	0.05	0.03	0.51	0.06	0.08	2.16	0.06	0.07	1.67	0.12
sp.gr.-1	1	*Roseovarius* sp.	8.31	8.79	0.00	2.08	5.74	0.00	6.31	1.01	0.00	0.18
	7	*Roseovarius litoreus*	1.63	2.11	0.00	1.44	1.32	0.00	0.12	0.17	0.00	0.00
	10	*Roseovarius* sp.	0.33	0.53	0.66	1.25	0.54	0.75	2.34	1.60	0.22	0.03
sp.gr.-2	256	*Halorhodospira* sp.	0.01	0.01	0.49	0.01	0.00	0.38	0.01	0.02	0.00	4.18
	257	*Halorhodospira* sp.	0.00	0.00	0.00	0.01	0.02	0.00	0.01	0.02	0.00	0.92
sp.gr.-3	300	*Desulfovermiculus* sp.	0.48	0.27	3.44	0.95	0.57	2.01	1.28	1.09	2.26	1.88
	301	*Desulfovermiculus* sp.	0.49	0.27	0.16	1.21	1.13	1.00	1.57	1.31	0.97	0.30
	302	*Desulfovermiculus* sp.	0.13	0.20	0.33	0.32	0.27	0.63	0.43	0.56	0.43	1.27
	304	*Desulfovermiculus* sp.	1.76	1.25	4.10	3.57	2.61	4.39	5.89	7.89	4.74	2.15
	933	*Desulfovermiculus* sp.	0.00	0.00	0.16	0.00	0.00	1.25	0.00	0.00	0.32	0.10
sp.gr.-6	86	Unc. *Rhodobacteraceae*	0.13	0.06	0.16	0.39	0.40	0.00	0.60	0.84	0.00	0.78
sp.gr.-8	133	*Aurantimonas coralicida / A. manganoxydans*	0.01	0.03	4.75	0.01	0.01	8.66	0.05	0.00	5.06	0.01
sp.gr.-9	167	*Rhodovibrio* sp.	0.03	0.06	0.00	0.14	0.13	0.38	0.16	0.18	0.43	1.30
sp.gr.-11	481	*Halanaerobium* sp.	0.25	0.27	2.30	0.59	0.43	2.51	1.08	1.64	1.83	1.24
	482	*Halanaerobium* sp.	0.13	0.10	0.66	0.25	0.18	0.75	0.21	0.46	0.32	0.75
	484	*Halanaerobium* sp.	0.10	0.17	2.30	0.35	0.32	1.00	0.65	0.98	0.97	0.64
	491	*Halanaerobium* sp.	0.07	0.06	0.98	0.21	0.20	1.25	0.36	0.36	1.18	0.22
	493	*Halanaerobium* sp.	0.04	0.03	4.10	0.19	0.06	1.63	0.08	0.23	0.32	0.22
	646	*Halanaerobium* sp.	0.04	0.06	0.49	0.08	0.12	0.13	0.32	0.31	0.32	1.09
sp.gr.-13	522	*Salinivenus iranica*	4.54	5.20	0.16	3.35	3.04	0.25	1.82	2.84	0.00	0.30
	523	*Salinivenus lutea*	19.19	18.20	0.66	3.06	2.27	0.00	1.71	1.32	0.00	0.62
sp.gr.-14	521	*Salinibacter ruber*	33.86	32.41	0.82	24.07	19.44	0.50	21.61	9.01	1.18	3.32
	635	*Salinibacter* sp.	0.28	0.24	0.16	1.48	1.16	0.00	0.00	0.17	0.00	0.01
sp.gr.-15	566	Unc. MVP-94	0.48	0.42	2.30	0.73	0.83	3.39	1.57	1.80	8.29	2.77
	567	Unc. MVP-94	0.06	0.06	1.64	0.10	0.16	1.00	0.17	0.17	2.26	0.00
sp.gr.-16	313	Unc. *Desulfobacteraceae*	0.17	0.13	0.16	0.52	0.43	1.76	0.88	1.17	0.43	0.04
sp.gr.-18	399	Unc. TM6	0.06	0.00	1.80	0.12	0.12	0.25	0.13	0.21	0.11	1.61
sp.gr.-20	494	Unc. *Halarsenatibacter* sp.	0.07	0.07	0.33	0.24	0.22	0.38	0.35	0.63	0.43	1.32
sp.gr.-23	531	Unc. *Marinilabiliaceae*	0.81	0.49	0.98	1.48	1.27	1.00	2.50	2.81	0.43	0.01
sp.gr.-24	533	Unc. *Marinilabiliaceae*	0.12	0.04	1.80	0.19	0.23	2.01	0.49	0.69	0.54	0.55
sp.gr.-25	538	Unc. *Marinilabiliaceae*	0.60	0.40	0.33	1.05	0.95	0.13	2.06	1.92	0.43	0.17
sp.gr.-26	563	Unc. SAR406 clade	0.10	0.01	1.48	0.18	0.15	2.26	0.32	0.21	2.05	0.65
sp.gr.-27	640	Unc. PB79	0.00	0.00	5.90	0.00	0.02	13.80	0.00	0.07	23.47	3.08
sp.gr.-28	714	Unc. *Acetothermia*	0.07	0.07	0.16	0.16	0.11	0.00	0.27	0.26	0.00	1.52
sp.gr.-29	740	Unc. *Candidatus* Falkowbacteria	0.00	0.01	1.15	9.4E-03	0.02	1.13	0.05	0.02	1.08	0.45
sp.gr.-30	741	Unc. *Acetothermia*	0.44	0.63	22.95	1.12	1.17	14.68	2.14	2.41	10.23	0.65
sp.gr.-31	742	Unc. *Acetothermia*	0.07	0.11	0.82	0.18	0.15	1.25	0.36	0.33	0.86	6.95
sp.gr.-32	743	Unc. *Acetothermia*	0.55	0.43	0.82	1.70	1.33	0.88	2.66	1.65	0.54	0.17
sp.gr.-33	744	Unc. *Acetothermia*	0.22	0.14	3.44	0.31	0.15	3.39	0.47	0.58	2.15	1.28
sp.gr.-34	745	Unc. *Acetothermia*	0.41	0.43	2.62	0.97	0.97	2.01	1.59	2.08	2.26	4.31
sp.gr.-35	746	Unc. *Acetothermia*	1.05	0.83	4.10	2.33	2.11	4.14	3.71	4.47	2.69	2.75
sp.gr.-36	747	Unc. *Acetothermia*	0.13	0.27	0.66	0.42	0.53	1.63	0.74	1.12	2.58	0.27
sp.gr.-37	748	Unc. *Acetothermia*	0.35	0.29	0.16	0.49	0.71	0.50	0.82	1.22	0.43	3.95
sp.gr.-38	749	Unc. *Acetothermia*	0.07	0.04	1.48	0.19	0.15	1.38	0.25	0.36	1.51	1.89
sp.gr.-39	750	Unc. *Acetothermia*	0.04	0.01	0.82	0.11	0.04	1.13	0.11	0.08	0.22	16.67
sp.gr.-41	969	*Halothermothrix orenii*	0.00	0.00	0.49	0.00	0.00	0.13	0.00	0.00	0.65	0.99
sp.gr.-44	1131	Unc. *Parcubacteria*	0.00	0.00	2.95	0.00	0.00	1.25	0.00	0.00	1.51	0.61

Species group (sp.gr.) = Species clustered at the genus level, from OPUs with relative abundances ≥ 1% (first column). The species (OPUs; number and affiliation in the second and third columns) belonging to the same genus were grouped into a single "species group", and relative abundances calculated for each OPU and sample are listed in the subsequent columns. Relative abundances of listed genera in Tables A and B (above) are the sum of the relative abundances of grouped OPUs in Table C, for both Archaea and Bacteria.

Supplementary Table S1.5. MAGs recovered from S, U, M and L and their most relevant features. From left to right, the first column indicates the MAG taxonomic domain (Archaea or Bacteria); *ID* indicates the MAG denomination where the first letter indicates the metagenome of origin; *ANI* indicates the average nucleotide identity with the closest genome or MAG and *Geno%* the percentage aligned genome stretches used to calculate the ANI; *AAI* indicates the average amino acid identity with the closest genome or MAG and *Prot.%* the percentage of aligned proteins; *Contigs* indicate the number of assembled contigs that were binned; *GC%* is the G+C mol percentage; *N50*, *N90* and average sequence (*sdep*) depth are basic quality parameters. The last six columns indicate the categories to which each MAG could be identified to. Empty boxes indicate that the category could not be determined. MAGs sharing >96% ANI identity and therefore identified as the same species are shaded in grey. i.h indicates the lack of sufficient hits to calculate ANI or AAI parameters.

	ID	ANI%	Geno%	AAI%	Prot.%	Contigs	GC%	N50	N90	sdep	Domain	Phylum	Class	Order	Family	Genus	Species
Arch	U04	76.7	0.03	58.8	49.1	486	60.7	14,415	1,630	6.5	*Archaea*	*Euryarchaeota*	*Halobacteria*	*Natrialbales*	*Natrialbaceae*	*Salinarchaeum*	
Arch	M04	76.4	0.02	58.9	49.8	421	61.8	18,561	1,644	6.3	*Archaea*	*Euryarchaeota*	*Halobacteria*	*Natrialbales*	*Natrialbaceae*	*Salinarchaeum*	
Arch	L02	77.0	0.03	58.8	49.1	529	59.1	12,772	1,622	11.6	*Archaea*	*Euryarchaeota*	*Halobacteria*	*Natrialbales*	*Natrialbaceae*	*Salinarchaeum*	
Arch	S09	76.2	2.4	59.3	61.1	197	61.6	25,442	4,714	147.4	*Archaea*	*Euryarchaeota*	*Halobacteria*	*Natrialbales*	*Natrialbaceae*	*Salinarchaeum*	
Arch	U01	i.h.	i.h.	43.0	62.0	216	42.6	33,291	4,357	63.0	*Archaea*	*Euryarchaeota*	DHVE2				
Arch	S02	i.h.	i.h.	42.7	61.8	453	43.0	10,972	2,574	31.1	*Archaea*	*Euryarchaeota*	DHVE2				
Arch	S05	i.h.	i.h.	42.4	47.0	431	61.7	5,345	1,363	9.8	*Archaea*	*Euryarchaeota*	DHVE2				
Arch	U05	i.h.	i.h.	42.3	57.0	630	56.8	22,947	1,292	4.1	*Archaea*	*Euryarchaeota*	DHVE2				
Arch	U03	i.h.	i.h.	43.2	62.5	229	47.6	23,547	5,792	13.0	*Archaea*	*Euryarchaeota*	DHVE2				
Arch	M03	i.h.	i.h.	43.2	63.0	278	46.0	28,09	4,887	14.6	*Archaea*	*Euryarchaeota*	DHVE2				
Arch	L03	i.h.	i.h.	43.2	53.4	685	47.8	3,817	1,383	4.0	*Archaea*	*Euryarchaeota*	DHVE2				
Arch	S23	i.h.	i.h.	43.5	53.9	766	48.1	3,117	1,335	14.4	*Archaea*	*Euryarchaeota*	DHVE2				
Arch	M10	68.9	21.7	49.9	62.3	206	44.6	14,959	4,310	7.8	*Archaea*	*Euryarchaeota*	MSBL1				
Arch	U09	68.7	22.9	55.0	46.5	411	44.0	11,224	1,752	5.2	*Archaea*	*Euryarchaeota*	MSBL1				
Arch	S13	67.9	17.2	47.5	63.4	417	43.5	6,757	1,460	9.0	*Archaea*	*Euryarchaeota*	MSBL1				
Bac	M05	90.9	72.7	93.7	75.8	1,226	65.4	3,963	1,532	4.0	*Bacteria*	*Proteobacteria*	*Alphaproteobacteria*	*Rhizobiales*	*Aurantimonadaceae*	*Aureimonas*	
Bac	L06	90.8	71.1	92.4	61.8	1,306	65.1	2,217	1,214	3.2	*Bacteria*	*Proteobacteria*	*Alphaproteobacteria*	*Rhizobiales*	*Aurantimonadaceae*	*Aureimonas*	
Bac	M02	i.h.	i.h.	39.3	36.0	1,392	54.3	6,927	1,463	7.7	*Bacteria*	*Planctomycetes*	*Planctomycetia*				
Bac	L01	i.h.	i.h.	39.3	34.5	903	54.4	9,941	2,235	18.6	*Bacteria*	*Planctomycetes*	*Planctomycetia*				
Bac	M12	63.4	1.6	37.3	38.7	1,385	56.8	1,874	1,122	3.2	*Bacteria*	*Kiritimatiellota*					
Bac	L09	i.h.	i.h.	39.5	44.0	1,600	57.5	3,143	1,210	3.9	*Bacteria*	*Kiritimatiellota*					
Arch	S12	79.3	22.6	74.4	75.2	269	62.7	10,077	3,273	12.7	*Archaea*	*Euryarchaeota*	*Halobacteria*	*Halobacteriales*	*Halobacteriaceae*	*Halodesulfurarchaeum*	*H. formicicum*
Arch	S20	79.3	7.9	68.6	71.0	243	67.3	1,737	1,110	8.8	*Archaea*	*Euryarchaeota*	*Halobacteria*	*Halobacteriales*	*Halobacteriaceae*	*Halodesulfurarchaeum*	*H. formicicum*
Arch	S19	83.7	19.7	73.9	50.5	921	70.5	3,366	1,223	11.2	*Archaea*	*Euryarchaeota*	*Halobacteria*	*Haloferacales*	*Halorubraceae*	*Halorubrum*	*H. lacusprofundi*
Arch	S21	75.0	3.2	58.7	54.0	684	67.3	2,699	1,241	9.1	*Archaea*	*Euryarchaeota*	*Halobacteria*	*Halobacteriales*	*Halobacteriaceae*	*Halomicrobium*	
Arch	S22	75.4	4.0	57.5	54.9	640	68.6	1,897	1,152	8.0	*Archaea*	*Euryarchaeota*	*Halobacteria*	*Halobacteriales*	*Halobacteriaceae*	*Halomicrobium*	
Arch	S32	i.h.	i.h.	54.8	65.6	308	69.5	1,729	1,090	7.8	*Archaea*	*Euryarchaeota*	*Halobacteria*	*Halobacteriales*	*Haloarculaceae*	*Halorientalis*	
Arch	S10	75.8	0.6	56.9	52.4	334	54.5	17,018	2,668	83.2	*Archaea*	*Euryarchaeota*	*Halobacteria*	*Natrialbales*	*Natrialbaceae*	*Salinarchaeum*	
Arch	S01	i.h.	i.h.	57.3	51.1	807	54.1	7,772	1,762	32.5	*Archaea*	*Euryarchaeota*	*Halobacteria*	*Natrialbales*	*Natrialbaceae*	*Salinarchaeum*	

Arch	**S31**	75.7	5.3	56.9	62.3	306	67.5	1,624	1,082	7.7	*Archaea*	*Euryarchaeota*	*Halobacteria*	*Halobacteriales*	*Haloarculaceae*	*Halorientalis*	
Arch	**S30**	83.8	3.3	47.5	29.9	1,259	58.2	2,252	1,153	9.0	*Archaea*	*Euryarchaeota*	*Halobacteria*	*Haloferacales*			
Arch	**U08**	i.h.	i.h.	38.8	45.3	1,177	37.0	1,676	1,090	9.4	*Archaea*	*Euryarchaeota*	DHVE2				
Arch	**M01**	i.h.	i.h.	43.2	49.5	542	39.2	5,611	1,613	8.1	*Archaea*	*Euryarchaeota*	DHVE2				
Arch	**U10**	i.h.	i.h.	39.0	36.3	505	36.0	4,307	1,44	7.8	*Archaea*	*Euryarchaeota*	DHVE2				
Arch	**L04**	i.h.	i.h.	41.4	47.2	1,391	38.0	1,51	1,070	7.5	*Archaea*	*Euryarchaeota*	DHVE2				
Arch	**L08**	i.h.	i.h.	40.0	38.2	339	39.7	2,617	1,204	4.0	*Archaea*	*Euryarchaeota*	DHVE2				
Arch	**S25**	i.h.	i.h.	42.6	51.2	197	46.5	7,561	2,060	11.8	*Archaea*	*Euryarchaeota*	DHVE2				
Arch	**S03**	i.h.	i.h.	42.6	43.7	611	40.1	3,498	1,377	13.1	*Archaea*	*Euryarchaeota*	DHVE2				
Arch	**L07**	i.h.	i.h.	40.3	37.1	342	35.8	6,004	1,678	5.5	*Archaea*	*Euryarchaeota*	DHVE2				
Arch	**U02**	i.h.	i.h.	43.1	51.9	242	42.0	16,889	3,912	17.3	*Archaea*	*Euryarchaeota*	DHVE2				
Arch	**U11**	i.h.	i.h.	40.2	40.1	770	36.1	2,525	1,224	3.8	*Archaea*	*Euryarchaeota*	DHVE2				
Arch	**M07**	i.h.	i.h.	39.6	48.9	1,443	37.8	1,586	1,076	8.6	*Archaea*	*Euryarchaeota*	DHVE2				
Arch	**L10**	i.h.	i.h.	41.7	41.2	451	46.1	2,74	1,267	3.7	*Archaea*	*Euryarchaeota*	DHVE2				
Arch	**S17**	i.h.	i.h.	39.1	34.7	510	43.4	5,504	1,512	10.3	*Archaea*	*Euryarchaeota*	*Archaeoglobi*				
Arch	**M08**	70.2	6.0	43.8	35.2	1,241	49.5	1,43	1,064	6.6	*Archaea*	*Euryarchaeota*	MSBL1				
Arch	**S36**	i.h.	i.h.	40.2	47.0	349	39.3	1,618	1,094	7.3	*Archaea*	*Euryarchaeota*	MSBL1				
Arch	**L05**	68.0	1.0	36.9	42.8	1,029	50.8	1,361	1,051	8.1	*Archaea*	*Euryarchaeota*	MSBL1				
Arch	**U12**	72.1	5.3	40.7	58.9	1,214	45.6	1,423	1,057	7.3	*Archaea*	*Euryarchaeota*	MSBL1				
Arch	**S18**	72.5	5.9	40.4	47.8	649	40.1	3,042	1,230	8.7	*Archaea*	*Euryarchaeota*	MSBL1				
Arch	**U07**	i.h.	i.h.	37.6	50.5	1,870	33.0	2,283	1,131	3.6	*Archaea*	*Euryarchaeota*	*Methanomicrobia*				
Arch	**U06**	i.h.	i.h.	39.7	39.5	380	46.3	3,948	1,532	4.7	*Archaea*	*Euryarchaeota*	*Methanobacteria*				
Arch	**S34**	i.h.	i.h.	39.3	31.9	756	37.2	1,834	1,124	6.7	*Archaea*	*Euryarchaeota*	*Thermococci*				
Arch	**S08**	i.h.	i.h.	40.6	57.7	178	41.0	1,825	1,114	7.2	*Archaea*	*Euryarchaeota*	*Thermococci*				
Arch	**M06**	i.h.	i.h.	40.5	47.1	1,933	33.2	2,063	1,125	3.3	*Archaea*	*Euryarchaeota*	*Thermococci*				
Arch	**S35**	i.h.	i.h.	38.6	57.9	168	40.4	2,050	1,231	7.1	*Archaea*	*Euryarchaeota*	*Thermococci*				
Arch	**S28**	63.3	1.6	36.5	36.1	704	37.2	2,560	1,196	9.7	*Archaea*	*Euryarchaeota*	*Thermoplasmata*				
Arch	**S06**	i.h.	i.h.	38.8	33.9	1,920	49.0	2,189	1,133	8.9	*Archaea*	*Euryarchaeota*					
Arch	**S33**	i.h.	i.h.	37.8	35.7	889	39.5	1,968	1,119	7.4	*Archaea*	*Euryarchaeota*					
Arch	**M11**	i.h.	i.h.	37.1	37.5	1,123	40.3	1,674	1,100	3.1	*Archaea*						
Bac	**S16**	81.1	33.4	76.5	71.1	354	70.6	10,504	1,861	14.0	*Bacteria*	*Proteobacteria*	*Gammaproteobacteria*	*Chromatiales*	*Ectothiorhodospiraceae*	*Halorhodospira*	
Bac	**S24**	98.8	54.4	92.6	64.2	1,427	66.2	2,111	1,143	13.2	*Bacteria*	*Bacteroidetes*	*Rhodothermia*	*Rhodothermales*	*Salinibacteraceae*	*Salinibacter*	
Bac	**S04**	73.9	0.6	46.4	39.7	1,146	60.7	3,136	1,227	9.7	*Bacteria*	*Proteobacteria*	*Deltaproteobacteria*				
Bac	**S07**	i.h.	i.h.	37.7	36.0	2,322	42.1	1,792	1,103	7.9	*Bacteria*	*Proteobacteria*	*Deltaproteobacteria*				
Bac	**S29**	61.7	1.7	39.2	34.4	949	50.0	2,064	1,133	7.9	*Bacteria*	*Firmicutes*	*Clostridia*				
Bac	**S14**	i.h.	i.h.	38.6	48.0	658	49.4	6,044	1,595	52.3	*Bacteria*	*Thermotogae*	*Thermotogae*				
Bac	**S15**	i.h.	i.h.	38.9	41.8	651	49.5	3,880	1,449	27.2	*Bacteria*	*Thermotogae*	*Thermotogae*				
Bac	**S11**	i.h.	i.h.	39.2	44.9	541	47.9	4,200	1,539	14.0	*Bacteria*	*Thermotogae*	*Thermotogae*				
Bac	**S27**	i.h.	i.h.	34.7	31.6	380	35.3	3,655	1,297	11.7	*Bacteria*	*Thermotogae*					
Bac	**S26**	59.8	0.3	34.2	42.2	226	45.3	5,617	1,532	11.2	*Bacteria*	*Thermotogae*					
Bac	**M09**	63.3	1.0	34.0	32.0	442	36.0	6,846	1,913	6.6	*Bacteria*						

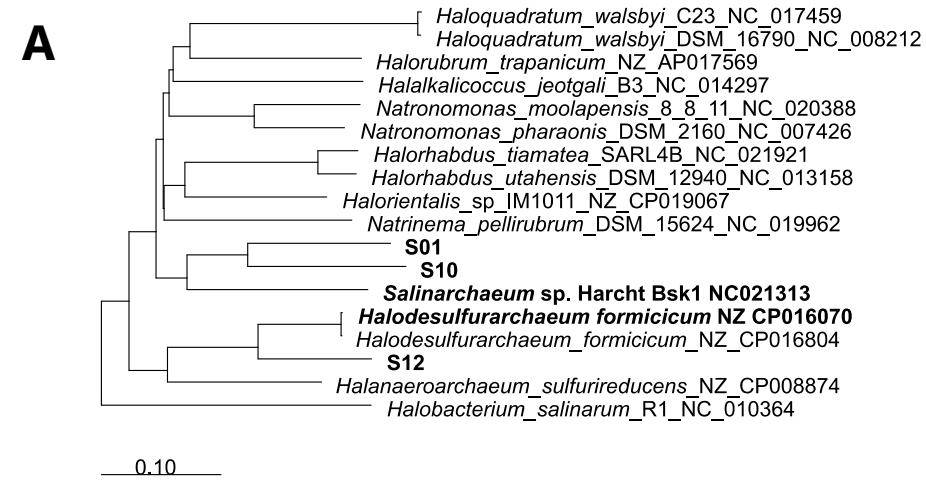
A
Haloquadratum_walsbyi_C23_NC_017459
Haloquadratum_walsbyi_DSM_16790_NC_008212
Halorubrum_trapanicum_NZ_AP017569
Halalkalicoccus_jeotgali_B3_NC_014297
Natronomonas_moolapensis_8_8_11_NC_020388
Natronomonas_pharaonis_DSM_2160_NC_007426
Halorhabdus_tiamatea_SARL4B_NC_021921
Halorhabdus_utahensis_DSM_12940_NC_013158
Halorientalis_sp_IM1011_NZ_CP019067
Natrinema_pellirubrum_DSM_15624_NC_019962
S01
S10
Salinarchaeum sp. Harcht Bsk1 NC021313
Halodesulfurarchaeum formicicum NZ CP016070
Halodesulfurarchaeum_formicicum_NZ_CP016804
S12
Halanaeroarchaeum_sulfurireducens_NZ_CP008874
Halobacterium_salinarum_R1_NC_010364
0.10

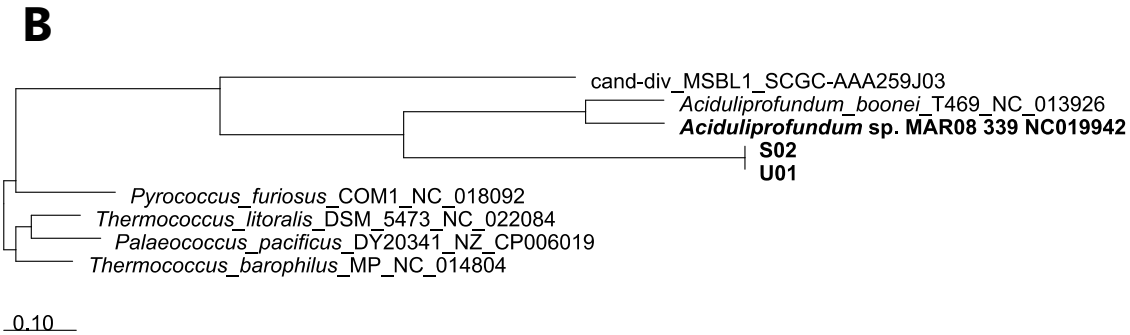
B
cand-div_MSBL1_SCGC-AAA259J03
Aciduliprofundum_boonei_T469_NC_013926
Aciduliprofundum sp. MAR08 339 NC019942
S02
U01
Pyrococcus_furiosus_COM1_NC_018092
Thermococcus_litoralis_DSM_5473_NC_022084
Palaeococcus_pacificus_DY20341_NZ_CP006019
Thermococcus_barophilus_MP_NC_014804
0.10

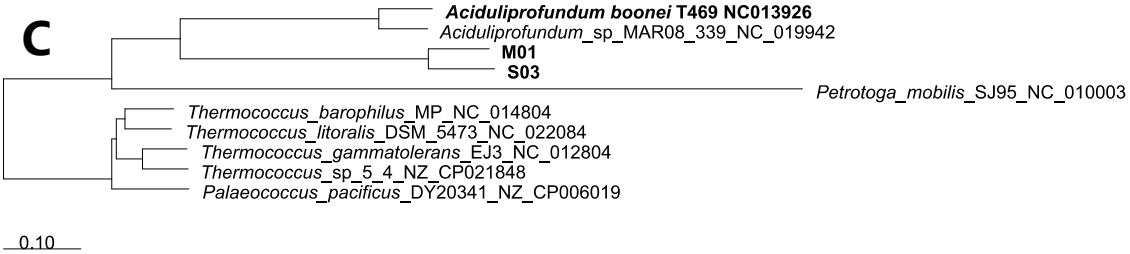
C
Aciduliprofundum boonei T469 NC013926
Aciduliprofundum_sp_MAR08_339_NC_019942
M01
S03
Petrotoga_mobilis_SJ95_NC_010003
Thermococcus_barophilus_MP_NC_014804
Thermococcus_litoralis_DSM_5473_NC_022084
Thermococcus_gammatolerans_EJ3_NC_012804
Thermococcus_sp_5_4_NZ_CP021848
Palaeococcus_pacificus_DY20341_NZ_CP006019
0.10

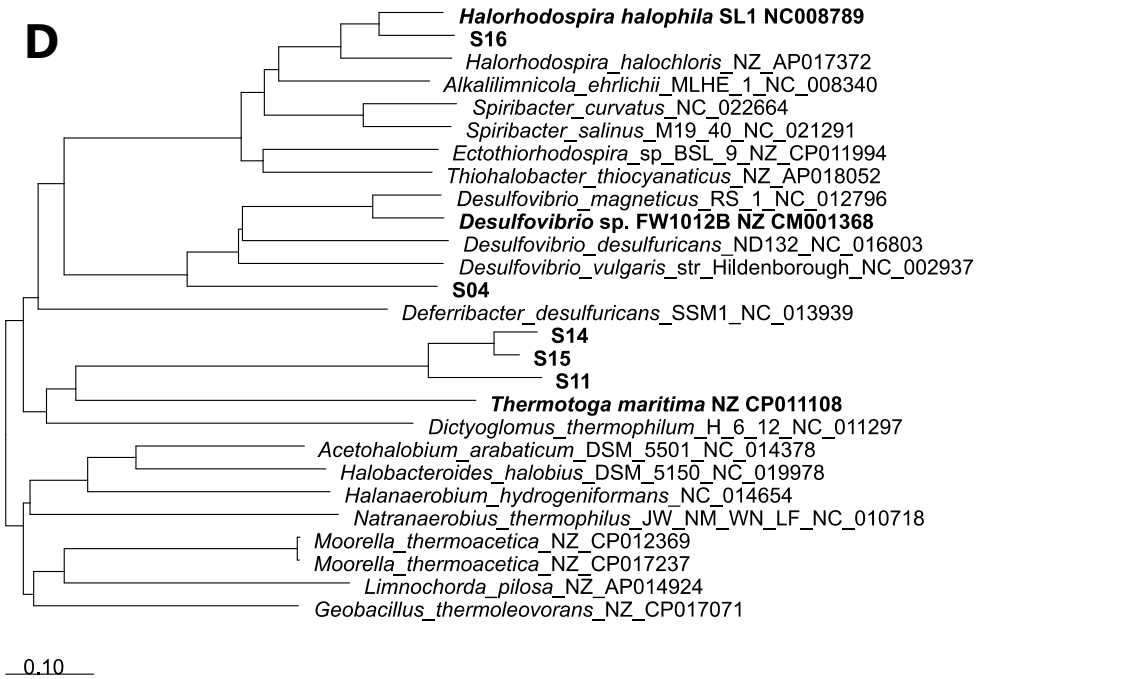
D
Halorhodospira halophila SL1 NC008789
S16
Halorhodospira_halochloris_NZ_AP017372
Alkalilimnicola_ehrlichii_MLHE_1_NC_008340
Spiribacter_curvatus_NC_022664
Spiribacter_salinus_M19_40_NC_021291
Ectothiorhodospira_sp_BSL_9_NZ_CP011994
Thiohalobacter_thiocyanaticus_NZ_AP018052
Desulfovibrio_magneticus_RS_1_NC_012796
Desulfovibrio sp. FW1012B NZ CM001368
Desulfovibrio_desulfuricans_ND132_NC_016803
Desulfovibrio_vulgaris_str_Hildenborough_NC_002937
S04
Deferribacter_desulfuricans_SSM1_NC_013939
S14
S15
S11
Thermotoga maritima NZ CP011108
Dictyoglomus_thermophilum_H_6_12_NC_011297
Acetohalobium_arabaticum_DSM_5501_NC_014378
Halobacteroides_halobius_DSM_5150_NC_019978
Halanaerobium_hydrogeniformans_NC_014654
Natranaerobius_thermophilus_JW_NM_WN_LF_NC_010718
Moorella_thermoacetica_NZ_CP012369
Moorella_thermoacetica_NZ_CP017237
Limnochorda_pilosa_NZ_AP014924
Geobacillus_thermoleovorans_NZ_CP017071
0.10

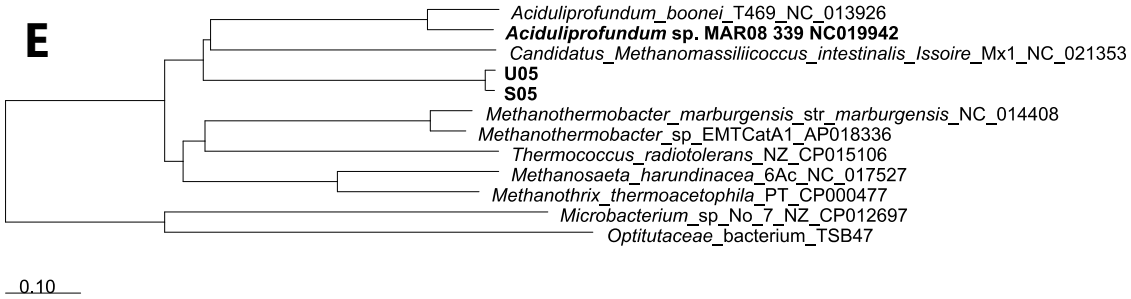
E
Aciduliprofundum_boonei_T469_NC_013926
Aciduliprofundum sp. MAR08 339 NC019942
Candidatus_Methanomassiliicoccus_intestinalis_Issoire_Mx1_NC_021353
U05
S05
Methanothermobacter_marburgensis_str_marburgensis_NC_014408
Methanothermobacter_sp_EMTCatA1_AP018336
Thermococcus_radiotolerans_NZ_CP015106
Methanosaeta_harundinacea_6Ac_NC_017527
Methanothrix_thermoacetophila_PT_CP000477
Microbacterium_sp_No_7_NZ_CP012697
Optitutaceae_bacterium_TSB47
0.10

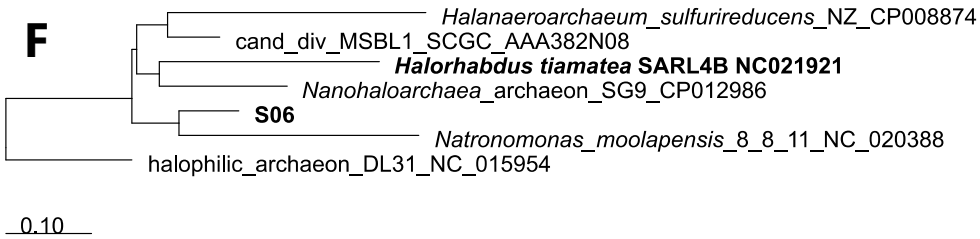
F
Halanaeroarchaeum_sulfurireducens_NZ_CP008874
cand_div_MSBL1_SCGC_AAA382N08
Halorhabdus tiamatea SARL4B NC021921
Nanohaloarchaea_archaeon_SG9_CP012986
S06
Natronomonas_moolapensis_8_8_11_NC_020388
halophilic_archaeon_DL31_NC_015954
0.10

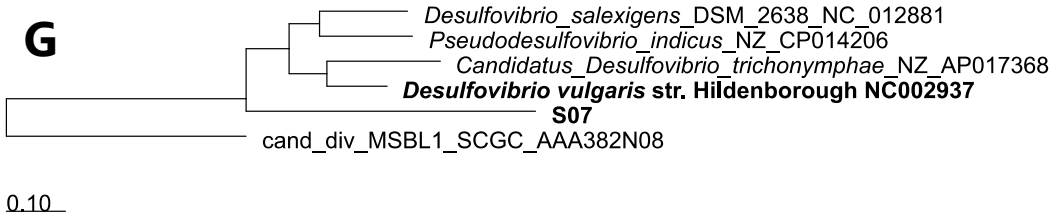
G
Desulfovibrio_salexigens_DSM_2638_NC_012881
Pseudodesulfovibrio_indicus_NZ_CP014206
Candidatus_Desulfovibrio_trichonymphae_NZ_AP017368
Desulfovibrio vulgaris str. Hildenborough NC002937
S07
cand_div_MSBL1_SCGC_AAA382N08
0.10

H

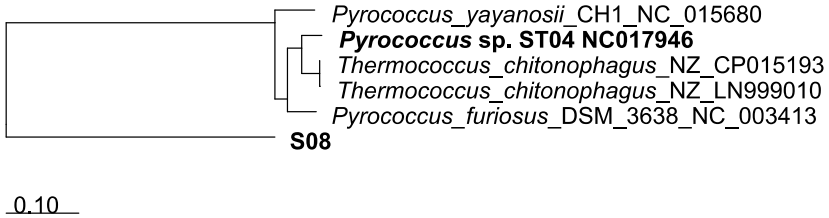
Pyrococcus_yayanosii_CH1_NC_015680
Pyrococcus sp. ST04 NC017946
Thermococcus_chitonophagus_NZ_CP015193
Thermococcus_chitonophagus_NZ_LN999010
Pyrococcus_furiosus_DSM_3638_NC_003413
S08
0.10

I

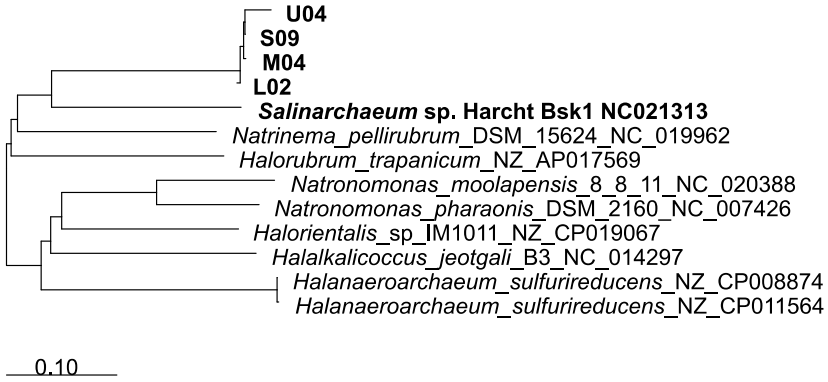
U04
S09
M04
L02
Salinarchaeum sp. Harcht Bsk1 NC021313
Natrinema_pellirubrum_DSM_15624_NC_019962
Halorubrum_trapanicum_NZ_AP017569
Natronomonas_moolapensis_8_8_11_NC_020388
Natronomonas_pharaonis_DSM_2160_NC_007426
Halorientalis_sp_IM1011_NZ_CP019067
Halalkalicoccus_jeotgali_B3_NC_014297
Halanaeroarchaeum_sulfurireducens_NZ_CP008874
Halanaeroarchaeum_sulfurireducens_NZ_CP011564
0.10

J

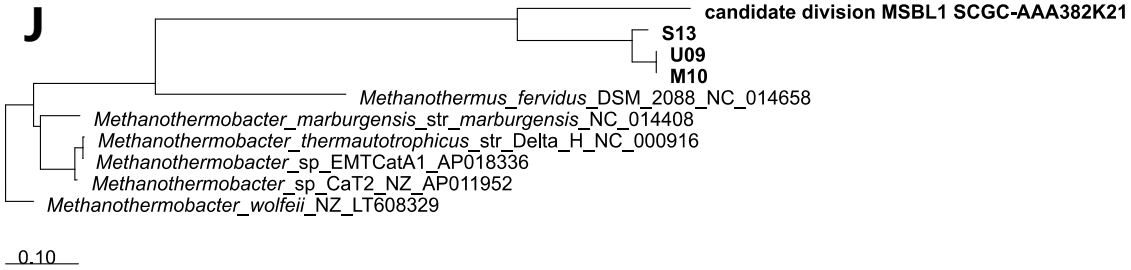
candidate division MSBL1 SCGC-AAA382K21
S13
U09
M10
Methanothermus_fervidus_DSM_2088_NC_014658
Methanothermobacter_marburgensis_str_marburgensis_NC_014408
Methanothermobacter_thermautotrophicus_str_Delta_H_NC_000916
Methanothermobacter_sp_EMTCatA1_AP018336
Methanothermobacter_sp_CaT2_NZ_AP011952
Methanothermobacter_wolfeii_NZ_LT608329
0.10

K

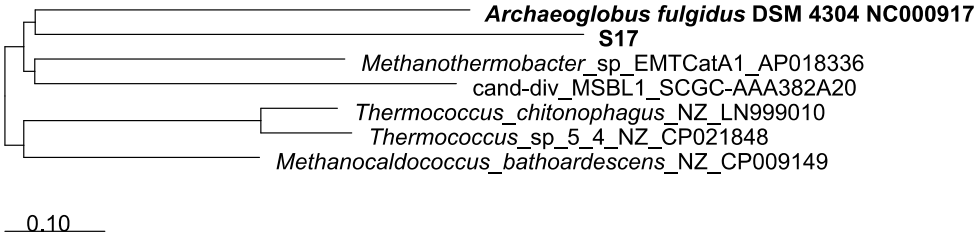
Archaeoglobus fulgidus DSM 4304 NC000917
S17
Methanothermobacter_sp_EMTCatA1_AP018336
cand-div_MSBL1_SCGC-AAA382A20
Thermococcus_chitonophagus_NZ_LN999010
Thermococcus_sp_5_4_NZ_CP021848
Methanocaldococcus_bathoardescens_NZ_CP009149
0.10

L

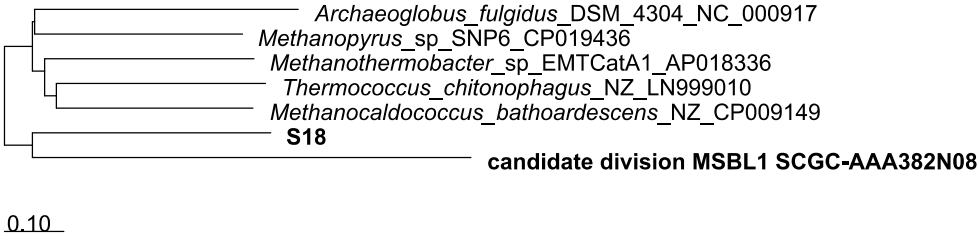
Archaeoglobus_fulgidus_DSM_4304_NC_000917
Methanopyrus_sp_SNP6_CP019436
Methanothermobacter_sp_EMTCatA1_AP018336
Thermococcus_chitonophagus_NZ_LN999010
Methanocaldococcus_bathoardescens_NZ_CP009149
S18
candidate division MSBL1 SCGC-AAA382N08
0.10

M

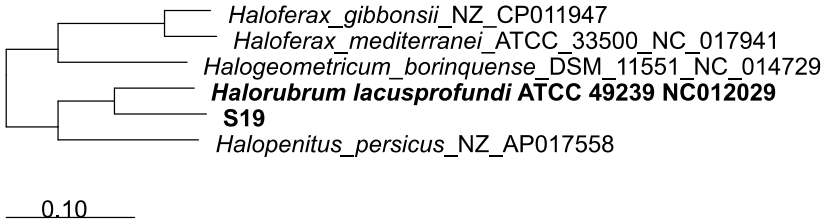
Haloferax_gibbonsii_NZ_CP011947
Haloferax_mediterranei_ATCC_33500_NC_017941
Halogeometricum_borinquense_DSM_11551_NC_014729
Halorubrum lacusprofundi ATCC 49239 NC012029
S19
Halopenitus_persicus_NZ_AP017558
0.10

N

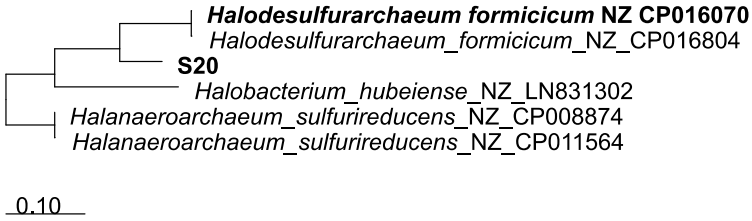
Halodesulfurarchaeum formicicum NZ CP016070
Halodesulfurarchaeum_formicicum_NZ_CP016804
S20
Halobacterium_hubeiense_NZ_LN831302
Halanaeroarchaeum_sulfurireducens_NZ_CP008874
Halanaeroarchaeum_sulfurireducens_NZ_CP011564
0.10

O

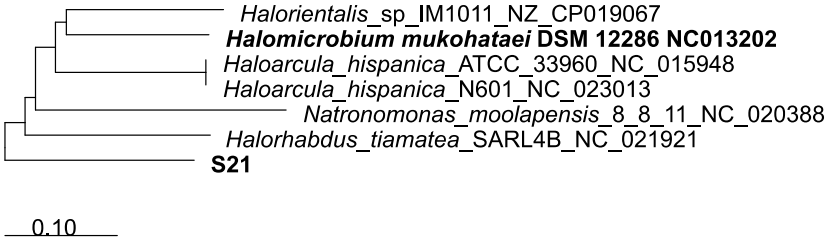
Halorientalis_sp_IM1011_NZ_CP019067
Halomicrobium mukohataei DSM 12286 NC013202
Haloarcula_hispanica_ATCC_33960_NC_015948
Haloarcula_hispanica_N601_NC_023013
Natronomonas_moolapensis_8_8_11_NC_020388
Halorhabdus_tiamatea_SARL4B_NC_021921
S21
0.10

P

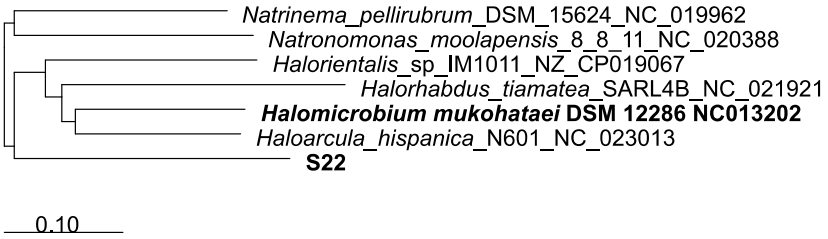
Natrinema_pellirubrum_DSM_15624_NC_019962
Natronomonas_moolapensis_8_8_11_NC_020388
Halorientalis_sp_IM1011_NZ_CP019067
Halorhabdus_tiamatea_SARL4B_NC_021921
Halomicrobium mukohataei DSM 12286 NC013202
Haloarcula_hispanica_N601_NC_023013
S22
0.10

Q

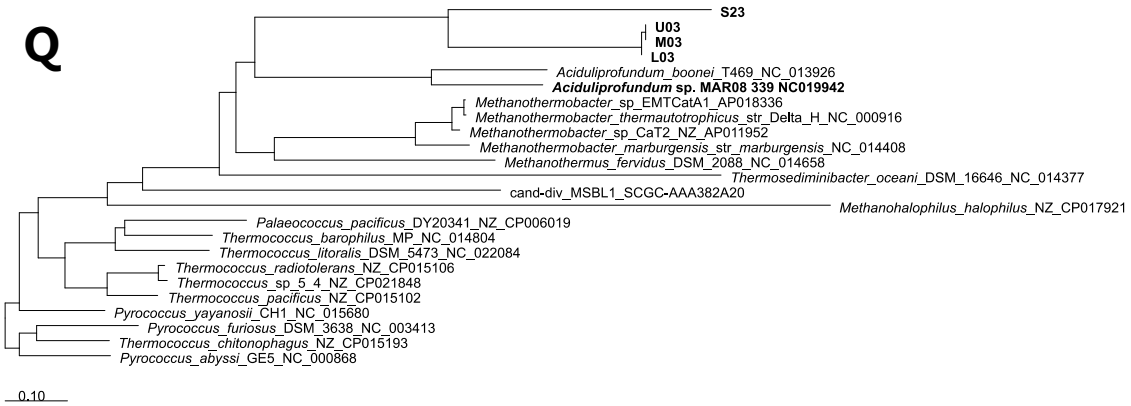
S23
U03
M03
L03
Aciduliprofundum_boonei_T469_NC_013926
Aciduliprofundum sp. MAR08 339 NC019942
Methanothermobacter_sp_EMTCatA1_AP018336
Methanothermobacter_thermautotrophicus_str_Delta_H_NC_000916
Methanothermobacter_sp_CaT2_NZ_AP011952
Methanothermobacter_marburgensis_str_marburgensis_NC_014408
Methanothermus_fervidus_DSM_2088_NC_014658
Thermosediminibacter_oceani_DSM_16646_NC_014377
cand-div_MSBL1_SCGC-AAA382A20
Methanohalophilus_halophilus_NZ_CP017921
Palaeococcus_pacificus_DY20341_NZ_CP006019
Thermococcus_barophilus_MP_NC_014804
Thermococcus_litoralis_DSM_5473_NC_022084
Thermococcus_radiotolerans_NZ_CP015106
Thermococcus_sp_5_4_NZ_CP021848
Thermococcus_pacificus_NZ_CP015102
Pyrococcus_yayanosii_CH1_NC_015680
Pyrococcus_furiosus_DSM_3638_NC_003413
Thermococcus_chitonophagus_NZ_CP015193
Pyrococcus_abyssi_GE5_NC_000868
0.10

R

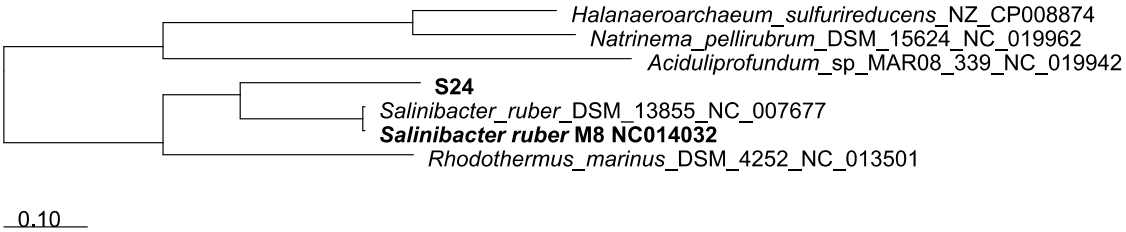
Halanaeroarchaeum_sulfurireducens_NZ_CP008874
Natrinema_pellirubrum_DSM_15624_NC_019962
Aciduliprofundum_sp_MAR08_339_NC_019942
S24
Salinibacter_ruber_DSM_13855_NC_007677
Salinibacter ruber M8 NC014032
Rhodothermus_marinus_DSM_4252_NC_013501
0.10

S

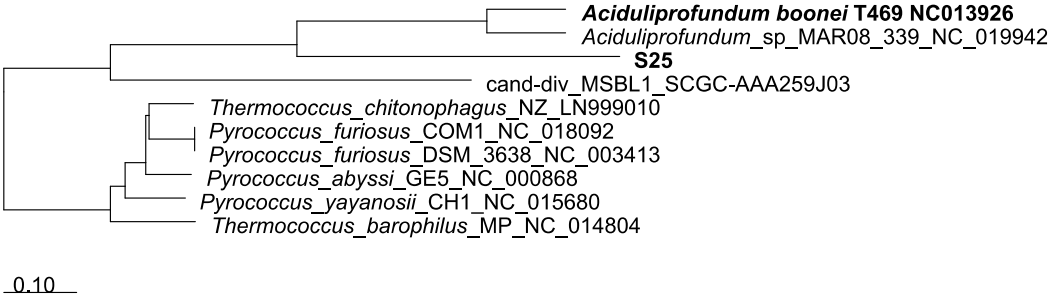
Aciduliprofundum boonei T469 NC013926
Aciduliprofundum_sp_MAR08_339_NC_019942
S25
cand-div_MSBL1_SCGC-AAA259J03
Thermococcus_chitonophagus_NZ_LN999010
Pyrococcus_furiosus_COM1_NC_018092
Pyrococcus_furiosus_DSM_3638_NC_003413
Pyrococcus_abyssi_GE5_NC_000868
Pyrococcus_yayanosii_CH1_NC_015680
Thermococcus_barophilus_MP_NC_014804
0.10

T

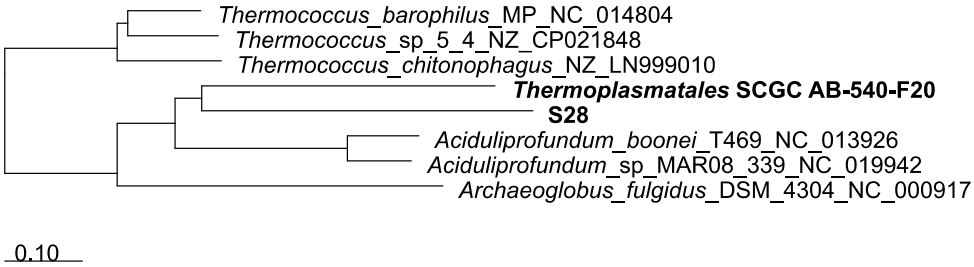
Thermococcus_barophilus_MP_NC_014804
Thermococcus_sp_5_4_NZ_CP021848
Thermococcus_chitonophagus_NZ_LN999010
Thermoplasmatales SCGC AB-540-F20
S28
Aciduliprofundum_boonei_T469_NC_013926
Aciduliprofundum_sp_MAR08_339_NC_019942
Archaeoglobus_fulgidus_DSM_4304_NC_000917
0.10

U

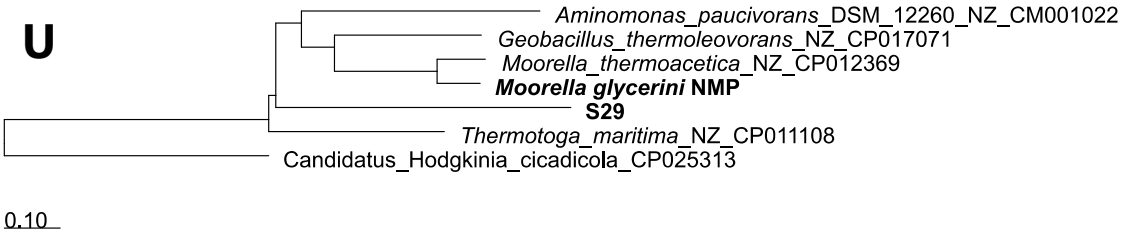
Aminomonas_paucivorans_DSM_12260_NZ_CM001022
Geobacillus_thermoleovorans_NZ_CP017071
Moorella_thermoacetica_NZ_CP012369
Moorella glycerini NMP
S29
Thermotoga_maritima_NZ_CP011108
Candidatus_Hodgkinia_cicadicola_CP025313
0.10

V

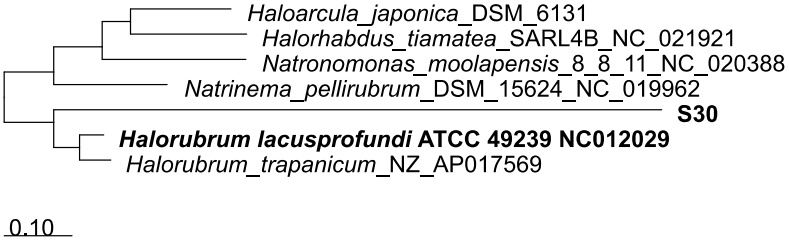
Haloarcula_japonica_DSM_6131
Halorhabdus_tiamatea_SARL4B_NC_021921
Natronomonas_moolapensis_8_8_11_NC_020388
Natrinema_pellirubrum_DSM_15624_NC_019962
S30
Halorubrum lacusprofundi ATCC 49239 NC012029
Halorubrum_trapanicum_NZ_AP017569
0.10

W

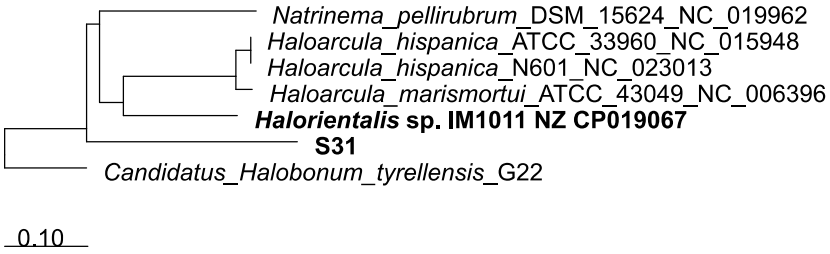
Natrinema_pellirubrum_DSM_15624_NC_019962
Haloarcula_hispanica_ATCC_33960_NC_015948
Haloarcula_hispanica_N601_NC_023013
Haloarcula_marismortui_ATCC_43049_NC_006396
Halorientalis sp. IM1011 NZ CP019067
S31
Candidatus_Halobonum_tyrellensis_G22
0.10

X

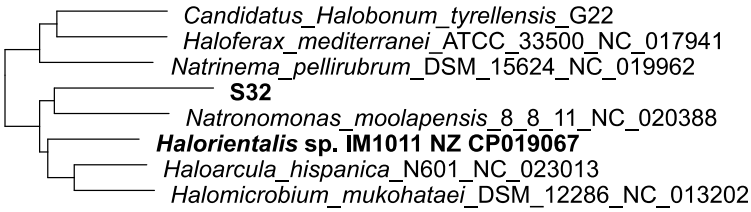
Candidatus_Halobonum_tyrellensis_G22
Haloferax_mediterranei_ATCC_33500_NC_017941
Natrinema_pellirubrum_DSM_15624_NC_019962
S32
Natronomonas_moolapensis_8_8_11_NC_020388
Halorientalis sp. IM1011 NZ CP019067
Haloarcula_hispanica_N601_NC_023013
Halomicrobium_mukohataei_DSM_12286_NC_013202
0.10

Y

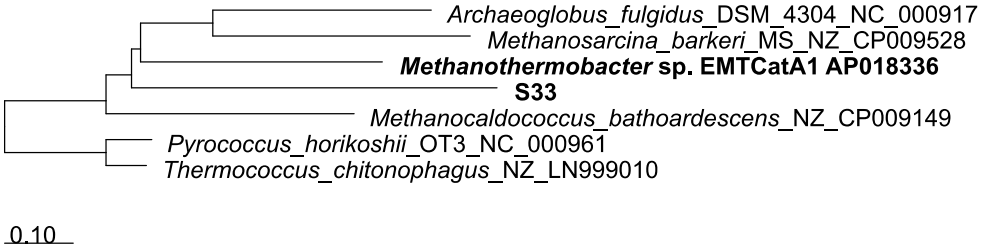
Archaeoglobus_fulgidus_DSM_4304_NC_000917
Methanosarcina_barkeri_MS_NZ_CP009528
Methanothermobacter sp. EMTCatA1 AP018336
S33
Methanocaldococcus_bathoardescens_NZ_CP009149
Pyrococcus_horikoshii_OT3_NC_000961
Thermococcus_chitonophagus_NZ_LN999010
0.10

Z

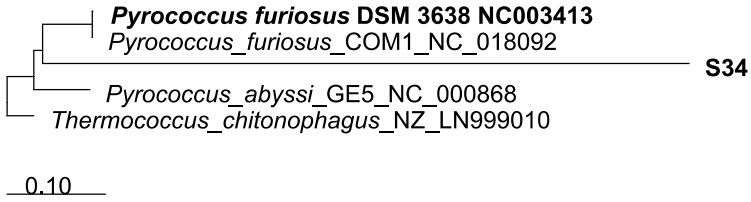
Pyrococcus furiosus DSM 3638 NC003413
Pyrococcus_furiosus_COM1_NC_018092
S34
Pyrococcus_abyssi_GE5_NC_000868
Thermococcus_chitonophagus_NZ_LN999010
0.10

AA

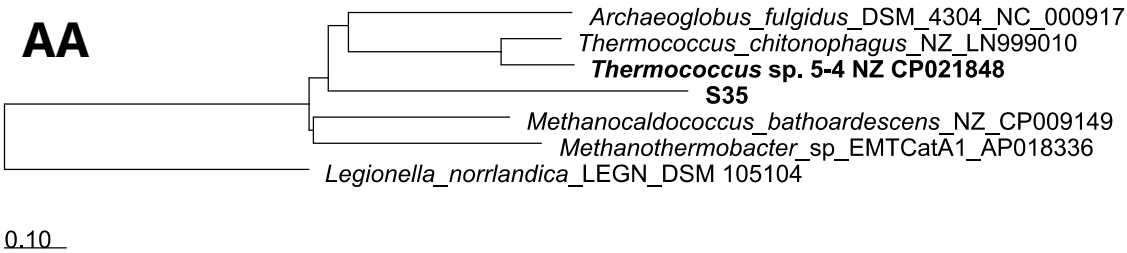
Archaeoglobus_fulgidus_DSM_4304_NC_000917
Thermococcus_chitonophagus_NZ_LN999010
Thermococcus sp. 5-4 NZ CP021848
S35
Methanocaldococcus_bathoardescens_NZ_CP009149
Methanothermobacter_sp_EMTCatA1_AP018336
Legionella_norrlandica_LEGN_DSM 105104
0.10

AB

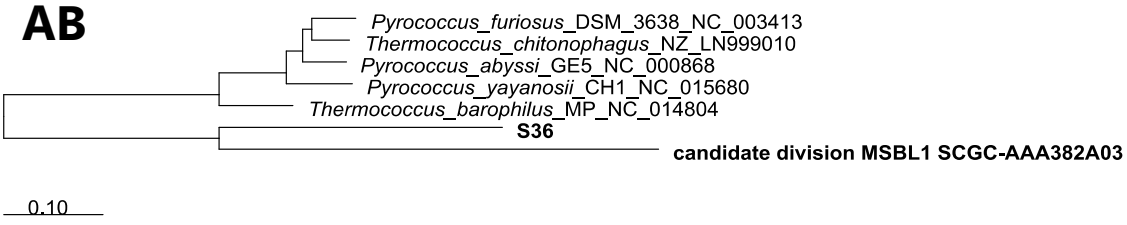
Pyrococcus_furiosus_DSM_3638_NC_003413
Thermococcus_chitonophagus_NZ_LN999010
Pyrococcus_abyssi_GE5_NC_000868
Pyrococcus_yayanosii_CH1_NC_015680
Thermococcus_barophilus_MP_NC_014804
S36
candidate division MSBL1 SCGC-AAA382A03
0.10

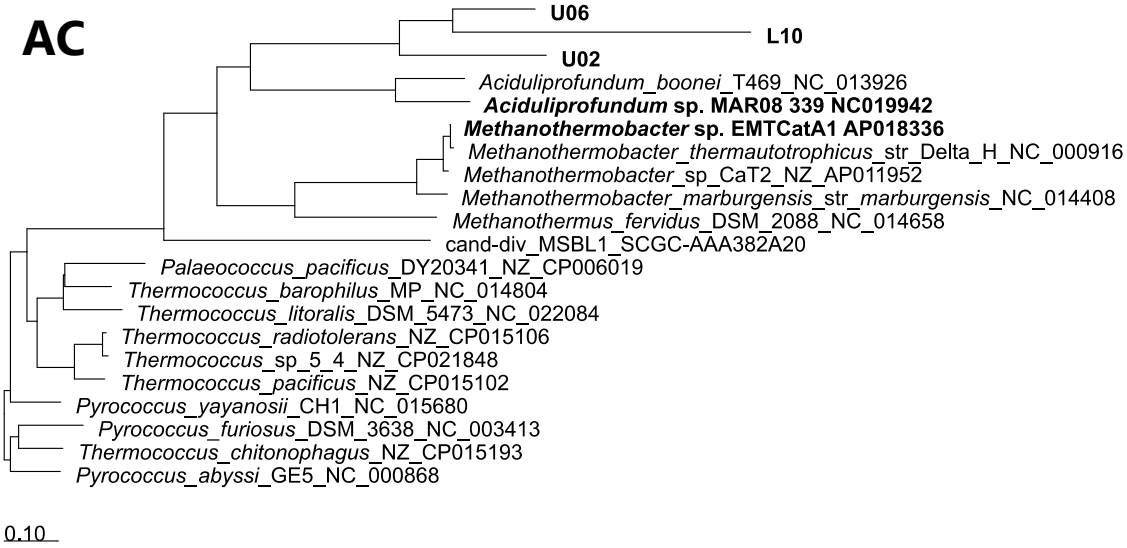
AC
U06
L10
U02
Aciduliprofundum_boonei_T469_NC_013926
Aciduliprofundum sp. MAR08 339 NC019942
Methanothermobacter sp. EMTCatA1 AP018336
Methanothermobacter_thermautotrophicus_str_Delta_H_NC_000916
Methanothermobacter_sp_CaT2_NZ_AP011952
Methanothermobacter_marburgensis_str_marburgensis_NC_014408
Methanothermus_fervidus_DSM_2088_NC_014658
cand-div_MSBL1_SCGC-AAA382A20
Palaeococcus_pacificus_DY20341_NZ_CP006019
Thermococcus_barophilus_MP_NC_014804
Thermococcus_litoralis_DSM_5473_NC_022084
Thermococcus_radiotolerans_NZ_CP015106
Thermococcus_sp_5_4_NZ_CP021848
Thermococcus_pacificus_NZ_CP015102
Pyrococcus_yayanosii_CH1_NC_015680
Pyrococcus_furiosus_DSM_3638_NC_003413
Thermococcus_chitonophagus_NZ_CP015193
Pyrococcus_abyssi_GE5_NC_000868
0.10

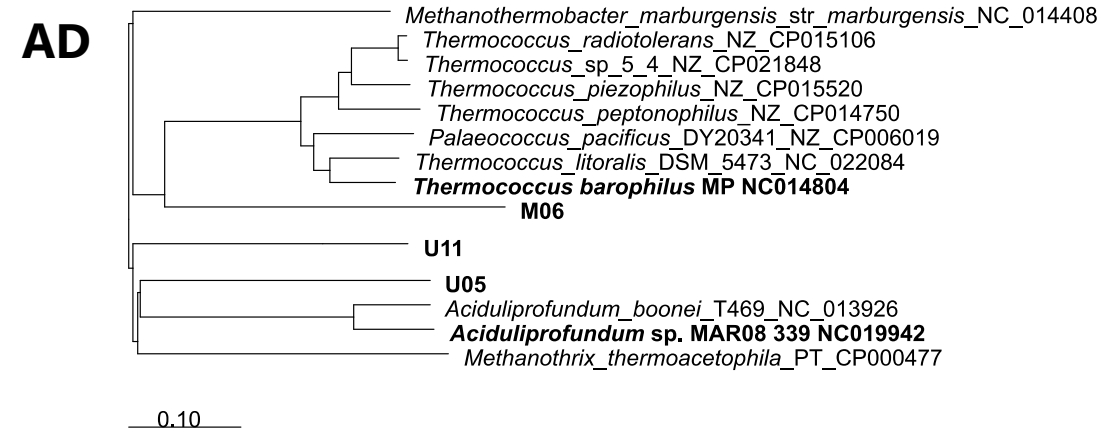
AD
Methanothermobacter_marburgensis_str_marburgensis_NC_014408
Thermococcus_radiotolerans_NZ_CP015106
Thermococcus_sp_5_4_NZ_CP021848
Thermococcus_piezophilus_NZ_CP015520
Thermococcus_peptonophilus_NZ_CP014750
Palaeococcus_pacificus_DY20341_NZ_CP006019
Thermococcus_litoralis_DSM_5473_NC_022084
Thermococcus barophilus MP NC014804
M06
U11
U05
Aciduliprofundum_boonei_T469_NC_013926
Aciduliprofundum sp. MAR08 339 NC019942
Methanothrix_thermoacetophila_PT_CP000477
0.10

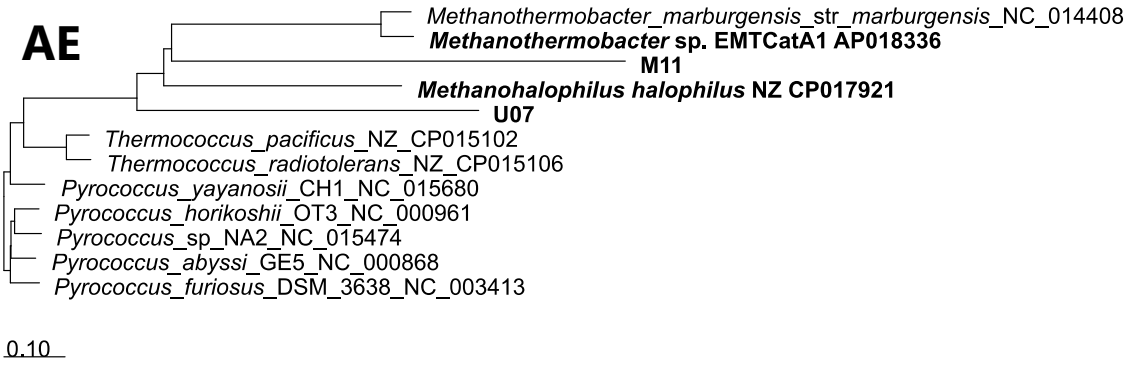
AE
Methanothermobacter_marburgensis_str_marburgensis_NC_014408
Methanothermobacter sp. EMTCatA1 AP018336
M11
Methanohalophilus halophilus NZ CP017921
U07
Thermococcus_pacificus_NZ_CP015102
Thermococcus_radiotolerans_NZ_CP015106
Pyrococcus_yayanosii_CH1_NC_015680
Pyrococcus_horikoshii_OT3_NC_000961
Pyrococcus_sp_NA2_NC_015474
Pyrococcus_abyssi_GE5_NC_000868
Pyrococcus_furiosus_DSM_3638_NC_003413
0.10

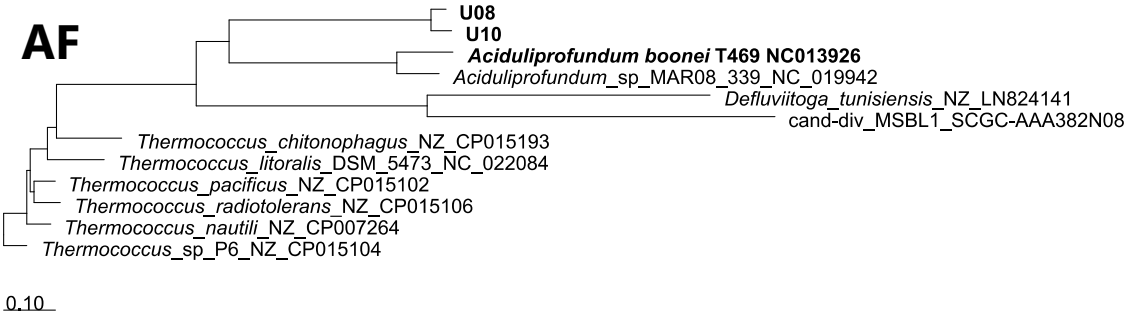
AF
U08
U10
Aciduliprofundum boonei T469 NC013926
Aciduliprofundum_sp_MAR08_339_NC_019942
Defluviitoga_tunisiensis_NZ_LN824141
cand-div_MSBL1_SCGC-AAA382N08
Thermococcus_chitonophagus_NZ_CP015193
Thermococcus_litoralis_DSM_5473_NC_022084
Thermococcus_pacificus_NZ_CP015102
Thermococcus_radiotolerans_NZ_CP015106
Thermococcus_nautili_NZ_CP007264
Thermococcus_sp_P6_NZ_CP015104
0.10

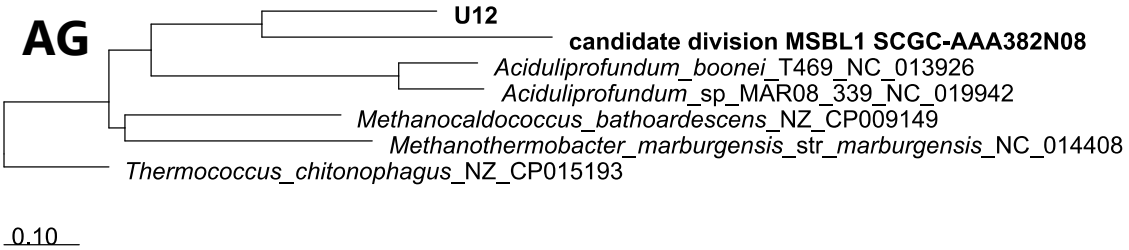
AG
U12
candidate division MSBL1 SCGC-AAA382N08
Aciduliprofundum_boonei_T469_NC_013926
Aciduliprofundum_sp_MAR08_339_NC_019942
Methanocaldococcus_bathoardescens_NZ_CP009149
Methanothermobacter_marburgensis_str_marburgensis_NC_014408
Thermococcus_chitonophagus_NZ_CP015193
0.10

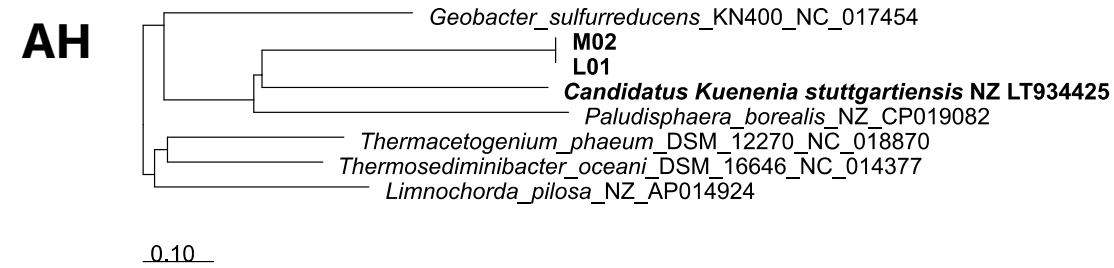
AH
Geobacter_sulfurreducens_KN400_NC_017454
M02
L01
Candidatus Kuenenia stuttgartiensis NZ LT934425
Paludisphaera_borealis_NZ_CP019082
Thermacetogenium_phaeum_DSM_12270_NC_018870
Thermosediminibacter_oceani_DSM_16646_NC_014377
Limnochorda_pilosa_NZ_AP014924
0.10

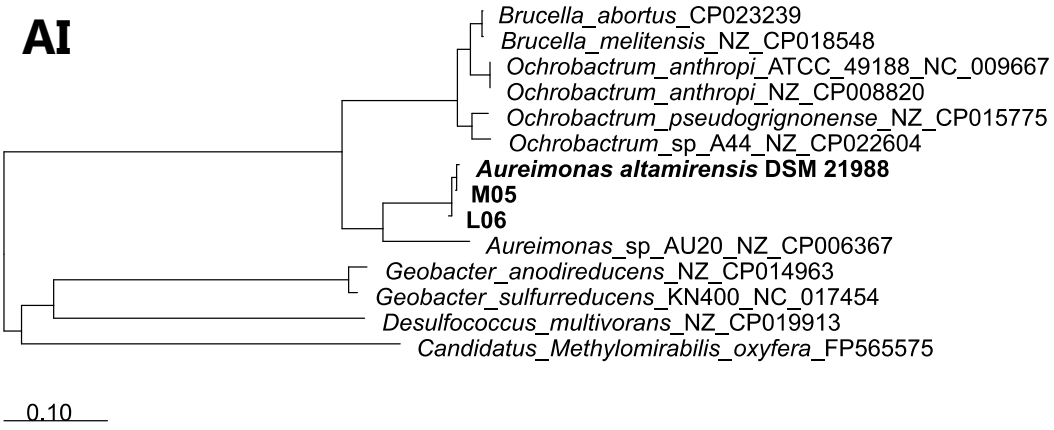
AI
Brucella_abortus_CP023239
Brucella_melitensis_NZ_CP018548
Ochrobactrum_anthropi_ATCC_49188_NC_009667
Ochrobactrum_anthropi_NZ_CP008820
Ochrobactrum_pseudogrignonense_NZ_CP015775
Ochrobactrum_sp_A44_NZ_CP022604
Aureimonas altamirensis DSM 21988
M05
L06
Aureimonas_sp_AU20_NZ_CP006367
Geobacter_anodireducens_NZ_CP014963
Geobacter_sulfurreducens_KN400_NC_017454
Desulfococcus_multivorans_NZ_CP019913
Candidatus_Methylomirabilis_oxyfera_FP565575
0.10

AJ

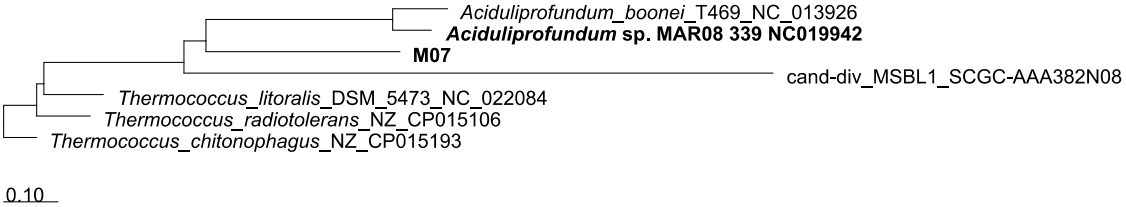
*Aciduliprofundum_boonei*_T469_NC_013926
***Aciduliprofundum* sp. MAR08 339 NC019942**
M07
cand-div_MSBL1_SCGC-AAA382N08
*Thermococcus_litoralis*_DSM_5473_NC_022084
*Thermococcus_radiotolerans*_NZ_CP015106
*Thermococcus_chitonophagus*_NZ_CP015193
0.10

AK

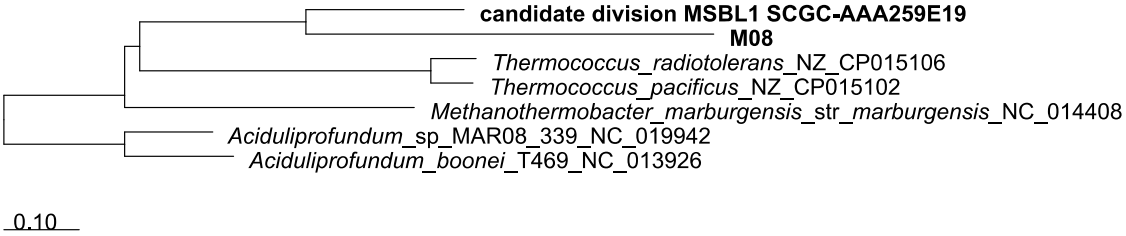
candidate division MSBL1 SCGC-AAA259E19
M08
*Thermococcus_radiotolerans*_NZ_CP015106
*Thermococcus_pacificus*_NZ_CP015102
*Methanothermobacter_marburgensis*_str_*marburgensis*_NC_014408
*Aciduliprofundum*_sp_MAR08_339_NC_019942
*Aciduliprofundum_boonei*_T469_NC_013926
0.10

AL

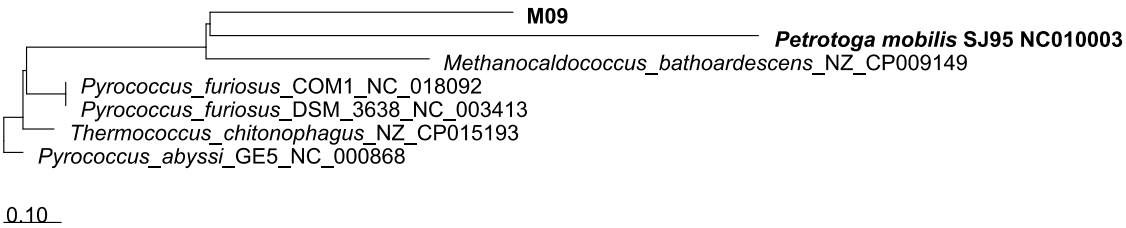
M09
***Petrotoga mobilis* SJ95 NC010003**
*Methanocaldococcus_bathoardescens*_NZ_CP009149
*Pyrococcus_furiosus*_COM1_NC_018092
*Pyrococcus_furiosus*_DSM_3638_NC_003413
*Thermococcus_chitonophagus*_NZ_CP015193
*Pyrococcus_abyssi*_GE5_NC_000868
0.10

AM

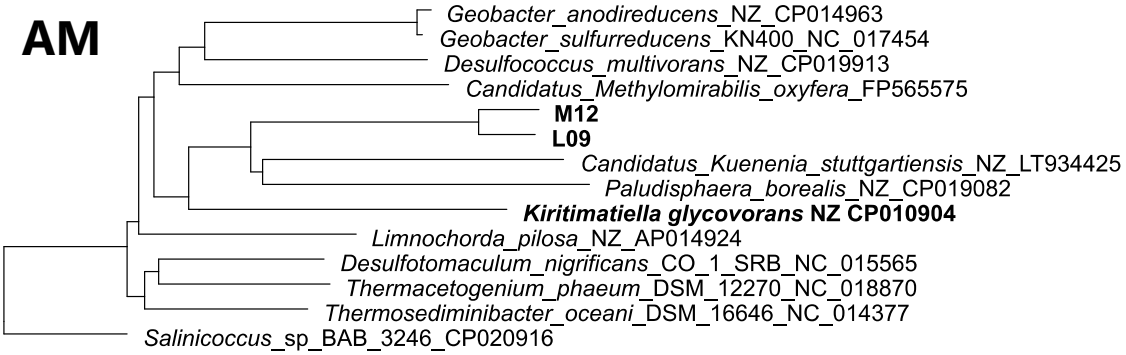
*Geobacter_anodireducens*_NZ_CP014963
*Geobacter_sulfurreducens*_KN400_NC_017454
*Desulfococcus_multivorans*_NZ_CP019913
*Candidatus_Methylomirabilis_oxyfera*_FP565575
M12
L09
*Candidatus_Kuenenia_stuttgartiensis*_NZ_LT934425
*Paludisphaera_borealis*_NZ_CP019082
***Kiritimatiella glycovorans* NZ CP010904**
*Limnochorda_pilosa*_NZ_AP014924
*Desulfotomaculum_nigrificans*_CO_1_SRB_NC_015565
*Thermacetogenium_phaeum*_DSM_12270_NC_018870
*Thermosediminibacter_oceani*_DSM_16646_NC_014377
*Salinicoccus*_sp_BAB_3246_CP020916
0.10

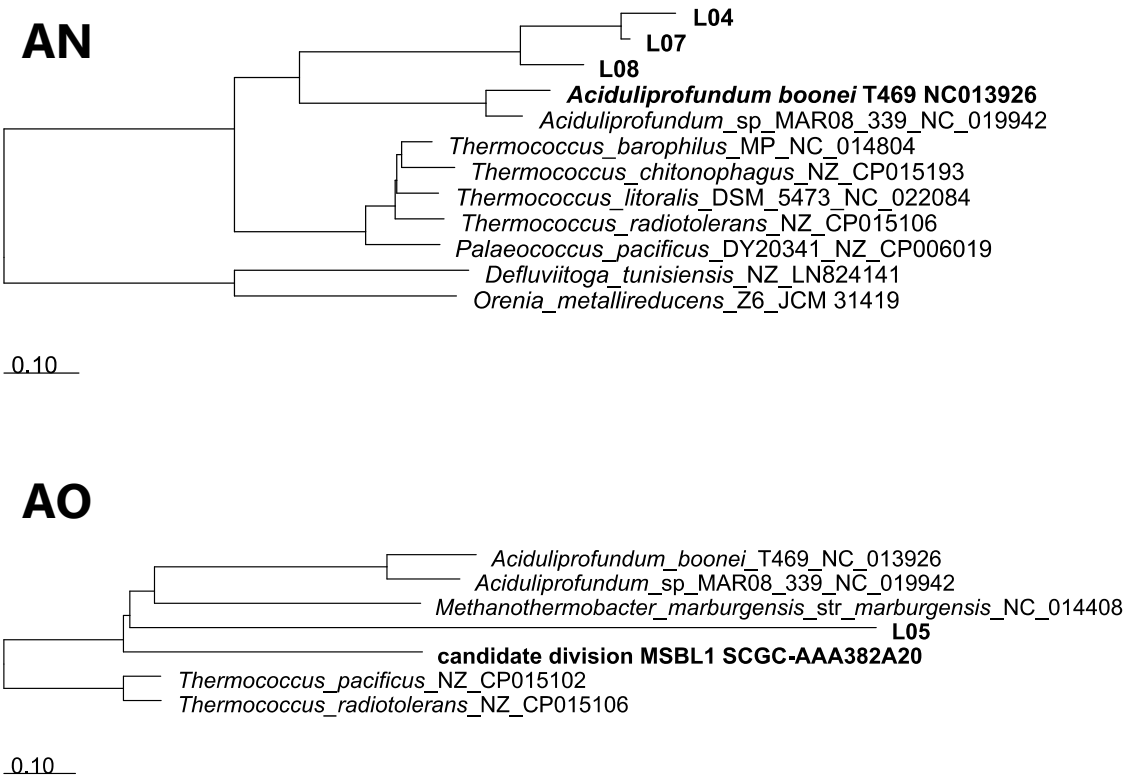

Supplementary Figure S1.5. Phylogenetic reconstruction from essential genes for the taxonomic identification of MAGs. The phylogenetic trees presented were created according to shared essential genes and/or because they were the same MAG recruited in slurry and vertical profile metagenomes. Reference genomes in trees were mostly the five closest species in comparison with %AAI. The closest reference genome after phylogenetic reconstruction and taking into account %ANI, %AAI, genome completeness and size, are marked in bold.

Supplementary Table S1.6. Percentage average nucleotide identity (ANI) values and shared nucleotide rates of the genomes in brackets, for the MAGs of the S, U, M and L metagenomes.

	U01	S02	U05	S05	U03	M03	L03	S23	M05	L06	M02	L01	U09	M10	S13	U04	M04	L02	S09	M12	L09
U01	100%(100%)	100% (81.9%)																			
S02	100% (81.9%)	100%(100%)																			
U05			100%(100%)	99.9% (87.5%)																	
S05			99.9% (87.5%)	100%(100%)																	
U03					100%(100%)	100% (92.4%)	99.9% (76.5%)	99.5% (78.4%)													
M03					100% (92.4%)	100%(100%)	99.8% (78.3%)	99.4% (79.7%)													
L03					99.9% (76.5%)	99.8% (78.3%)	100%(100%)	99.4% (46.8%)													
S23					99.5% (78.4%)	99.4% (79.7%)	99.4% (46.8%)	100%(100%)													
M05									100%(100%)	99.8% (33.8%)											
L06									99.8% (33.8%)	100%(100%)											
M02											100%(100%)	99.7% (80.7%)									
L01											99.7% (80.7%)	100%(100%)									
U09													100%(100%)	100% (80.5%)	99.9% (77%)						
M10													100% (80.5%)	100%(100%)	100% (71.7%)						
S13													99.9% (77%)	100% (71.7%)	100%(100%)						
U04																100%(100%)	99.8% (84%)	99.8% (80.5%)	99.8% (88.5%)		
M04																99.8% (84%)	100%(100%)	99.8% (82.1%)	99.8% (88.7%)		
L02																99.8% (80.5%)	99.8% (82.1%)	100%(100%)	99.8% (85.2%)		
S09																99.8% (88.5%)	99.8% (88.7%)	99.8% (85.2%)	100%(100%)		
M12																				100%(100%)	99.6% (37.4%)
L09																				99.6% (37.4%)	100%(100%)

Supplementary Table S1.7. Percentage average amino acid identity (AAI) values and shared protein rates of the genomes in brackets, between the non-monophyletic MAGs of the S, U, M and L metagenomes.

	S11	S14	S15	S12	S20	S19	S30	S21	S22	S31	S32	U06	M11
S11	100%(100%)	69.2% (63.7%)	70.6% (58.3%)										
S14	69.2% (63.7%)	100%(100%)	83.6% (60.1%)										
S15	70.6% (58.3%)	83.6% (60.1%)	100%(100%)										
S12				100%(100%)	67.8% (69.2%)								
S20				67.8% (69.2%)	100%(100%)								
S19						100%(100%)	43.4% (29%)						
S30						43.4% (29%)	100%(100%)						
S21								100%(100%)	57.3% (44.5%)				
S22								57.3% (44.5%)	100%(100%)				
S31										100%(100%)	42.3% (31.7%)		
S32										42.3% (31.7%)	100%(100%)		
U06												100%(100%)	36.6% (41.7%)
M11												36.6% (41.7%)	100%(100%)

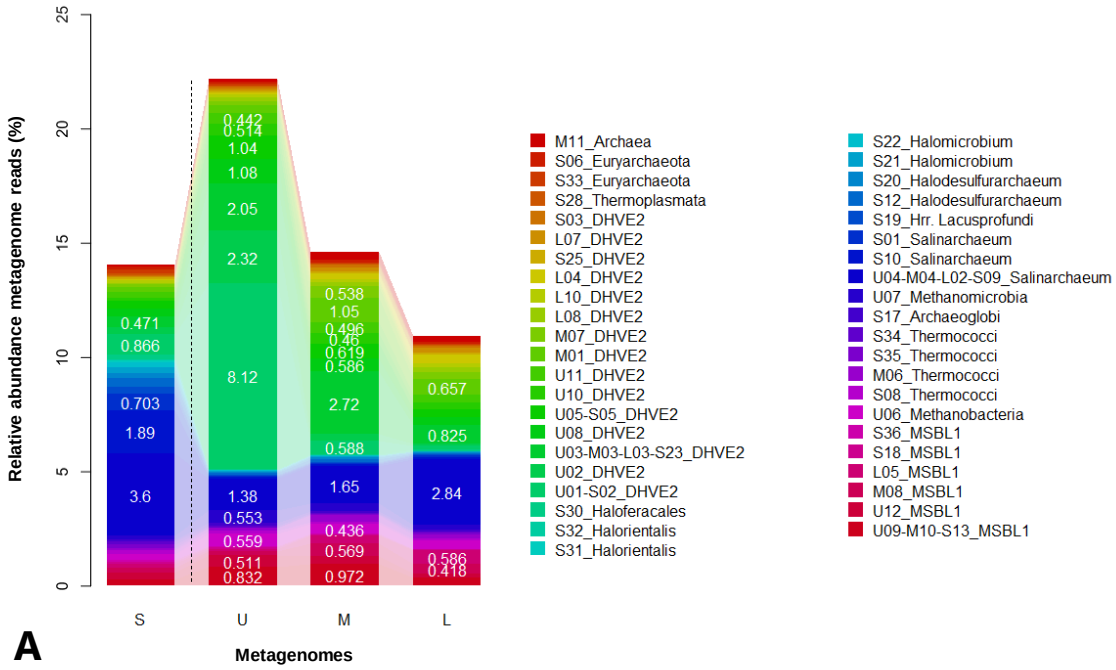

Supplementary Figure S1.6. Relative abundance of mapped reads (%) at 98% identity and 70% coverage for the MAGs at the species level against the four metagenomes (S, U, M and L). Taxonomic categories between brackets in the legend correspond to the assignation level of MAGs (Table 1.1). Relative abundances of metagenome reads above 0.4% for Archaea (**A**) and 0.1% for Bacteria (**B**) are indicated with a blank over the bars.

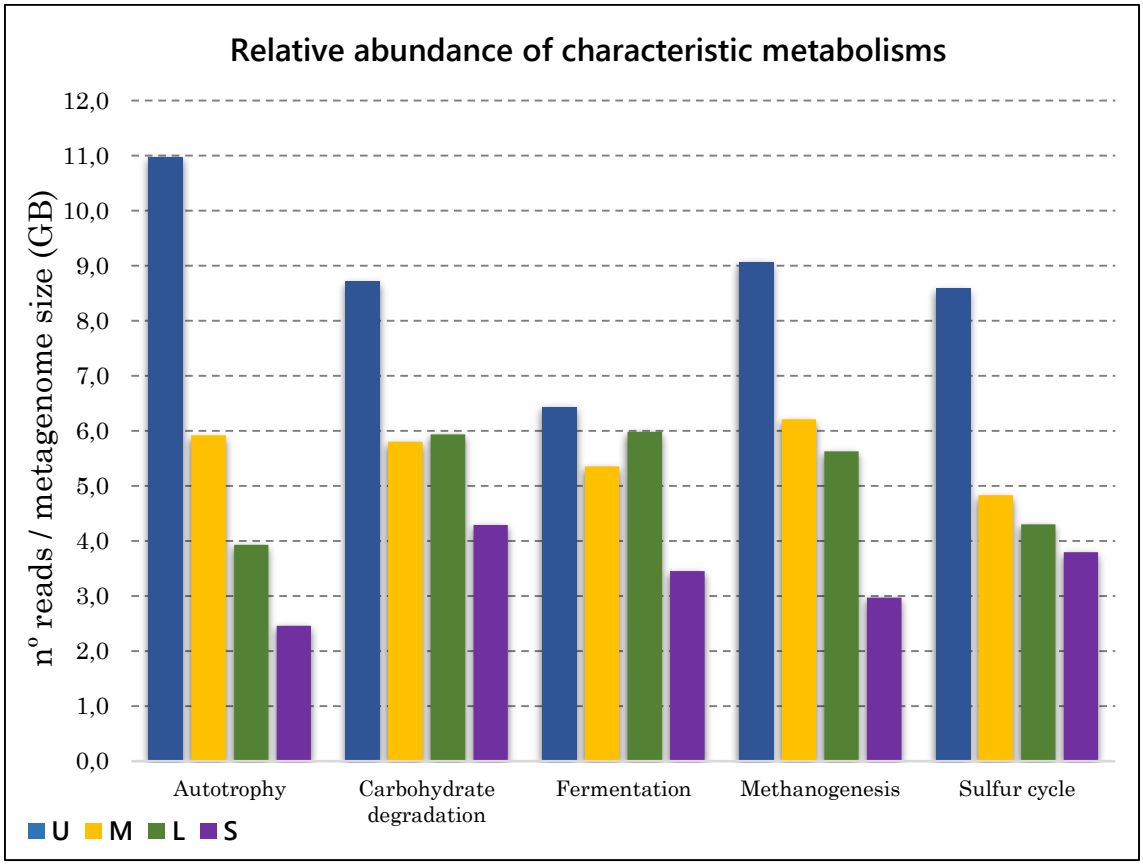

Supplementary Figure S1.7. Bar plots of relative abundance of five characteristic metabolisms in anaerobic sediments (Carbohydrate degradation, Methanogenesis, Fermentation, Autotrophy and the Sulfur cycle). Annotated genes in UniProtKB Swiss-Prot with quality parameters of 40% identity and 70% coverage involved in the cited routes were considered for mapping. Relative abundances were calculated from mapped reads of the metagenomes S, U, M and L at 95% identity and 90% coverage, in reads per metagenome size.

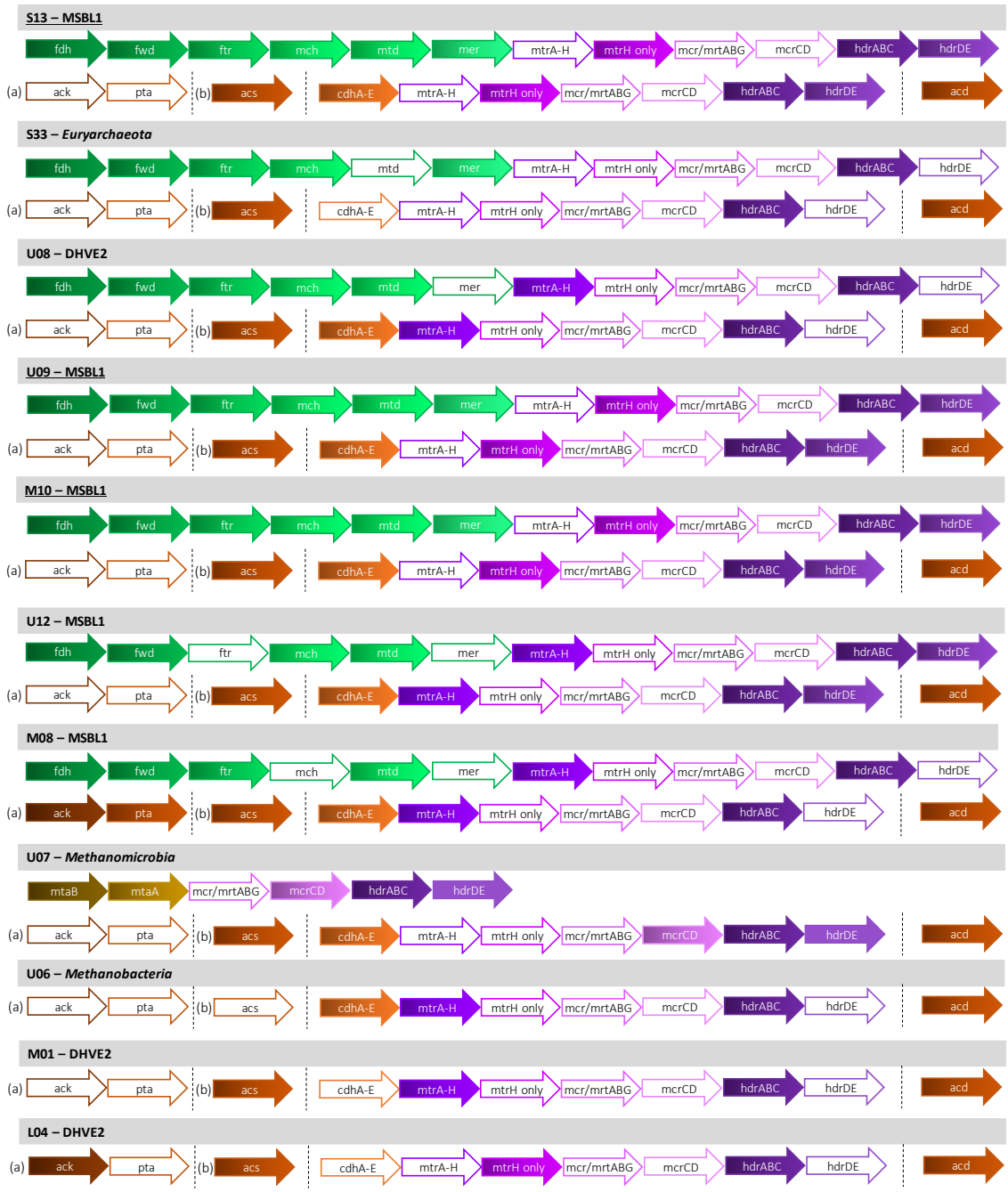

Supplementary Figure S1.8. Schematic view of the gene structure in methanogenic metabolic pathways of interesting MAGs. Filled or empty arrows indicate the presence or absence of genes, respectively.

Supplementary Table S1.8. Relative abundances of non-binned genes related to total annotated genes of the methanogenic pathways, nitrogen and sulfur cycles in metagenomes S, U, M and L are shown.

		%S	%U	%M	%L	%ALL
METHANOGENIC PATHWAYS	Hydrogenotrophic	0.97	3.88	2.43	4.13	**11.41**
	Aceticlastic	3.75	0.00	2.10	0.93	**6.78**
	Methylotrophic (CH_3OH)	0.73	0.49	0.49	0.49	**2.18**
	Methylotrophic (CH_3-amines)	0.97	0.97	1.46	0.49	**3.88**
	Methane synthesis	1.21	3.16	1.21	3.16	**8.74**
	ALL	**7.63**	**8.50**	**7.68**	**9.18**	**32.99**
NITROGEN CYCLE GENES	Denitrification	2.56	0.00	2.56	6.41	**11.54**
	N_2 fixation	0.00	0.00	0.00	11.54	**11.54**
	Dissimilatory nitrate reduction	0.00	1.28	1.28	0.00	**2.56**
	Nitrification	0.00	0.00	0.00	1.28	**1.28**
	Urea break down into NH_4^+	2.56	2.56	6.41	2.56	**14.10**
	Assimilatory nitrate reduction	0.00	1.28	1.28	3.85	**6.41**
	ALL	**5.13**	**5.13**	**11.54**	**25.64**	**47.44**
SULFUR CYCLE GENES	Dissimilatory sulfate reduction	0.81	0.81	0.40	0.81	**2.83**
	Assimilatory sulfate reduction	0.00	0.40	0.40	4.45	**5.26**
	Sulfur-oxidizing	0.00	0.81	2.02	0.40	**3.24**
	ALL	**0.81**	**2.02**	**2.83**	**5.67**	**11.34**

A

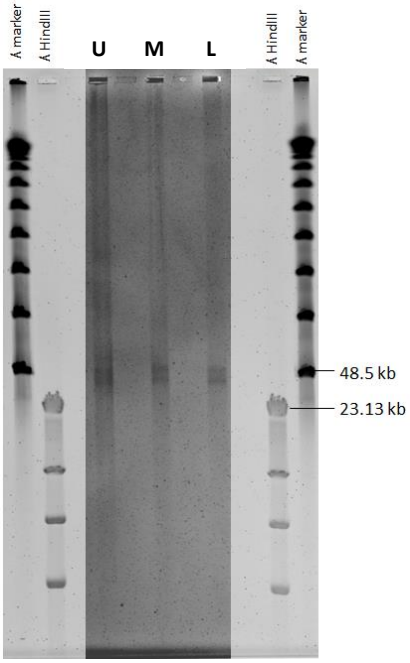

B

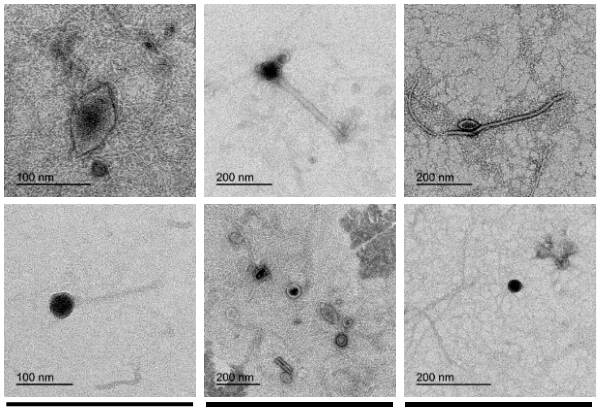

C

% shared reads (95% id, 70% qcov)

	U	M	L
U		56.66	53.81
M	59.11		66.44
L	59.52	68.15	

% shared reads (100% id, 100% qcov)

	U	M	L
U		12.21	11.35
M	13.96		16.57
L	13.82	16.74	

Supplementary Figure S1.9. General features of the viral assemblages analyzed in horizons U, M and L (April 2017). **A**. Predominant genome sizes of the virus communities estimated by PFGE. **B**. Selection of transmission electron microscopy images where different viral morphotypes can be observed. **C**. BLASTN-based comparison between the three viral metagenomes, where percentage shared reads above 95% identity (and ≥ 70% query coverage) and identical shared reads (100% identity and query coverage) are shown.

Supplementary Table S1.9. Main features of the three viral metagenomes (U, M and L) analyzed from April 2017 sediments.

Sample	Number reads	Nucleotides	%GC	Coverage	% reads 16S	Number contigs	Contigs > 5kb	Largest contig	vOTUs
U	4.65E+06	1.08E+09	54.32	84.97	0.0017	1.50E+05	253	27,395	190
M	3.95E+06	8.97E+08	56.17	84.62	0.0005	1.29E+05	271	22,946	
L	4.15E+06	9.51E+08	55.63	84.67	0.0009	1.38E+05	294	23,045	

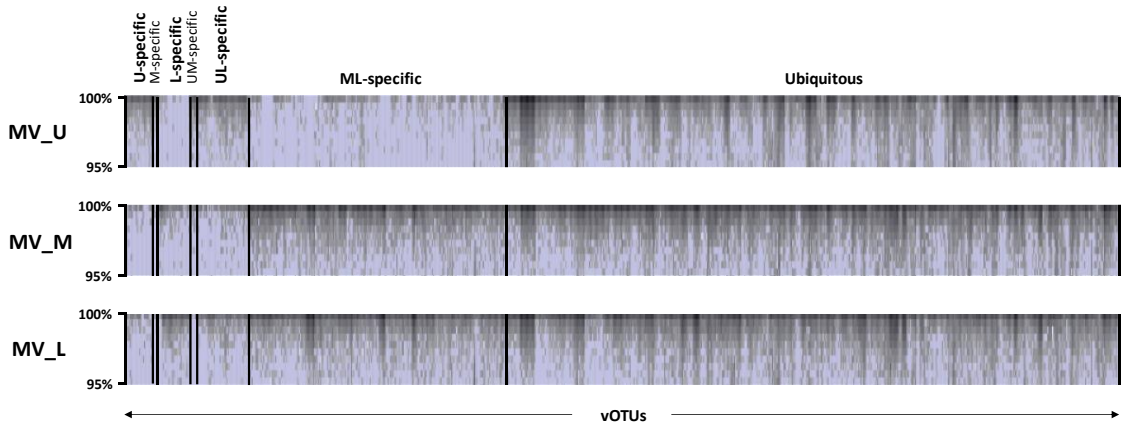

Supplementary Figure S1.10. Fragment recruitment plots of all viral OTUs (X axis), against the total reads from each analyzed metavirome (MV_U, MV_M and MV_L). Only those reads (queries) matching the vOTUs (database) above a 95% identity (Y axis) and 70% coverage are shown.

Supplementary Table S1.10. Presence of vOTUs in the set of viral (MV) and cellular (MG) metagenomes (U, M and L) from April 2017 sediments. Information about their putative hosts and the presence of integrases is also provided. Nomenclature of the vOTUs is as shown in spreadsheet Table ST1.3. Relative abundances for each of the vOTUs (red scale) are expressed as recruited base pairs per metagenome size and contig size. vOTUs associated with MAGs are highlighted in grey.

vOTU		Length	MV_U	MV_M	MV_L	MG_U	MG_M	MG_L	Integrase	Host
U-specific (4.21%)	vOTU_U_042	9642	2.00							
	vOTU_U_049	9077	1.72						YES	
	vOTU_U_089	7612	1.78							
	vOTU_U_125	6747	1.94							
	vOTU_U_191	5680	1.64							
	vOTU_U_196	5585	1.75						YES	
	vOTU_U_230	5180	1.64			0.28				
	vOTU_U_253	5001	1.61			0.47				
M-specific (0.53%)	vOTU_M_209	5608		1.97						
L-specific (3.16%)	vOTU_L_056	9104			1.83				YES	
	vOTU_L_076	8470			1.91					
	vOTU_L_141	6816			1.92			0.45		
	vOTU_L_150	6668			2.11				YES	
	vOTU_L_152	6652			1.97					
	vOTU_L_159	6564			1.88					
UM-specific (0.53%)	vOTU_UM_020(U)	12169	1.64	0.19		0.22			YES	
UL-specific (4.74%)	vOTU_UL_006(U)	17598	1.69		0.27					*Halobacteria* class
	vOTU_UL_039(L)	10374	0.41		1.99				YES	
	vOTU_UL_045(U)	9413	1.83		0.47				YES	
	vOTU_UL_048(U)	9168	1.85		0.36	0.23		0.22		
	vOTU_UL_053(U)_*UL	9002	1.93		1.21				YES	*Halobacteria* class
	vOTU_UL_059(U)	8711	1.94		0.32					
	vOTU_UL_165(U)	6026	1.87		0.68				YES	
	vOTU_UL_187(U)	5755	1.78		0.20					
	vOTU_UL_239(U)	5072	1.93		0.48				YES	
ML-specific (23.68%)	vOTU_ML_001(L)_*ML	23045		3.05	1.86					
	vOTU_ML_002(L)_*ML	19842		2.43	1.79				YES	

	vOTU_ML_003(L)_*ML	18846		3.12	1.87					
	vOTU_ML_003(M)	19801		2.06	1.12					
	vOTU_ML_011(L)_*ML	13837		1.41	2.17		0.45	0.67	YES	
	vOTU_ML_011(M)_*ML	13352		1.91	5.52			0.20		
	vOTU_ML_013(L)_*ML	13349		0.76	1.99		1.46	1.87		MAG L01: *Planctomycetia* class
	vOTU_ML_013(M)	13329		2.10	0.89		0.24	0.22	YES	
	vOTU_ML_021(L)	11993		1.11	2.05					
	vOTU_ML_022(L)_*ML	11832		3.43	1.84		0.21		YES	
	vOTU_ML_023(L)	11639		0.31	1.84		0.69	1.34		
	vOTU_ML_023(M)_*ML	11651		1.93	1.44					
	vOTU_ML_024(L)	11541		3.42	1.19		0.41			
	vOTU_ML_042(L)	10112		0.66	0.56				YES	*Halobacteria* class
	vOTU_ML_042(M)	9813		2.02	1.43					
	vOTU_ML_045(L)	9886		0.41	1.08			0.03		
	vOTU_ML_057(L)	9040		0.91	1.89				YES	
	vOTU_ML_062(M)	8850		2.32	2.55					
	vOTU_ML_071(M)	8633		1.95	0.92				YES	*Halobacteria* class
	vOTU_ML_080(L)	8408		1.43	2.11					
	vOTU_ML_088(L)	8137		1.15	2.11					*Gammaproteobacteria*
	vOTU_ML_096(L)	7977		0.64	1.79		0.02	0.08		
	vOTU_ML_105(M)	7297		2.35	1.58					
	vOTU_ML_115(L)	7309		3.52	2.45					
	vOTU_ML_117(L)	7293		0.39	1.82		0.79	1.50		MAG L05: *Euryarchaeota* (uncultured lineage MSBL1)
	vOTU_ML_124(L)	7152		0.37	1.84		0.78	1.57		
	vOTU_ML_126(M)	6794		2.12	0.54					
	vOTU_ML_136(L)	6950		0.45	1.08					
	vOTU_ML_139(M)	6641		2.08	0.57				YES	
	vOTU_ML_140(M)	6617		2.51	1.96					
	vOTU_ML_158(M)	6254		2.03	1.68					
	vOTU_ML_161(M)	6224		2.14	1.01					
	vOTU_ML_174(L)	6354		2.49	2.40		3.20	2.74	YES	
	vOTU_ML_179(M)	6029		2.23	1.83					
	vOTU_ML_194(M)	5798		2.01	1.29		0.21			
	vOTU_ML_204(M)	5639		2.09	1.31			0.48		

	vOTU_ML_212(M)	5561		2.69	1.16					
	vOTU_ML_222(M)	5463		2.24	0.71					
	vOTU_ML_242(L)	5462		0.58	2.08			0.74		
	vOTU_ML_244(L)	5426		1.69	2.35					
	vOTU_ML_249(L)	5393		0.72	1.99					
	vOTU_ML_250(L)	5391		0.25	0.32		0.12			
	vOTU_ML_263(L)	5278		1.69	2.08					
	vOTU_ML_269(L)	5225		2.23	1.97		1.00	0.68		
	vOTU_ML_281(L)	5089		1.05	2.62		0.49	0.64		
Ubiquitous (63.16%)	vOTU_UML_002(U)_*UML	27395	1.59	0.24	0.65	0.15			YES	
	vOTU_UML_001(M)_*ML	22946	21.60	1.88	4.13	1.53	0.24	0.45	YES	
	vOTU_UML_003(U)	22466	1.62	0.22	0.14	1.36		0.15	YES	MAG U02: *Euryarchaeota* (uncultured lineage DHVE2)
	vOTU_UML_004(U)_*UML	22450	1.64	1.30	1.36	0.12			YES	
	vOTU_UML_004(L)_*UML	18775	1.83	1.31	1.49	0.17				
	vOTU_UML_006(L)_*ML	17297	2.53	1.19	1.95				YES	
	vOTU_UML_004(M)	16683	0.34	2.01	0.33		0.15		YES	
	vOTU_UML_006(M)	15428		1.91		0.39	1.04	0.55	YES	
	vOTU_UML_009(L)_*UL	15011	6.88	1.50	1.89					
	vOTU_UML_014(M)_*ML	13312	0.56	1.84	3.34			0.27	YES	
	vOTU_UML_014(L)_*ML	13165	1.07	2.15	1.39					
	vOTU_UML_017(L)_*ML	12601	0.96	2.95	1.87	0.29	0.40	1.01		
	vOTU_UML_016(M)_*ML	12509	0.53	2.28	1.96					
	vOTU_UML_018(L)_*ML	12447	0.96	1.35	1.42				YES	
	vOTU_UML_022(U)_*UL	11354	1.82	0.28	0.23	0.13				
	vOTU_UML_031(L)_*ML	11169	0.69	1.53	2.19		0.93	0.59		
	vOTU_UML_028(M)	11123	1.17	1.89	1.07					
	vOTU_UML_025(U)_*UML	10992	1.74	0.85	0.36	0.08			YES	
	vOTU_UML_035(M)	10688	0.17	2.50	5.01					
	vOTU_UML_040(L)	10280	0.94	1.17	1.96				YES	*Halobacteria* class
	vOTU_UML_038(M)_*UM	10174	0.58	2.03	7.01			0.10		
	vOTU_UML_035(U)	9958	2.01	0.92	1.52			0.35		
	vOTU_UML_036(U)_*UM	9943	2.32	5.87	5.51					*Halobacteria* class
	vOTU_UML_049(M)	9596	0.20	2.15	0.69					
	vOTU_UML_051(M)	9546	1.19	2.26	4.87		0.42	1.36		

	vOTU_UML_052(M)_*ML	9450	9.23	2.16	1.56	0.68	0.28	0.23	YES	
	vOTU_UML_054(M)	9412	0.41	2.07	5.79	0.98	12.27	7.24		
	vOTU_UML_058(L)	9036	0.07	0.76	1.95					
	vOTU_UML_055(U)_*UL	8935	1.64	0.52	0.76	0.18			YES	
	vOTU_UML_060(L)_*ML	8829	0.80	2.39	2.51					
	vOTU_UML_061(L)	8798		2.26	2.25	0.41	2.11	1.70		MAG M02: *Planctomycetia* class
	vOTU_UML_062(L)	8758	0.38	0.95	1.70					*Gammaproteobacteria*
	vOTU_UML_058(U)	8726	1.71	0.33	0.16					*Gammaproteobacteria*
	vOTU_UML_066(M)	8724	0.45	1.98	1.75					
	vOTU_UML_067(M)	8721	4.38	2.76	3.07					
	vOTU_UML_065(L)	8689	0.81	0.14	0.15	0.06	0.02	0.02	YES	
	vOTU_UML_066(L)	8680	0.22	0.95	1.63					*Gammaproteobacteria*
	vOTU_UML_069(M)	8655	0.62	2.01	1.64					
	vOTU_UML_062(U)	8621	1.65	0.34	0.50	0.75	1.32	0.41		
	vOTU_UML_071(L)	8568	0.16	0.49	1.27		0.12	0.29		
	vOTU_UML_075(M)_*ML	8548	22.27	2.23	1.22					
	vOTU_UML_074(L)	8492	0.63	0.39	0.25				YES	
	vOTU_UML_078(M)	8410	0.78	2.07	1.83					
	vOTU_UML_082(L)	8393	0.27	0.94	2.05					
	vOTU_UML_082(M)	8322	4.01	1.90	1.03				YES	
	vOTU_UML_067(U)	8320	1.65	0.22	0.43	1.66	0.32	0.30		
	vOTU_UML_087(M)	7933	0.72	2.15	2.05		0.92	0.86		
	vOTU_UML_098(L)	7853	0.01	0.02	0.04			0.00	YES	
	vOTU_UML_099(L)	7841	0.65	1.34	1.90		0.33	0.65		
	vOTU_UML_100(L)	7806	3.82	1.70	0.90	0.17				
	vOTU_UML_094(M)	7677	0.85	2.07	5.09		0.62	1.19		
	vOTU_UML_095(M)_*ML	7669	0.14	2.07	5.33		0.11	0.10		
	vOTU_UML_087(U)	7654	1.95	0.90	1.31					
	vOTU_UML_105(L)	7604	0.92	2.17	2.52					
	vOTU_UML_109(L)	7491	6.36	2.57	2.07	0.34				
	vOTU_UML_111(L)_*ML	7439	3.13	2.13	2.19					
	vOTU_UML_114(L)	7342	5.89	2.98	2.34	0.33				*Gammaproteobacteria*
	vOTU_UML_102(M)	7327	0.23	2.36	6.12		0.13	0.14		
	vOTU_UML_103(U)	7311	2.05	11.27	22.94	1.12	4.89	5.59		MAGs L01, M02: *Planctomycetia* class
	vOTU_UML_116(L)	7295	0.66	1.02	1.18					

	vOTU_UML_108(M)	7275	0.22	1.55	2.98	0.13	0.66	0.80		MAGs L01, M02: *Planctomycetia* class
	vOTU_UML_106(U)_*UM	7211	1.67	0.32	0.11					
	vOTU_UML_130(L)	7024	3.22	1.61	2.06				YES	
	vOTU_UML_123(M)	6834	0.96	2.21	0.77		1.00	0.75		
	vOTU_UML_142(L)	6804	1.01	2.73	2.98					
	vOTU_UML_127(U)	6737	2.25	0.65	0.38					*Halobacteria* class
	vOTU_UML_131(M)	6702	0.30	1.99	0.69		0.26	0.15		
	vOTU_UML_136(M)_*UML	6668	0.70	1.83	1.24			0.54		
	vOTU_UML_137(M)	6665		2.07	0.77	0.44	4.34	3.15		
	vOTU_UML_138(M)	6647		1.89	0.75	0.35	2.75	2.18		
	vOTU_UML_141(U)	6446	1.74	0.46	0.49	0.26	0.13	0.11	YES	
	vOTU_UML_170(L)	6429	1.53	2.63	2.78				YES	
	vOTU_UML_148(M)	6403	21.53	3.05	4.25				YES	
	vOTU_UML_172(L)	6381	5.00	2.13	2.62					
	vOTU_UML_151(M)	6375	6.33	2.39	1.76					*Halobacteria* class
	vOTU_UML_152(M)_*ML	6367	17.77	2.04	2.32	4.04	0.77	0.54	YES	
	vOTU_UML_173(L)	6364	1.50	9.59	2.64					
	vOTU_UML_176(L)	6321	0.63	1.45	2.28					*Halobacteria* class
	vOTU_UML_154(U)	6246	1.77	1.75	3.56					
	vOTU_UML_160(M)	6230	1.91	1.05	0.89				YES	
	vOTU_UML_181(L)	6184	0.33	0.77	2.12	0.14	0.43	0.31		
	vOTU_UML_186(L)	6125	8.70	1.22	2.29	0.86				
	vOTU_UML_161(U)	6084	2.27	6.72	6.98		0.72			
	vOTU_UML_177(M)	6049	3.73	2.07	1.01	0.24				
	vOTU_UML_164(U)	6028	1.59	0.78	0.54	0.54				
	vOTU_UML_197(L)	5977	0.87	0.78	2.14					
	vOTU_UML_169(U)	5976	1.63	1.67	1.68				YES	
	vOTU_UML_182(M)	5969	6.41	2.09	1.02	0.21				
	vOTU_UML_204(L)	5889	0.31	0.03	0.06	0.03	0.01	0.02	YES	
	vOTU_UML_215(L)	5760	3.32	2.63	2.37					
	vOTU_UML_219(L)	5714	0.10	1.18	1.21					
	vOTU_UML_189(U)	5712	1.88	1.45	1.29					
	vOTU_UML_193(U)	5630	1.83	1.40	1.50					
	vOTU_UML_195(U)_*UL	5615	1.62	1.45	2.02				YES	
	vOTU_UML_207(M)	5615	0.07	0.09	0.06				YES	

	vOTU_UML_225(L)	5602	0.09	0.46	1.03	0.04	0.22	0.26		MAGs L01, M02: *Planctomycetia* class
	vOTU_UML_226(L)	5593	0.65	0.65	2.01				YES	
	vOTU_UML_197(U)	5583	2.00	0.66	1.16					
	vOTU_UML_198(U)_*UM	5562	1.74	1.86	1.11					
	vOTU_UML_234(L)	5525	0.22	2.28	1.78		0.16			
	vOTU_UML_203(U)	5510	2.09	8.52	6.86					*Halobacteria* class
	vOTU_UML_237(L)	5501	0.74	0.94	2.09	1.13	1.09	1.25		
	vOTU_UML_229(M)	5371	14.11	2.84	2.38					
	vOTU_UML_218(U)	5333	1.56	1.04	0.54	0.36				
	vOTU_UML_256(L)	5323	0.64	2.48	1.87					
	vOTU_UML_237(M)	5289	8.16	2.02	1.40	0.58	0.32	0.13	YES	
	vOTU_UML_242(M)	5228	1.09	2.99	1.62					
	vOTU_UML_244(M)	5224	0.70	2.14	2.63					
	vOTU_UML_226(U)	5196	1.68	0.88	0.85				YES	
	vOTU_UML_250(M)	5182	1.67	1.97	3.31	0.88	0.73	1.31	YES	
	vOTU_UML_256(M)	5137	1.61	2.27	1.61	3.22	5.57	3.03		
	vOTU_UML_234(U)	5134	2.28	1.24	1.31					
	vOTU_UML_276(L)	5133	1.11	1.73	2.90					
	vOTU_UML_259(M)	5096	2.33	3.03	1.66	1.12				
	vOTU_UML_261(M)	5089	1.07	2.32	4.67					
	vOTU_UML_265(M)	5064	3.30	2.06	1.11	0.07	0.05	0.03		
	vOTU_UML_288(L)	5036	0.13	2.75	2.01		0.16			
	vOTU_UML_247(U)	5032	1.64	0.25	0.16	0.08	0.06			
	vOTU_UML_291(L)	5022	0.48	1.31	2.12					
	vOTU_UML_294(L)	5008	1.32	0.98	2.09					

Chapter 2. Study of the effect of salinity, antibiotic and carbon source concentration in structuring the microbial communities from S'Avall hypersaline sediments

Supplementary Table S2.1. Permutation D-test, Kolmogorov-Smirnov, Kolmogorov-Smirnov (with Bonferroni correction), Wilcoxon and T-test results obtained from the comparison among the potential duplicates of microcosms at the same salinity, substrate concentration and ampicillin addition (those with identifiers finished with 1 and 2). The statistically significance of the data is according to consider the samples as equal. D-values are presented for the Permutation D-test, D-values and p-values are displayed for the Kolmogorov-Smirnov test and Bonferroni correction, whilst p-values from Wilcoxon test and t-values of T-test are shown.

Permutation D-test: D ≤ 1.36 (p ≥ 0.05)																
D_{value}	**5_0.1A1**	**5_0.1_1**	**5_1A1**	**5_1_1**	**5_10A1**	**5_10_1**	**10_0.1A1**	**10_0.1_1**	**10_1A1**	**10_1_1**	**10_10A1**	**10_10_1**	**12_0.1A1**	**12_0.1_1**	**12_1A1**	**12_1_1**
	5_0.1A2	**5_0.1_2**	**5_1A2**	**5_1_2**	**5_10A2**	**5_10_2**	**10_0.1A2**	**10_0.1_2**	**10_1A2**	**10_1_2**	**10_10A2**	**10_10_2**	**12_0.1A2**	**12_0.1_2**	**12_1A2**	**12_1_2**
	0.843	2.017	1.826	1.784	1.829	0.918	1.427	2.333	2.323	1.780	1.597	1.098	1.311	2.208	1.614	0.736
	12_10A1	**12_10_1**	**15_0.1A1**	**15_0.1_1**	**15_1A1**	**15_1_1**	**15_10A1**	**15_10_1**	**18_0.1A1**	**18_0.1_1**	**18_1A1**	**18_1_1**	**18_10A1**	**18_10_1**	**20_0.1A1**	**20_0.1_1**
	12_10A2	**12_10_2**	**15_0.1A2**	**15_0.1_2**	**15_1A2**	**15_1_2**	**15_10A2**	**15_10_2**	**18_0.1A2**	**18_0.1_2**	**18_1A2**	**18_1_2**	**18_10A2**	**18_10_2**	**20_0.1A2**	**20_0.1_2**
	1.821	2.565	1.990	0.696	1.763	1.446	2.056	2.068	1.382	1.977	1.623	1.564	1.996	2.226	1.318	1.301
	20_1A1	**20_1_1**	**20_10A1**	**20_10_1**	**25_0.1A1**	**25_0.1_1**	**25_1A1**	**25_1_1**	**25_10A1**	**25_10_1**	**30_0.1A1**	**30_0.1_1**	**30_1A1**	**30_1_1**	**30_10A1**	**30_10_1**
	20_1A2	**20_1_2**	**20_10A2**	**20_10_2**	**25_0.1A2**	**25_0.1_2**	**25_1A2**	**25_1_2**	**25_10A2**	**25_10_2**	**30_0.1A2**	**30_0.1_2**	**30_1A2**	**30_1_2**	**30_10A2**	**30_10_2**
	1.036	1.325	1.106	1.843	1.383	0.868	2.360	0.461	1.427	1.647	0.936	1.531	0.442	2.101	2.205	1.575
Kolmogorov-Smirnov: D ≤ 1.36 and p ≥ 0.05																
D_{value} / p_{value}	**5_0.1A1**	**5_0.1_1**	**5_1A1**	**5_1_1**	**5_10A1**	**5_10_1**	**10_0.1A1**	**10_0.1_1**	**10_1A1**	**10_1_1**	**10_10A1**	**10_10_1**	**12_0.1A1**	**12_0.1_1**	**12_1A1**	**12_1_1**
	5_0.1A2	**5_0.1_2**	**5_1A2**	**5_1_2**	**5_10A2**	**5_10_2**	**10_0.1A2**	**10_0.1_2**	**10_1A2**	**10_1_2**	**10_10A2**	**10_10_2**	**12_0.1A2**	**12_0.1_2**	**12_1A2**	**12_1_2**
	0.010	0.012	0.014	0.033	0.033	0.080	0.006	0.009	0.016	0.029	0.017	0.015	0.042	0.019	0.033	0.057
	1.000	1.000	0.999	0.413	0.413	1.52E-04	1.000	1.000	0.994	0.585	0.984	0.997	0.159	0.952	0.387	0.018

	12_10A1	**12_10_1**	**15_0.1A1**	**15_0.1_1**	**15_1A1**	**15_1_1**	**15_10A1**	**15_10_1**	**18_0.1A1**	**18_0.1_1**	**18_1A1**	**18_1_1**	**18_10A1**	**18_10_1**	**20_0.1A1**	**20_0.1_1**
	12_10A2	**12_10_2**	**15_0.1A2**	**15_0.1_2**	**15_1A2**	**15_1_2**	**15_10A2**	**15_10_2**	**18_0.1A2**	**18_0.1_2**	**18_1A2**	**18_1_2**	**18_10A2**	**18_10_2**	**20_0.1A2**	**20_0.1_2**
	0.040	0.020	0.007	0.037	0.014	0.012	0.007	0.020	0.065	0.006	0.006	0.013	0.005	0.006	0.020	0.005
	0.187	0.937	1.000	0.274	0.999	1.000	1.000	0.919	0.004	1.000	1.000	1.000	1.000	1.000	0.919	1.000
	20_1A1	**20_1_1**	**20_10A1**	**20_10_1**	**25_0.1A1**	**25_0.1_1**	**25_1A1**	**25_1_1**	**25_10A1**	**25_10_1**	**30_0.1A1**	**30_0.1_1**	**30_1A1**	**30_1_1**	**30_10A1**	**30_10_1**
	20_1A2	**20_1_2**	**20_10A2**	**20_10_2**	**25_0.1A2**	**25_0.1_2**	**25_1A2**	**25_1_2**	**25_10A2**	**25_10_2**	**30_0.1A2**	**30_0.1_2**	**30_1A2**	**30_1_2**	**30_10A2**	**30_10_2**
	0.027	0.025	0.020	0.027	0.014	0.015	0.005	0.053	0.052	0.011	0.032	0.005	0.040	0.010	0.004	0.004
	0.647	0.740	0.937	0.647	0.999	0.997	1.000	0.032	0.039	1.000	0.439	1.000	0.202	1.000	1.000	1.000
Bonferroni correction (post Kolmogorov-Smirnov): D ≤ 1.36 and p ≥ 0.05																
	5_0.1A1	**5_0.1_1**	**5_1A1**	**5_1_1**	**5_10A1**	**5_10_1**	**10_0.1A1**	**10_0.1_1**	**10_1A1**	**10_1_1**	**10_10A1**	**10_10_1**	**12_0.1A1**	**12_0.1_1**	**12_1A1**	**12_1_1**
	5_0.1A2	**5_0.1_2**	**5_1A2**	**5_1_2**	**5_10A2**	**5_10_2**	**10_0.1A2**	**10_0.1_2**	**10_1A2**	**10_1_2**	**10_10A2**	**10_10_2**	**12_0.1A2**	**12_0.1_2**	**12_1A2**	**12_1_2**
	0.010	0.012	0.014	0.033	0.033	0.080	0.006	0.009	0.016	0.029	0.017	0.015	0.042	0.019	0.033	0.057
	1.000	1.000	1.000	1.000	1.000	0.007	1.000	1.000	1.000	1.000	1.000	1.000	1.000	1.000	1.000	0.879
D_{value} / p_{value}	**12_10A1**	**12_10_1**	**15_0.1A1**	**15_0.1_1**	**15_1A1**	**15_1_1**	**15_10A1**	**15_10_1**	**18_0.1A1**	**18_0.1_1**	**18_1A1**	**18_1_1**	**18_10A1**	**18_10_1**	**20_0.1A1**	**20_0.1_1**
	12_10A2	**12_10_2**	**15_0.1A2**	**15_0.1_2**	**15_1A2**	**15_1_2**	**15_10A2**	**15_10_2**	**18_0.1A2**	**18_0.1_2**	**18_1A2**	**18_1_2**	**18_10A2**	**18_10_2**	**20_0.1A2**	**20_0.1_2**
	0.040	0.020	0.007	0.037	0.014	0.012	0.007	0.020	0.065	0.006	0.006	0.013	0.005	0.006	0.020	0.005
	1.000	1.000	1.000	1.000	1.000	1.000	1.000	1.000	0.205	1.000	1.000	1.000	1.000	1.000	1.000	1.000
	20_1A1	**20_1_1**	**20_10A1**	**20_10_1**	**25_0.1A1**	**25_0.1_1**	**25_1A1**	**25_1_1**	**25_10A1**	**25_10_1**	**30_0.1A1**	**30_0.1_1**	**30_1A1**	**30_1_1**	**30_10A1**	**30_10_1**
	20_1A2	**20_1_2**	**20_10A2**	**20_10_2**	**25_0.1A2**	**25_0.1_2**	**25_1A2**	**25_1_2**	**25_10A2**	**25_10_2**	**30_0.1A2**	**30_0.1_2**	**30_1A2**	**30_1_2**	**30_10A2**	**30_10_2**
	0.027	0.025	0.020	0.027	0.014	0.015	0.005	0.053	0.052	0.011	0.032	0.005	0.040	0.010	0.004	0.004
	1.000	1.000	1.000	0.647	1.000	1.000	1.000	1.000	1.000	1.000	1.000	1.000	1.000	1.000	1.000	1.000
Wilcoxon: p ≤ 0.5																
p_{value}	**5_0.1A1**	**5_0.1_1**	**5_1A1**	**5_1_1**	**5_10A1**	**5_10_1**	**10_0.1A1**	**10_0.1_1**	**10_1A1**	**10_1_1**	**10_10A1**	**10_10_1**	**12_0.1A1**	**12_0.1_1**	**12_1A1**	**12_1_1**
	5_0.1A2	**5_0.1_2**	**5_1A2**	**5_1_2**	**5_10A2**	**5_10_2**	**10_0.1A2**	**10_0.1_2**	**10_1A2**	**10_1_2**	**10_10A2**	**10_10_2**	**12_0.1A2**	**12_0.1_2**	**12_1A2**	**12_1_2**

	0.459	0.392	0.572	0.042	0.056	1.02E-07	0.632	0.546	0.537	0.024	0.317	0.278	0.002	0.191	0.035	4.8E-06
	12_10A1	**12_10_1**	**15_0.1A1**	**15_0.1_1**	**15_1A1**	**15_1_1**	**15_10A1**	**15_10_1**	**18_0.1A1**	**18_0.1_1**	**18_1A1**	**18_1_1**	**18_10A1**	**18_10_1**	**20_0.1A1**	**20_0.1_1**
	12_10A2	**12_10_2**	**15_0.1A2**	**15_0.1_2**	**15_1A2**	**15_1_2**	**15_10A2**	**15_10_2**	**18_0.1A2**	**18_0.1_2**	**18_1A2**	**18_1_2**	**18_10A2**	**18_10_2**	**20_0.1A2**	**20_0.1_2**
	0.003	0.990	0.625	0.002	0.410	0.583	0.594	0.073	1.29E-07	0.761	0.787	0.259	0.990	0.690	0.069	0.960
	20_1A1	**20_1_1**	**20_10A1**	**20_10_1**	**25_0.1A1**	**25_0.1_1**	**25_1A1**	**25_1_1**	**25_10A1**	**25_10_1**	**30_0.1A1**	**30_0.1_1**	**30_1A1**	**30_1_1**	**30_10A1**	**30_10_1**
	20_1A2	**20_1_2**	**20_10A2**	**20_10_2**	**25_0.1A2**	**25_0.1_2**	**25_1A2**	**25_1_2**	**25_10A2**	**25_10_2**	**30_0.1A2**	**30_0.1_2**	**30_1A2**	**30_1_2**	**30_10A2**	**30_10_2**
	0.020	0.026	0.062	0.016	0.526	0.139	0.986	4.34E-08	8.76E-06	0.375	0.004	0.954	3.72E-04	0.373	0.789	0.994
t-test: |t| ≤ 1 (*)																
t_{value}	**5_0.1A1**	**5_0.1_1**	**5_1A1**	**5_1_1**	**5_10A1**	**5_10_1**	**10_0.1A1**	**10_0.1_1**	**10_1A1**	**10_1_1**	**10_10A1**	**10_10_1**	**12_0.1A1**	**12_0.1_1**	**12_1A1**	**12_1_1**
	5_0.1A2	**5_0.1_2**	**5_1A2**	**5_1_2**	**5_10A2**	**5_10_2**	**10_0.1A2**	**10_0.1_2**	**10_1A2**	**10_1_2**	**10_10A2**	**10_10_2**	**12_0.1A2**	**12_0.1_2**	**12_1A2**	**12_1_2**
	-0.279	-0.092	-0.513	-1.240	0.947	-0.158	-0.184	-0.407	0.518	-0.569	-0.208	0.388	-0.011	-0.351	0.141	-0.407
	12_10A1	**12_10_1**	**15_0.1A1**	**15_0.1_1**	**15_1A1**	**15_1_1**	**15_10A1**	**15_10_1**	**18_0.1A1**	**18_0.1_1**	**18_1A1**	**18_1_1**	**18_10A1**	**18_10_1**	**20_0.1A1**	**20_0.1_1**
	12_10A2	**12_10_2**	**15_0.1A2**	**15_0.1_2**	**15_1A2**	**15_1_2**	**15_10A2**	**15_10_2**	**18_0.1A2**	**18_0.1_2**	**18_1A2**	**18_1_2**	**18_10A2**	**18_10_2**	**20_0.1A2**	**20_0.1_2**
	-0.529	0.504	0.092	0.062	-0.290	0.124	-0.083	-0.067	0.602	0.212	0.570	-0.226	0.372	-0.007	0.513	0.001
	20_1A1	**20_1_1**	**20_10A1**	**20_10_1**	**25_0.1A1**	**25_0.1_1**	**25_1A1**	**25_1_1**	**25_10A1**	**25_10_1**	**30_0.1A1**	**30_0.1_1**	**30_1A1**	**30_1_1**	**30_10A1**	**30_10_1**
	20_1A2	**20_1_2**	**20_10A2**	**20_10_2**	**25_0.1A2**	**25_0.1_2**	**25_1A2**	**25_1_2**	**25_10A2**	**25_10_2**	**30_0.1A2**	**30_0.1_2**	**30_1A2**	**30_1_2**	**30_10A2**	**30_10_2**
	-0.694	0.133	-0.203	-0.308	0.137	-0.203	-0.256	0.116	-0.200	0.784	0.476	-0.499	-0.794	0.811	0.046	0.214
	(*) As there are so many degrees of freedom (df > = 2700) we could consider accepting the null hypothesis H_0, where H_0: $\mu_1 = \mu_2$ (the samples are equal) when |t| ≤ 1															

Supplementary Table S2.2. Sequencing features of the ninety-six microcosms and S (slurry), before and after applying the rarefaction to the set of sequences, classified by domain (Archaea and Bacteria).

	Number sequences		Number of OPUs		Number sequences (post-rarefaction)		Number of OPUs (post-rarefaction)	
SAMPLES	***Archaea***	***Bacteria***	***Archaea***	***Bacteria***	***Archaea***	***Bacteria***	***Archaea***	***Bacteria***
5_0.1A1	9,243	37,181	58	157	6,624	27,157	59	156
5_0.1A2	7,433	43,436	52	149	4,877	28,904	53	148
5_0.1_1	3,293	51,410	23	164	2,044	31,737	25	159
5_0.1_2	5,260	51,568	34	168	3,090	30,691	34	167
5_1A1	7,397	38,930	62	190	5,480	28,301	63	188
5_1A2	9,327	44,332	65	185	5,781	28,000	64	178
5_1_1	10,591	43,001	37	224	6,717	27,064	37	220
5_1_2	12,406	62,863	43	269	5,649	28,132	45	260
5_10A1	18,732	47,928	55	223	9,463	24,318	56	217
5_10A2	12,793	41,741	86	229	7,831	25,950	85	228
5_10_1	16,646	40,495	25	259	9,894	23,887	25	256
5_10_2	16,472	44,252	63	336	9,238	24,543	65	327
10_0.1A1	17,791	43,861	33	133	9,800	23,981	34	130
10_0.1A2	22,320	43,710	40	141	11,398	22,383	38	135
10_0.1_1	13,472	32,521	26	126	9,890	23,891	25	125
10_0.1_2	17,641	37,265	27	134	10,740	23,041	27	134
10_1A1	23,332	38,375	33	136	12,840	20,941	34	129
10_1A2	19,950	28,321	31	124	14,013	19,768	31	123
10_1_1	26,342	26,698	23	134	16,827	16,954	23	132
10_1_2	22,682	45,493	38	162	11,234	22,547	38	159
10_10A1	13,489	35,877	21	114	9,212	24,569	21	112
10_10A2	11,066	42,451	24	126	6,907	26,874	24	124
10_10_1	21,884	44,407	27	193	11,198	22,583	27	180
10_10_2	13,729	43,818	29	159	8,082	25,699	29	156
12_0.1A1	22,963	35,875	29	134	13,132	20,649	28	133
12_0.1A2	8,125	50,979	60	158	4,670	29,111	60	156
12_0.1_1	11,647	44,607	53	145	7,026	26,755	53	144
12_0.1_2	12,020	51,673	52	175	6,476	27,305	53	172
12_1A1	15,650	40,130	39	131	9,453	24,328	40	126
12_1A2	12,170	41,077	63	141	7,823	25,958	64	137
12_1_1	22,212	30,750	23	122	14,167	19,614	23	119
12_1_2	11,769	49,432	47	182	6,297	27,484	47	178
12_10A1	9,289	42,434	53	128	6,086	27,695	53	127
12_10A2	10,251	52,133	69	172	5,625	28,156	70	166
12_10_1	9,727	47,013	43	154	5,795	27,986	43	151
12_10_2	8,123	38,972	43	150	5,877	27,904	43	148
15_0.1A1	23,095	31,080	26	103	14,244	19,537	26	101
15_0.1A2	22,144	29,805	24	114	14,242	19,539	23	112
15_0.1_1	22,582	33,190	26	123	13,723	20,058	26	120
15_0.1_2	10,861	43,682	55	147	6,826	26,955	54	146
15_1A1	23,902	29,570	28	114	15,083	18,698	28	111
15_1A2	25,897	35,324	35	125	14,295	19,486	34	119
15_1_1	22,891	33,658	31	134	13,690	20,091	31	130
15_1_2	20,373	33,856	29	124	12,700	21,081	30	122
15_10A1	18,045	34,024	27	110	11,662	22,119	28	107
15_10A2	14,741	38,805	23	104	9,274	24,507	23	103
15_10_1	11,479	37,507	19	115	7,986	25,795	18	114
15_10_2	17,181	32,954	30	136	11,644	22,137	29	133
18_0.1A1	31,834	44,722	51	171	13,969	19,812	51	163
18_0.1A2	20,935	36,273	30	93	12,301	21,480	31	88
18_0.1_1	30,418	36,059	37	132	15,546	18,235	37	129
18_0.1_2	25,063	36,017	40	121	13,878	19,903	40	120
18_1A1	27,475	41,715	35	131	13,321	20,460	36	128
18_1A2	22,893	30,911	39	127	14,371	19,410	38	121
18_1_1	20,782	25,207	30	97	15,377	18,404	31	95
18_1_2	15,680	34,375	28	116	10,597	23,184	28	116
18_10A1	21,588	43,866	33	104	11,090	22,691	32	97
18_10A2	18,443	39,171	28	103	10,778	23,003	29	100
18_10_1	18,373	32,718	24	107	12,306	21,475	24	106
18_10_2	16,735	34,489	21	105	11,047	22,734	22	102
20_0.1A1	11,089	47,677	30	102	6,412	27,369	29	101
20_0.1A2	17,449	29,637	37	125	12,476	21,305	36	123
20_0.1_1	21,276	33,784	31	105	12,933	20,848	31	104
20_0.1_2	23,179	31,861	34	101	14,238	19,543	34	100
20_1A1	23,335	25,591	36	110	16,010	17,771	35	109
20_1A2	18,363	46,360	58	129	9,632	24,149	57	127
20_1_1	16,350	35,214	25	97	10,646	23,135	25	94

20_1_2	20,715	27,897	39	116	14,391	19,390	40	114
20_10A1	19,333	33,022	33	109	12,453	21,328	34	107
20_10A2	16,975	40,011	30	86	10,031	23,750	29	84
20_10_1	14,637	24,004	30	83	12,783	20,998	29	83
20_10_2	17,661	25,339	37	115	13,931	19,850	38	114
25_0.1A1	6,828	31,479	29	77	6,098	27,683	29	75
25_0.1A2	8,491	27,063	28	86	8,096	25,685	28	84
25_0.1_1	9,387	30,628	32	76	7,988	25,793	31	74
25_0.1_2	18,544	24,841	33	96	14,448	19,333	33	94
25_1A1	10,802	41,569	42	104	6,876	26,905	42	102
25_1A2	10,880	48,615	38	108	6,223	27,558	38	106
25_1_1	7,784	44,185	19	50	5,074	28,707	19	50
25_1_2	22,744	26,055	38	111	15,685	18,096	37	110
25_10A1	13,131	37,985	24	96	8,747	25,034	24	94
25_10A2	25,097	30,418	46	153	15,248	18,533	46	148
25_10_1	27,518	35,320	35	112	14,884	18,897	35	111
25_10_2	23,249	22,781	39	92	17,158	16,623	39	92
30_0.1A1	18,976	40,142	35	125	10,811	22,970	34	124
30_0.1A2	8,477	39,942	28	87	5,935	27,846	27	86
30_0.1_1	20,883	20,618	37	113	17,081	16,700	37	112
30_0.1_2	22,877	26,693	42	109	15,651	18,130	41	109
30_1A1	7,355	26,426	31	82	7,471	26,310	31	82
30_1A2	18,895	30,476	44	132	12,876	20,905	43	128
30_1_1	29,605	29,669	33	114	16,957	16,824	33	114
30_1_2	23,274	20,212	38	94	17,963	15,818	38	94
30_10A1	14,047	30,770	37	126	10,609	23,172	37	123
30_10A2	13,706	30,367	37	129	10,535	23,246	37	128
30_10_1	16,550	24,722	30	85	13,627	20,154	30	84
30_10_2	15,439	22,977	33	83	13,571	20,210	32	82
S	6,579	31,433	40	116	5,878	27,903	39	116
ALL	**1,632,127**	**3,559,770**	**213**	**1,301**	**1,032,632**	**2,244,125**	**210**	**1,258**
Total of sequences	**5,191,897**				**3,276,757**			
Total OPUs			**1,514**				**1,468**	

Supplementary Table S2.3. Change percentage (%) with standard deviation for each duplicate of microcosms calculated for the alpha-diversity indices of Chao-1, Shannon and Dominance in relation to the inoculum (S). This equivalent percentage is estimated from the change that each sample experiments considering the slurry (S) as reference value. A positive or negative percentage indicate that the values have incremented or decremented respectively regarding to the slurry.

	Change percentage in Archaea (%)			Change percentage in Bacteria (%)		
	Chao-1	**Shannon**	**Dominance**	**Chao-1**	**Shannon**	**Dominance**
5_0.1A	43.6±10.9	15.6±3.7	-2.2±18.9	32.1±5.2	18.7±3.8	-35.4±18.1
5_1A	62.8±1.8	17.9±6.5	-0.4±17.9	58±6.4	27.1±3.8	-50.3±0.6
5_10A	80.8±52.6	19.1±19.6	-10.3±42	93.8±5.5	39.5±1.4	-73.9±0.3
5_0.1	-24.4±16.3	-45.7±7.9	402.9±99.7	41.9±5.4	17.7±2.4	-9.9±16.1
5_1	5.1±14.5	-51.2±0.4	479.2±24.1	112.5±25.4	43.6±4	-74.8±3.8
5_10	15.4±72.5	-46±39.4	381.3±307.3	152.2±42.9	36.4±33.9	-33.1±73
10_0.1A	-7.7±7.3	-39.1±8.3	276.8±94	15.6±3.2	14.9±0.9	-43.6±0.2
10_1A	-16.7±5.4	-55.7±3.8	434.9±28.2	9.4±3.7	10.3±6.8	-29.2±19.1
10_10A	-42.3±5.4	-46.1±6.7	296.2±70	2.9±8.7	5.1±10.4	-16±29.7
10_0.1	-33.3±3.6	-34±5.7	175.9±64.2	12.5±4.3	0±2.1	29.6±10.2
10_1	-21.4±27.8	-35.6±4.9	190.2±5.1	26.6±17.9	7.7±8	1.3±38.7
10_10	-26.9±5.4	-41.6±14.3	256.8±165.5	47.1±17.6	17.6±4.4	-45.5±11.2
12_0.1A	12.8±58	-19.4±47.5	177.9±255.7	25.1±13.3	12.2±5	-35.3±22.1
12_1A	33.3±43.5	-15.3±37.9	171.9±213.9	16.1±5.9	15.3±2.2	-44.6±3.7
12_10A	57.7±30.8	21.9±10.8	-35.2±21.1	29.7±20.1	10.8±7.1	-20±8.6
12_0.1	35.9±0	10±5	-14.7±11.1	37.7±18	15.1±2.8	-16.6±2.2
12_1	-10.3±43.5	-11.7±25.7	40.4±72.2	28.2±36.2	12.6±6.7	-19.2±0.5
12_10	10.3±0	6.9±7.3	-7.6±29	29±2	14.5±2.8	-15.4±2.1
15_0.1A	-37.2±5.4	-50.2±0.9	304.8±9.5	-7.8±6.5	4.6±4.3	-15.7±21.2
15_1A	-20.5±10.9	-48.2±3.3	306.4±34.6	-0.7±4.6	5.2±3.5	-11.5±21.1
15_10A	-34.6±9.1	-40.1±3.5	193.6±21.7	-5.2±0	9.8±3	-43.9±6.7
15_0.1	2.6±50.8	-10.6±31.4	62.9±100.2	16.4±18	13.8±3	-25.6±32.1
15_1	-21.8±1.8	-27.8±5.9	121.4±48.6	8.9±4.9	14.6±5.6	-41.3±13.7
15_10	-39.7±19.9	-36.7±7.6	171.4±31.4	6.6±11.6	11.9±4.1	-34.3±10.1
18_0.1A	5.6±36.9	-38.6±0.4	226.7±30.9	14.4±42.3	-8.4±1.8	46.3±34.5
18_1A	-3.9±5.4	-39.4±4.6	212.6±23.9	9.2±3.3	-3.7±0.1	16.3±15.4
18_10A	-21.8±5.4	-38.3±1	167.7±12.9	-14.6±2.4	4.8±2.3	-39.9±4
18_0.1	-1.3±5.4	-34.1±0.4	207.9±41.4	8.2±4.6	10.5±1.4	-39.1±4.8
18_1	-24.4±5.4	-36.8±0.3	201.4±12	-9.1±12.8	9.2±1.1	-40±3.5
18_10	-41±3.6	-41.4±6.2	193±40.7	-9.9±2.4	3.9±2.6	-31±5.4
20_0.1A	-16.7±12.7	-19.8±5.6	112.4±33.2	-3.3±13.4	-4.9±13.3	18.1±22.6
20_1A	18±39.9	-15.9±28.7	97.1±143.2	2.2±10.6	-1.1±6.1	17±32.3
20_10A	-19.2±9.1	-31.6±11.6	153.7±70.4	-17±14.3	-6±14	13.3±50.1
20_0.1	-14.7±2.7	-27.8±2.4	150±8	-11.1±3.1	9.2±1.8	-38.5±10.1
20_1	-16.7±27.2	-31.5±8.4	172.9±41.3	-10.3±12.3	-3.6±17	25.9±81.5
20_10	-14.1±16.3	-24.5±0.5	106.5±7.1	-14.8±19.3	6.5±2.7	-33.4±13.5
25_0.1A	-26.9±1.8	-11.7±3.2	44.2±36.2	-31.2±5.1	-21.1±12.5	97.1±64.7
25_1A	2.6±7.3	-7.6±3.7	43.7±25.8	-9.9±3	-17.1±2.7	63.2±13.8
25_10A	-10.3±39.9	-21.7±4.7	94.6±3.5	5.7±33.6	-4.5±14.9	20.4±33.3
25_0.1	-18±3.6	-5.8±3.8	9.7±12.5	-27.6±12.2	-7.1±16.4	22.9±62.9
25_1	-28.2±32.6	-15.6±10.7	52.8±39.4	-30.8±36.6	-15.4±43.6	72.9±180.8
25_10	-3.2±4.5	-23.6±9.3	109.2±46.2	-11.9±11.2	0.7±0.4	-8±2.6
30_0.1A	-21.8±12.7	-8.8±4.9	43.4±14.4	-9.2±23	-9.9±16.8	25.6±59.6
30_1A	-5.1±21.8	-11.6±6.3	70.1±42.6	-8.4±29.6	-14.7±31.7	98.3±176.3
30_10A	-5.1±0	-16.1±2.4	91.5±10.1	8.8±2.7	1.5±1.1	-9.9±8.6
30_0.1	0.4±7.9	-13.6±6.7	86.8±47.5	-2.4±0.9	6.3±0	-30±0.1
30_1	-9±9.1	-16±2.5	102±21.5	-8.3±11.4	6.2±0.2	-31.9±4.4
30_10	-20.5±3.6	-6.9±1.9	27.2±10.1	-27.8±1.5	-0.1±4.8	-8.4±26.1

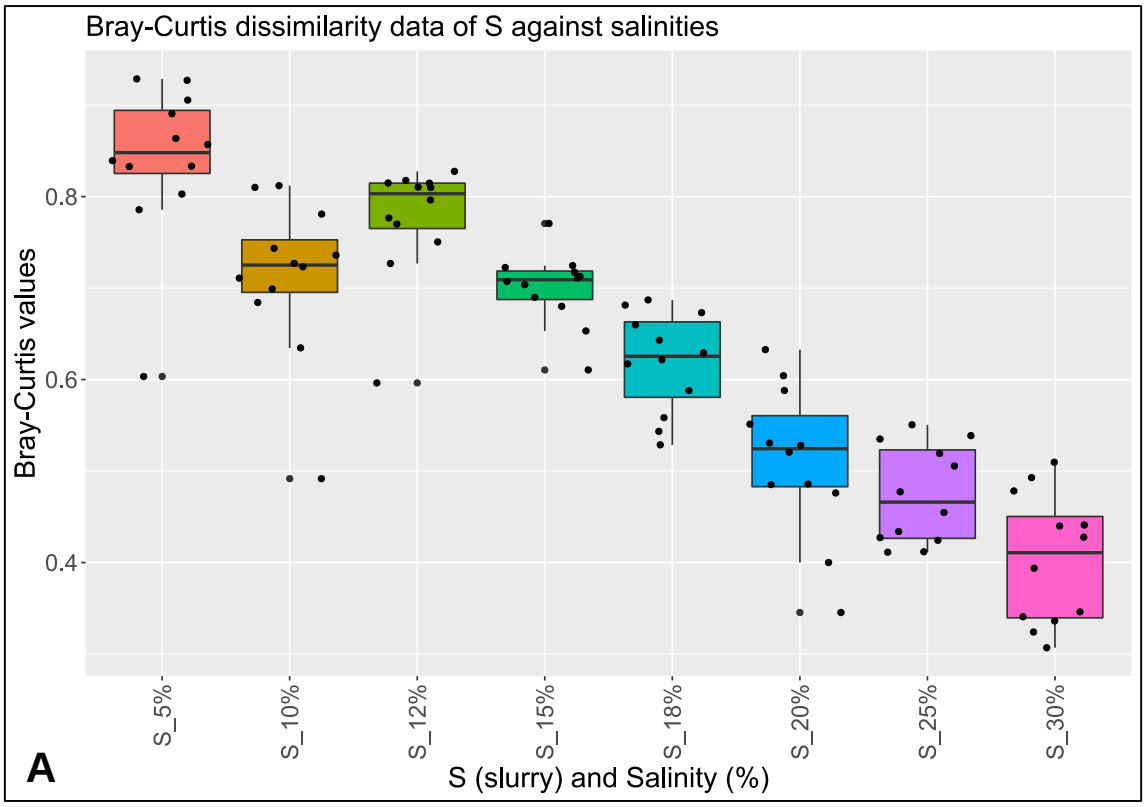
Bray-Curtis dissimilarity data of S against salinities
Bray-Curtis values
0.8
0.6
0.4
S_5%
S_10%
S_12%
S_15%
S_18%
S_20%
S_25%
S_30%
S (slurry) and Salinity (%)
A

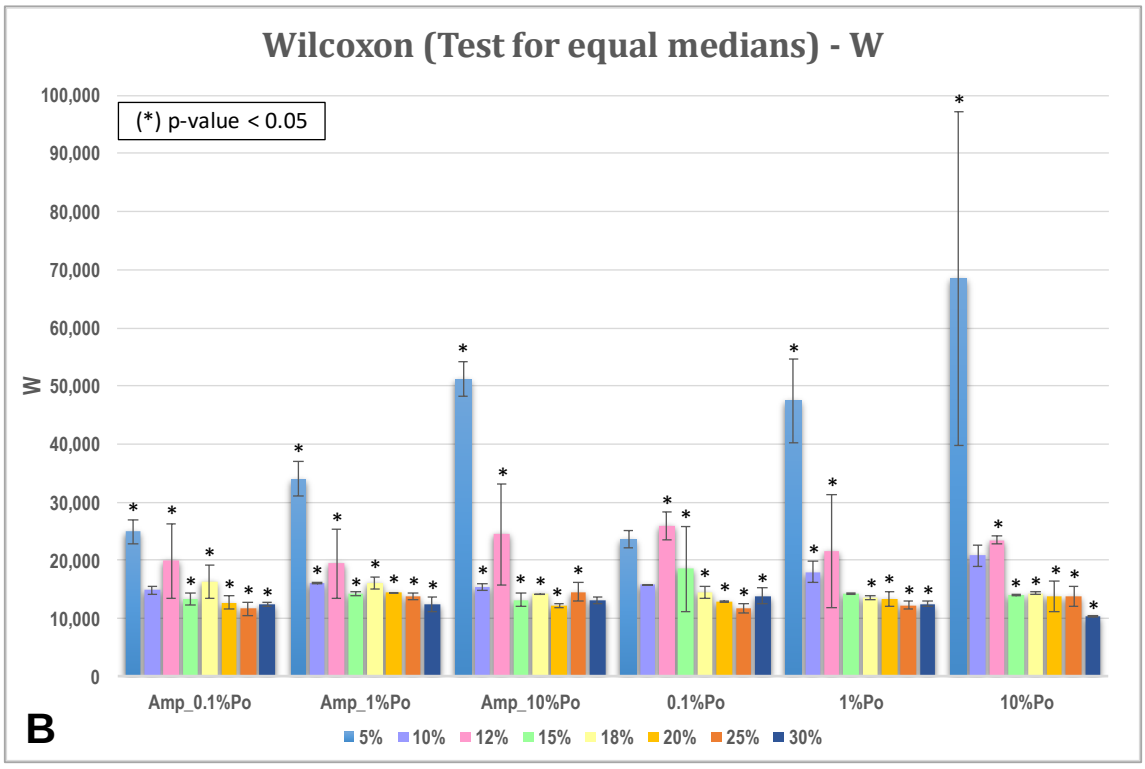
Wilcoxon (Test for equal medians) - W
(*) p-value < 0.05
W
100,000
90,000
80,000
70,000
60,000
50,000
40,000
30,000
20,000
10,000
0
Amp_0.1%Po
Amp_1%Po
Amp_10%Po
0.1%Po
1%Po
10%Po
5%
10%
12%
15%
18%
20%
25%
30%
B

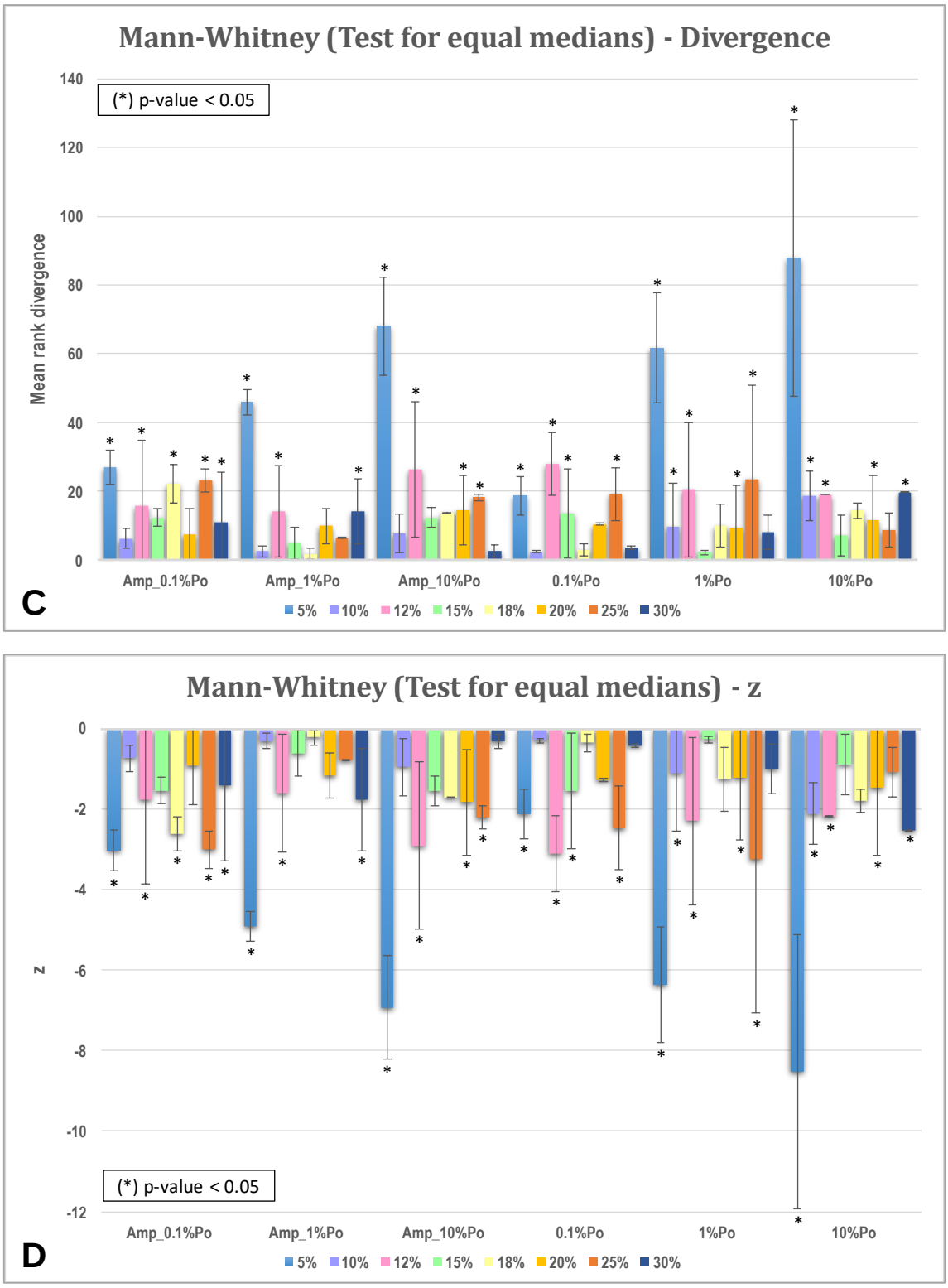

Supplementary Figure S2.1. A. Boxplots of Bray-Curtis dissimilarity data of S (slurry) against the eight salinities. From left to right, salinities of 5%, 10%, 12%, 15%, 18%, 20%, 25% and 30% are shown. **B**. Wilcoxon scores (W) from Wilcoxon non-parametric test applied to the microcosms against S. **C**. Divergence results from Mann-Whitney non-parametric test applied to the microcosms against S. **D**. Z-scores from Mann-Whitney non-parametric test applied to the microcosms against S. Scores W, z and the Divergence are displayed in six groups

according to ampicillin presence and substrate concentration, with the eight salinities differentiated by colors. Statistically significant values are marked with ***** (p-value < 0.05) in barplots.

Supplementary Table S2.4. Kolmogorov-Smirnov and T-test results obtained from the comparison among the microcosms of 30% of salinity and the slurry (S). The statistically significance of the data is according to consider the samples as equal, where D-values (in the first row) and p-values (second row) for the Kolmogorov-Smirnov test and t-values of T-test are displayed.

Kolmogorov-Smirnov: D ≤ 1.36 and p ≥ 0.05											
30_0.1A1	**30_0.1A2**	**30_0.1_1**	**30_0.1_2**	**30_1A1**	**30_1A2**	**30_1_1**	**30_1_2**	**30_10A1**	**30_10A2**	**30_10_1**	**30_10_2**
0.011	0.039	0.020	0.022	0.031	0.011	0.021	0.024	0.018	0.017	0.031	0.028
1.000	0.218	0.919	0.852	0.495	1.000	0.899	0.798	0.965	0.984	0.495	0.616
t-test: |t| ≤ 1 (*)											
30_0.1A1	**30_0.1A2**	**30_0.1_1**	**30_0.1_2**	**30_1A1**	**30_1A2**	**30_1_1**	**30_1_2**	**30_10A1**	**30_10A2**	**30_10_1**	**30_10_2**
1.195	0.509	0.225	0.738	-0.219	0.739	1.145	0.341	0.444	0.385	0.231	0.028

(*) As there are so many degrees of freedom (df > = 3200) we could consider accepting the null hypothesis H_0, where H_0: $\mu_1 = \mu_2$ (the samples are equal) when $|t| \leq 1.2$

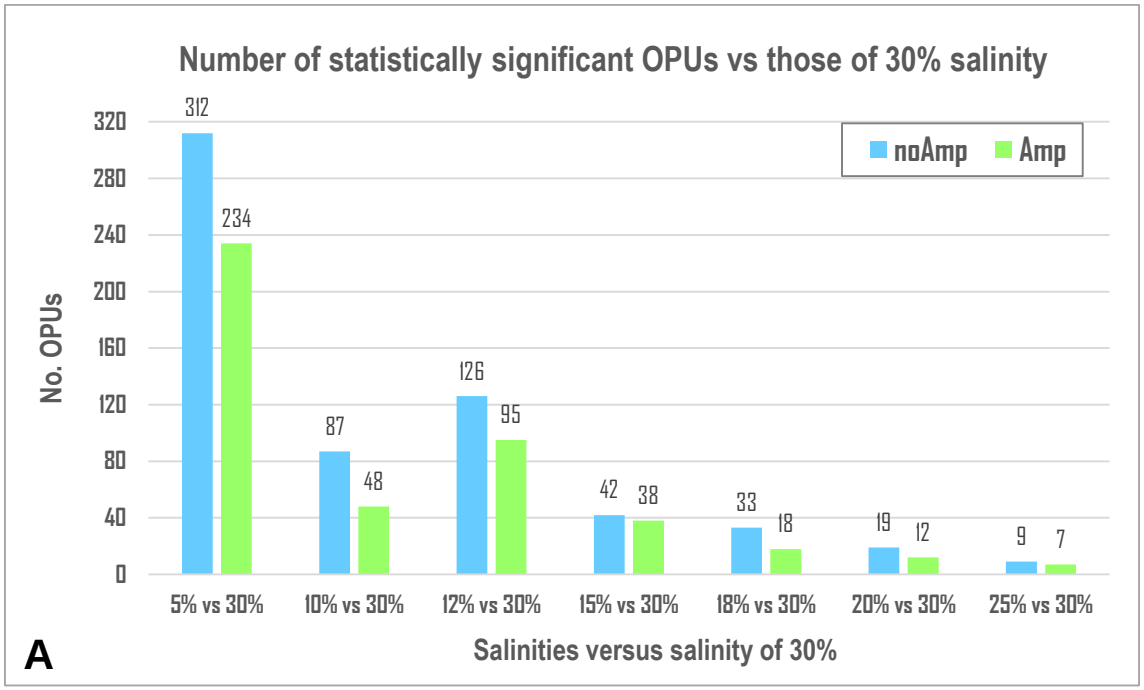

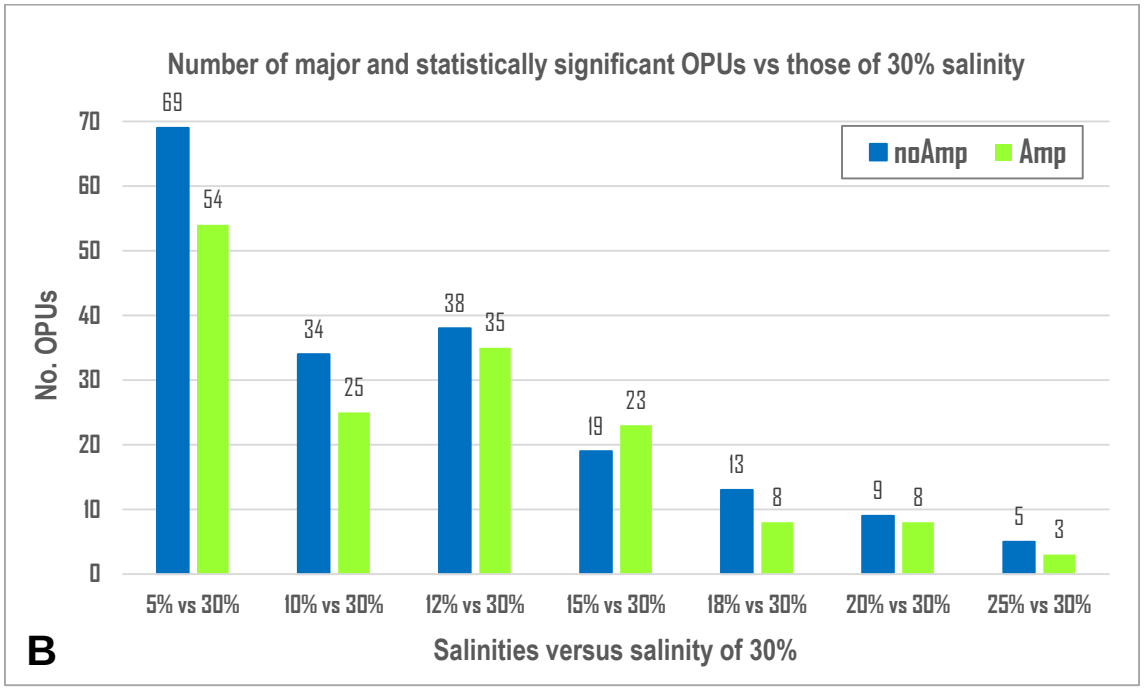

Supplementary Figure S2.2. A. Graphic of number of statistically significant OPUs of a salinity against OPUs at 30% of salinity. **B**. Representation of number of major (≥1% of relative abundances) and statistically significant OPUs versus OPUs at 30% of salinity. Each plot bar on the left signifies samples without ampicillin and on the right those with antibiotic. The complete list of counted OPUs in plot B is shown in the spreadsheet Table ST2.3.

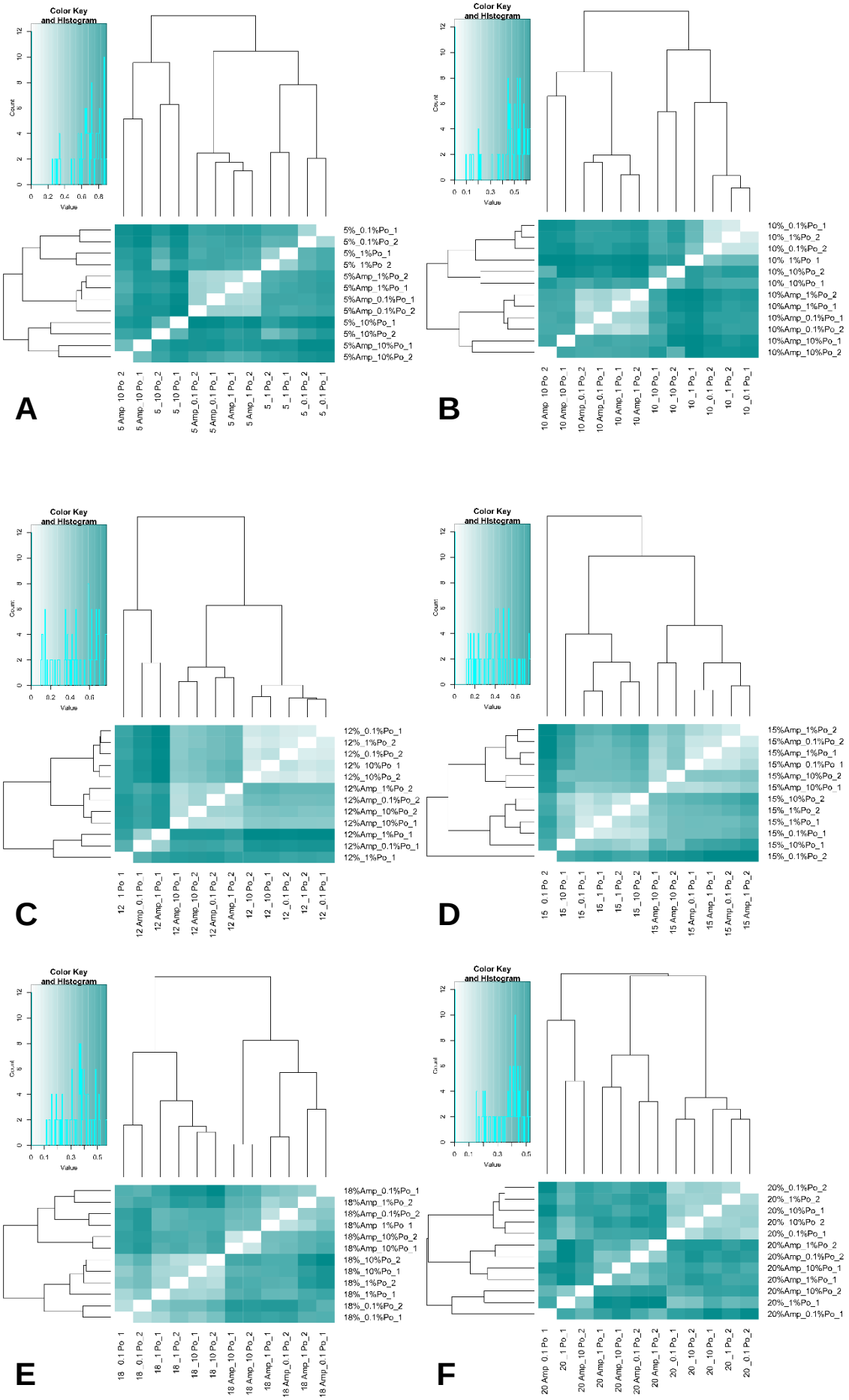
Color Key and Histogram
Count
Value
A
5%_0.1%Po_1
5%_0.1%Po_2
5%_1%Po_1
5%_1%Po_2
5%Amp_1%Po_2
5%Amp_1%Po_1
5%Amp_0.1%Po_1
5%Amp_0.1%Po_2
5%_10%Po_1
5%_10%Po_2
5%Amp_10%Po_1
5%Amp_10%Po_2
5 Amp_10 Po_2
5 Amp_10 Po_1
5 _10 Po_2
5 _10 Po_1
5 Amp_0.1 Po_2
5 Amp_0.1 Po_1
5 Amp_1 Po_1
5 Amp_1 Po_2
5 _1 Po_2
5 _1 Po_1
5 _0.1 Po_2
5 _0.1 Po_1
B
10%_0.1%Po_1
10%_1%Po_2
10%_0.1%Po_2
10%_1%Po_1
10%_10%Po_2
10%_10%Po_1
10%Amp_1%Po_2
10%Amp_1%Po_1
10%Amp_0.1%Po_1
10%Amp_0.1%Po_2
10%Amp_10%Po_1
10%Amp_10%Po_2
10 Amp_10 Po_2
10 Amp_10 Po_1
10 Amp_0.1 Po_2
10 Amp_0.1 Po_1
10 Amp_1 Po_1
10 Amp_1 Po_2
10 _10 Po_1
10 _1 Po_1
10 _0.1 Po_2
10 _1 Po_2
10 _0.1 Po_1
C
12%_0.1%Po_1
12%_1%Po_2
12%_0.1%Po_2
12%_10%Po_1
12%_10%Po_2
12%Amp_1%Po_2
12%Amp_0.1%Po_2
12%Amp_10%Po_2
12%Amp_10%Po_1
12%Amp_1%Po_1
12%Amp_0.1%Po_1
12%_1%Po_1
12 _1 Po_1
12 Amp_0.1 Po_1
12 Amp_1 Po_1
12 Amp_10 Po_1
12 Amp_10 Po_2
12 Amp_0.1 Po_2
12 Amp_1 Po_2
12 _10 Po_1
12 _0.1 Po_2
12 _1 Po_2
12 _0.1 Po_1
D
15%Amp_1%Po_2
15%Amp_0.1%Po_2
15%Amp_1%Po_1
15%Amp_0.1%Po_1
15%Amp_10%Po_2
15%Amp_10%Po_1
15%_10%Po_2
15%_1%Po_2
15%_1%Po_1
15%_0.1%Po_1
15%_10%Po_1
15%_0.1%Po_2
15 _0.1 Po_2
15 _10 Po_1
15 _0.1 Po_1
15 _1 Po_1
15 _1 Po_2
15 _10 Po_2
15 Amp_10 Po_1
15 Amp_10 Po_2
15 Amp_0.1 Po_1
15 Amp_1 Po_1
15 Amp_0.1 Po_2
15 Amp_1 Po_2
E
18%Amp_0.1%Po_1
18%Amp_1%Po_2
18%Amp_0.1%Po_2
18%Amp_1%Po_1
18%Amp_10%Po_2
18%Amp_10%Po_1
18%_10%Po_2
18%_10%Po_1
18%_1%Po_2
18%_1%Po_1
18%_0.1%Po_2
18%_0.1%Po_1
18 _0.1 Po_1
18 _0.1 Po_2
18 _1 Po_1
18 _1 Po_2
18 _10 Po_1
18 _10 Po_2
18 Amp_10 Po_1
18 Amp_10 Po_2
18 Amp_1 Po_1
18 Amp_0.1 Po_2
18 Amp_1 Po_2
18 Amp_0.1 Po_1
F
20%_0.1%Po_2
20%_1%Po_2
20%_10%Po_1
20%_10%Po_2
20%_0.1%Po_1
20%Amp_1%Po_2
20%Amp_0.1%Po_2
20%Amp_10%Po_1
20%Amp_1%Po_1
20%Amp_10%Po_2
20%_1%Po_1
20%Amp_0.1%Po_1
20 Amp_0.1 Po_1
20 _1 Po_1
20 Amp_10 Po_2
20 Amp_1 Po_1
20 Amp_10 Po_1
20 Amp_0.1 Po_2
20 Amp_1 Po_2
20 _0.1 Po_1
20 _10 Po_2
20 _10 Po_1
20 _1 Po_2
20 _0.1 Po_2

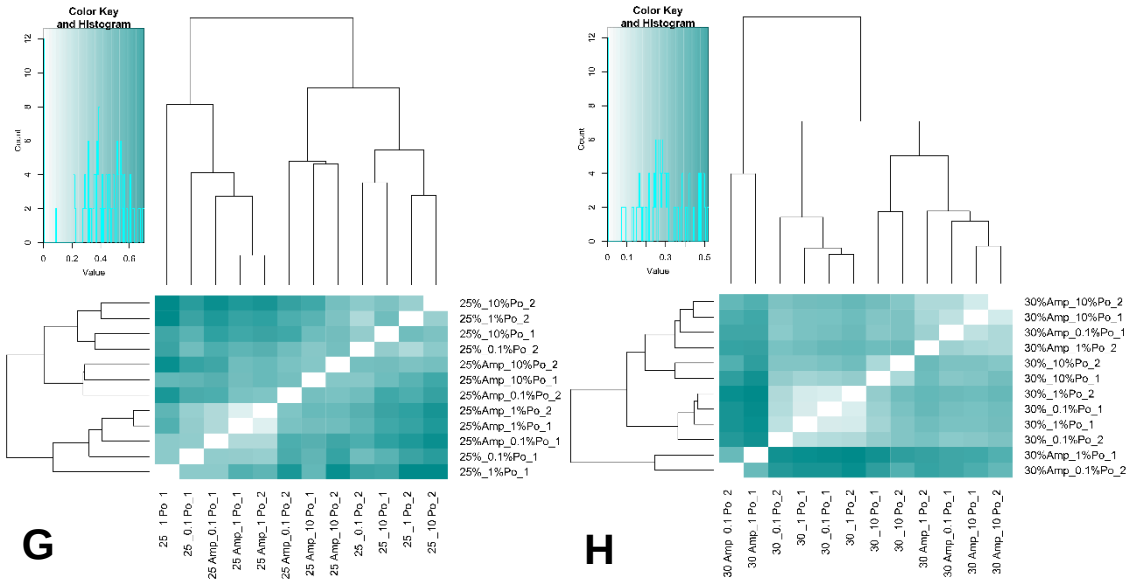

Supplementary Figure S2.3. A-H. Dendrograms based on Bray-Curtis dissimilarity using OPUs from 16S rRNA gene amplicons of the ninety-six microcosms, for the twelve samples at 5%, 10%, 12%, 15%, 18%, 20%, 25% and 30%, correspondingly.

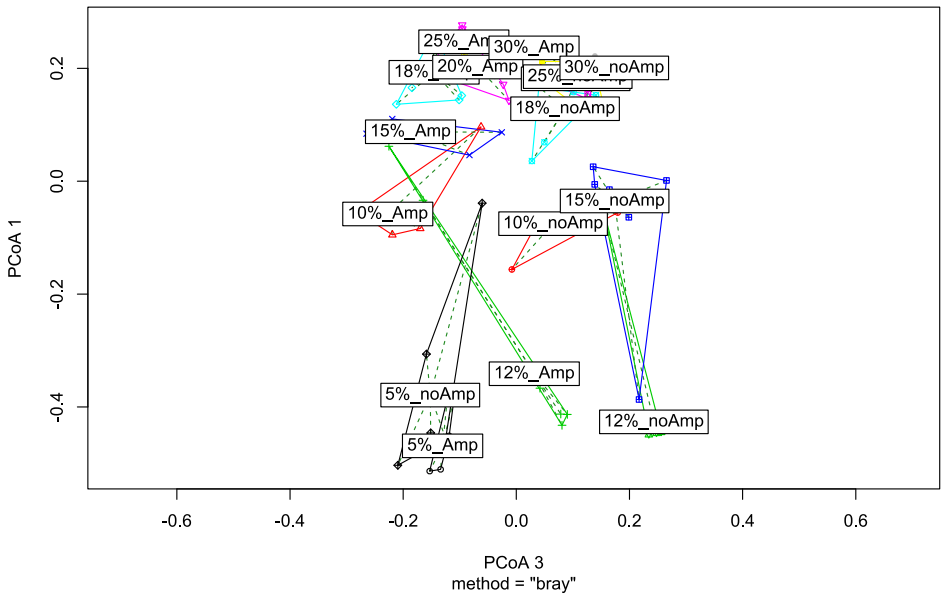

Supplementary Figure S2.4. Betadisper (with vegan package) performed to microcosms according to salinity and ampicillin presence. Data with same characteristic are grouped in colored polygons.

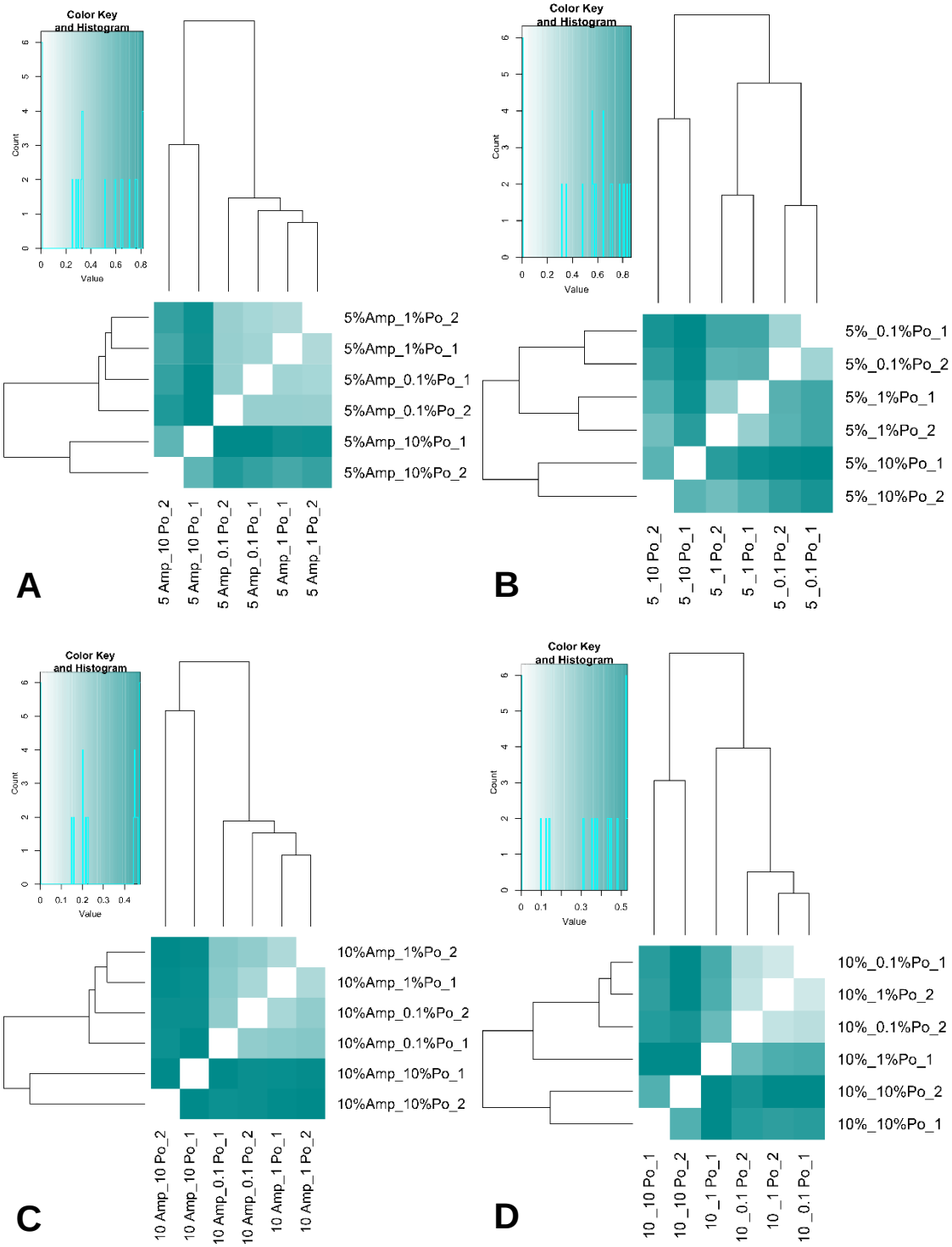
Color Key and Histogram
Count
Value
5%Amp_1%Po_2
5%Amp_1%Po_1
5%Amp_0.1%Po_1
5%Amp_0.1%Po_2
5%Amp_10%Po_1
5%Amp_10%Po_2
5 Amp_10 Po_2
5 Amp_10 Po_1
5 Amp_0.1 Po_2
5 Amp_0.1 Po_1
5 Amp_1 Po_1
5 Amp_1 Po_2
A
5%_0.1%Po_1
5%_0.1%Po_2
5%_1%Po_1
5%_1%Po_2
5%_10%Po_1
5%_10%Po_2
5 _10 Po_2
5 _10 Po_1
5 _1 Po_2
5 _1 Po_1
5 _0.1 Po_2
5 _0.1 Po_1
B
10%Amp_1%Po_2
10%Amp_1%Po_1
10%Amp_0.1%Po_2
10%Amp_0.1%Po_1
10%Amp_10%Po_1
10%Amp_10%Po_2
10 Amp_10 Po_2
10 Amp_10 Po_1
10 Amp_0.1 Po_1
10 Amp_0.1 Po_2
10 Amp_1 Po_1
10 Amp_1 Po_2
C
10%_0.1%Po_1
10%_1%Po_2
10%_0.1%Po_2
10%_1%Po_1
10%_10%Po_2
10%_10%Po_1
10 _10 Po_1
10 _10 Po_2
10 _1 Po_1
10 _0.1 Po_2
10 _1 Po_2
10 _0.1 Po_1
D

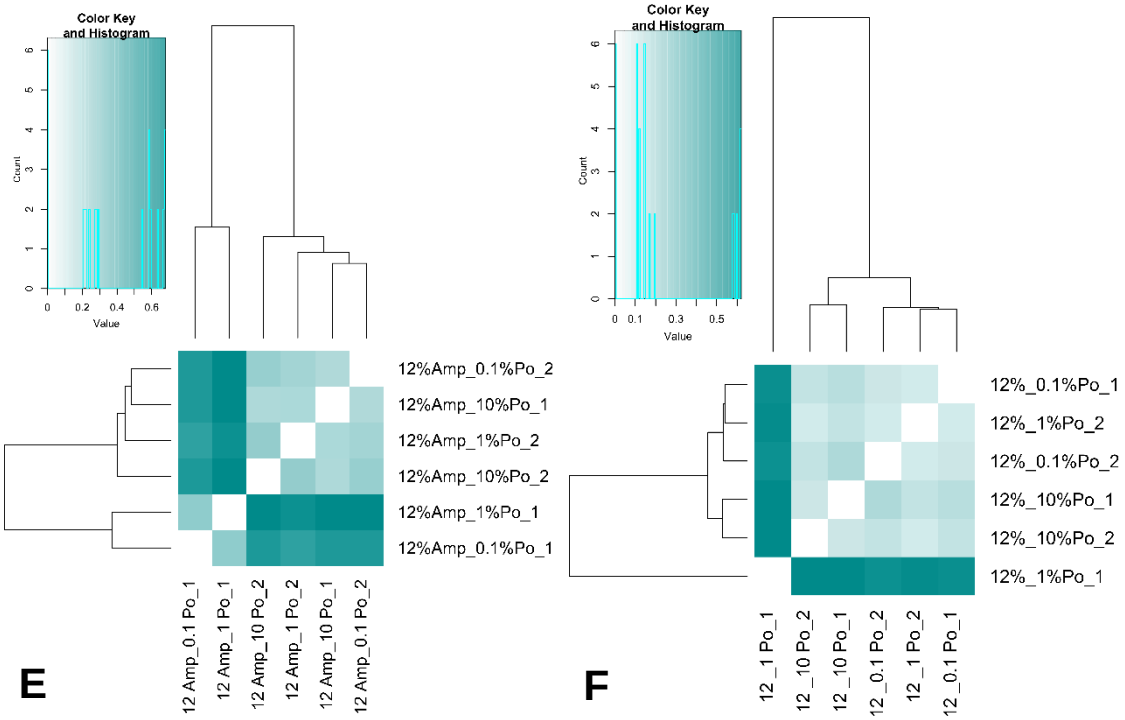
Color Key and Histogram
Count
Value
12%Amp_0.1%Po_2
12%Amp_10%Po_1
12%Amp_1%Po_2
12%Amp_10%Po_2
12%Amp_1%Po_1
12%Amp_0.1%Po_1
12 Amp_0.1 Po_1
12 Amp_1 Po_1
12 Amp_10 Po_2
12 Amp_1 Po_2
12 Amp_10 Po_1
12 Amp_0.1 Po_2
E
12%_0.1%Po_1
12%_1%Po_2
12%_0.1%Po_2
12%_10%Po_1
12%_10%Po_2
12%_1%Po_1
12 _1 Po_1
12 _10 Po_2
12 _10 Po_1
12 _0.1 Po_2
12 _1 Po_2
12 _0.1 Po_1
F

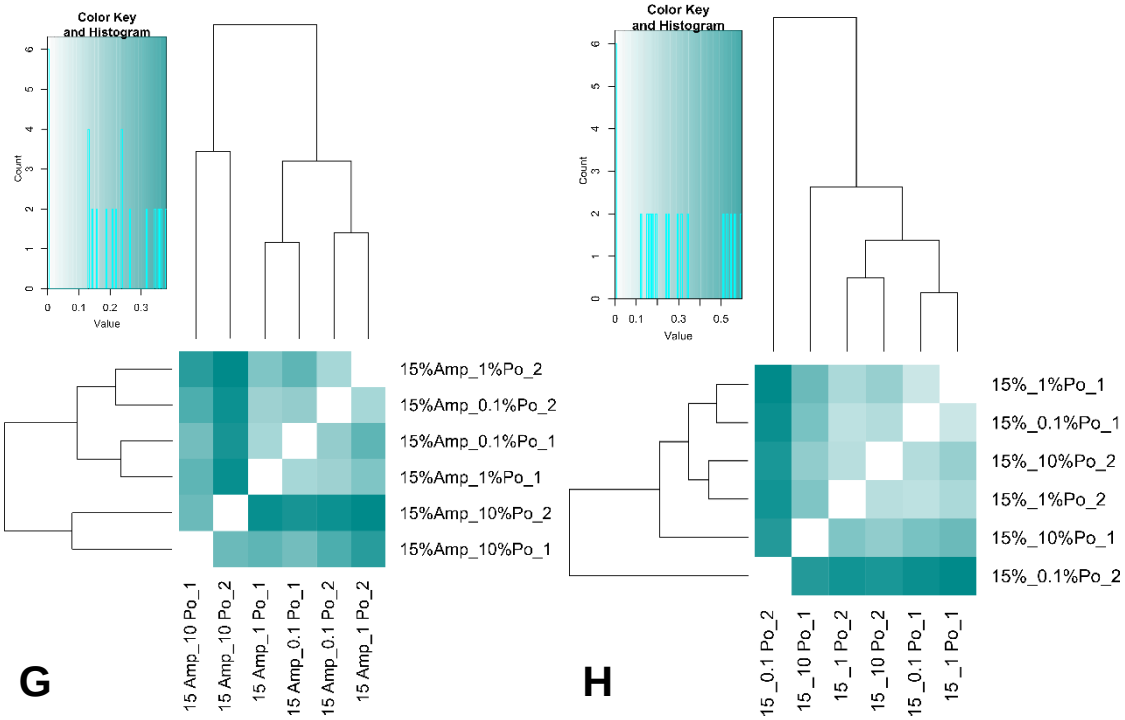
Color Key and Histogram
Count
Value
15%Amp_1%Po_2
15%Amp_0.1%Po_2
15%Amp_0.1%Po_1
15%Amp_1%Po_1
15%Amp_10%Po_2
15%Amp_10%Po_1
15 Amp_10 Po_1
15 Amp_10 Po_2
15 Amp_1 Po_1
15 Amp_0.1 Po_1
15 Amp_0.1 Po_2
15 Amp_1 Po_2
G
15%_1%Po_1
15%_0.1%Po_1
15%_10%Po_2
15%_1%Po_2
15%_10%Po_1
15%_0.1%Po_2
15 _0.1 Po_2
15 _10 Po_1
15 _1 Po_2
15 _10 Po_2
15 _0.1 Po_1
15 _1 Po_1
H

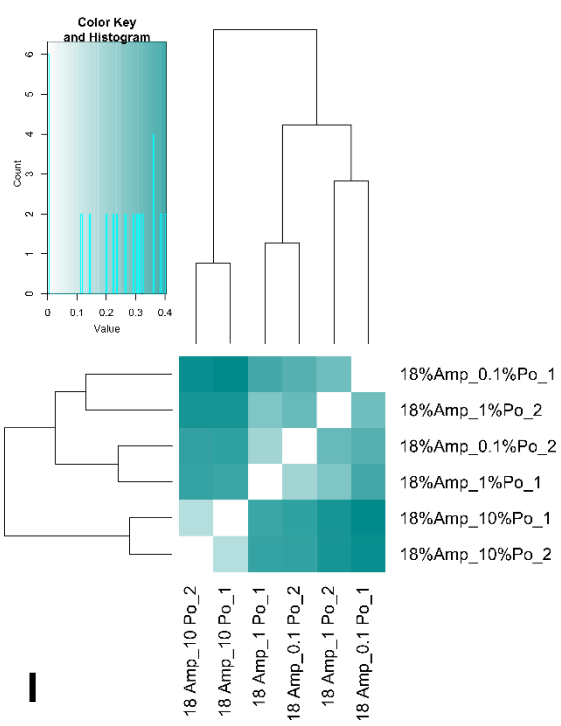
Color Key and Histogram
Count
Value
18%Amp_0.1%Po_1
18%Amp_1%Po_2
18%Amp_0.1%Po_2
18%Amp_1%Po_1
18%Amp_10%Po_1
18%Amp_10%Po_2
18 Amp_10 Po_2
18 Amp_10 Po_1
18 Amp_1 Po_1
18 Amp_0.1 Po_2
18 Amp_1 Po_2
18 Amp_0.1 Po_1

I

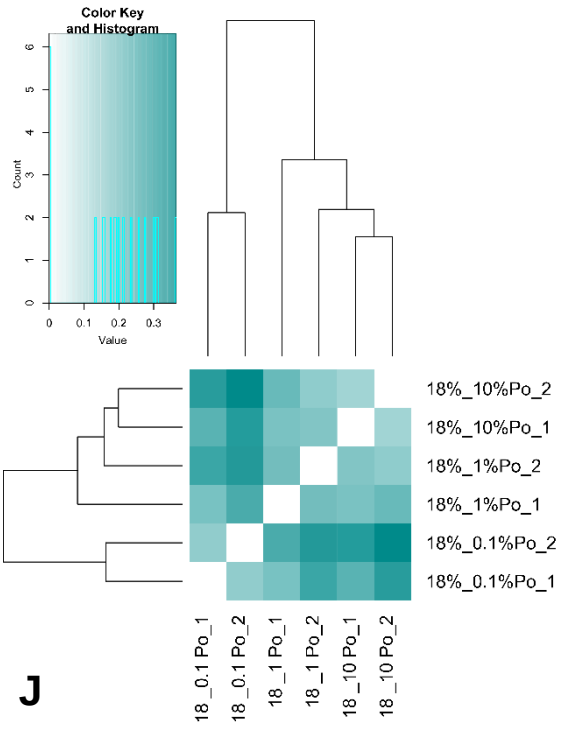
Color Key and Histogram
Count
Value
18%_10%Po_2
18%_10%Po_1
18%_1%Po_2
18%_1%Po_1
18%_0.1%Po_2
18%_0.1%Po_1
18 _0.1 Po_1
18 _0.1 Po_2
18 _1 Po_1
18 _1 Po_2
18 _10 Po_1
18 _10 Po_2

J

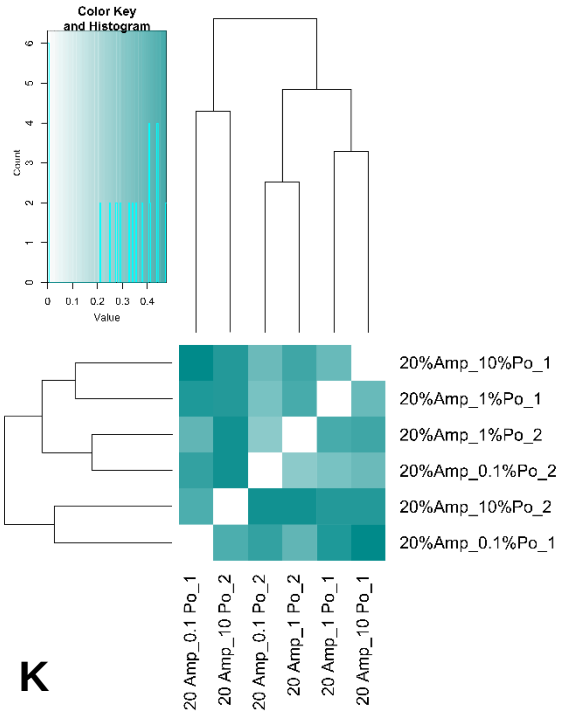
Color Key and Histogram
Count
Value
20%Amp_10%Po_1
20%Amp_1%Po_1
20%Amp_1%Po_2
20%Amp_0.1%Po_2
20%Amp_10%Po_2
20%Amp_0.1%Po_1
20 Amp_0.1 Po_1
20 Amp_10 Po_2
20 Amp_0.1 Po_2
20 Amp_1 Po_2
20 Amp_1 Po_1
20 Amp_10 Po_1

K

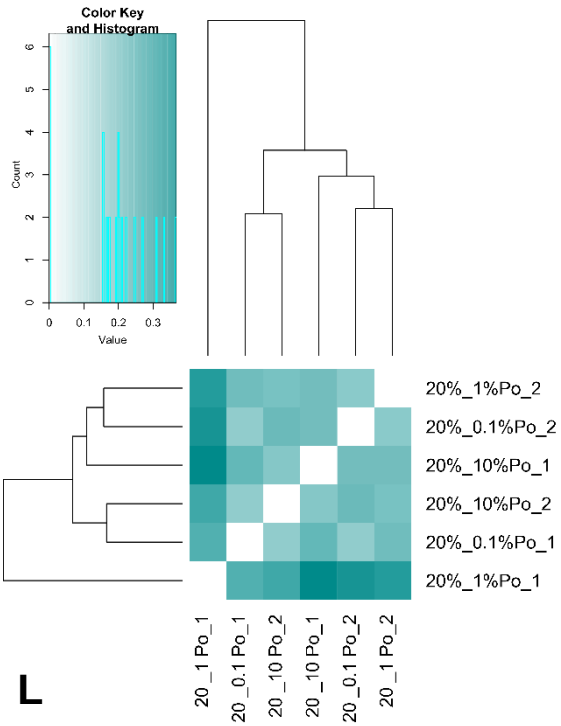
Color Key and Histogram
Count
Value
20%_1%Po_2
20%_0.1%Po_2
20%_10%Po_1
20%_10%Po_2
20%_0.1%Po_1
20%_1%Po_1
20 _1 Po_1
20 _0.1 Po_1
20 _10 Po_2
20 _10 Po_1
20 _0.1 Po_2
20 _1 Po_2

L

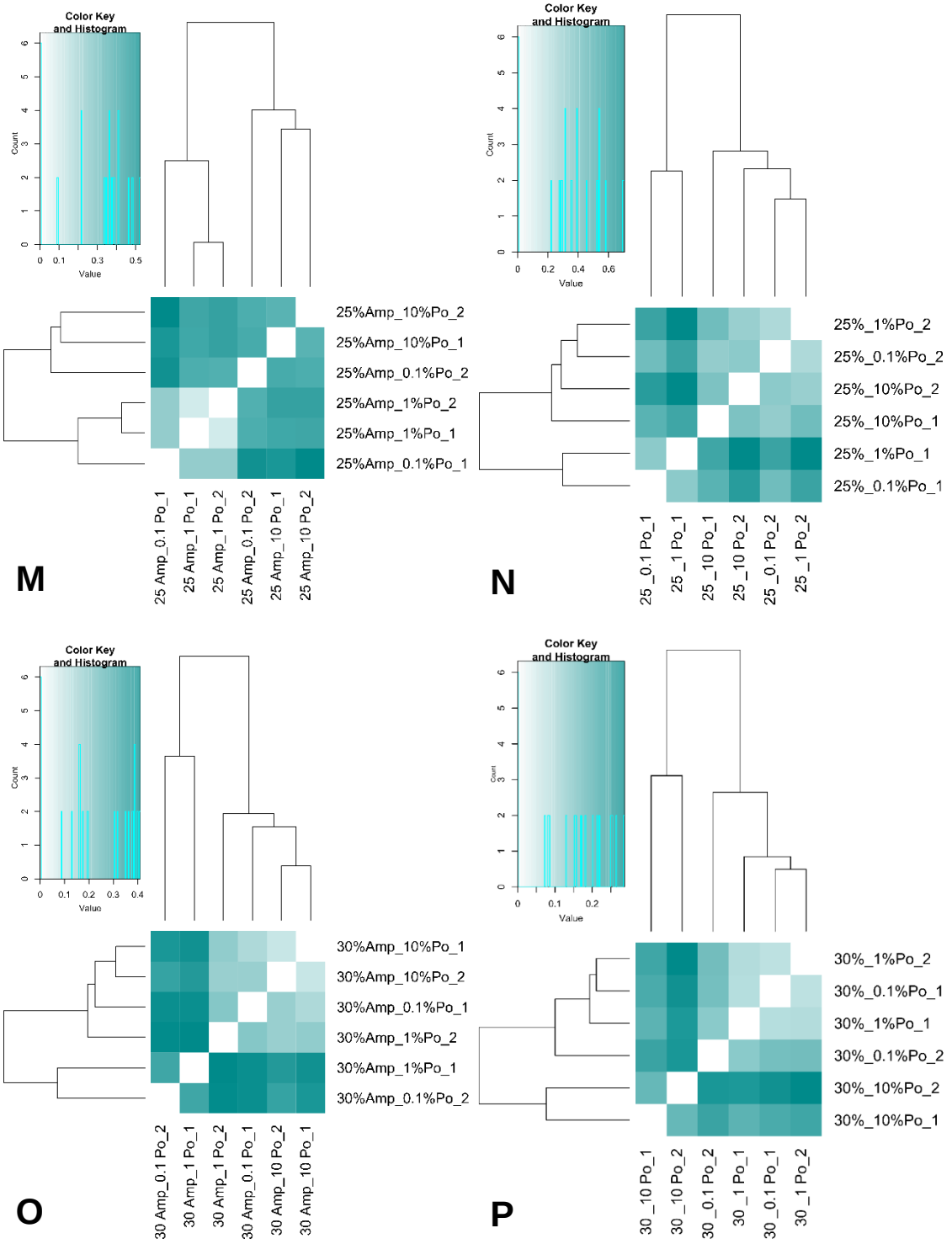

Supplementary Figure S2.5. Dendrograms according to Bray-Curtis dissimilarity based on OPUs from 16S rRNA gene amplicons of microcosms. Clustering dendrograms for the six samples with or without ampicillin and salinities of 5% (**A** and **B**), 10% (**C** and **D**), 12% (**E** and **F**), 15% (**G** and **H**), 18% (**I** and **J**), 20% (**K** and **L**), 25% (**M** and **N**) and 30% (**O** and **P**) are shown.

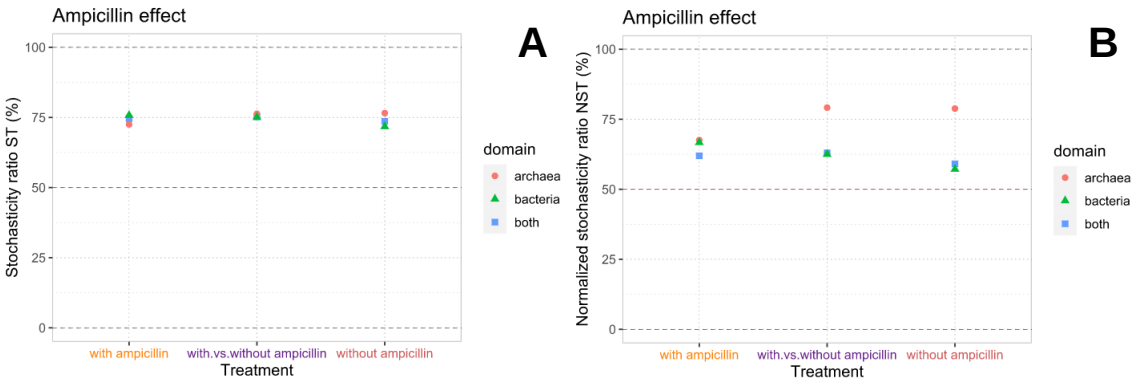
Ampicillin effect
A
Stochasticity ratio ST (%)
100
75
50
25
0
with ampicillin
with.vs.without ampicillin
without ampicillin
Treatment
domain
archaea
bacteria
both
Ampicillin effect
B
Normalized stochasticity ratio NST (%)
100
75
50
25
0
with ampicillin
with.vs.without ampicillin
without ampicillin
Treatment
domain
archaea
bacteria
both

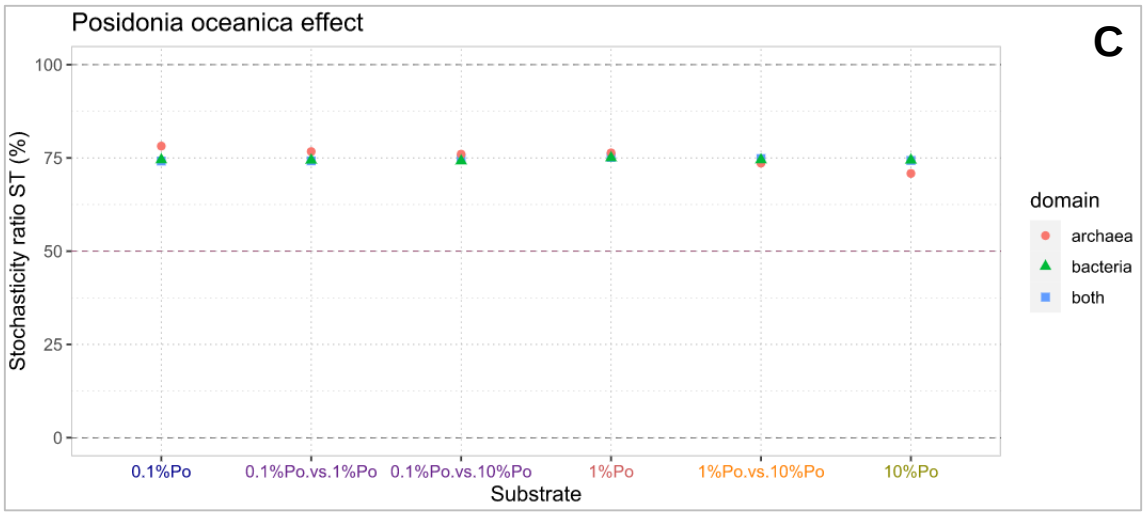
Posidonia oceanica effect
C
Stochasticity ratio ST (%)
100
75
50
25
0
0.1%Po
0.1%Po.vs.1%Po
0.1%Po.vs.10%Po
1%Po
1%Po.vs.10%Po
10%Po
Substrate
domain
archaea
bacteria
both

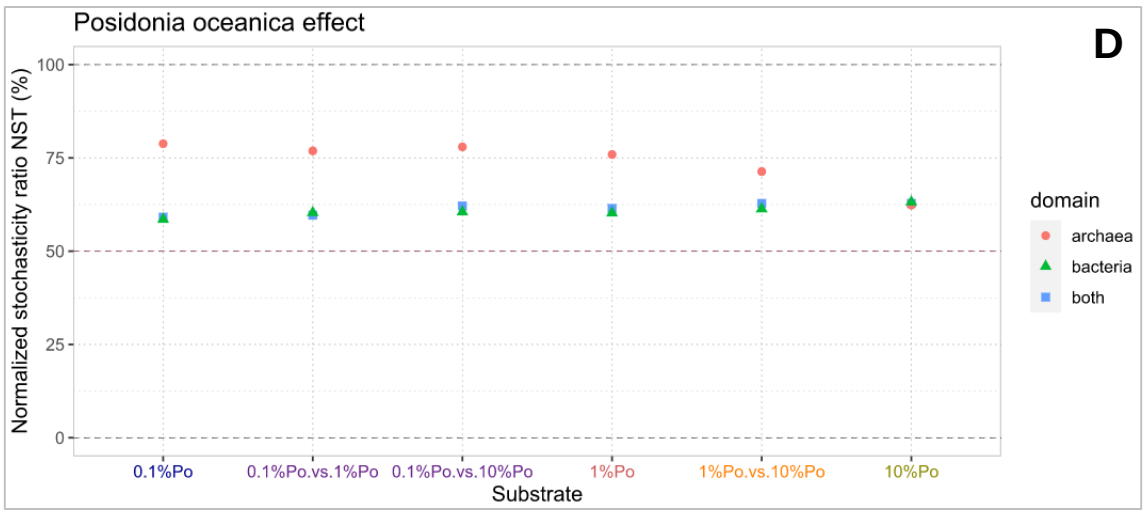
Posidonia oceanica effect
D
Normalized stochasticity ratio NST (%)
100
75
50
25
0
0.1%Po
0.1%Po.vs.1%Po
0.1%Po.vs.10%Po
1%Po
1%Po.vs.10%Po
10%Po
Substrate
domain
archaea
bacteria
both

Supplementary Figure S2.6. Stochasticity ratio (ST; **A**) and Normalized stochasticity ratio (NST; **B**) in percentage regarding to the ampicillin effect (group mean of ST and NST is plotted). In the x axis, treatments with and without ampicillin are compared. Stochasticity ratio (ST; **C**) and Normalized stochasticity ratio (NST; **D**) in percentage regarding to the susbtrate effect (group mean of ST and NST is plotted). In the x axis, the three substrate concentrations are evaluated individually or among them. Data from archaeal, bacterial or both domains are drawn in red, green and blue, respectively. Stochasticity ratio (ST; **E**) in percentage regarding to the ampicillin effect in relation to S for the microcosms. Data from Archaea, Bacteria or both are represented in circles, triangles and squares, respectively, whereas samples regarding to ampicillin are colored in red (with) or blue (without antibiotic).

Supplementary Table S2.5. Most relevant OPUs with relative abundances ≥ 5% and their putative associated metabolism. From left to right: OPU number and taxonomic classification from the closest relative reference. Potential metabolism hypothesized for each OPU is shown in the last column. OPUs belonging to Archaea are grey shaded, whereas bacterial OPUs are shown in blank.

#OPU	Closest relative reference	Putative metabolism (according to description of species)
4	Deep Sea Euryarchaeotic Group	Fermentation and Carbohydrate metabolism
23	Unc. KTK 4A	- Heterotrophic, Fermentative metabolism - Anaerobic formate and CO oxidation
25	Unc. Marine Benthic Group D and DHVEG-1	Two autotrophic pathways: Wood–Ljundahl using both H_4MPT and H_4folate as C_1carriers, and an incomplete dicarboxylate/4-hydroxybutyratecycle with alternative bypasses from pyruvate to malate/oxaloacetate during decarboxylation.
62	Unc. *Halobacteria* class	- Sugar-fermentation, lithoheterotrophic sulfur dissimilatory reduction - Sulfate- nitrate- dissimilatory reduction
138	Unc. 20c-4	Sugar fermentation
159	Unc. MSBL1	Methanogen hydrogenotrophic
170	Unc. MSBL1	Methanogen hydrogenotrophic
195	Unc. DHVEG-6	Fermentation and Carbohydrate metabolism
205	Unc. DHVEG-6	Fermentation and Carbohydrate metabolism
18	Unc. TM6 (*Dependentiae*)	Sugar fermentation (glucose)
24	Unc. WS1	Carbohydrate metabolism
39	Unc. *Acetothermia*	Chemolithoautotrophy, with assimilation of glycine betaine into acetate and trimethylamine
158	Unc. *Marinilabiliaceae*	Heterotrophic, not performing photosynthesis. - Some genera have a strictly fermentative metabolism - Other genera are facultative anaerobic with respiratory and fermentative types of metabolism
159	Unc. *Marinilabiliaceae*	
167	Unc. *Marinilabiliaceae*	
283	Unc. *Simkaniaceae*	Sugar fermentation (glycolysis)
288	*Prosthecochloris vibrioformis*	Anaerobe, phototroph and mesophilic bacterium
312	Unc. *Anaerolineaceae*	Anaerobic, heterotrophic with a fermentative metabolism
325	Unc. *Anaerolineaceae*	
392	*Halobacillus halophilus*	Carbohydrate metabolism, chemoorganotrophic
393	*Halobacillus mangrove*	Carbohydrate metabolism, chemoorganotrophic
416	*Paraliobacillus ryukyuensis*	Fermentation and Carbohydrate metabolism
421	Unc. *Bacillus* sp.	Fermentation and Carbohydrate metabolism
432	*Virgibacillus salarius*	Hydrocarbon metabolism
468	Unc. MAT-CR-H4-C10	Heterotrophic/Chemolithotrophic
477	Unc. *Christensenellaceae* R-7 group	Chemoautotroph and Mixotrophic
563	Unc. *Halanaerobium* sp.	Fermentation of carbohydrates and sulfide production through thiosulfate reduction
567	Unc. *Halanaerobium* sp.	
572	Unc. *Halocella* sp.	Fermentative or Homoacetogenic metabolism
574	Unc. *Halocella* sp.	
651	Unc. SAR406 clade	Carbohydrates degradation
697	Unc. PB79	Sugar fermentation / Autotrophic metabolism / Anammox
1021	Unc. *Desulfobacteraceae*	Sulfate dissimilatory reduction
1051	Unc. *Desulfovermiculus* sp.	Sulfate dissimilatory reduction
1285	Unc. NB1-n	Anaerobic fermentation of simple sugars
1287	*Haloplasma contractile*	Strictly anaerobic and halophilic. Nitrate and nitrite reduction. Lactate is a fermentation product

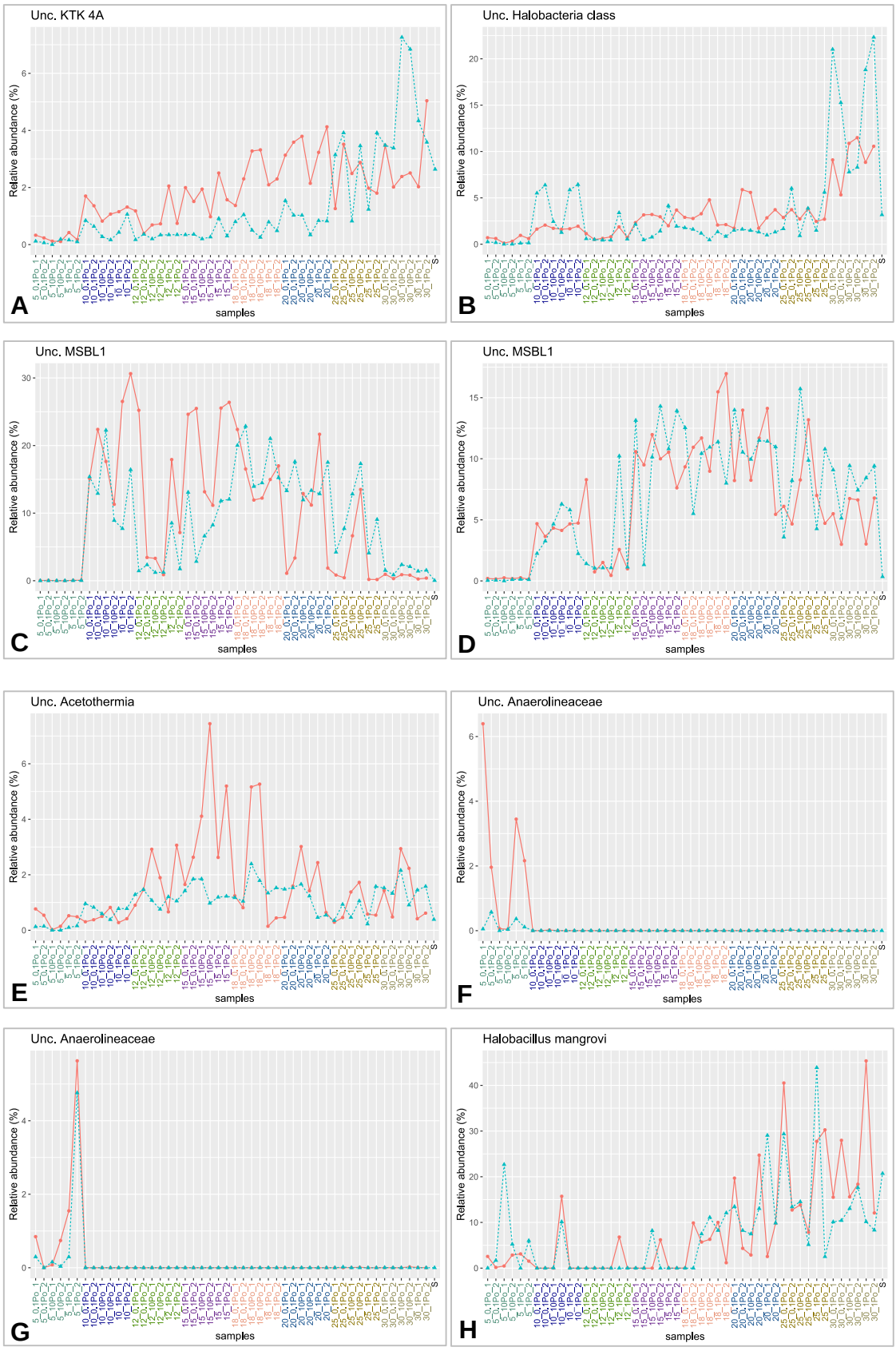
Unc. KTK 4A
A
Unc. Halobacteria class
B
Unc. MSBL1
C
Unc. MSBL1
D
Unc. Acetothermia
E
Unc. Anaerolineaceae
F
Unc. Anaerolineaceae
G
Halobacillus mangrovi
H
Relative abundance (%)
samples

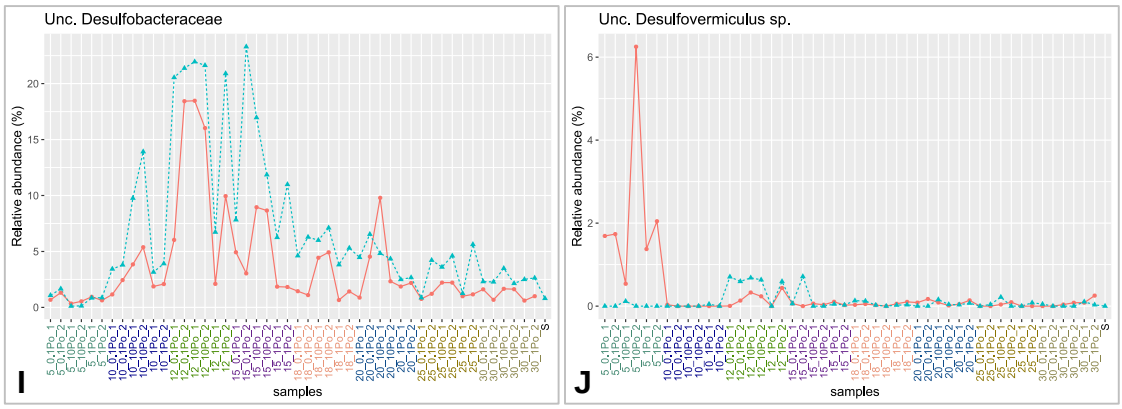

Supplementary Figure S2.7. Graphics of relevant OPUs (a selection of ten OPUs from Table 2.1) associated to diverse and most characteristic metabolisms. In the x axis, the microcosms at the eight salinities with the three substrate compositions (0.1% *Po*, 1% *Po* and 10% *Po* w/w) and the S sample are represented. Samples with and without ampicillin are plotted in red and blue, respectively.

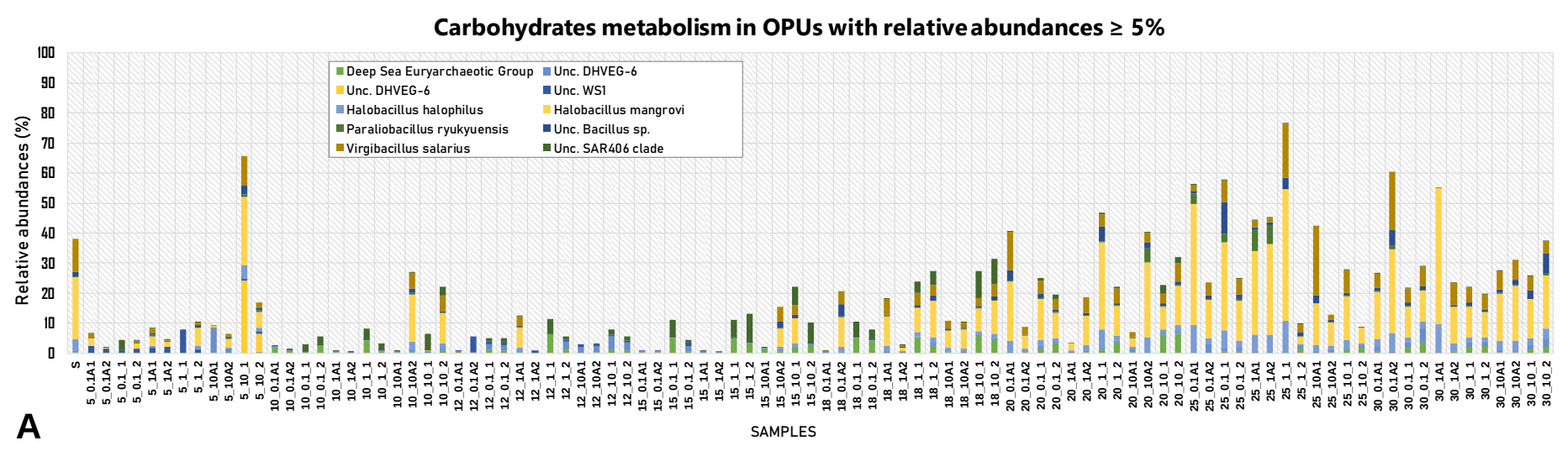
Carbohydrates metabolism in OPUs with relative abundances ≥ 5%
Relative abundances (%)
Deep Sea Euryarchaeotic Group
Unc. DHVEG-6
Unc. DHVEG-6
Unc. WS1
Halobacillus halophilus
Halobacillus mangrovi
Paraliobacillus ryukyuensis
Unc. Bacillus sp.
Virgibacillus salarius
Unc. SAR406 clade
A
SAMPLES

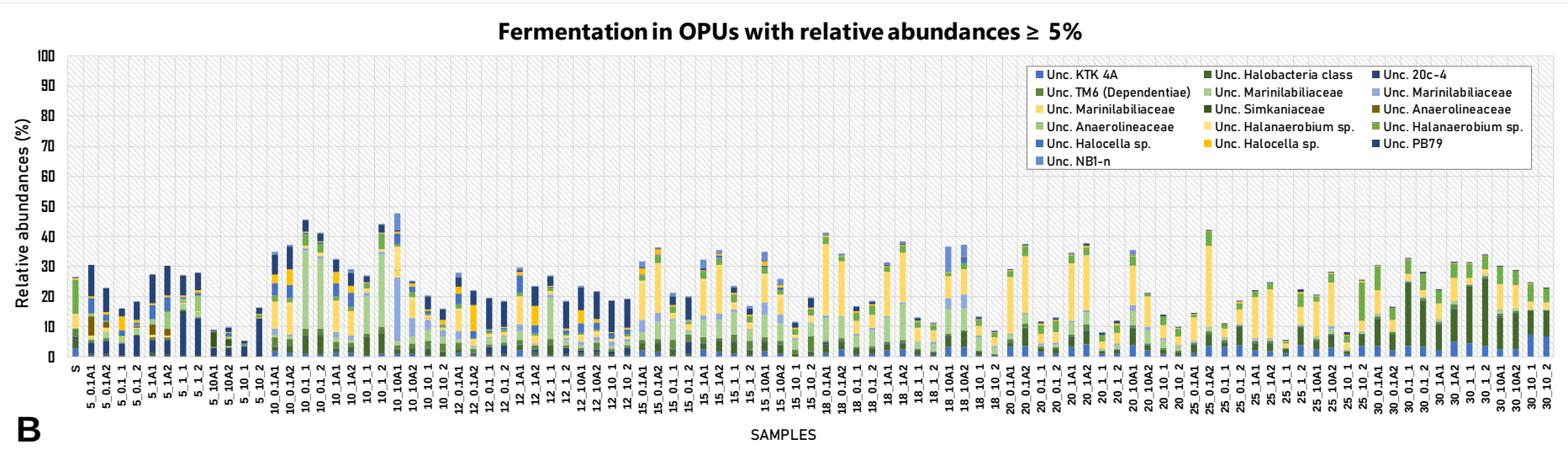
Fermentation in OPUs with relative abundances ≥ 5%
Relative abundances (%)
Unc. KTK 4A
Unc. Halobacteria class
Unc. 20c-4
Unc. TM6 (Dependentiae)
Unc. Marinilabiliaceae
Unc. Marinilabiliaceae
Unc. Marinilabiliaceae
Unc. Simkaniaceae
Unc. Anaerolineaceae
Unc. Anaerolineaceae
Unc. Halanaerobium sp.
Unc. Halanaerobium sp.
Unc. Halocella sp.
Unc. Halocella sp.
Unc. PB79
Unc. NB1-n
B
SAMPLES

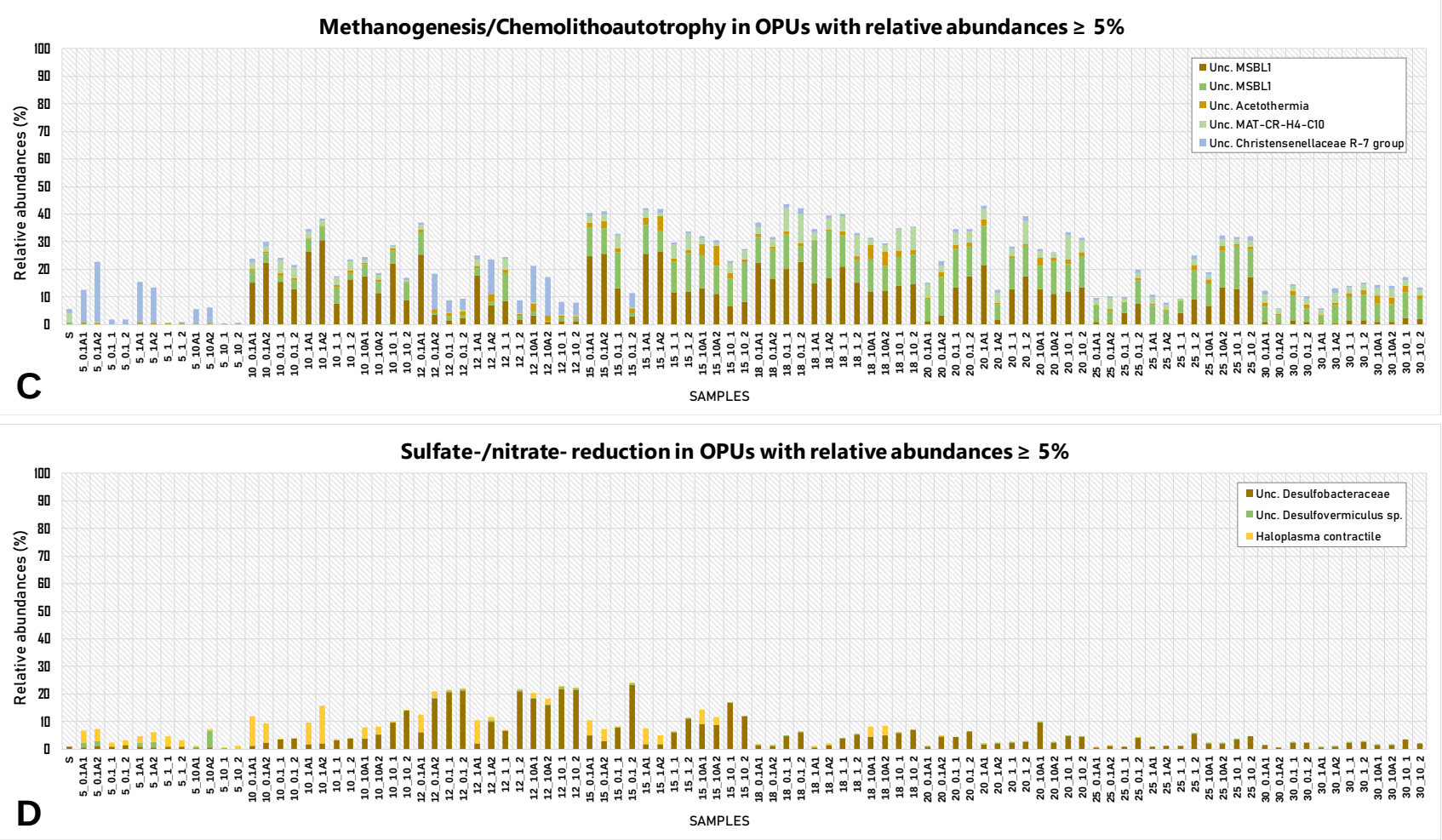

Supplementary Figure S2.8. Grouped barplots representing the described metabolisms regarding to carbohydrates degradation or synthesis (**A**), fermentation (**B**), methanogenesis / chemolithoautotrophy (**C**) and sulfate- / nitrate- reduction (**D**) for those OPUs with relative abundances above 5% in one sample at least.

Chapter 3. Improvement and selection of methanogenic consortia. Description of the most efficient microcosms in methane generation

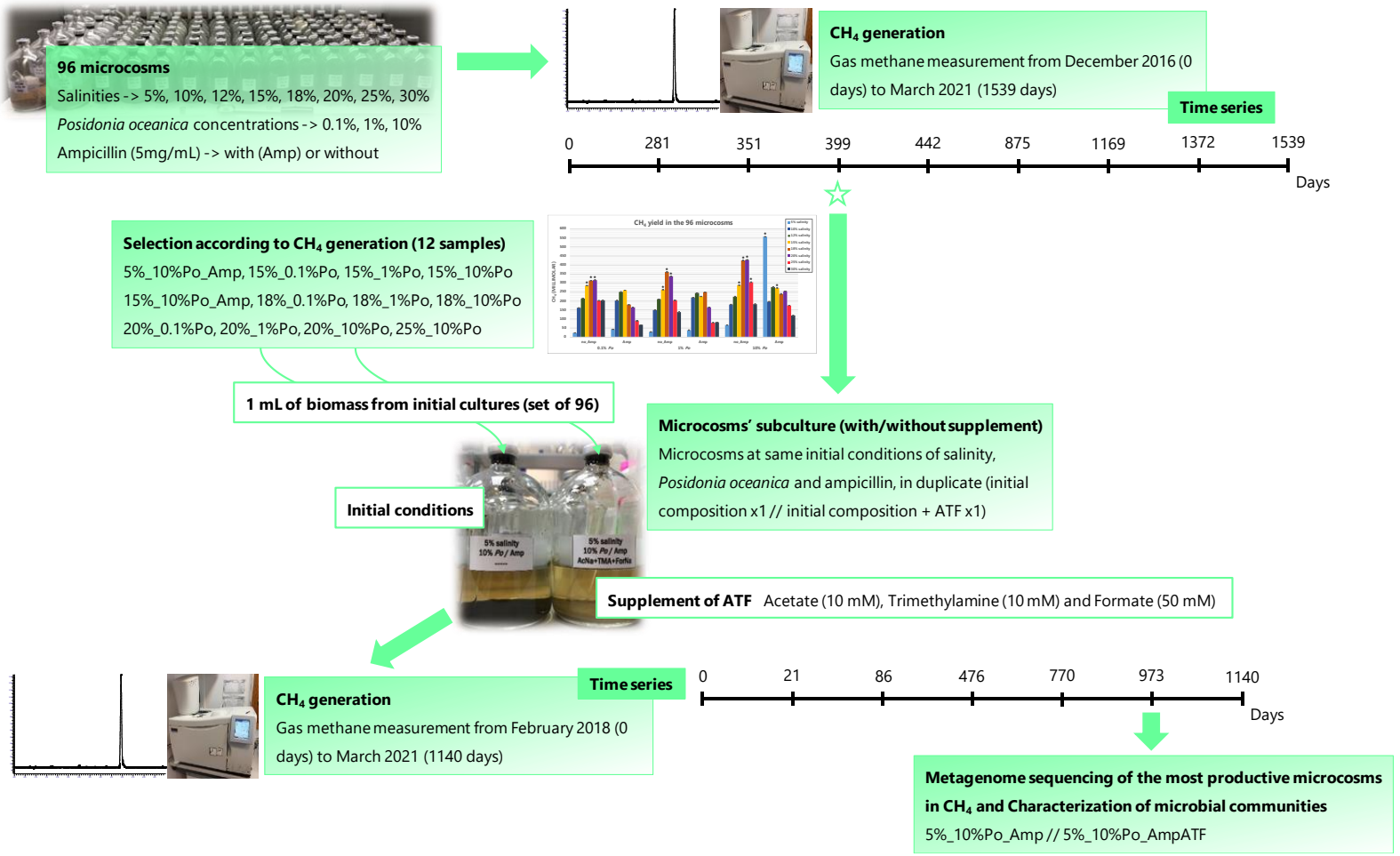

Supplementary Figure S3.1. Flowchart of the methodology applied in the Chapter 3.

Supplementary Table S3.1. Data of methane yield (in millimolar) from the duplicate microcosms (with the standard deviations) at 399 days. Samples are classified depending on the salinity (rows), and the substrate concentration (0.1%, 1% and 10% *Po*) and the ampicillin addition (both in columns). The selected microcosms are grey shaded.

CH_4 (mM)	0.1% *Po*		1% *Po*		10% *Po*	
Salinity	**WITHOUT Amp**	**WITH Amp**	**WITHOUT Amp**	**WITH Amp**	**WITHOUT Amp**	**WITH Amp**
5%	23.33±0	42.67±0.69	28.64±1.1	38.49±0.9	67.29±0.77	557.29±0.75
10%	162.09±0.78	203.26±0.49	150.07±1.32	219.54±0.54	180.64±0.9	196.85±0.53
12%	214.69±0.77	250.96±1.04	210.4±0.34	244.07±0.14	224.7±0.97	271.39±0.9
15%	285.79±1.03	260.19±0.56	263.59±0.52	225.34±0.3	288.31±0.92	272.7±0.23
18%	313.64±0.52	179.76±0.89	361.07±1.77	249.64±0.46	425.21±1.45	239.32±1.36
20%	316.38±0.07	165.59±0.09	337.74±0.66	165.64±0.16	428.36±0.01	254.84±0.58
25%	202.59±1.09	90.68±0.09	203.97±0.39	79.98±0.18	304.79±1.51	175.3±0.03
30%	203.83±1.21	67.7±0.42	138.77±0.86	81.97±0.2	182.85±0.52	119.86±0.73

Supplementary Table S3.2. Metagenomic sequencing features of the two metagenomes E and ES. In the last row, Nonpareil index of S (slurry) is shaded in grey.

	E	ES
Number of raw reads	84,298,626	83,138,476
Number of trimmed and merged reads	64,610,744	70,703,906
Trimmed reads mean length (pb)	120.49	127.43
Number of assembled contigs	169,676	197,933
Number of contigs >500pb	94,525	112,841
Total size assembled contigs (pb)	267,600,671	296,097,299
Total size contigs >500pb (pb)	239,266,301	264,153,869
Coverage (%)	92.29%	92.36%
N50 (assembled contigs)	5,393	3,803
N50 (contigs >500pb)	7,787	5,570
G+C mol% (assembled contigs)	53.9	52.3
G+C mol% (contigs >500pb)	53.5	52.3
Longer contig size (pb)	654,592	400,714
Num. gene contigs >500pb	277,726	311,538
% reads mapped to trimmed reads *	85.22%	81.39%
% reads from MAGs mapped *	81.17%	72.73%
Nonpareil diversity index (Nd)	18.08	17.96
Nonpareil diversity index (Nd) of S	**19.76**	

*At 98% identity and 70% coverage.

Supplementary Table S3.3. Additional MAGs recovered from E and ES metagenomes and their most relevant features. From left to right, *D* indicates taxonomic domain (Archaea or Bacteria); *Gsp* indicates the genomospecies designation; *ID* indicates the MAG designation; *same sp.* indicates the high quality MAG, sharing ANI >99% with the designated MAG, and therefore identified as the same genomospecies (Table 3.1); *Id rank* indicates the lowest taxonomic rank to which the genomospecies could be assigned; *Category* indicates the taxonomic group to which the MAG could be assigned; the *Closest reference sequence* is the nearest genome or MAG available in the public repositories; *Comp.* indicates genome completeness; *Con.* indicates contamination; *AAI* indicates the average amino acid identity with the closest genome or MAG, *Prot%* indicates the percentage of aligned proteins; *contigs* indicates the number of assembled and binned contigs; *Mb* is the size in Mb of the binned MAG.

D	Gsp	ID	same sp.	Id rank	Category	Closest reference sequence	Comp	Con	AAI	Prot%	contigs	Mb
B	Gsp1	ES46	E27	Family	*Acholeplasmataceae*	AD A	43.5	4.3	41.2	24.3	674	1.66
B	Gsp14	E14	ES11	Genus	*Brevefilum*	*Anaerolineaceae* bacterium	82.6	4.3	59.0	64.8	334	4.94
B	Gsp15	E18	ES22	Genus	*Pelolinea*	*Pelolinea submarina*	91.3	0.0	85.9	80.0	120	3.08
B	Gsp19	ES43	E31	Class	*Anaerolineae*	-	69.6	17.4	-	-	1,747	4.15
B	Gsp21	E17	ES41	Order	*Rhodospirillales*	TARA MED MAG 00125	60.9	4.3	53.8	54.0	827	3.11
B	Gsp32	E09	ES06	Order	*Desulfatiglandales*	AK5YR 20 metabat2 7 fa	91.3	4.3	45.1	53.8	968	4.86
B	Gsp33	E01	ES15	Family	*Desulfarculaceae*	*Desulfarculus* sp. genome	100.0	13.0	67.5	72.2	113	4.63
B	Gsp36	E40	ES37	Family	*Desulfovibrionaceae*	*Desulfovibrionaceae* bacterium UBA6814	39.1	0.0	58.0	60.4	964	2.02
B	Gsp37	ES19	E12	Family	*Desulfohalobiaceae*	*Desulfovermiculus halophilus* DSM 18834	91.3	17.4	56.3	58.7	567	3.80
B	Gsp41	ES32	E13	Order	*Bacteroidales*	-	82.6	4.3	-	-	263	2.92
B	Gsp44	E05	ES17	Class	*Gemmatimonadetes*	TARA ANE MAG 00005	100.0	4.3	53.6	67.9	157	4.46
B	Gsp46	ES39	E24	Order	*Pirellulales*	TARA RED MAG 00100	21.7	8.7	43.1	46.2	1,818	3.89
B	Gsp48	E30	ES21	Order	*Pirellulales*	TARA RED MAG 00100	91.3	0.0	49.1	45.2	1,446	6.64
B	Gsp51	ES18	E22	Family	*Anaerohalophaeraceae*	*Phycisphaerales* bacterium PLanc-01	95.7	0.0	65.5	63.8	715	6.82
B	Gsp53	ES30	E03	Family	*Anaerohalophaeraceae*	*Phycisphaerales* bacterium PLanc-01	56.5	8.7	66.5	55.6	546	5.86
B	Gsp57	ES10	E45	Family	*Sphaerochaetaceae*	-	100.0	0.0	-	-	32	2.55
B	Gsp60	ES04	E06	Class	*Bipolaricaulia*	*Candidatus* Atribacteria bacterium	100.0	0.0	66.7	70.9	122	2.68
A	Gsp65	ES09	E02	Genus	*Methanosarcina*	*Methanosarcina* sp. DTU009	91.3	0.0	73.9	70.5	166	3.81
A	Gsp67	ES05	E04	Family	DHVEG-1	-	4.3	0.0	-	-	192	0.37
A	Gsp69	E08	ES02	Family	DHVEG-1	*Thermoplasmatales* archaeon ex4572_165	100.0	8.7	59.3	76.8	624	3.10
A	Gsp71	E20	ES13	Class	*Bathyarchaeia*	*Candidatus* Bathyarchaeota archaeon	95.7	26.1	71.6	53.7	281	2.04

Supplementary Table S3.4. MAGs recovered from E and ES and their most relevant features. From left to right, the first column indicates the MAG taxonomic domain (*Arch* or *Bact* for Archaea or Bacteria, respectively); *Gsp* indicates the genomospecies designation; *ID* indicates the MAG denomination; *GC%* is the G+C mol percentage; *N50* and *N90* are basic quality parameters. The last six columns indicate the taxonomic categories to which each MAG could be identified to. Empty boxes indicate that the category could not be determined. MAGs sharing >99% ANI identity and therefore identified as a genomospecies are shaded in grey.

	Gsp	ID	GC%	N50	N90	Domain	Phylum	Class	Order	Family	Genus	Species
Bact	Gsp1	E27	32.5	9,228	1,510	*Bacteria*	*Firmicutes*	*Bacilli*	*Acholeplasmatales*	*Acholeplasmataceae*		
Bact		ES46	34.1	3,136	1,203	*Bacteria*	*Firmicutes*	*Bacilli*	*Acholeplasmatales*	*Acholeplasmataceae*		
Bact	Gsp2	ES42	41.2	2,240	1,151	*Bacteria*	*Firmicutes*	UBA994	PWPR01			
Bact	Gsp3	E21	40.5	18,822	4,114	*Bacteria*	*Firmicutes*	*Clostridia*	*Acetivibrionales*	DSM-8532	*Thermoclostridium*	
Bact	Gsp4	ES36	35.1	8,610	1,897	*Bacteria*	*Firmicutes*	*Clostridia*	*Acetivibrionales*			
Bact	Gsp5	E39	51.6	3,311	1,307	*Bacteria*	*Firmicutes*	*Clostridia*	*Christensenellales*	*Christensenellaceae*		
Bact	Gsp6	ES24	49.1	55,479	24,331	*Bacteria*	*Firmicutes*	*Clostridia*	*Christensenellales*	*Christensenellaceae*		
Bact	Gsp7	E36	51.6	4,759	1,586	*Bacteria*	*Firmicutes*	*Clostridia*	*Christensenellales*	SZUA-584	SZUA-584	
Bact	Gsp8	ES16	34.2	61,088	16,743	*Bacteria*	*Firmicutes*	*Halanaerobiia*	*Halanaerobiales*	*Halanaerobiaceae*	*Halanaerobium*	
Bact	Gsp9	ES20	34.5	74,775	20,097	*Bacteria*	*Firmicutes*	*Halanaerobiia*	*Halanaerobiales*			
Bact	Gsp10	E29	35.9	13,171	3,667	*Bacteria*	*Firmicutes*	*Halanaerobiia*	*Halanaerobiales*	DTU029		
Bact	Gsp11	ES26	39.3	6,431	1,832	*Bacteria*	*Firmicutes*	*Halanaerobiia*	*Halanaerobiales*			
Bact	Gsp12	E32	62.7	5,573	2,222	*Bacteria*	*Actinobacteriota*	*Thermoleophilia*	RBG-16-64-13	RBG-16-64-13		
Bact	Gsp13	ES33	31.4	3,736	1,260	*Bacteria*	*Actinobacteriota*	UBA1414				
Bact	Gsp14	ES11	47.5	136,041	13,475	*Bacteria*	*Chloroflexota*	*Anaerolineae*	*Anaerolineales*	*Anaerolineaceae*	*Brevefilum*	
Bact		E14	47.0	58,218	5,435	*Bacteria*	*Chloroflexota*	*Anaerolineae*	*Anaerolineales*	*Anaerolineaceae*	*Brevefilum*	
Bact	Gsp15	ES22	52.8	72,115	20,318	*Bacteria*	*Chloroflexota*	*Anaerolineae*	*Anaerolineales*	*Anaerolineaceae*	*Pelolinea*	
Bact		E18	52.7	50,705	14,593	*Bacteria*	*Chloroflexota*	*Anaerolineae*	*Anaerolineales*	*Anaerolineaceae*	*Pelolinea*	
Bact	Gsp16	E43	51.6	2,440	1,194	*Bacteria*	*Chloroflexota*	*Anaerolineae*	*Anaerolineales*	UBA11858		
Bact	Gsp17	E42	59.1	2,252	1,152	*Bacteria*	*Chloroflexota*	*Anaerolineae*	*Anaerolineales*	UBA11579		
Bact	Gsp18	ES47	56.5	2,214	1,166	*Bacteria*	*Chloroflexota*	*Anaerolineae*	B4-G1	SLSP01		
Bact	Gsp19	E31	60.9	9,598	1,468	*Bacteria*	*Chloroflexota*	*Anaerolineae*	UBA1429			
Bact		ES43	62.2	2,747	1,156	*Bacteria*	*Chloroflexota*	*Anaerolineae*	UBA1429			
Bact	Gsp20	E34	51.8	7,668	1,407	*Bacteria*	*Chloroflexota*	*Dehalococcoidia*	GIF9			
Bact	Gsp21	ES41	64.4	3,323	1,508	*Bacteria*	*Proteobacteria*	*Alphaproteobacteria*	*Rhodospirillales*			
Bact		E17	64.9	5,034	1,749	*Bacteria*	*Proteobacteria*	*Alphaproteobacteria*	*Rhodospirillales*			
Bact	Gsp22	ES45	51.5	3,256	1,317	*Bacteria*	*Desulfobacterota*	*Desulfobacteria*	*Desulfobacterales*	SURF-3		
Bact	Gsp23	E38	57.5	1,711	1,101	*Bacteria*	*Desulfobacterota*	*Desulfobacteria*	*Desulfobacterales*	SURF-3		
Bact	Gsp24	E11	52.3	42,849	13,310	*Bacteria*	*Desulfobacterota*	*Desulfobacteria*	*Desulfobacterales*	SURF-15		
Bact	Gsp25	ES14	44.0	22,934	5,683	*Bacteria*	*Desulfobacterota*	*Desulfobacteria*	*Desulfobacterales*	SKZT01		
Bact	Gsp26	ES50	52.5	1,847	1,124	*Bacteria*	*Desulfobacterota*	*Desulfobacteria*				
Bact	Gsp27	ES28	46.4	38,981	4,083	*Bacteria*	*Desulfobacterota*	*Desulfobacteria*	*Desulfatiglandales*	NaphS2		
Bact	Gsp28	ES38	48.1	5,352	1,311	*Bacteria*	*Desulfobacterota*	*Desulfobacteria*	*Desulfatiglandales*	NaphS2		
Bact	Gsp29	ES08	47.4	44,281	9,232	*Bacteria*	*Desulfobacterota*	*Desulfobacteria*	*Desulfatiglandales*	NaphS2		
Bact	Gsp30	E26	52.7	15,960	1,643	*Bacteria*	*Desulfobacterota*	*Desulfobacteria*	*Desulfatiglandales*	HGW-15		
Bact	Gsp31	ES51	56.5	1,873	1,127	*Bacteria*	*Desulfobacterota*	*Desulfobacteria*	*Desulfatiglandales*			
Bact	Gsp32	ES06	60.3	28,502	8,523	*Bacteria*	*Desulfobacterota*	*Desulfobacteria*	*Desulfatiglandales*			

Bact		E09	60.8	8,893	1,843	*Bacteria*	*Desulfobacterota*	*Desulfobacteria*	*Desulfatiglandales*			
Bact	Gsp33	ES15	64.6	85,611	29,712	*Bacteria*	*Desulfobacterota*	*Desulfarculia*	*Desulfarculales*	*Desulfarculaceae*	SURF-10	
Bact		E01	64.0	86,422	28,361	*Bacteria*	*Desulfobacterota*	*Desulfarculia*	*Desulfarculales*	*Desulfarculaceae*	SURF-10	
Bact	Gsp34	E37	51.7	3,812	1,474	*Bacteria*	*Desulfobacterota*	*Desulfobulbia*	*Desulfobulbales*	*Desulfocapsaceae*	*Desulforhopalus*	
Bact	Gsp35	E33	45.1	2,924	1,233	*Bacteria*	*Desulfobacterota*	*Desulfobulbia*	*Desulfobulbales*	*Desulfocapsaceae*	*Desulforhopalus*	
Bact	Gsp36	ES37	65.6	7,042	2,080	*Bacteria*	*Desulfobacterota*	*Desulfovibrionia*	*Desulfovibrionales*	*Desulfovibrionaceae*		
Bact		E40	66.4	2,284	1,218	*Bacteria*	*Desulfobacterota*	*Desulfovibrionia*	*Desulfovibrionales*	*Desulfovibrionaceae*		
Bact	Gsp37	E12	45.6	18,452	3,897	*Bacteria*	*Desulfobacterota*	*Desulfovibrionia*	*Desulfovibrionales*	*Desulfohalobiaceae*		
Bact		ES19	45.6	11,995	2,675	*Bacteria*	*Desulfobacterota*	*Desulfovibrionia*	*Desulfovibrionales*	*Desulfohalobiaceae*		
Bact	Gsp38	E23	37.8	18,084	1,833	*Bacteria*	*Desulfobacterota*	*Desulfovibrionia*	*Desulfovibrionales*	*Desulfohalobiaceae*		
Bact	Gsp39	ES35	40.3	4,015	1,452	*Bacteria*	*Desulfobacterota*	*Desulfovibrionia*	*Desulfovibrionales*	*Desulfohalobiaceae*		
Bact	Gsp40	ES34	39.0	24,495	3,596	*Bacteria*	*Bacteroidota*	*Bacteroidia*	*Bacteroidales*	UBA10428	UBA10428	
Bact	Gsp41	E13	37.6	86,703	18,135	*Bacteria*	*Bacteroidota*	*Bacteroidia*	*Bacteroidales*	UBA10428		
Bact		ES32	36.7	24,859	4,844	*Bacteria*	*Bacteroidota*	*Bacteroidia*	*Bacteroidales*	UBA10428		
Bact	Gsp42	E44	36.1	2,253	1,208	*Bacteria*	*Bacteroidota*	*Ignavibacteria*	*Ignavibacteriales*	*Melioribacteraceae*	SURF-28	
Bact	Gsp43	ES25	40.4	129,223	45,856	*Bacteria*	SM23-31	SM23-31	QNDG01			
Bact	Gsp44	ES17	66.0	52,576	17,132	*Bacteria*	*Gemmatimonadota*	*Gemmatimonadetes*	SG8-23	UBA6960		
Bact		E05	65.8	55,945	17,001	*Bacteria*	*Gemmatimonadota*	*Gemmatimonadetes*	SG8-23	UBA6960		
Bact	Gsp45	ES40	63.1	4,079	1,469	*Bacteria*	*Aureabacteria*	PUNC01	PUNC01	PWXJ01	PWXJ01	
Bact	Gsp46	E24	66.2	6,801	1,391	*Bacteria*	*Planctomycetota*	*Planctomycetes*	*Pirellulales*	Ga0077529		
Bact		ES39	66.3	2,374	1,186	*Bacteria*	*Planctomycetota*	*Planctomycetes*	*Pirellulales*	Ga0077529		
Bact	Gsp47	ES23	65.2	17,073	4,319	*Bacteria*	*Planctomycetota*	*Planctomycetes*	*Pirellulales*	Ga0077529		
Bact	Gsp48	ES21	63.7	83,695	20,336	*Bacteria*	*Planctomycetota*	*Planctomycetes*	*Pirellulales*	UBA11386		
Bact		E30	64.0	8,233	1,674	*Bacteria*	*Planctomycetota*	*Planctomycetes*	*Pirellulales*	UBA11386		
Bact	Gsp49	E19	45.6	48,026	13,042	*Bacteria*	*Planctomycetota*	*Phycisphaerae*	*Sedimentisphaerales*	*Anaerohalophaeraceae*		
Bact	Gsp50	ES44	61.0	2,312	1,184	*Bacteria*	*Planctomycetota*	*Phycisphaerae*	*Sedimentisphaerales*	*Anaerohalophaeraceae*	PLanc-01	
Bact	Gsp51	E22	53.9	12,898	2,305	*Bacteria*	*Planctomycetota*	*Phycisphaerae*	*Sedimentisphaerales*	*Anaerohalophaeraceae*	PLanc-01	
Bact		ES18	53.8	18,161	4,179	*Bacteria*	*Planctomycetota*	*Phycisphaerae*	*Sedimentisphaerales*	*Anaerohalophaeraceae*	PLanc-01	
Bact	Gsp52	ES29	59.7	33,771	6,018	*Bacteria*	*Planctomycetota*	*Phycisphaerae*	*Sedimentisphaerales*	*Anaerohalophaeraceae*	PLanc-01	
Bact	Gsp53	ES30	61.4	18,071	5,036	*Bacteria*	*Planctomycetota*	*Phycisphaerae*	*Sedimentisphaerales*	*Anaerohalophaeraceae*	PLanc-01	
Bact		E03	60.6	52,274	10,954	*Bacteria*	*Planctomycetota*	*Phycisphaerae*	*Sedimentisphaerales*	*Anaerohalophaeraceae*	PLanc-01	
Bact	Gsp54	ES49	48.8	1,900	1,113	*Bacteria*	*Planctomycetota*	*Phycisphaerae*	*Sedimentisphaerales*	*Anaerohalophaeraceae*	4572-13	
Bact	Gsp55	E41	60.5	1,798	1,087	*Bacteria*	*Planctomycetota*	*Phycisphaerae*	*Sedimentisphaerales*			
Bact	Gsp56	E10	54.9	72,665	22,870	*Bacteria*	*Planctomycetota*	UBA8108	UBA8890	UBA8898		
Bact	Gsp57	E45	50.5	187,952	84,721	*Bacteria*	*Spirochaetota*	*Spirochaetia*	*Sphaerochaetales*	*Sphaerochaetaceae*		
Bact		ES10	51.0	259,281	80,913	*Bacteria*	*Spirochaetota*	*Spirochaetia*	*Sphaerochaetales*	*Sphaerochaetaceae*		
Bact	Gsp58	E46	59.7	71,475	20,534	*Bacteria*	*Bipolaricaulota*	*Bipolaricaulia*	UBA7950	UBA9294	RXOA01	
Bact	Gsp59	E15	55.1	61,124	12,391	*Bacteria*	*Bipolaricaulota*	*Bipolaricaulia*	UBA7950	UBA9294	SPBW01	
Bact	Gsp60	E06	61.5	70,609	12,295	*Bacteria*	*Bipolaricaulota*	*Bipolaricaulia*	UBA7950	UBA9294	SPBW01	
Bact		ES04	61.4	70,609	11,871	*Bacteria*	*Bipolaricaulota*	*Bipolaricaulia*	UBA7950	UBA9294	SPBW01	
Arch	Gsp61	E35	40.7	3,176	1,308	*Archaea*	*Nanoarchaeota*	*Nanoarchaeia*	*Woesearchaeales*	GW2011-AR15	GW2011-AR15	
Arch	Gsp62	ES12	30.4	81,692	2,481	*Archaea*	*Nanoarchaeota*	*Nanoarchaeia*	*Pacearchaeales*	GW2011-AR1	ARS1301	
Arch	Gsp63	E16	60.7	24,531	7,827	*Archaea*	*Euryarchaeota*	*Methanomicrobia*	*Methanomicrobiales*	*Methanoculleaceae*	*Methanoculleus*	
Arch	Gsp64	ES07	59.5	58,221	19,542	*Archaea*	*Euryarchaeota*	*Methanomicrobia*	*Methanomicrobiales*	*Methanoculleaceae*	*Methanoculleus*	
Arch	Gsp65	E02	46.3	34,240	9,971	*Archaea*	*Euryarchaeota*	*Methanomicrobia*	*Methanosarcinales*	*Methanosarcinaceae*	*Methanosarcina*	
Arch		ES09	46.8	36,655	11,615	*Archaea*	*Euryarchaeota*	*Methanomicrobia*	*Methanosarcinales*	*Methanosarcinaceae*	*Methanosarcina*	
Arch	Gsp66	ES01	42.0	4,752	1,723	*Archaea*	*Thermoplasmatota*	E2	DHVEG-1	DHVEG-1		
Arch	Gsp67	E04	41.3	8,166	2,637	*Archaea*	*Thermoplasmatota*	E2	DHVEG-1	DHVEG-1		
Arch		ES05	43.0	1,991	1,118	*Archaea*	*Thermoplasmatota*	E2	DHVEG-1	DHVEG-1		

Arch	Gsp68	ES03	40.2	8,157	2,013	*Archaea*	*Thermoplasmatota*	E2	DHVEG-1	DHVEG-1		
Arch	Gsp69	ES02	33.5	229,543	27,296	*Archaea*	*Thermoplasmatota*	E2	DHVEG-1	DHVEG-1	EX4572-165	
Arch		E08	33.2	7,286	2,161	*Archaea*	*Thermoplasmatota*	E2	DHVEG-1	DHVEG-1	EX4572-165	
Arch	Gsp70	E28	47.1	22,392	2,610	*Archaea*	*Thermoproteota*	*Bathyarchaeia*	B26-1	UBA233	PALSA-986	
Arch	Gsp71	ES13	38.3	16,960	3,797	*Archaea*	*Thermoproteota*	*Bathyarchaeia*	B26-1	BA1	BIN-L-1	
Arch		E20	39.3	23,264	2,464	*Archaea*	*Thermoproteota*	*Bathyarchaeia*	B26-1	BA1	BIN-L-1	
Arch	Gsp72	ES27	39.6	2,537	1,236	*Archaea*	*Thermoproteota*	*Bathyarchaeia*	B26-1	BA1	BIN-L-1	
Arch	Gsp73	E25	58.6	11,091	2,526	*Archaea*	*Thermoproteota*	*Bathyarchaeia*	TCS64	TCS64	RBG-16-57-9	
Arch	Gsp74	E07	47.3	179,341	10,821	*Archaea*	*Thermoproteota*	*Bathyarchaeia*	TCS64	TCS64	RBG-16-57-9	
Arch	Gsp75	ES48	49.6	2,539	1,245	*Archaea*	*Asgardarchaeota*	*Lokiarchaeia*	CR-4	CR-4		
Arch	Gsp76	ES31	36.1	38,515	9,067	*Archaea*	*Asgardarchaeota*	*Lokiarchaeia*	CR-4	AMARA-1		

Supplementary Table S3.5. Percentage average nucleotide identity (ANI) values and shared nucleotide rates of the genomes in brackets, for the MAGs of the E and ES metagenomes, therefore identified as genomospecies.

	E06	E02	E45	E01	E05	E18	E13	E14	E30	E40	E27	E31	E12	E22	E09	E03	E17	E24	E08	E20	E04
ES04	100%(95.1%)																				
ES09		100%(99.3%)																			
ES10			100%(95.7%)																		
ES15				100%(97.5%)																	
ES17					100%(99.6%)																
ES22						100%(90.4%)															
ES32							100%(87%)														
ES11								100%(63.4%)													
ES21									100%(87.6%)												
ES37										100%(76%)											
ES46											100%(62.8%)										
ES43												100%(50.9%)									
ES19													99.9%(81.4%)								
ES18														99.9%/79.7%)							
ES06															99.8%(71.7%)						
ES30																99.8%(80.9%)					
ES41																	99.8%(58%)				
ES39																		99.8%(63.8%)			
ES02																			99.5%(75.1%)		
ES13																				99.3%(67%)	
ES05																					99%(61.2%)

Supplementary Table S3.6. Amino acid identity comparison between the retrieved MAGs from original sediments previously analyzed (Font-Verdera *et al.*, 2021), belonging to the vertical profile (U, M and L for the upper, middle and lower fractions, respectively) and the slurry (S), and the MAGs obtained from the E and ES metagenomes. From left to right: MAGs designation and the taxonomic group where were assigned, from U, M, L and S (first column) and from E and ES (second column). In the third and fourth columns, *AAI* indicates the average amino acid identity among the MAGs and *Prot%* indicates the percentage of aligned and shared proteins between the genomes. MAGs identified as same species (genomospecies; ANI >99%) are grouped in a single row and grey shaded. Data percentage are shown for AAI values >45% (family rank).

MAGs from U, M, L and S (original sediments)	MAGs from E and ES (subcultured/enriched sediments)	AAI	Prot%
S04 - *Deltaproteobacteria*	Gsp37: E12_ES19 - *Desulfohalobiaceae*	54.44	46.98
S04 - *Deltaproteobacteria*	Gsp38: E23 - *Desulfohalobiaceae*	52.47	44.29
S04 - *Deltaproteobacteria*	Gsp39: ES35 - *Desulfohalobiaceae*	50.78	37.97
M05_L06 - *Aureimonas*	Gsp21: E17_ES41 - *Rhodospirillales*	46.63	43.65
S04 - *Deltaproteobacteria*	Gsp36: E40 - *Desulfovibrionaceae*	46.02	41.20
S05 - DHVE2	Gsp69: E08_ES02 - *Thermoplasmatota*	45.57	46.46